

Experimental and Theoretical Investigations into the Development  
of an Efficient Wind Turbine

Charles Amoge Ikonwa

Submitted in accordance with the requirements for the degree of  
Doctor of Philosophy

Under the supervision of

Professor William Gale

Professor Lin Ma

Professor Derek Ingham

Professor Mohamed Pourkashanian

School of Chemical and Process Engineering

The University of Leeds

December 2016

The candidate confirms that the work submitted is his own, except where work which has formed part of jointly authored publications has been included. The contribution of the candidate and the other authors to this work has been explicitly indicated below. The candidate confirms that appropriate credit has been given within the thesis where reference has been made to the work of others.

Chapter 4 includes the following submitted work:

C. A. Ikonwa, W. F. Gale, D. B. Ingham, L. Ma, and M. Pourkashanian, *Wind resource assessment and economic analysis for the potential installation of small-scale wind turbines using site pre-assessment, measurement and reanalysis data*. Renewable Energy (under review), 2016.

Chapter 7 includes the following published work:

C. A. Ikonwa, W. F. Gale, D. B. Ingham, L. Ma, and M. Pourkashanian, *Investigation of Airfoil Profiles for Use in Self-starting, Small-scale, Low Reynolds Number Vertical Axis Wind Turbines*. The International Journal of Environmental Sustainability 2016, 12 (3): 33-52.

All the research and analysis within these papers are solely conducted by the lead author with guidance and review provided by the co-authors.

This copy has been supplied on the understanding that it is copyright material and that no quotation from the thesis may be published without proper acknowledgement. The right of Charles Amoge Ikonwa to be identified as the author of this work has been asserted by him in accordance with the Copyright, Designs and Patents Act 1988.

© 2016 The University of Leeds and Charles Amoge Ikonwa.

## Conferences and Publications

### Conference:

C. A. Ikonwa, W. F. Gale, D. B. Ingham, L. Ma, and M. Pourkashanian

*Investigation of Airfoil Profiles for use in Self-Starting Small-Scale, Low Reynolds Number VAWTs.*

11<sup>th</sup> International Conference on Sustainability Copenhagen, Denmark 21-23 January 2015.

### Journal Papers:

C. A. Ikonwa, W. F. Gale, D. B. Ingham, L. Ma, and M. Pourkashanian,

*Investigation of Airfoil Profiles for Use in Self-starting, Small-scale, Low Reynolds Number Vertical Axis Wind Turbines.*

The International Journal of Environmental Sustainability 2016, 12 (3): 33-52.

C. A. Ikonwa, W. F. Gale, D. B. Ingham, L. Ma, and M. Pourkashanian,

*Wind resource assessment and economic analysis for the potential installation of small-scale wind turbines using site pre-assessment, measurement and reanalysis data.*

Renewable Energy (under review), 2016.

## **Acknowledgements**

I would like to begin by thanking my primary supervisor Professor William Gale for his expert advice, encouragement and direction throughout the period of this thesis. I would also like to sincerely appreciate Professor Derek Ingham, Professor Lin Ma and Professor Mohamed Pourkashanian, who were my main supervisors during the first and second year of my PhD, because their initial support and advice lead to the development of the research project and for their commitment to continue to act as my supervisors even when they were not based at the University of Leeds. Their invaluable insight and consistent mentoring in our weekly meetings have made my work very interesting and is strongly appreciated.

Sincere appreciation to the University of Leeds training units for all the numerous training sessions that I received during the period of this thesis.

Special thanks are also due to the staffs and management of the Low Carbon Combustion Centre, Beighton who were responsible for the installation and operation of the wind measurements stations installed as part of the work done in Chapter 5.

I am also very grateful to the National Aeronautics and Space Administration (NASA) which allowed access into historical reference data through the modern-era retrospective analysis for research and applications (MERRA) whose data formed part of the work presented in Chapters 4 and 5 for validation.

I gratefully acknowledge the financial support from my brother, Hon. Bright Ikonwa who funded my PhD. I really cannot thank him enough for this kind gesture.

On a more personal note, I would like to thank my family, my mother in-law, father-in-law, and my parents for all the sacrifices they have made since I ventured into this journey. Their prayers and supplications unto God was what sustained me throughout this period.

I would also like to thank my beloved wife Jennie, my daughter Christabel for being my inspiration and for their unwavering support, prayers and patience throughout this journey.

Above all, I would like to wholeheartedly thank the almighty God for the unusual strength and good health he has given me throughout these years, without which I wouldn't have completed this work.

## **Abstract**

The small-scale wind turbine is considered as one of the most effective renewable technologies due to their potential to provide useful amount of electricity, particularly in “off-grid” settings as well as promising future prospects to decarbonise the power sector and ultimately stabilise energy security. Due to the huge potential of the wind resources and financial incentives, the UK is a promising region for small-scale wind energy development but there has been lack of comprehensive assessment of the wind resource for relevant locations. Thus efficient and low cost techniques are urgently needed to assess the resource potential since the long-term measurement techniques usually employed in the large-scale industry are very expensive and often not feasible for small-scale development.

The research developed during this thesis focuses on cost effective techniques for predicting the wind resource using two main approaches, namely the boundary layer meteorology and measure-correlate-predict (MCP). These approaches were evaluated using a long-term dataset from the Modern Era Retrospective-Analysis and short-term onsite dataset from meteorological measurement station.

To begin with, the performance of a modified methodology based on the boundary layer meteorology was evaluated at four UK sites, and the results were validated using traditional error metrics. Averaged across all sites, the percentage error in the predicted wind power density was found to be about 25% due to the uncertainties associated with the choice of the input parameters. Although the result is very encouraging, it was concluded that such a method is better applied in a “preliminary” analysis to identify viable sites worthy of further investigation.

To reduce these uncertainties, an MCP technique was utilised along with onsite measurements over a period of 12 months at a subset of 1 of the 4 UK sites, and the results show a significant improvement on the predicted wind speed and power density. Comparison of both approaches show that the best performing MCP approaches resulted in percentage error in the predicted mean wind speed and power density of 7.2 % and 12.9 % in contrast to the 18.9 % and 17.0% obtained using the boundary layer approach. Seasonal trends, direction behaviours and frequency distribution were analysed and

their characteristics reflected the general wind conditions across most UK sites.

Based on the output of the wind resource assessment, the potential of a small-scale vertical axis wind turbine (VAWT) was assessed using the double multiple streamtube model. VAWTs based on the Darrieus concept are potentially more efficient and economical, but those with fixed pitch blades are inherently non self-starting and are unsuitable for decentralised application. It is shown that the self-starting problem can be alleviated by a combination of a suitable aerofoil sections, solidity and pitch angles. The thesis provides a technique for inexpensive wind resource assessment where direct long-term measurements are not feasible. In addition, it provides a suitable solution strategy to the problem of self-starting in small-scale fixed pitch wind turbines.

## **Table of Contents**

<b>Conferences and Publications .....</b>	<b>ii</b>
Conference:.....	ii
Journal Papers:.....	ii
<b>Acknowledgements .....</b>	<b>iii</b>
<b>Abstract .....</b>	<b>v</b>
<b><u>Table of Contents</u> .....</b>	<b>vii</b>
<b>List of Figures .....</b>	<b>xiii</b>
<b>List of Tables .....</b>	<b>xx</b>
<b>Chapter 1: Introduction.....</b>	<b>1</b>
1.1 Energy and Sustainability .....	1
1.2 Challenges and constraints of Wind Resource Assessment .....	3
1.2.1 Wind Atlas Methodology.....	4
1.2.2 NOABL-Microgeneration Certification Scheme (MCS) method .....	5
1.2.3 Boundary Layer Methodology .....	5
1.2.4 Hindcasting/Measure-Correlate-Predict methods .....	5
1.3 The reason for this research .....	6
1.4 Vertical axis wind turbine (VAWTs): the need to self-start.....	7
1.5 Aims and objectives of this research .....	9
1.6 Structure of the Thesis .....	10
<b>Chapter 2: Literature Review .....</b>	<b>13</b>
2.1 Background.....	13
2.2 Overview of Small-Scale Wind Energy .....	16
2.2.1 What is a small-scale wind turbine? .....	16
2.2.2 Environmental Viability of Wind Energy .....	17
2.2.3 Environmental Reliability of Wind Energy .....	18
2.2.4 Variability of Wind Energy .....	20
2.2.5 Financial Viability .....	21
2.3 The Wind as an Energy Source .....	22
2.3.1 Theoretical power in the wind.....	23
2.3.2 Real power in the wind .....	23
2.4 Describing the wind resource .....	24
2.4.1 The Weibull distribution .....	25
2.4.2 Alternative methods to the Weibull distribution.....	29



2.5 Energy needs that could be met by small-scale wind turbines .....	31
2.5.2 Very small systems .....	31
2.5.3 Hybrid systems: .....	31
2.5.4 Wind-diesel systems:.....	31
2.5.5 Wind-pump systems: .....	32
2.6 Wind in the boundary layer .....	32
2.6.1 The atmospheric boundary layer .....	33
2.6.2 The inertial sublayer.....	33
2.6.3 Internal boundary layer over a sudden change of surface roughness.....	35
2.6.4 Wind flow over multiple internal boundary layers.....	37
2.6.5 Wind flow over complex orography .....	40
2.6.6 Summary of boundary layer approaches.....	42
2.7 Review of Vertical Axis Wind Turbines (VAWTs) .....	42
2.7.2 Darrieus VAWT .....	44
2.7.3 Advantages and disadvantages of VAWTs relative to HAWTs.....	46
2.7.4 Vertical axis wind turbine design parameters .....	48
2.8 Review of self-starting.....	55
2.8.2 Reynolds number effects .....	56
2.8.3. Savonius auxiliary rotor .....	57
2.8.4 Blade thickness.....	58
2.8.5 Cambered blades .....	59
2.8.6 Rotor solidity.....	63
2.8.7 Leading/Trailing Edge.....	66
2.8.8 Variable pitch .....	66
2.9 Review of mathematical models for performance prediction.....	73
2.9.1 Momentum Model.....	74
2.9.2 Vortex Model .....	77
2.9.3 Cascade Model .....	78
2.9.4 Summary.....	79
<b>Chapter 3: Methodologies for Wind Resource Assessment .....</b>	<b>81</b>
3.1 The Boundary Layer Methodology .....	81
3.1.1 Long-term reference climatology .....	82
3.1.2 Wind speed at a blending height.....	83
3.1.3 Wind speed at a propose turbine hub height .....	83

3.1.2 Limitations of the methodology .....	84
3.2 Hindcasting/Measure-Correlate-Predict (MCP) methodology .....	85
3.2.1 Determinants of the MCP methods .....	88
3.3 MCP models .....	91
3.3.1 Climatological reduction .....	92
3.3.2 Linear regression .....	92
3.3.3 Variance ratio (VR) method .....	93
3.3.4 Matrix method .....	94
3.3.5 Weibull parameter scaling .....	95
3.3.6 Alternative regression models .....	95
3.3.7 Artificial Neural Networks (ANNs) .....	96
3.4 Short-term measurement periods .....	97
3.5 MCP uncertainties .....	98
3.6 Summary of the methodologies for small-scale wind resource assessment .....	99

#### **Chapter 4: Performance Evaluation of the Boundary Layer Methodology to Wind Resource Assessment**

4.1 Overview .....	100
4.2 Methodology .....	101
4.2.1 Potential modification to the original methodology .....	101
4.2.2 Estimation of the local aerodynamic parameters .....	106
4.2.3 The Numerical Objective Analysis of the Boundary Layer (NOABL) – Microgeneration Certification Scheme (MCS) Method .....	108
4.2.4 Terrain classification .....	109
Beighton .....	110
Ilkeston .....	110
Bilsthorpe .....	110
Colby .....	111
4.2.5 Metrological measurements .....	111
4.2.6 Error Metrics .....	115
4.3 Results and discussions .....	116
4.3.1 Comparison of the observed wind speed with the predicted wind speed (data validation) .....	116
4.3.2 Wind speed probability distribution and direction analysis .....	121
4.3.3 Sensitivity to the Weibull shape parameter .....	124

4.3.4 Overall performance of the prediction methodology .....	128
4.4 Boundary layer prediction methodology as a site screening tool .....	129
4.5 Conclusions .....	133
<b>Chapter 5 Data Driven Measure-Correlate-Predict Approaches to Wind Resource Assessment .....</b>	<b>136</b>
5.1 Overview .....	136
5.2 Methodology .....	139
5.2.1 Evaluation of the MCP techniques .....	140
5.2.2 Choice of long-term data sites.....	140
5.2.3 Correlation of the target site (PACT, Beighton) wind speed to the MERRA reference (RF4) wind speed .....	143
5.2.4 Uncertainties associated with the different MCP methods .....	144
5.3 Results and discussion .....	146
5.3.1 Comparison of linear MCP approaches with measured wind speed data.....	146
5.3.2 Adjustment to the target site wind speed data.....	150
5.3.3 The added value of the Measure-Correlate-Predict (MCP) method.....	152
5.3.4 Overall error statistics .....	153
5.3.5 Seasonal characteristics and variations in the percentage error of the predicted wind resource .....	155
5.3.6 Seasonal variations in the mean bias error .....	157
5.3.7 Summary of seasonal effects .....	158
5.3.8 Comparison between boundary layer scaling model and data-driven MCP approach .....	159
5.4 Energy production estimates .....	160
5.5 Economic evaluation .....	162
5.6 Summary .....	164
<b>Chapter 6 The Design of a Small-Scale Wind Turbine .....</b>	<b>166</b>
6.1 Darrieus-type VAWT .....	166
6.2 Design requirements .....	167
6.3 Modelling approaches of the VAWTs self-starting .....	168
6.3.1 Viscous aerofoil data.....	168
6.4 Wind turbine simulations .....	173
6.4.1 The Double Multiple Streamtube Algorithm .....	173
6.4.2 Summary.....	179

## **Chapter 7: Evaluation of a Darrieus VAWT with self-starting capabilities**

7.1 Overview .....	182
7.2 Variables and equations governing the performance of a vertical axis wind turbine (VAWT) .....	183
7.3 Conceptual design .....	192
7.3.1 Design considerations .....	192
7.3.2 Design conditions .....	192
7.3.3 Aerofoil profile features.....	194
7.3.4 Design Philosophy.....	196
7.4 Evaluation of Aerofoils for self-starting.....	197
7.4.1 Comparison of XFOIL results with published experimental data .....	198
7.5 Results and discussion.....	200
7.5.1 Comparison of the performance of selected asymmetrical aerofoils .....	200
7.5.2 Stall characteristics .....	201
7.5.3 Drag polar .....	203
7.5.4 Lift-Drag Ratio .....	203
7.5.5 Pitching Moment.....	204
7.5.6 Drag Coefficient .....	205
7.5.7 Overall comparison of the aerofoil performance .....	206
7.6 Aerofoil design.....	209
7.6.1 Thickness.....	209
7.6.2 Fixed pitch .....	211
7.6.3 Solidity.....	213
7.6.4 Final design .....	217
7.7 Design proposal.....	218
7.7.1 Improved start-up performance.....	218
7.7.2 Maximum power performance.....	220
7.7.3 Comparison with NACA 0018 and the original DU-06-W-200.....	221
7.8 Summary .....	223

## **Chapter 8: Overall conclusions and suggestions for future research**

8.1 Research outcomes .....	227
8.1.1 Boundary layer model.....	227

8.1.2 MCP approaches.....	227
8.2 Design for self-starting improvement.....	228
8.2.1 Failure to achieve self-starting .....	228
8.2.2 Summary of ways to achieve self-starting.....	229
8.2.3 Design proposals for an efficient and economical self-starting of a small-scale VAWT .....	230
8.2.4 A cautionary note.....	231
8.3 Limitations and recommendations for further research opportunities.....	233
8.3.1 Boundary layer model.....	233
8.3.2 MCP approaches.....	234
8.3.3 Design for a self-starting vertical axis wind turbine.....	235
8.4 Research impacts .....	235
8.4.1 The big picture .....	237
Bibliography.....	<b>238</b>
<b>Appendix I .....</b>	<b>266</b>
<b>Appendix II: Photographs of the experimental set up .....</b>	<b>268</b>

## List of Figures

Figure 1.1: Regions of negative tangential force experienced by a NACA 0018 blade section at $\lambda=1.5$ under static condition (dynamic stall and wake effects are neglected).....	8
Figure 1.2: Hypothetical tangential force coefficient $C_Q$ Vs tip speed ratio $\lambda$ showing the presence of dead band.....	9
Figure 1.3: Problems encountered and possible solution methodologies proposed in this thesis.....	11
Figure 2.1: World wind turbine market breakdown for 2014.....	15
Figure 2.2: Cumulative breakdown of installed wind capacity at the end of 2014 (Euroobserver, 2015).....	15
Figure 2.3: Sketch of the development of an internal boundary layer from a smooth to rough transition. (Adapted from Rao et al. 1973).....	36
Figure 2.4: Sketch of internal boundary layers over terrain consisting of well-defined repeating patches.....	37
Figure 2.5: Wind flow over a hill with (a) moderate and (b) steep slope (Adapted from Taylor and Lee, 1984).....	41
Figure 2.6: Plan view of a VAWT showing the lift $L$ , drag $D$ , and angle of attack $\alpha$ , with freestream velocity $V_\infty$ (Adopted from Sharpe, 1990).....	43
Figure 2.7: Sketch of Savonius-type VAWT. (Adapted from Boss, 2012).....	44
Figure 2.8: Sketch of the curved-blade (or “egg-beater” type) Darrieus VAWT (Adapted from Bos, 2012).....	45
Figure 2.9: The effect of the laminar separation bubble on the hysteresis behaviour of different aerofoils (adapted from Selig et al., 1995).....	53
Figure 2.10: (a) Lift, and (b) drag coefficients of NACA 0012 as a function of the angles of attack (Adapted from Sheldahl and Klimas, 1981).....	54
Figure 2.11: Lift and drag coefficients as a function of the angle of attack of two DU aerofoil sections (reproduced from Timmer, 2001).....	55
Figure 2.12: Schematic of a Darrieus-Savonius wind turbine where the two rotors have a phase difference of $\Delta\theta_2$ (reproduced from Bos, 2012).....	58
Figure 2.13: Schematic of the Darrieus cam driven design (Darrieus, 1931).....	68

Figure 2.14: A schematic of the design patented by Sicard (1977).....	69
Figure 2.15: Schematics of the elastic (left) and inertial design patents (Reproduced from Brenneman, 1983).....	70
Figure 2.16: Schematic of the Liljegren passive variable pitch design (reproduced from Liljegren, 1984).....	71
Figure 2.17: Schematic of the Sharp's design (reproduced from Sharp, 1982).....	72
Figure 2.18: Schematic of the Kirke-Lazauskas initial design (Adapted from Kirke, 1998).....	74
Figure 2.19: Schematic of Templin's single streamtube model (Adapted from Danao, 2012).....	75
Figure 2.20: Schematic of Strickland's streamtube model (Adapted from Danao, 2012).....	77
Figure 2.21: Schematic of the DMST model showing the induced velocities.....	78
Figure 2.22: Schematic representation of a simple vortex model for a single blade element (reproduced from Islam et al. 2008).....	79
Figure 3.1: Schematic diagram of the Measure-Correlate-Predict process (Adapted from Jane, 2011).....	88
Figure 4.1: An illustration of the methodology used by the Met Office to predict the spatially averaged mean wind speed.....	103
Figure 4.2: Modified methodology based on the boundary layer model.....	105
Figure 4.3: An approximate geographical location map of the study sites (Google Earth, 2015).....	112
Figure 4.4 (a-d) shows the average wind speeds variations, hour by hour and month by month, at a height 10 m for a 12 months period.....	116
Figure 4.5: Comparison of predicted wind speed (red coloured symbol) versus observed wind speed (MERRA database).....	119
Figure 4.6: Predicted annual mean wind speed at all sites using Model A compared with a benchmark predication obtained directly from the NOABL-MCS database at a hub height of 10 m.....	120
Figure 4.7: Distribution of the residual errors in the mean wind speed for different implementations of the prediction methodology.....	122

Figure 4.8: Weibull probability distribution function calculated using the maximum likelihood method and histogram of the actual wind speed data (green bars) for the 4 investigated sites.....	123
Figure 4.9: Wind rose plots showing the prevailing wind directions at the investigate sites.....	124
Figure 4.10: Predicted wind power density as a function of the shape parameter for the 4 investigated sites.....	126
Figure 4.11: Error metrics using the coefficient of correlation ( $R^2$ ) to compare how the observed Weibull shape parameter fits the predicted wind power density.....	126
Figure 4.12: Comparison of the observed and predicted wind power density at all 4 sites. The solid line represents a one-to-one relationship.....	127
Figure 5.1: A workflow diagram illustrating the process involved in the long-term correction of onsite wind measurements.....	136
Figure 5.2: Long and short term mean wind speeds for the MERRA reference (RF4) dataset.....	143
Figure 5.3: Illustration of the method used to test the prediction capacity of the different MCP approaches.....	145
Figure 5.4 Target and reference site wind speeds for a single directional sector (135°- 165°) from the reference/target site pair.....	147
Figure 5.5: Comparison of the measured and the predicted wind speed using linear regression (LR) and Variance ratio MCP approaches.....	151
Figure 5.6: Measured and predicted wind frequency roses at 10m.....	151
Figure 5.7: Mean absolute prediction error as a function of the measurement period length based on the linear regression (LR) and variance ratio (VR) MCP approaches.....	154
Figure 5.8: Residual percentage error distribution at the target (measurement) site: (a) predicted mean wind speed, and (b) predicted wind power density.....	156
Figure 5.9: Variation of the %error in the predicted wind speed and power density as a function of the seasons. ....	159
Figure 5.10: Seasonal variation of the mean bias error in the predicted wind speed using two MCP approaches at the target site. The vertical lines	



represent the seasons of autumn (Sept-Nov), winter (Dec-Feb), spring (Mar-May) and summer (June-Aug).....	160
Figure 5.11: Output of individual wind turbines, (a) annual energy production, and (b) the corresponding capacity factors at the PACT measurement site Beighton.....	163
Figure 5.12: Cost of electricity as a function of the wind turbines at the target site.....	166
Figure 6.1: Comparison of NACA 4418 aerofoil characteristics with wind tunnel experiments at a Reynolds number, $Re = 3000000$ .....	173
Figure 6.2: Comparison of NACA 64-218 aerofoil characteristics with wind tunnel experiment at a Reynolds number, $Re = 3000000$ .....	173
Figure 6.3: Performance prediction of a NACA 0018 profile at 0.070% and 0.046% turbulence levels.....	175
Figure 6.4: Illustration of the Doubles Multiple Streamtube Model with actuator discs and velocity vectors at the upstream, equilibrium and downstream cycles of the actuator disc (Adapted from Newman, 1983; Paraschavoui, 1981).....	177
Figure 6.5: (a) Plan view of the DMST showing velocity triangle to determine the relative velocity. (b) A single blade illustrating the concept of pitching.....	178
Figure 6.6: Simulation sequence and data flow.....	183
Figure 7.1 Schematic of a blade element showing the components of the lift and drag coefficients contributing to the tangential force coefficient.....	188
Figure 7.2: Tangential force coefficient as a function of the angle of attack for a single NACA 0018 aerofoil at rest ( $\lambda=0$ ) based on a simple model of Eqn. (7.1) and experimental data from Sheldahl and Klimas (1981).....	189
Figure 7.3: Angle of attack variation as a function the azimuthal position and tip speed ratio experienced by a blade under static conditions.....	191
Figure 7.4: Torque, $T$ as a function of azimuthal positions and tip speed ratio for NACA 0018 section blades at $Re = 80,000$ .....	192
Figure 7.5: (a) Power coefficient, (b) Torque coefficient as a function of tip speed ratios for NACA 0018 section blades at a wind speed of 5 m/s.....	193

Figure 7.6: The predicted lift and drag coefficient as a function of angle of attack at several Reynolds number for the NACA 0018 aerofoil.....	194
Figure 7.7: Predicted performance of a small-scale VAWT utilising the NACA 0018 blade showing the operating conditions during start-up.....	196
Figure 7.8: Performance comparison of the NACA 0018 aerofoil with the available experimental data: (a) Lift as a function of the angle of attack, (b) Drag as a functions of the angle of attack.....	202
Figure 7.9: Tangential force coefficient $C_t$ as a function of the blade azimuthal position $\theta$ for the investigated aerofoils at $Re=383,200$ , $N_{crit} = 9$ .....	204
Figure 7.10: Lift coefficient $C_l$ as a function of the angle of attack for the prospective aerofoils at $Re=383,200$ , $N_{crit} = 9$ .....	205
Figure 7.11: Lift coefficient $C_l$ as a function of the drag coefficient for the prospective aerofoils at $Re=383,200$ , $N_{crit} = 9$ .....	206
Figure 7.12: Comparison of the lift-drag ratio of the prospective aerofoils in comparison with the NACA 0018 at different angles of attack at $Re = 383,200$ , $N_{crit} = 9$ .....	207
Figure 7.13: Comparison of the aerofoil pitching moment coefficient as a function of the angle of attack of the prospective aerofoils at $Re = 383,200$ , $N_{crit} = 9$ .....	208
Figure 7.14: Comparison of drag coefficients as a function of the lift coefficients of the prospective aerofoils at $Re = 383,200$ , $N_{crit} = 9$ .....	209
Figure 7.15: Torque output as a function of blade azimuthal position for the prospective aerofoils at a wind speed 5 m/s, rotational speed 18.5 rpm.....	211
Figure 7.16: (a) Lift coefficient as a function of drag coefficients, and (b) lift coefficients as a function of the angles of attack showing the several variations in the thickness of the original DU-06-W-200 at $Re = 383,200$ .....	212
Figure 7.17: Power coefficient as a function of tip speed ratios for DU-06-W-200 profiles with different thicknesses and $Re = 383, 200$ .....	213

Figure 7.18: Schematic of an aerofoil section set under a fixed pitched angle.....	214
Figure 7.19: Predicted power coefficient as a function of the tip speed ratios for the DU-06-200 (19% chord) aerofoil as a function of the pitch angles and wind speed 5 m/s.....	215
Figure 7.20: (a) Torque as a function of the blade azimuthal position for a three bladed DU-06-W-200 (19% c) for wind speeds 5 m/s, 7 m/s, 9 m/s at a pre-set pitch angle $\gamma = 4^\circ$ and Reynolds number 383,200; (b) Torque coefficient as a function of the tip speed ratio for various pitch angles at the same operating conditions.....	216
Figure 7.21: Predicted power coefficient for the DU-06-W-200 as a function of the pitch angle $\gamma = 4^\circ$ for different solidities.....	217
Figure 7.22: Predicted power as a function of the rotor rotational speed with respect to wind speed and pitch angle $\gamma = 4^\circ$ ; (a) chord length $c = 0.03\text{m}$ ( $\sigma = 0.1$ ), (b) $c = 0.06\text{m}$ ( $\sigma = 0.2$ ) and $c = 0.1\text{m}$ ( $\sigma = 0.3$ ).....	218
Figure 7.23: Predicted maximum power as a function of both wind speed and rotor solidity.....	219
Figure 7.24: Power coefficient as a function of both rotor rotational speed and wind speed, (a) chord length $c = 0.03\text{m}$ ( $\sigma = 0.1$ ), (b) $c = 0.06\text{m}$ ( $\sigma = 0.2$ ) and $c = 0.1\text{m}$ ( $\sigma = 0.3$ ).....	219
Figure 7.25: Schematic of the investigated aerofoils. (a) Final shape of the transformed aerofoil section. (b) The original and the transformed profiles.....	220
Figure 7.26: The torque as a function of the rotational speed for the fixed of NACA 0018, and the pre-set pitched-blade for the DU-06-W-200 rotors.....	222
Figure 7.27: Predicted performance of start-up and maximum power configuration at a cut in wind speed of 5 m/s.....	222
Figure 7.28: Predicted power as a function of the wind speed and the rotor solidity for start-up ( $c = 0.03\text{m}$ , $\sigma = 0.1$ ), and maximum power configurations ( $c = 0.06\text{m}$ , $\sigma = 0.2$ ).....	223
Figure 7.29: Power coefficient as a function of the tip speed ratio for the hypothetical three bladed rotor with chord length $c = 0.03$ , $R = 1$ and	

wind speed = 5 m/s using either the DU-06-W-200, the present design  
(transformed DU-06-W-200) or the NACA 0018 aerofoil.....227

## List of Tables

Table 2.1: Classification of micro-medium wind turbines (Renewable UK, 2013).....	16
Table 4.1: Local terrain classification and associated mean height of the roughness elements $h_m$ , and frontal area density $\lambda_f$ . (Reproduced from Grimmond and Oke, 1999).....	107
Table 4.2: Comparison of the predicted absolute winds speed using Model A with MERRA wind speed.....	117
Table 4.3: Error metrics associated with the predicted wind speed compared over four target sites using Model A.....	120
Table 4.4: Predicted wind power density with associated errors across all the 4 sites investigated at a hub height of 10 m.....	128
Table 4.5: Summary of the sites used to compare predicted and measured wind power density. The sites are defined by the letter in the parenthesis as <u>R</u> ural, <u>U</u> rban and <u>S</u> ub- <u>U</u> rban.....	131
Table 4.6: Comparison of observed and predicted viability for the 10 sites based on a criterion of $\bar{p}_d \geq 47 W/m^2$ . Tick depict viable sites, and crosses depict non- viable sites. Correct prediction are highlighted in green, and incorrect predictions are red.....	132
Table 5.1: The PACT low carbon combustion centre, Beighton is at position (N53.60°, W2.18°). Column 3-6 show the locations of the reference sites in which long- term data are available.....	142
Table 5.2: MERRA reference (RF4) long-term wind data at 10 m (Jan 1, 2015- Dec 31, 2015).....	143
Table 5.3: Coefficient of correlations for the PACT (target) and Reference sites.....	144
Table 5.4: Correlation between the target site (PACT, Beighton) and the MERRA reference site (RF4).....	149
Table 5.5: Correlation between the target site (PACT, Beighton) and the MERRA reference site (RF4).....	149
Table 5.6: Comparison of short-term to long-term predicted wind speed at the target site at six heights commonly used for small scale-wind energy installation. LR and VR represents linear regression and variance ratio, respectively.....	152

Table 5.7: Direct comparison of the error metrics at the target predicted using linear regression (LR), variance ratio (VR) MCP approaches and the boundary layer (BL) model discussed in Chapter 4.....	154
Table 5.8: Specifications of the analysed wind turbines, including the output mean hub height wind speed (AWE, 2013; ECI, 2013; BWPC, 2013; EWPC, 2013).....	161
Table 6.1: Typical turbulence values of $N_{crit}$ for various scenarios as listed in the XFOIL user manual (Drela, 1995).....	172
Table 7.1: Selected prospective aerofoils based on the availability of experimental data.....	199
Table 7.2: Ratings of the investigated airfoils based on the desirable aerodynamic characteristics.....	208
Table 7.3: Characteristics for improved start-up and maximum power configuration.....	222

## Glossary of terms

### List of Symbols:

$a_d$	Downstream interference factor
$A_r$	Blade aspect ratio
$a_v-C_{qd}$	Average torque coefficient
$a_v-T$	Total average torque
$a_v-T_w$	Average downstream torque
$a_v-C_{qu}$	Average power coefficient
$c$	Chord length
$C_d$	Drag coefficient
$C_l$	Lift coefficient
$C_m$	Moment coefficient
$C_n$	Normal coefficient
$C_t$	Tangential coefficient
$C_p$	Power coefficient
$C_Q$	Torque coefficient
$C_{pu}$	Upstream power coefficient
$C_{pd}$	Downstream power coefficient
$C_{qav}$	Average torque coefficient
$D$	Rotor diameter
$\varepsilon$	Residual error
$\varepsilon\%$	Residual percentage error
$F_d$	Drag force
$F_l$	Lift force
$f(u)$	Probability distribution function
$F_{up}$	Upwind flow condition
$\Gamma$	Gamma function
$N$	Number of blades
$P_w$	Power from the wind
$P_R$	Actual Power captured by the Turbine
$P_d$	Wind power density
$\bar{P}_d$	Mean wind power density

$k$	Weibull shape factor
$k_{ass}$	Assumed shape factor
$k_{obs}$	Observed Weibull shape factor
$\kappa$	Von Karman constant
$Q$	Torque Produced by the Blade
$R_e$	Reynolds number
$\rho$	Air density
$\theta$	Blade azimuthal angle
$S$	Rotor swept area
$V$	Wind speed
$\overline{V^3}$	Mean of the cubed wind speed
$\bar{V}$	Mean wind speed
$V_e$	Induced velocity at equilibrium plane
$V_\infty$	Free stream velocity
$V_{ref}$	Observed reference site wind speed
$\bar{V}_{ref}$	Observed reference site mean wind speed
$V_{tar}$	Observed target site wind speed
$\bar{V}_{tar}$	Observed target site mean wind speed
$\hat{V}_{tar}$	Observed target site mean wind speed
$V_u$	Upstream induced velocity
$V_d$	Downstream induced velocity
$\alpha$	Angle of attack
$\gamma$	Blade pitch angle
$\lambda$	Tip speed ratio
$\omega$	Rotor angular velocity
$\sigma$	Turbine solidity
$W$	Relative Velocity of Wind with respect to Blade
$Z_0$	Roughness length
$Z_{0, eff}$	Effective roughness length



**Abbreviations:**

BEM	Blade Element Momentum
DMST	Double Multiple Stream Tube
%Error	Absolute percentage error
FiT	Feed in Tariff
HAWT	Horizontal Axis Wind Turbine
IBL	International boundary layer
ISL	Inertia sublayer
LR	Linear regression
MAE	Mean absolute error
MBE	Mean bias error
MCS	Microgeneration Certification Scheme
MCP	Measure-correlate-predict
MERRA	Modern Era Retrospective Analysis for Research and Applications
MTOE	Million Tonnes of Oil Equivalent
NACA	National Advisory Committee for Aeronautics
NOABL	Numerical Objective Analysis of Boundary Layer
PBL	Planetary boundary layer
RMSE	Root mean square error
SWT	Small Wind Turbines
TSR	Tip Speed Ratio
VAWT	Vertical Axis Wind Turbine
VR	Variance ratio

## Chapter 1: Introduction

### 1.1 Energy and Sustainability

Energy is the mainstream of modern society, enabling everything from heating, lighting, computers and agricultural production through to manufacturing, medicine, and transportation. Future energy projections indicate that the Total Primary Energy Supply (TPES) should be increased to 16, 3000 MTOE by 2030 (IEA, 2003). Thus, energy supply is critically a basic requirement for the development and sustenance of the global economies and societies. At present, among the main energy utilised by mankind is electricity. The World's electricity production is projected to increase due to the improvement in the living standards of mankind along with industrial and economic developments around the World. Currently, about 78% of the world total energy consumption is produced by burning fossil fuels- coal, oil and natural gas (IEA, 2016). Although, these generation technologies are affordable and reliable and have been used increasingly for many decades in powering the World economies, they are finite resources which are non-renewables and unsustainable. The proven fossil fuel reserves- oil, coal and natural gas are currently estimated at 1.3 trillion barrels, 909,064 billion tonnes and 204.7 trillion cubic meters, respectively (IEA, 2016) in the world's major fields, which at present rates of consumption will be sufficient to last for about 40 years (Sharma et al., 2012). Although, new discoveries of these resources could be made, the rate of discovery has been declining in recent years. Furthermore, the environmental catastrophes of fossil fuel consumption add another dimension to this problem. Fossil fuels emit greenhouse gases (GHG) and particulates to the environment which contributes to climate change, intensive rainfalls, floods and droughts (IPPC, 2007; Solomon et al., 2007). Consequently, many countries and governments are advocating for sustainable energy systems that are both renewable and environmental friendly such as wind, solar, biofuel, geothermal, biomass, etc. The contribution of renewable energy technologies has been increasing in recent years, for example in 2012 the World relied on renewable energy sources for around 13.2% of its primary energy supply (IEA, 2013). In 2013 renewable energy accounted for almost 22% of the global electricity generation and

future projections foresee renewable share reaching at least 26% in 2020 (IEA, 2016). Renewable energy utilisation has some disadvantages as well, such as high cost and controllability (Jane, 2011). Some renewable energy systems are currently more expensive than the conventional energy sources and thus require some sort of government subsidy to make it economically viable to be exploited. They are also less controllable than fossil based technologies since the primary energy source cannot be controlled. The only exception to these limitations are geothermal, hydro and biomass. Therefore, the realisation of a low carbon economy through renewable energy technologies is technically and economically challenging.

In the UK, the main source of electricity generation is from fossil fuels which account for about 27% of the total emissions (HM Government, 2011). Furthermore, the UK coal generation is heading to extinction as the government plans to decommission the ageing power stations (DECC, 2012). In addition, the government plan of diversification into other sources of energy (HM Government, 2011), the 2020 target of 15% of primary energy use from renewables (EC, 2009) and the 2050 commitment to reduce the amount of carbon emissions (CO<sub>2</sub>) by 80% compared to the 1990 levels present enormous challenges to the UK's energy industries. Overcoming these head-on challenges requires the deployment of different "large-scale" renewable energy technologies in the coming years to decarbonise the power sector (HM Government, 2011).

Among the several renewable energy sources, wind energy has been recognised as one of the most significant and attractive renewable energy sources due to its availability and prospects in climate change mitigation as well as the opportunity to stabilise energy security (Mustafaeipour, 2010; Akpınar, 2013).

In addition to these energy technologies, distributed energy sources such as the small-scale wind energy must also be fully exploited in order to increase access to cheap and sustainable energy systems (DECC, 2011). The small-scale wind energy is often considered as one of the microgeneration technologies that can potentially provide clean energy sources for houses and buildings. The industry is rapidly growing, with a total generating capacity of over 102 MW at the end of 2012 (Renewable UK, 2013). However, in order to

make the small-scale wind turbine industry a huge success, several engineering challenges need to be overcome.

Two of the most important of these challenges are the “accurate” assessment of the wind resource and the “installation of matching” wind energy conversion systems (wind turbines). An estimate of the wind energy potential is essential because it is the basis for determining the initial feasibility of any wind energy project and is ultimately vital for acquiring financing. However, predicting the wind resource for potential wind turbine installation presents a number of challenges and constraints such as accuracy, costs and timescales (WWEA, 2013) as stated below.

## **1.2 Challenges and constraints of Wind Resource Assessment**

A wind resource assessment, like other technical projects, requires careful planning and considerations that are guided by a clear set of objectives. It is often complicated by several factors, namely: the cubic relationship between the wind speed and power, the variability of wind speed at different times and seasons as well as the spatial variability in the mean speed. A small change in the wind speed often results in a large change in the wind power because of the cubic relationship between the wind speed and the power, which necessitates a highly accurate wind speed prediction. In addition, due to the temporal and spatial variability in the wind flows, long-term measurements at the planned project sites are generally required to reflect the true wind characteristics. The long-term measurements are utilised to produce the wind characteristics in the form of frequency distribution over a certain period of time, from which, long-term statistical averages of the studied site can be realised. These statistical representations of the wind speed, along with other estimates of the atmospheric variables, are used to characterise the resource potential of any specific site. The resource information, along with a specific wind turbine power curve, can be utilised to predict the average wind energy yield for a specific wind turbine and location. Supposing the performance of the wind turbine has been well characterised, the subject of wind resource assessment ultimately becomes one of the most important statistical averages which describe the wind flow pattern at a specific location or site.

The most reliable way to estimate the potential wind resource is to carry an out onsite long-term measurement campaign. For a large-scale wind project, long-term measurements over a period of about 2-3 years is required in order to obtain the adequate statistical information that represents the location wind pattern (Jain, 2011). However, for a small-scale wind energy project, long-term measurements are not often realisable due to the huge investment cost and time associated with such a method (Jain, 2011). Consequently, potential customers must adopt an alternative method of estimating the wind resource. These methods should be cost effective and quick to implement, applicable to different kinds of sites, and should be reasonably accurate enough to reduce the degree of uncertainty and high project risks.

### **1.2.1 Wind Atlas Methodology**

The wind atlas method is a traditional wind resource assessment technique which can be used to quickly determine the mean wind speed at any specific location. In the UK, two main wind atlases, namely the Numerical Objective Analysis of Boundary Layer (NOABL) and the National Climate Information Centre (NCIC) are widely used in the wind industry (Weekes and Tomlin, 2013). The NOABL database comprises long term data sets of annual wind speed estimates for every 1 km grid square of the UK (Carbon Trust, 2008), at the heights 10 m, 25 m and 45 m, above the ground. The NOABL has been used increasingly over the years because it is freely available to the general public. However, these two databases have some issues in common. Firstly, while organography is taken into account in the development of the databases, they do not account for local variations in the roughness and ground effects. This implies that the models give a limited representation of the local topographical features which may have a significant impact on the predicted wind resource. Previous studies using the NOABL revealed an overestimation of the wind speeds, particularly for areas with a high surface roughness (Energy Saving Trust, 2009), and so various adjustment are required to account for these factors (Carbon Trust, 2008). As will be shown in Chapter 3 these correction factors presents a number of uncertainty in the predicted wind resource.

### **1.2.2 NOABL-Microgeneration Certification Scheme (MCS) method**

A new financial incentive and an increasing interest in self-generation of renewable energy is creating a potentially lucrative UK market for small-scale wind energy conversion system. However, to qualify for this incentive, the installation system products must be certified against some robust industry standards in the Microgeneration Certification Scheme that include MCS 010, MCS 011 and MCS 006 (Renewable UK, 2010). These standards set out a method for applying a correction factors to the NOABL database where there are obstructions close to the proposed site (Renewable UK, 2010). While this method may offer an improvement in the prediction of the wind resource, the approach as will be shown in Chapter 4 has some limitations which could potentially exclude some suitable sites from development.

### **1.2.3 Boundary Layer Methodology**

The principles of the boundary layer meteorology can be used to provide a more reliable estimate of the mean wind speed compared to those obtained from the methods described above. This method uses wind atlas as input and takes into account the local and regional roughness to reduce the margin of uncertainty in the predicted wind speed (Best et al., 2008, Weekes, 2014). The boundary layer approaches are promising since they can be utilised to assess the wind resource potentials at several sites without huge financial investment. However, there are a number of limitations which could potentially affect the overall accuracy of the predicted wind speed and power density (Weekes, 2012). While this technique can result in general siting recommendations to investors, they require site specific modelling which negates some of the benefits of a simple scaling method. Further, since they use wind atlas as input into the model, they tend to predict an estimate of the mean wind speed rather than the full wind speed distribution and this could potentially results in higher uncertainties in the predicted wind power.

### **1.2.4 Hindcasting/Measure-Correlate-Predict methods**

Hindcasting methodology involves the process of generating the wind resource that predicts 10 or more years of wind data. It is a data-driven approach that uses onsite wind measurement for few a years and then these

measurements are correlated to reflect the long-term climatology of the site of interest (Jain, 2011). It should be noted that while the MCP technique has the potential of predicting the long-term wind resource using short-term measurement periods, it has not been widely investigated in the context of small-scale wind industry where measurement periods are significantly lower than 2-3 years. A similar technique to MCP approach may use forecast wind data as the target data in place of onsite measurements.

### **1.3 The reason for this research**

Firstly, as discussed in Section 1.1, wind resource assessment for small-scale wind energy project is constrained with a number of challenges such as timescales and costs as well as the availability of modern tools and instrumentations. These challenges have contributed to the lack of adequate site specific wind resource data and information. Ultimately, this has contributed to the installation of wind turbines at some sites that are not economically viable (Energy Saving Trust, 2009).

The need for accurate wind resource assessment has been examined by several studies, for example the Warwick Wind Trials (Encraft, 2009) investigated the prospects of building mounted small-wind turbines across different locations in the UK. The study revealed the potential of using simple numerical method such as the NOABL in predicting the wind resource in a complex environment. In addition, the studies highlighted the challenges in predicting the wind resource using this method and the importance of choosing a viable location for potential wind turbine installations. Another large field trial of building mounted small wind turbines was performed across different sites in the UK by the energy saving trust (Energy Saving Trust, 2009). The field test revealed the underperformance of many wind turbines and the significance of installing these turbines at viable locations (Energy Saving Trust, 2009; James et al., 2010; Sissons et al., 2011).

Ideally, due to the significance of year-to-year variations in the wind speeds, the small-scale wind industry should aim to adopt the rigorous process of large-scale wind industry in assessing a potential wind turbine site. However, to achieve this aim, high quality instrumentations and equipment's are required. Such instrumentations should be able to function efficiently at

different locations and sites without the need for rigorous site-specific modelling. While this may appear to be a difficult task, it must be emphasised that the development of a small-scale wind resource assessment methodology does not translate to the same accuracy standard of the industrial wind resource approaches. However, the methodologies for a small-scale wind resource assessment should be reasonably cost effective and accurate enough to determine the associated uncertainties and inform investment decisions.

Secondly, the need for the provision of sustainable energy supplies is vitally important to all mankind. At the most basic level of human development, people need food, medicine, water, clothing and shelter over their heads. In most environment today, energy is required in the provision of these fundamental needs. Our modern society has relied heavily on the conventional energy sources (fossil fuels) to supply the bulk of this energy, but the increasing concern of hazardous greenhouse emissions along with the dwindling reserves of fossil fuels sources, the need for an environmentally friendly renewable energy sources become paramount. It is argued in this thesis that the small-scale wind turbine technology could play a significant role in the provision of sustainable energy systems. In particular, the vertical axis wind turbine with the Darrieus-type are examined and their potential in electricity generation for standalone or decentralised application is assessed. Furthermore, avenues to improve the performance of this concept of turbine, particularly self-starting are reviewed and evaluated.

#### **1.4 Vertical axis wind turbine (VAWTs): the need to self-start**

The vertical axis wind turbines (VAWTs) have numerous advantages over the horizontal axis wind turbine (HAWTs). The relative merits of these turbines are discussed in **Chapter 2**. The modern VAWTs are subdivided into two forms, namely Savonius VAWT and the Darrieus VAWTs, the later having either curved or straight blades.



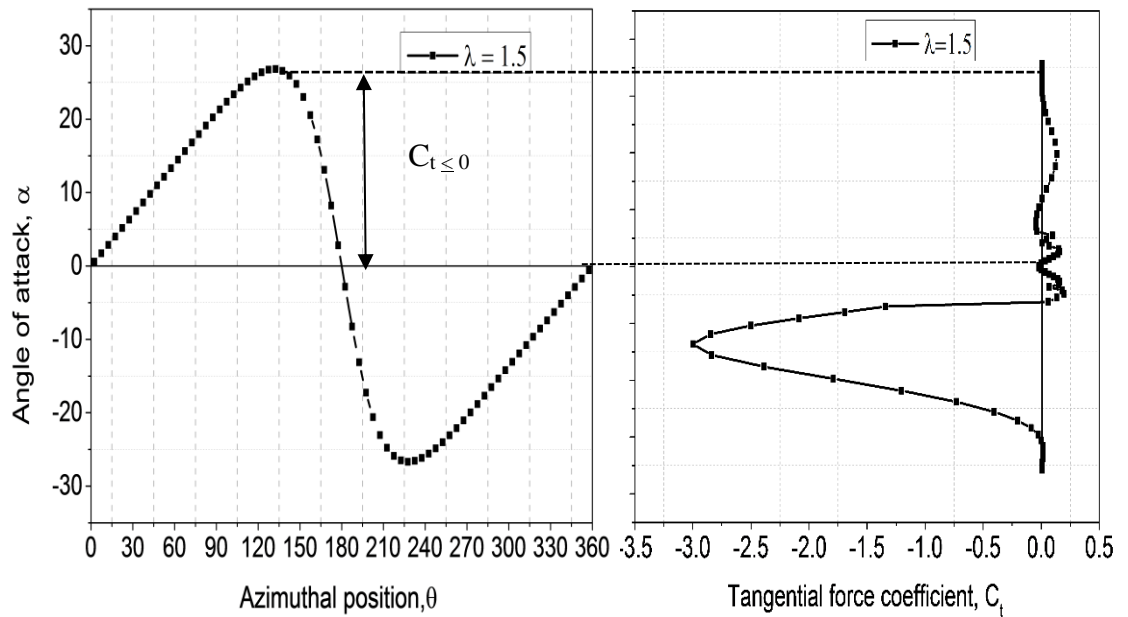


Figure 1.1: Regions of negative tangential force experienced by a NACA 0018 blade section at  $\lambda=1.5$  under static condition (dynamic stall and wake effects are neglected).

The Darrieus type VAWTs are potentially far more efficient and economical than the Savonius type but suffer from one major weakness. They do not self-start at low tip speed ratios  $\lambda$  due to the cyclical variation in the blade angles of attack  $\alpha$ , so that the blades are frequently stalled and generate low or negative torque for most azimuthal positions  $\theta$ . As a result of this variation and other operating conditions, most fixed-pitch Darrieus VAWTs do not self-start without an external mechanism to bring the turbine to an operating speed. This phenomenon can be visualised in Figure 1.1 by comparing the angles of attack variation with the tangential force  $C_t(\alpha)$  plot. At a tip speed ratio  $\lambda=1.5$ , the blades enter into a region of negative torque often referred to as the dead-band (Baker, 1983) in the literature. This is again reflected by a dip region in the torque curve of the rotor shown in Figure 1.2. It is only at higher tip speed ratios  $\lambda$  about 3 and above that the blades remain unstalled and the turbine can achieve high efficiency.

The severity of this dead-band depends on the design of the turbine including the aerofoil section used as well as other factors, namely the drive train friction and parasitic drag. Therefore, one of the objective of this thesis is to

investigate the methods of increasing the torque produced by the Darrieus VAWT at low tip speed ratios so that they may be able to reliably self-start.

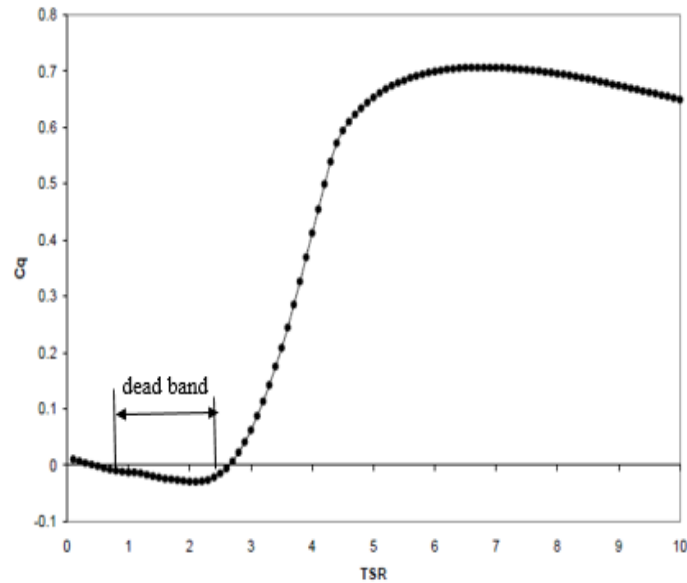


Figure 1.2: Hypothetical torque coefficient  $C_Q$  as a function of the tip speed ratio  $\lambda$  showing the presence of a dead band.

### 1.5 Aims and objectives of this research

Accurate wind resource assessment is the linchpin of energy production simulations. Only direct measurement from within the project site captured with high level of confidence reflects the true wind conditions that determines the energy production potential. Without them, it is rare that wind energy investors or financial institutions will risk money on building a wind project or turbine of a significant size.

Therefore, the main aim of this thesis is to accurately assess the wind resource at potential sites for the installation of a small wind turbine that is capable of self-starting without the aid of an external mechanism. This aim is vigorously pursued through two main approaches, namely: (i) development of a low cost design methodology to assess potential small-scale wind turbine sites and accurately predict the wind resource, and (ii) development of a Measure-Correlate-Predict (MCP) technique to predict the long-term wind conditions at a potential small-scale wind turbine site. It is believed that these approaches will offer flexibility to the wind resource assessment since it is tailored to the specific requirement of the project including the available time.

Specifically, the objectives of the thesis are as follows:

- (i) To accurately assess the wind energy potential and economic analyses for small-scale wind power generation at some locations in the UK.
- (ii) To determine the correlation between the measured wind speed at the target site and some reference data.
- (iii) Using the results from objectives (i) to (ii), perform an aerodynamic design of a small-scale vertical axis wind turbine based on the wind resource conditions of the site.
- (iv) Investigate the avenues to improve the self-starting performance of the turbine.

The research objectives and the problems encountered, along with their possible solution methodologies, are summarised in Figure 1.3.

## **1.6 Structure of the Thesis**

This thesis is divided into eight chapters, following a natural progression from problem definition to solution. Chapter 2 outlines the relevant literatures in utilising wind energy and begins with the background of wind power development. Next, an overview of wind energy is presented, including an explanation on the causes and variability of wind. Further, a brief review on the cost of wind energy is given, followed by the environmental impacts and reliability of wind energy. Next, a technical background, including the types of wind turbines, and the theoretical and real power in the wind are discussed. The wind resource and applications of wind energy systems are also discussed. The chapter culminates with the fundamental performance basics of wind turbine operations.

In Chapter 3, analytical methods for wind resource assessment are presented. A detailed review for each of the approaches employed in the subsequent chapters is presented.

Chapter 4 presents an evaluation of the onsite measurement approach to wind resource assessment. The performance of this methodology is evaluated quantitatively using observed wind data at four different sites. Based on this methodology, comparisons are made based on the economic evaluations and

energy estimations from each site. Some possible errors are predicted and discussed for future improvements.

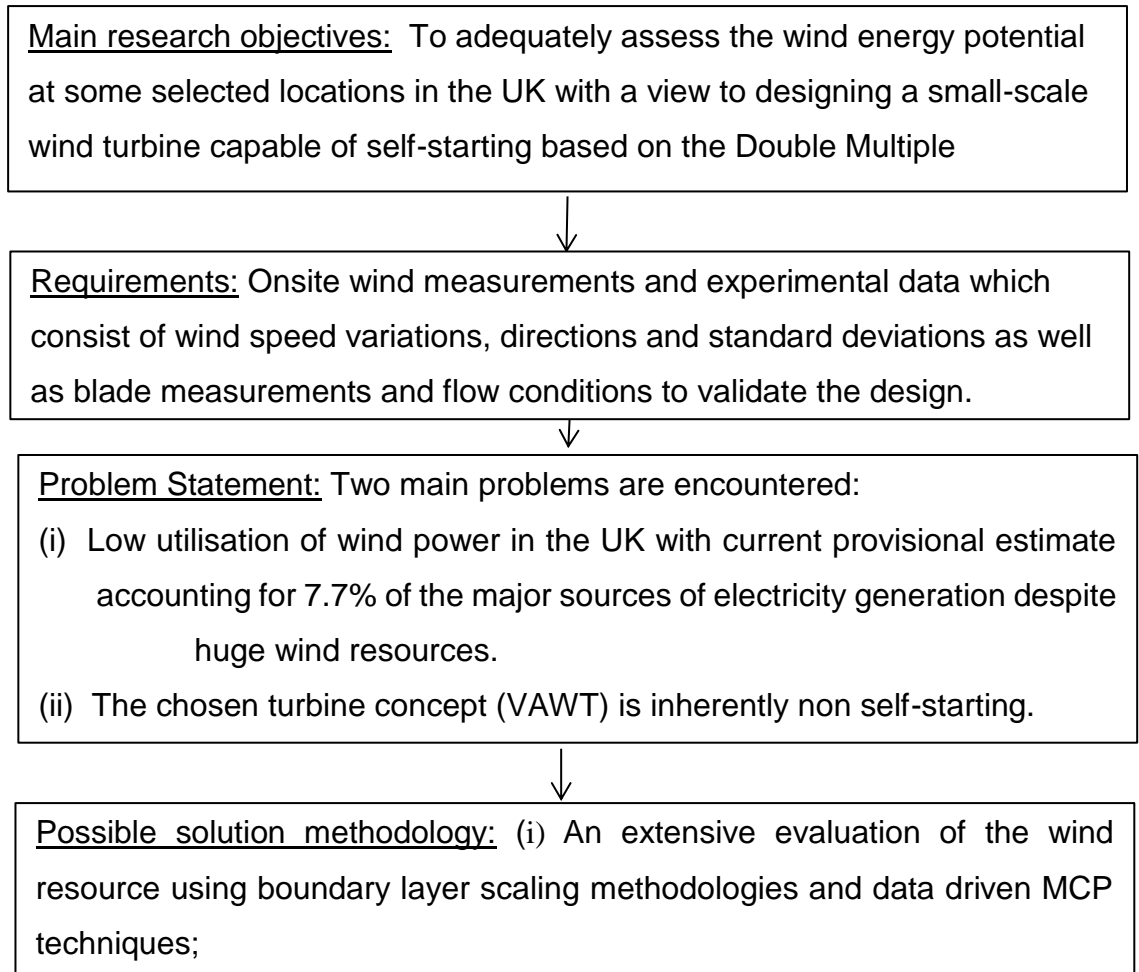


Figure 1.3: Problems encountered and possible solution methodologies proposed in this thesis.

Chapter 5 extends the work of Chapter 4 through the prediction of the long term energy yield using a data driven approach, namely Measure-Correlate-Predict (MCP). The MCP approach developed in this chapter is used to compare the performance of the long-term prediction with meteorological measurements at a target site. Using the output and climatological information from the wind resource assessment as a guide, Chapters 6 and 7 explore the fundamentals of designing a small-scale vertical axis wind turbine with straight blades. The design parameters, including the aerodynamic characteristics of the turbine, are discussed with reference to the simulation of rotors of VAWTs. A set of parametric studies of the designed rotor is then presented and discussed. The power coefficients, aerodynamic power on the blade are the

primary focus. Further, avenues for performance improvement of the designed turbine are presented. Firstly, the problems that affect the performance of the turbine concept, particularly its ability to reliably self-start, is considered. Evaluation of aerofoil profile as an avenue to improve the self-starting characteristics is investigated in detail. The performance of the aerofoil is compared with traditional NACA symmetrical aerofoil in order to assess their self-starting performance.

Chapter 8 highlights the main outcomes of the thesis, covering both the theoretical contributions to the small-scale wind resource assessment as well as wind turbines aerodynamics. The thesis concludes with suggestions for future work.

## **Chapter 2: Literature Review**

This chapter presents a state of the art literature review on small-scale wind energy. The chapter is structured as follows: Section 2.1 gives a background on the use of wind energy for various applications, including power generation, the current market trends and future prospect of harnessing energy from the wind. Section 2.2 presents an overview of small-scale wind energy, including the definition of the term “small-scale”. In addition, a review of environmental viability and reliability as well as the financial viability of small-scale wind energy are presented in this section. In Sections 2.3 and 2.4, the fundamental equations and analytical distributions required for describing the wind resource is presented. Section 2.5 highlights the energy needs that could be met by small-scale wind energy while Section 2.6 examines the boundary layer processes relevant to wind resource assessment, including the effects of roughness change in the boundary layer and additional complexities due to complex orography. Section 2.7 reviews vertical axis wind turbines, the advantages and disadvantages, including the design parameters that affects VAWT performance. Section 2.8 reviews the self-starting performance of VAWTs, including the definition of the concept “self-starting”. In addition, various solution strategies to improve self-starting performance as well as previous studies on self-starting have been reviewed.

### **2.1 Background**

The application of wind energy for power generation is not a new concept. Wind energy has been utilised for many centuries for mechanical power applications, water pumping, milling grain etc. The first accepted establishment of a windmill for power generation dates back to the tenth century when the first wind machines were built by the Persians between 500 and 900 AD (Manwell et al., 2009). The machine has a vertical axis orientation and is powered by a drag force which pushes the turbine blades to generate power. The use of the Persian windmill for power generation subsequently spread throughout the Islamic world. In the 11<sup>th</sup> century AD, wind energy was utilised in Europe. These wind machines were horizontal axis wind turbines which were introduced from the Middle East. The machines were primarily used for mechanical operations, such as water pumping, grinding mill, sawing

wood, and powering tools, etc. By the 14th century, the Dutch were ahead in improving wind machines and subsequently utilised them for draining the marshes and lakes of the Rhine River delta (Dannemand, 1999). Wind energy was the fastest growing renewable energy technology in the 1990s, in terms of the percentage of annual growth of installed capacity. However, the growth rate of installed capacity is not equally distributed around the globe. For example, by the end of 1999, about 69% of the worldwide wind energy capacity was installed in Europe, while 19% was installed in North America and a further 10% was installed in the Asia and Pacific region (Ackerman and Soder, 2000). By the end of 2014, the global installed wind capacity increased significantly with a record-breaking output estimated 52,129 MW bringing the world total of installed capacity to 371,191 MW (GWEC, 2015).

The market breakdown of wind energy development shows that the Asian market is leading in total installed capacity with more than 50.2% of the world newly installed capacity followed by the European market which accounts for more than a quarter of the global markets (25.8%). The North American market has a market share of 13.9% while the Pacific region, South America and Africa hold a total of 10.1% of the global market share. The market breakdown of the installed capacities is shown in Figure 2.1. In terms of the global total installed capacity to date, Figure 2.2 shows that the Asia has overtaken Europe as the leading wind energy installation region, and now tops Europe's 36.5% share of the world fleet with 38.3%. North America is still in third place with a 21% share.

Wind energy is forecasted to play an increasingly significant role in the future of the national energy portfolio (Ezio and Claudio, 1998), and according to Greenpeace, about 10% of electricity can be supplied by wind by the year 2020 (Goselin, 2007).

The wind turbines are among the best energy sources in terms of energy payback time (3-7 months) (EE A/S, 2004). Once the turbines are installed, their impact is virtually negligible, given proper design and consideration of the local site of installation and wildlife. These strong economic and sustainability features make wind power attractive from many perspectives. Turbine design has attained a very high level of sophistication, enabling the

production of 120m diameter, 5 MW turbines, installed both onshore and offshore.

Progress from 5m diameter, 15 kW machines of the early 1980s to the present day evolutions has been possible by technical breakthroughs of the “Danish concept”. Today, there are close to a million windmills in operation around different regions in the world. Modern windmills are called wind turbines and this is partly because of their mode of operational that is similar to the steam and gas turbines and partly to differentiate them from their ancient designs (Boyle, 2004).

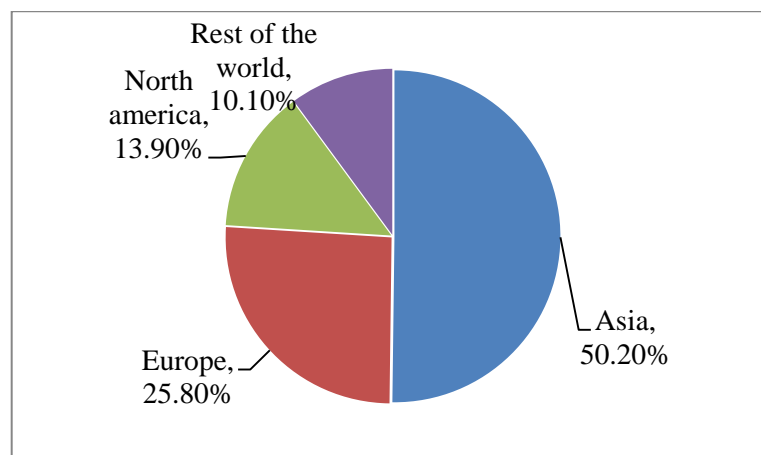


Figure 2.1: World wind turbine market breakdown for 2014 (Eurobserv'er, 2015).

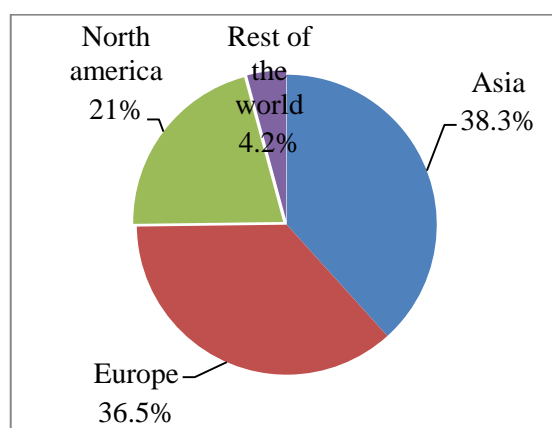


Figure 2.2: Cumulative breakdown of installed wind capacity at the end of 2014 (Eurobserv'er, 2015).



## 2.2 Overview of Small-Scale Wind Energy

### 2.2.1 What is a small-scale wind turbine?

Small wind turbines are a class of wind turbines that are mostly used for power generation to supply remote, off-grid loads, such as homes, sailing boats, telecommunication systems, etc. They are mainly used in combination with batteries and/or diesel generating systems.

According to Renewable UK, small-scale wind turbines are classified into three main categories, and these are shown in Table 2.1.

Table 2.1: Classification of micro-medium wind turbines (Renewable UK, 2013).

Rated Power(kW)	Height (m)	Sub-category
$0 < P_{\text{rated}} \leq 1.5 \text{ kW}$	10-18	micro
$1.5 \text{ kW} < P_{\text{rated}} \leq 50 \text{ kW}$	15-35	small
$50\text{kW} < P_{\text{rated}} < 500 \text{ kW}$	25-50	medium

This definition is a useful starting point for the modelling of the wind resource for small-scale wind turbine applications. Based on this definition, the hub height of a small-wind turbine is in the range 15-35 m. These hub heights are significantly lower than the large-scale turbines. Thus, wind resource assessment at these heights may be affected by topographical features. Hence, the prediction methodologies used in the large-scale wind industry may not be appropriate when applied to potential small-scale wind turbine sites due to the differences in the operating heights of the two turbines.

Despite the attention given to large-scale industrial wind turbines, the markets for small wind turbines can be attractive, especially when the price of conventional fossil based electricity are sufficiently high, or in many developing countries where the majority of the communities live without access to electricity.

The market for small wind turbines is dominated by off-grid applications and grid-connected applications. The bulk of the market for small-scale wind turbines in both developed and developing countries have been for small off-grid applications. They are mostly used for isolated applications, the most common of which is in rural electrification, professional applications

(telecommunications, etc.) and water pumping (Wood, 2011). There are other applications of small-scale wind turbines such as charging batteries in electric vehicles, producing hydrogen as an alternative to liquid fuels. However, these applications are beyond the scope of this thesis and will not be discussed further.

### **2.2.2 Environmental Viability of Wind Energy**

Generally, the main motive behind investing in small-scale wind energy technology is to reduce the amount of carbon emissions to the environment, thus, it is necessary to know if small-scale wind energy has the potential to reduce environmental emissions. Wind energy can be regarded as an environmentally friendly energy source; however, it is not totally free of emission. For a wind turbine to be environmentally viable, it must be able to save a substantial amount of carbon throughout the project lifetime to replace the amount of carbon released during the manufacture of blades, tower and other components of the turbine as well as the transport of equipment's for its installations. In order to establish environmental viability, two main processes must be accomplished, (i) a life cycle audit of the carbon emissions, and (ii) the predicted energy production over the lifecycle of the turbine. For a good understanding of these studies, the capacity factor of a wind turbine is introduced. The capacity factor is a fraction of the average power generated to its rated peak power as follows (Jain, 2011):

$$\text{Capacity factor} = \text{Average power} / \text{rated peak power} \quad (2.1)$$

The capacity factors are usually computed on annual basis from the actual energy produced from a wind turbine and measures the performance efficiency of wind turbines in any given location. It is a useful indicator when considering the environmental and financial viability of a wind turbine project since it allows a comparison of different turbines sizes to be made. A number of studies have been performed on the environmental viability of a wind turbine. For example, Allen et al. (2008) performed a life cycle assessment and energy potential for a 600 W capacity wind turbine based on onsite wind measurements at a height of 10 m. The study used a Meteorological Office wind database consisting of 26 sites and a correction factor was applied for turbulence based on both rural and urban areas. Their results revealed that the largest emissions emanated from building mounted wind turbines or the

scaffold pole in the case of the pole mounted turbines. Furthermore, the results show that the carbon payback was less than 15 years in urban areas. However, the adverse effect of heavy metal pollution was only compensated for in urban sites with the highest mean wind speed just over 5 m/s. Conversely, in rural areas, all pollutants were compensated for within the projected 15 years period even with the lowest observed mean wind speed. Overall, the displaced energy payback for the urban and rural wind turbines were found to be 3 and 0.6 years, respectively. The results were based on a capacity factor of 3% and 7% for the average urban and rural turbines, respectively. On the other hand, Celik et al. (2007) investigated the life-cycle emissions of a higher rated capacity (7.5 kW) off-grid wind turbine. The study was undertaken at an urban area in Turkey using wind measurements. They found an energy and carbon payback time of 1.4 years and 0.7 years, respectively.

The environmental viability of any wind energy will depend on a number of factors such as the chosen material for the construction of blades, the recycling process after the expected lifetime of the project is completed, and most importantly the wind resource. For instance, if the wind speed for a particular site is lower than the cut-in wind speed of a proposed wind turbine, such a turbine will not be environmentally viable, highlighting the importance of an accurate wind resource assessment before installation.

### **2.2.3 Environmental Reliability of Wind Energy**

There are a number of concerns in recent years about the reliability of wind turbine installations that are frequently expressed, although a proper design and siting could lead to their mitigation. The main concerns include the following:

Noise: early wind turbine designs are characterised with high noise, originating from blade aerodynamics and other mechanical sources in the system. Two-bladed turbines tend to produce more noise than three-bladed turbines (LDA, 2000). The noise impact can also be reduced with technical means, such as variable speed or reduced rotational speed of the turbine. This was taken into account in the choice of the number of blades and the value of the rotational speed in this thesis.

Aviation: siting the turbine away from flight paths reduces the possibility of collision with aircraft. National security might be threatened by blocking radar sites (Kirby, 2004) and may largely be reduced by radar placement and even stealth blades (Beck, 2004).

Direct mortality: Birds are sometimes killed in collision with wind turbine blades, meteorological towers and power transmission lines at land-based installations. Turbine related bat death have been reported in several studies, see for example Powlesland (2009); and Kingsley and Whittam (2005). These impacts can be reduced by proper siting of wind turbines in the landscape and a good understanding of the signals that birds use for navigation (Dooiling, 2002).

Land Use: wind turbines are often known to cover a large area of wind farms. However, in reality it only consists of the tower bases, and any sub-stations that may be present. It does not pose any threat to animals and neither does it disturbs farming operations (Love, 2003).

Visual Flicker: Accurate siting will mitigate sunlight shining through the turbine blades and casting a flickering shadow on occupants of buildings close to installation sites (LDA, 2000).

Clearly, from these reviews, the reliability of wind turbines is based on the performance of its components under a given environment, manufacturing process, handling, and the stress and ageing process. Reliability is a probabilistic concept involving a product's planned use, its operating environment and time. A number of studies have investigated the concept of reliability. Chands et al. (1998) had studied the expert-based maintenance methodology and suggested measures to ensure effective reliability of the wind turbine system. Denson (1998) analysed the failure causes for electronic systems and factors contributing to failure of components for electronic systems.

These studies highlight the necessity of accurate wind resource assessment and robust turbine design that will ensure the maximum functioning of the wind turbine system.

### **2.2.4 Variability of Wind Energy**

Wind energy relies on the energy of the sun. A small percentage of solar radiation is intercepted by the Earth and is converted into kinetic energy which provides all of the earth's energy requirements (Hubbert, 1971). The main cause of wind energy is the imbalance between the net outgoing radiation at high latitudes and the net incoming radiation at low altitudes. The nature of the resulting wind is affected by the Earth's rotation, geographical features and temperature gradients (Burton et al., 2011). The use of wind energy implies that the kinetic energy of the wind can be converted to useful energy. Consequently, the economics of using wind for power generation are extremely sensitive to the nature of the local wind conditions and the ability of the wind turbine to reliably extract energy over a wide range of wind speeds. Due to the variation of temperature across different regions of the world, and the rotation of Earth, wind can be found almost universally. Several studies have investigated the variability in wind energy. For example, Rohatgi (1994) investigated the variability in the wind pattern and grouped them into different classes of general or plenary variability, winds high above the Earth's surface, and local winds, being much closer to the surface of the Earth. General winds may include trade winds and the jet stream across a certain period of years, while local winds on the micro scale involve gusts that usually occur in seconds or minutes. Further, the variability of the wind is that it changes annually, seasonally, monthly and even daily. Due to this unpredictable variation in the wind pattern, the average wind speed at a typical location can change significantly up to twenty five percent annually (Gipe, 2004). The change in wind variability is even higher in complex terrains. However, the wind does exhibit some consistency, showing some diurnal and seasonal trends.

Typically, in the UK, wind is stronger during the day than night and it is mostly calm during the summer and increases in velocity throughout the summer months of June, July and August, with winter months of December, January and February exhibiting the highest greater than average wind speeds (Environmental Change Institute, 2005; Renewable UK, 2013).

Clearly, these studies indicate that the wind speed is highly variable, highlighting the necessity of accurate wind resource assessment that will capture the different trends in the wind speeds.

### **2.2.5 Financial Viability**

The question as to whether wind turbines are financially viable are much more difficult to address than the environmental viability discussed in the previous section. This is due to some strict policies and regulations by the UK government on the wind turbine and electricity markets which is having major implications for financial assessments (Weekes, 2014).

Due to the relative infancy of small-scale wind turbine market, along with other uncertainties, it may be argued that many small-scale wind turbines may not be financially viable without some form of financial incentives from the government (Bahaj et al., 2007). In the UK, the Feed-in Tariff (FiT) system is the major subsidy for small-scale renewable technologies. At present, the Feed-in Tariff for small-scale wind energy is 8.53 p/kW h for installations up to 100 kW. This amount is for every kilowatt hour of electricity generated with an additional 4.91 p/kWh paid for electricity exported to the grid (Energy Saving Trust, 2014).

A few studies have investigated the financial viability of installing a wind turbine in the UK.

Notable among these studies is the one undertaken by James et al. (2010). These authors reported that a 1 kW roof-mounted wind turbine, with a cost of £15000, would only achieve a payback within 10 years if it operated with an average capacity factor of 6%. The study incorporated the additional financial incentive available under the FiT program using a previous, higher tariff system. In all the wind turbines that were investigated, only those installed in rural areas were able to attain this level of performance. The turbines installed in urban areas performed poorly with a capacity factor as low as 3%, presumably due to poor siting decisions and low wind speeds (Energy Saving Trust, 2009).

On the other hand, Sissons et al. (2011) performed a similar study with an impressive result. They used a 6 kW turbine at an investment and operating cost of £20000 and £400, respectively. The study also included FiT incentive and the payback time was shown to be 12 years with a higher capacity factor

of 12%. When the capacity factor was increased to 25%, the payback time was reduced to 7 years. These results indicate that the capacity factor that can be achieved is strongly dependent on several factors, namely the turbine rated capacity, the wind speed and hence the height, and the nature of the land surface.

Based on the current market and financial support from the government, one can argue that small-scale wind turbines can be financially viable, particularly for the case of pole mounted turbines in rural locations which can achieve a quick payback period that is comparable to that for large-scale wind turbines. An additional point worthy of note is that since the energy production of a wind turbine is not linearly related to the turbine radius and wind speed, it is possible to achieve higher power production by ensuring that (i) turbines with higher rated capacity are installed, and (ii) turbines are installed at higher heights above local obstructions in order to access higher wind speeds. These important considerations favour the installation of pole mounted turbines in rural/ open regions where there are virtually no tall buildings and obstructions to hinder the wind flows.

### **2.3 The Wind as an Energy Source**

Wind is created by uneven heating of the surface of the earth. Solar energy absorbed by land or water is transferred to the atmosphere. A larger amount of solar radiation is received at the tropics compared to the poles, which causes hot air to rise or sink depending on the latitude. These flows which occur 10 to 15 km above the Earth's surface and are driven by the Coriolis force are responsible for the large-scale atmospheric circulation in different regions of the Earth (Jain, 2011). At these distances, within the range of heights of small-scale wind turbines, the frictional forces become particularly important causing large changes in the wind flow. Consequently, the prediction of the wind flow at these length scales tend to be difficult and strongly dependant on the nature of the surface (Jain, 2011). Thus, these effects must be taken into account when modelling the wind flows relevant to small-scale wind turbine in order to make the wind resource prediction more reliable and accurate.

### 2.3.1 Theoretical power in the wind

The power in the wind is the total available energy per unit time. This power is converted into electrical energy by the rotation of the wind turbine blades, which in turn induces a rotating magnetic flux in the turbine generator. The equation describing the energy and power in the wind is expressed as follows (Ackermann and Soder, 2000):

$$P = \frac{1}{2} \times \rho \times A \times V^3 \quad (2.2)$$

where  $\rho$  = air density,  $A$  = area of turbine blades, and  $V$  = wind speed.

The power in the wind depends on three factors, namely the density of the air, the area intercepted by the turbine blades and the cube of the wind speed. This cubic dependence is one of most important factor in evaluating the performance of a wind turbine at a particular site since a small change in the wind speed can produce a large effect on the power output of the turbine. In addition, since the power in the wind does not depend linearly on the wind speed, it is important to determine the shape of the wind speed frequency distribution as well as the mean wind speed in order to accurately assess a site wind resource.

### 2.3.2 Real power in the wind

The theory for utilising the real power in the wind was first proposed by Betz (1966). According to Betz, the maximum power that can be extracted from the wind can never attain the value expressed in Eqn. (2.1) regardless of the turbine design. Betz represented this effect by defining a power coefficient as follows (Burton et al., 2011):

$$C_p = \frac{\text{Generated power}}{0.5 \times \rho \times A \times V^3} \quad (2.3)$$

Using momentum theory, Betz established that the maximum power coefficient is equal to a value of  $C_p = 16/27 = 0.59$ .

Hence, the maximum theoretical power in the wind is expressed as follows (Burton et al., 2011):

$$P_{Betz} = 0.5 C_{pBetz} \times \rho \times A \times V^3 \quad (2.4)$$

According to the Betz theoretical equation, even if a power extraction without any losses would be possible, only 59% of the wind power could be utilised by a wind turbine.



In reality, the actual power from the wind turbine will usually be less than the Betz limit due to the time required for the turbine to respond to changes in the wind speed and direction; losses associated with conversion of energy processes as well as losses during the distribution of power to various sources. Since the power extracted from a wind turbine depends on the viability of the wind resource and the performance of the installed turbine, the Betz theory is a useful approximation for characterising a typical wind turbine site.

## **2.4 Describing the wind resource**

It is widely accepted in the research community that there is abundant resource in the Earth's winds to be harnessed for electricity generation (Marvel et al., 2013; EWEA, 1999). Several studies on the global wind resource potential have resulted in a phenomenal enhancement of knowledge of the wind energy resource. These studies show that the near surface winds on Earth that we can harness today for electricity generation, appears to be indicative of a potential, which in a sense is just the tip of the iceberg. The wind speed increases dramatically at higher altitudes, above about 2,000 m above ground level and up to 10,000 m. (WWEA, 2014). According to Acher and Caldeira (2009), the global average of the median wind power densities at 1,000 and 10,000 m are estimated at 422 and 2,228 W/m<sup>2</sup>, respectively, which implies that given a robust technology, wind in high altitudes can meet all the electricity needs on Earth in a reliable and sustainable manner. At present, most large-scale wind turbines are installed at a height below 100 m above ground level, but some turbines have been installed at a height of up to 120 m. Even at 80 m ABL, the resource potentials have been estimated in the order of 400 TW (WWEA, 2014). It must be emphasised that the global technical potential of wind energy is not fixed, but vary significantly over a wide range of timescales including annual, seasonal, daily and hourly.

Since wind speeds vary considerably over time and space, statistical distributions of the wind speeds are required for analysing the wind resource rather than just the simple mean. The wind speed distribution, along with the wind directions and possible turbulence characteristics, can be used to characterise the wind resource potential at a particular region or location. Furthermore, because the power in the wind depends on the cube of the wind

speed, the shape of the wind speed distribution provides important information on the available wind power that could be exploited from a given site. The next section describes the choice of the wind speed distribution.

### 2.4.1 The Weibull distribution

Investigations into an appropriate statistical distribution of wind speed to represent the wind resource potential of a site has been on-going for over 5 decades especially in the USA (Carta, Ramirez and Velazquez, 2009). During this period, several statistical distributions were proposed, namely univariate, bivariate, multivariate, bimodal and hybrid. However, in 1951 'A Statistical Distribution function of Wide Applicability', was published by Waloddi Weibull, and this is what is today known as the Weibull distribution (Weibull, 1959). The Weibull distribution was initially applied in the field of failure analysis of materials but was later utilised by researchers for wind resource assessment (Carta, Ramirez and Velazquez, 2009). Presently, the Weibull distribution is regarded as the most widely used and validated empirical distribution (He et al., 2010) in the literature of climatic surface wind speed studies (Klink, 2007; Capps and Zender, 2008), and wind power assessment (Pryor and Bathelmie, 2009; Ramirez and Carta, 2005) due to its success in describing different wind regimes. The probability density function (PDF) representing the Weibull distribution can be expressed as follows (Mirhosseini, Sharifi and Sedaghat 2011):

$$f(U) = \frac{k}{c} \left(\frac{v}{c}\right)^{k-1} \exp\left[-\left(\frac{v}{c}\right)^k\right] \quad k > 0, V > 0, c > 1 \quad (2.5)$$

where  $f(V)$  is the probability of the observed wind speed  $V$ ,  $k$  is the dimensionless Weibull shape parameter, and  $c$  is the Weibull scale parameter. It is important to note that the distribution is zero when the wind speed is zero, thus the Weibull distribution is not able to represent periods of zero wind speeds.

The cumulative density function (CDF) is the fraction of time (probability) of the wind speed at a given location. It is represented by the integral of the probability density function as follows (Manwell et al., 2009; Mirhosseini, Sharifi and Sedaghat 2011):

$$f(V) = 1 - \exp \left[ - \left( \frac{v}{c} \right)^k \right] \quad (2.6)$$

The Weibull parameters characterise the wind potential of a site under study. Basically, the scale parameter  $c$  indicates how ‘windy’ a wind location is and is a measure of central tendency (Pryor and Barthelmie, 2009), whereas the shape parameter  $k$  is a function of the skewness and kurtosis of the distribution (Capps and Zender, 2008). A special case of the Weibull distribution is assumed when the value of  $k = 2$  and is known as the Raleigh distribution. The Weibull distribution is generally characterised by  $k < 3.6$ , with a positively skewed curve. When the value of  $k = 3.6$ , the Weibull curve resembles a Gaussian curve, and if the value of  $k > 3.6$  the Weibull curve can be described by a negative skewness and will no longer have a long tail (Weekes, 2014).

The Weibull parameters may be obtained from a line of best fit to the actual wind speed data using a number of well-established methods (Manwell et al. 2009). Once the Weibull parameters has been computed, the wind speed probability density function (pdf) can be used to calculate the mean Betz power density,  $\bar{p}_d$  as follows (Manwell et al., 2009):

$$\bar{p}_d = C_p 0.5 \rho \int_0^{\infty} v^3 f(v) dv = \left( \frac{16}{27} \right) 0.5 \rho \bar{v}^3 \quad (2.7)$$

in which  $16/27$  is the Betz limit and  $\bar{v}^3$  is the mean of the cubed wind speed which is defined according to the following equation (Manwell et al., 2009):

$$\bar{v}^3 = c^3 \cdot \Gamma \left( 1 + \frac{3}{k} \right) \quad (2.8)$$

The mean wind velocity of a regime, according to the Weibull distribution, is expressed as follows (Manwell et al., 2009):

$$V_m = c \cdot \Gamma \left( 1 + \frac{1}{k} \right) \quad (2.10)$$

where  $\Gamma$  is the gamma function and can be expressed as follows:

$$\Gamma = \int_0^{\infty} e^{-x} x^{(n-1)} dx \quad (2.11)$$

The standard deviation of the wind velocity following the Weibull distribution is given as follows:

$$\sigma_v = V_m \sqrt{\frac{\Gamma(1+\frac{2}{k})}{[\Gamma(1+\frac{1}{k})]^2} - 1} \quad (2.12)$$

Furthermore, the expected energy yield from a wind turbine can be computed for a particular time  $t$  with reference to the manufacturer's power curve using the following expression (Manwell et al., 2009):

$$E = t \int_0^{\infty} PWT(u)f(v)dv \quad (2.13)$$

Describing the wind resource using the Weibull distribution is associated with a number of uncertainties. However, the distribution offers several advantages when compared to the other statistical methods. These advantages include: (i) greater flexibility in data manipulation and analysis to quickly determine the average annual production of wind turbine under a range of wind regimes, and (ii) the distribution allows the wind resource to be characterised in terms of mathematical parameters thereby making a simplified and accurate comparison between sites more relevant.

A wide range of researchers have utilised the Weibull distribution to represent the wind resource. For example, Dahmouni et al. (2011) studied the wind resource potential at the Centre of Research and Technologies in Bora Cedria Tunisia using a Weibull distribution along with wind measurements obtained at two heights 20 m and 30 m. The study was undertaken between 2008 and 2009 and the wind data were analysed and used to choose the best wind turbine for that site wind conditions. Gibescu et al. (2006) used a Weibull statistical distribution to evaluate the wind resource based on the measurement data from different weather stations and expresses the covariance between the locations as a function of their distances from the measurement stations. Zheng and Kusaik (2008) evaluated the wind energy potentials of a wind farm based on short-term onsite wind measurements using the Weibull distribution. Chandel, Ramasamy and Murthy (2014) used the Weibull distribution to assess the wind energy potential of a location. They provided a summary of the comparisons of some of the methods to evaluate the Weibull parameters  $k$  and  $c$ . The discussed methods include the maximum likelihood, modified maximum likelihood, empirical method, equivalent energy method, graphical method and the moment method. Clearly, these studies indicate that the Weibull distribution is the most widely used statistical distribution in the analysis of the wind resource.

### 2.4.1.1 Methods of fitting Weibull parameters

Several mathematical techniques have been used for fitting the Weibull distribution to the measured wind data and a number of studies are abound that adequately compares the relative advantage of each methods. The most widely used and validated methods are the maximum-likelihood method (MLM), the least square or graphical method (Nedaei, 2014) and the method of moments (Chang 2011).

#### Maximum-likelihood method (MLM)

The MLM method fits a Weibull distribution to a set of measured wind speeds using an iterative method. The likelihood function  $L$  is the joint density function of  $n$  random variable and the unknown distribution parameters. It defines the likelihood of observing the data as a function of the distribution parameters.

For convenience, the maximum likelihood method is expressed mathematically in the log-likelihood function which transforms the expression in to a summation by maximising the log-likelihood function ( $\ln L$ ). This can be achieved by differentiating ( $\ln L$ ) with respect to  $c$  and  $k$  and equating the partial derivative to zero as follows (Seguro and Lambert, 2000):

Using this method, the Weibull parameters can be estimated as follows (Manwell et al. 2009):

$$k = \left[ \frac{\sum_{i=1}^N v_i^k \ln(U_i)}{\sum_{i=1}^N v_i^k} - \frac{\sum_{i=1}^N v_i^k \ln(v_i)}{N} \right]^{-1} \quad (2.14)$$

where  $v_i$  is the wind speed in time step  $i$  and  $N$  is the number of time steps. Once the shape parameter has been found, the scale parameter is calculated as follows (Manwell et al. 2009):

$$c = \left[ \frac{\sum_{i=1}^N v_i^k}{N} \right]^{\frac{1}{k}} \quad (2.15)$$

#### The least square algorithm

The least square or the graphical method involves the transforming of the Weibull cumulative density function to a linear representation in order to obtain the Weibull parameters using linear regression (Manwell et al. 2009). In reality this implies binning the data sets according to the wind speed resulting in a regression line that give equal weight to each wind speed bin regardless of the number of data points. Therefore, wind speed bins at the extrema of the

distribution may significantly affect the regression fit and the values of the Weibull parameters (Manwell et al. 2009).

### Method of Moments

In this method, the coefficient of variation for the Weibull distribution can be expressed directly in terms of the Weibull parameters  $k$  and  $c$ . These values can then be obtained iteratively by solving the equation. However, the main limitations of the method is the occurrence of large deviations in the estimator (Carta, Ramirez and Velázquez, 2009). When the mean wind speed  $V_m$  and the standard deviation  $\sigma$  of the wind data are used, the following equation can be obtained (Akdağ, and Dinler, 2009):

$$(\sigma/V_m)^2 = \Gamma\left(1 + \frac{2}{k}\right)/\Gamma\left(1 + \frac{1}{k}\right)^2 - 1 \quad (2.16)$$

The shape parameter can be calculated from this equation using Newton-Raphson (NR) method as follows:

$$g(z) = \Gamma(1 + 2z)/\Gamma(1 + z)^2 - \left(\frac{\sigma}{V_m}\right)^2 - 1 \quad \rightarrow \quad \frac{dg(z)}{dz} = \frac{2\Gamma(1+3z)}{\Gamma(1+z)^2} [\Psi(1 + 2z) - \Psi(1 + z)] \quad (2.17)$$

where  $z = 1/k$ .

Nevertheless,  $k$  can also be estimated using the following approximation (Akdağ, and Dinler, 2009):

$$k = (\sigma/V_m)^{-1.086}, 1 \leq k \leq 10 \quad (2.18)$$

In wind resource assessment, the representativeness of a Weibull distribution, given a series of measured wind speeds may be assessed by evaluating the wind power density. Eqns. (2.16) and (2.17) can be used to compare the measured and Weibull estimates of the wind power density as well as provide the likely uncertainties (error) introduced through a fitted distribution in place of measured data.

### 2.4.2 Alternative methods to the Weibull distribution

Although the Weibull distribution is regarded as the most widely used wind speed distribution to represent the wind resource, it is not always justifiable from a theoretical point of view (Tuller and Brett, 1984). Thus, several studies have been published in recent years which argue on the validity of the Weibull

distribution by comparing the degree of accuracy of other methods in representing the wind resource. Unfortunately, some of these studies are based on wind data from either a single site or a small number of sites and hence the conclusion drawn from these studies may not be generalised. Some of these studies are reviewed as follows:

Celik et al. (2010) compared the performance of five different wind speed distributions using wind speed data obtained at a roof-top in Edinburgh. The authors showed that a bi-modal Weibull distribution sufficiently described the measured data than the standard Weibull distribution. However, they warn that the general conclusions cannot be drawn from a single site with a specific topography. On the other hand, Chang et al. (2011) compared the performance of six wind speed distributions using wind speed data from three different sites in Taiwan. The results of the investigation showed that the standard Weibull distribution adequately described the wind resource except in some instances where the observed wind speed showed bimodality. Nedaei, Assareh and Biglari (2014) compared the performance of five wind speed distributions using wind speed data from Mah-Shahr station in Iran. They concluded that the standard Weibull distribution accurately described the wind speed distribution at the Mah-Shahr site. A more comprehensive investigation combining different techniques was performed by Carta et al. (2009). The study was based on a wide range of wind regime in Canary Islands, and from the study they concluded that, while the Weibull distribution has a number of limitations, it offers some advantages over the other distributions. The advantages include: (i) wide applicability in a variety of wind regimes (ii) requires only two distribution parameters, and (iii) greater flexibility in estimating confidence intervals etc.

These reviews show that in the absence of information to other analytical distributions, the Weibull distribution provides a good starting point in the analyses of the wind resources at any location or region. However, if the wind speed data exhibits bimodality, it is possible that a different distribution method such as the Weibull mixture distributions will be appropriate to evaluate the wind resource.

## **2.5 Energy needs that could be met by small-scale wind turbines**

Wind energy can be utilised for different purposes and in different climates zones. The following section describe some energy needs that could be met by small-scale wind turbines.

### **2.5.1 Off-grid applications**

The bulk of the market for small wind turbines (SWTs) in both developed and developing countries have been for small off- grid applications. However, this trend has changed in the last few years due to the growth of grid-connections. They are mostly used for isolated applications, the most common of which is in rural electrification, professional applications (telecommunications, etc.) and water pumping (Wood, 2011). In terms of technology, three groups of isolated systems using SWTs are distinguished in the following sections.

### **2.5.2 Very small systems**

This class of SWTs have a generating capacity of less than about 1 kW (Paraschivoiu, 2002). They are mostly used for mobile applications, such as boats and caravans, and wind home systems (WHSs): the wind version of solar home system (SHS) used for rural electrification.

### **2.5.3 Hybrid systems:**

Hybrid refers to the systems including wind generation and other generation sources (usually photovoltaic). The power requirements for this system is less than 50kW (Paraschivoiu, 2002). A diesel generator is used in many systems in this configuration as a backup system to the power.

### **2.5.4 Wind-diesel systems:**

In this system the diesel engine generator (gen-set) plays a key role, not only as a back-up source but also as an integral component for proper control and functioning of the system. They are mostly used for large isolated applications (> 50 kW), and some systems in the MW range have been reported.

A good example of the wind-diesel system is located in the Australian city of Esperance, consisting of eight diesel generators with a combined capacity of 14 MW and two wind farms of 2.4 MW. These systems have been reported of



adequately responding to all power fluctuations caused by lightening in the region. At nights, with low system loads and high winds, the wind farms provide up to 75% of the total system load without any problems (Rosser, 1997). There are also examples of other wind diesel systems all over the world. However, most of the projects are located in countries with low population density, such as Canada and Australia.

### **2.5.5 Wind-pump systems:**

In 1500s, wind energy was used for water pumping applications. A good example of such an application is the watering of potato plantations in the Cretan plateau of Lassithi, and the wind pumps on the cattle farms in the American Midwest. Nowadays, in industrialised countries, wind energy is only scarcely utilised for water pumping. However, in developing countries, where many regions are not connected to the electricity grid, the utilisation of wind energy constitutes an economical and environmentally friendly option for improving the water supply. In developing countries, the majority of the operating wind pumps are currently applied for drinking-water supply and livestock watering. More recent approaches to use wind pumps for irrigation have failed and this is often due to the complexity of this application.

Different designs of wind pump are used all over the world. Depending on the water location, e.g. underground water or surface water, the required pumping height and pumping volume, the water contamination and the available wind conditions, different pumps and different wind turbines can be used. Simple piston pumps, for instance, are often used in remote locations and eccentric screw pumps are currently tested in more advanced applications (Ackermann and Soder, 2000).

## **2.6 Wind in the boundary layer**

An understanding of the wind flow in the boundary layer is necessary in order to develop analytical methods for wind resource assessment and therefore, a short review of the wind characteristics in the boundary layer is presented in the following sections.

### **2.6.1 The atmospheric boundary layer**

The atmospheric boundary layer (ABL), or planetary boundary layer (PBL), is a part of the troposphere. At the top of the ABL, at a distance approximately 1-2 km above the Earth's surface, the wind flow is governed by the geostrophic wind, i.e the wind created as a result of an exact balance between the Coriolis force and pressure gradient (Stull, 1988). The ABL is strongly affected by the buoyancy forces caused by the solar heating of the Earth. The interaction of these forces results in turbulent mixing which is triggered by free or forced convection. Since wind speeds increase at higher altitudes from the surface, the result of the turbulent mixing is a transfer of momentum from higher to lower levels (Oke, 1987). In the case of unstable conditions, turbulent mixing tends to increase, thus causing a higher transfer of momentum as well as a reduced vertical wind speed gradient.

Going down through the ABL, the effects of the surface roughness increases significantly and the wind speed changes from being geostrophic. The surface roughness effects cause turbulent stresses that spread upwards to create a shear in the vertical wind profile (Weekes, 2014). Due to the operating heights of small-scale wind turbines, as given in Table 2.1, they tend to be affected by these processes that occur in the lowest part of the ABL. A brief review of these processes are given in the subsequent sections.

### **2.6.2 The inertial sublayer**

The significance of the initial sublayer (ISL) cannot be over emphasised in the study of small-scale wind energy. The ISL occupies the lower part of the ABL up to a height greater than the average height of the roughness elements and much lower than the top of the ABL (Best, et al., 2008). The two main characteristics of the ISL are that the shear stress is approximately constant with height and the vertical wind profile may be described using a logarithmic expression. The logarithmic wind profile may be developed using two main approaches, namely vertical flux of horizontal momentum (Oke, 1987) and simple dimensional arguments (Best, et al., 2008). There is also a simplified approach based on the transfer of momentum as parcels of air that move between the different layers (Baldocchi, 2012; Millward-Hopkins, 2013). The

simplified approach based on the transfer of momentum can be obtained using the following mathematical formulations:

For an air parcel with mean wind speed  $\bar{v}$  moving through the initial sub layer (ISL) over a vertical distance  $l$ , the velocity fluctuations  $v'$  can be expressed as follows (Best et al., 2008; Weekes, 2014):

$$v' = \bar{v}(z - l) - \bar{v}(z) = -l \frac{d\bar{v}}{dz} \quad (2.19)$$

in which  $z$  is the height of the layer above ground level,  $l$  represents the Prandtl mixing length.

Using the formulation of Prandtl (Bradshaw,1975), Bradshaw developed a relationship between the vertical and streamwise velocity components to the vertical flow gradient with the boundary layer, Eqn. (2.19) can be written as follows:

$$\overline{v'w'} = -l^2 \left[ \frac{d\bar{v}}{dz} \right]^2 \quad (2.20)$$

The Prandtl mixing length  $l$  is related to the height above ground level with the von Karman constant  $\kappa$  (a constant of proportionality).

Eqn. (2.20), along with the expression for the Reynolds shear stress  $\tau$  in terms of the average of the fluctuating velocity components gives the following expression (Best et al., 2008; Weekes, 2014):

$$\tau = \overline{\rho v'w'} = \rho \kappa^2 z^2 \left[ \frac{d\bar{v}}{dz} \right]^2 \quad (2.21)$$

From this equation, it is possible to define a velocity at some reference height in which the shear stress is proportional to the square of the velocity (Oke, 1987). This is called the friction velocity  $v_*$  and it is given as follows (Oke, 1987):

$$v_* = \sqrt{\left( \frac{\tau}{\rho} \right)} \quad (2.22)$$

Combining Eqns. (2.21) and (2.22) and integrating produces a logarithmic vertical profile  $v_z$  as follows:

$$v_z = \frac{v_*}{\kappa} [\ln(z) + A] \quad (2.23)$$

where  $A$  is the integration which can be defined such that the wind speed is equal to zero at some given height, and where this height is equal to the roughness length  $z_0$  as follows:

$$v_z = \frac{v_*}{\kappa} \ln\left(\frac{z}{z_0}\right) \quad (2.24)$$

Assuming that the wind passes through a rough surface, a correction factor to the height above ground level must be added in Eqn. (2.24) in order to account for the blocking effects of the obstacles. This can be achieved through a displacement a displacement height which tends to change the profile to a new height  $z - d$ . The resulting equation is known as the log law and it is expressed as follows:

$$v_z = \frac{v_*}{\kappa} \ln\left(\frac{z-d}{z_0}\right) \quad (2.25)$$

It should be noted that Eqns. (2.24) and (2.25) are only valid in neutral stability conditions but they can be modified by introducing stability factors in cases where this assumption does not hold.

### **2.6.3 Internal boundary layer over a sudden change of surface roughness**

Eqn. (2.24) highlights the significance of the roughness parameter  $z_0$  in the vertical wind speed profile. It implies that the wind speed profile in the inertial sublayer ISL is strongly affected by the roughness length  $z_0$ . This is due to the differences in the land cover which can potentially affect the wind flow close to the Earth's surface.

According to Kaimal and Finnigan (1994), the internal boundary layer IBL is defined as the layer of air that is in immediate contact with the Earth's surface. Figure 2.3 depicts the development of an IBL from an abrupt roughness change. Above the internal boundary layer, the vertical wind speed profile is affected only by the upstream surface. However, within the IBL, the wind speed profile gradually adjusts to the properties of the local surface. Further,

downstream the developing IBL forms an equilibrium layer, where the wind flow is fully adjusted to the local surface.

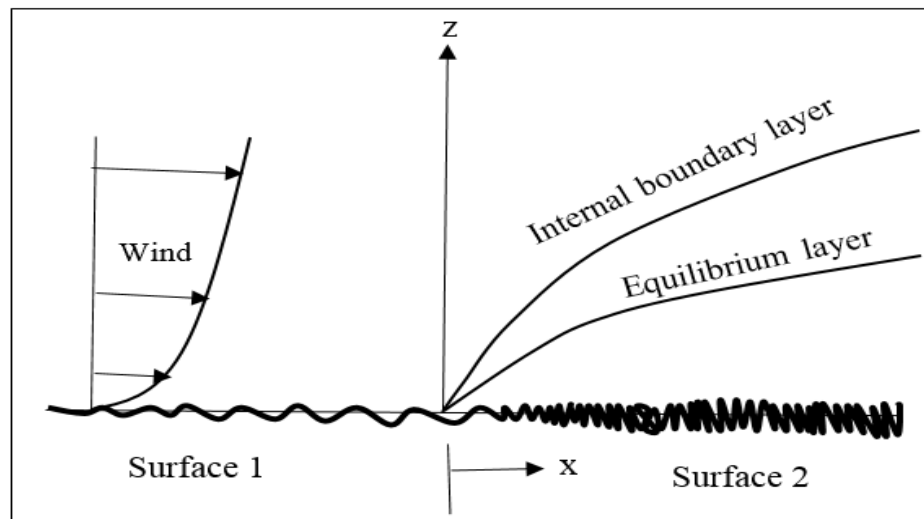


Figure 2.3: Sketch of the development of an internal boundary layer from a smooth to rough transition. (Adapted from Rao et al. 1973).

Several mathematical models have been developed to describe the development of an IBL as a function of the change in the surface roughness, see for example Elliot (1958), Rao et al. (1973) and Garratt (1990), etc. These models are derived from simple power laws based on the downstream surface roughness to more complex models that accounts for the upstream and downstream roughness changes as well as stability effects. Due to the different input parameters in these models, the predicted IBL depths tend to be large (Best, et al., 2008). The general rule for IBL development from smooth to rough transition is to use an IBM height to fetch ratio of 1/10, and since only a small fraction of this layer (about 10%) will be in full equilibrium with the downstream surface, this means that the equilibrium layer shown in Figure 2.3 has a height to fetch<sup>1</sup> ratio of approximately 1/100 (Rao, et al., 1974; Peterson, 1969). Conversely, transition from a rough to smooth surface is likely to have a smaller height to fetch ratio as the flow adjusts slowly to the direction of the smooth surface (Bradley, 1968).

---

<sup>1</sup> Fetch refers to the uninterrupted distance over which the wind blows without a significant change of direction

In theory, the logarithmic vertical wind speed profile, Eqn. (2.23) can be applied above the internal boundary layer IBL and within the equilibrium layer if the heights of the IBL and the equilibrium layer are given, thereby making the prediction of the wind speed possible.

#### 2.6.4 Wind flow over multiple internal boundary layers

In most situations, wind turbine sites are located in more complex topographies than the single surface roughness transition described in Section 2.4.3. Even in locations that are characterised with simple orography, the variations in the land cover may result in an upstream fetch that comprises several surfaces of different roughness elements. Assuming the sizes of these patches are such that the IBL is not fully developed before coming in contact with the next roughness change, the developing layer will interact with the surface layer resulting in a more complex wind flow (Best, et al., 2008). A pictorial representation of the development of regional internal boundary layer IBLs over a patchy surface is shown in Figure 2.4.

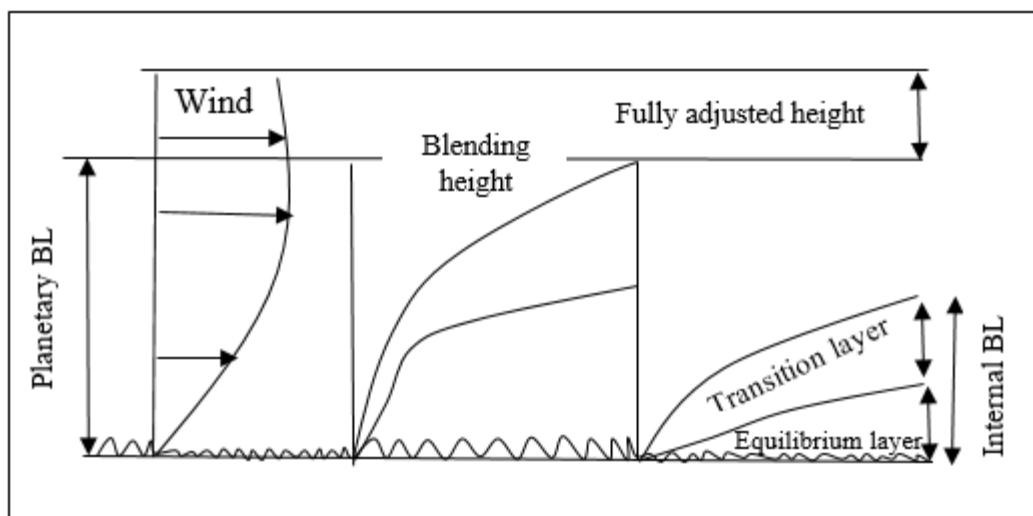


Figure 2.4: Sketch of the internal boundary layers over terrain consisting of well-defined repeating patches. (Adapted from Goode and Belcher, 1999).

Following Wieringa (1976), a blending height may be defined, above which, the individual contributions from multiple roughness patches may be combined into a single average. Wind flows crossing this height are

considered to be fully adjusted to some effective roughness that is representative of the overall surface. However, the actual definition of the term “blending height” has been debated (see Schmid and Bunzli, 1995; Mahrt, 1996). According to Claussen (1990), the blending height should represent the height above which the wind speed variations associated with the roughness changes are negligible so that the wind flow follows the logarithmic profile characterised by the effective roughness change  $Z_{0eff}$  and the effective friction velocity  $v_{*eff}$ . Hence Claussen (1990) associated the blending height with the depth of the internal boundary layers that develop downstream of the changes in surface roughness. It should be noted that the characteristics of the inertial sub layer (ISL), discussed in Section 2.8.2, may only be valid above the blending height, since below this height, the inertial sublayer ISL relating to each roughness patch may be invalid or partially developed (Cheng and Castro, 2002). Different rules are used to estimate a suitable blending height, for example Mason (1988) argued that a blending height of value of length/200 is suitable but stresses that this value is only an approximate scale. In reality, the value of such a length scale in which this estimate is based may not exist. Also, Mason stated that the blending height marks an abrupt transition between the local and regional surfaces. Despite the inherent challenges in estimating the blending height, the value based on the concept of single blending height is still a useful approximation and, in many practical applications, these estimates do not have a significant impact on the predicted wind speed (Best et al., 2008; Goode and Belcher, 1999).

The above discussion suggests that adequate measures must be taken when using the logarithmic vertical speed profile, namely Equation (2.23) to model any of the layer of the internal boundary layer IBL and suitable parametrisation of the roughness parameter must be applied. Further, below the blending height, the presence of multiple surfaces that the wind will have to pass through may result in large complexities that will further complicate the parameterisation of the surface.

#### **2.6.4.1 Blending methods**

As shown in Figure 2.4, wind flow above the blending height is significantly affected by the several surface patches and thus a procedure to determine the parameterisation of the spatially averaged roughness is required. To

achieve this, the effective roughness length  $Z_{0eff}$  applicable above the blending height must be achieved. The roughness length  $Z_{0eff}$  is defined as the roughness of an equivalent homogenous surface that would give rise to the same average stress as the homogenous surface (Mason, 1988). Two main approaches, namely the concept of source areas (Schmid and Oke, 1990) and the blending method (Mason, 1988) can be used to derive an expression for  $Z_{0eff}$ . The later provides an intuitive method that can be applied directly to gridded land cover data over different terrains and the approach is now presented:

Assuming alternating patches of the same size and different surface roughness, and making reference to Eqn. (2.23), the average surface stresses for these patches can be expressed in terms of the friction velocity as follows (Best, et al., 2008):

$$v_*^2 = 0.5(v_{*1}^2 + v_{*2}^2) \quad (2.26)$$

Combining Eqns. (2.22) and (2.264), the effective roughness length  $Z_{0eff}$  can be determined in terms of the roughness length of the two surfaces and the blending height  $z_{bh}$  as follows (Best et al., 2008):

$$\left[ \ln \left( \frac{z_{bh}}{Z_{0eff}} \right) \right]^{-2} = 0.5 \left\{ \left[ \ln \left( \frac{z_{bh}}{Z_{0,1}} \right) \right]^{-2} + \left[ \ln \left( \frac{z_{bh}}{Z_{0,2}} \right) \right]^{-2} \right\} \quad (2.27)$$

in which  $Z_{0,1}$  and  $Z_{0,2}$  represents the roughness lengths of the two surfaces.

For surfaces with multiple patches with varying sizes, Eqn. (2.27) can be written as follows (Best et al., 2008):

$$\left[ \ln \left( \frac{z_{bh}}{Z_{0eff}} \right) \right]^{-2} = \sum F_i \left\{ \left[ \ln \left( \frac{z_{bh}}{Z_{0,i}} \right) \right]^{-2} \right\} \quad (2.28)$$

in which  $F_i$  indicates the fraction of the surface  $i$  with roughness length  $Z_{0,i}$ . Eqn. (2.28) is the standard expression for estimating  $Z_{0eff}$  using techniques based on land cover data.



In developing a technique that is capable of downscaling the spatially average mean wind speed, the theories underpinning the blending height and effective roughness parameter discussed above leads to the idea of a regional and local downscaling which is discussed in the next section.

#### **2.6.4.2 Regional and local downscaling**

From the discussion in Section 2.6.2, wind speed at any specific height can be downscaled using a logarithmic wind speed profile and parameterisations of the regional and local roughness. There are two possible means of achieving this transformation. Firstly, the wind speed may be downscaled to a blending height by means of regional parameterisation. Secondly, a local downscaling can be applied using the surface roughness if the profiles match the blending heights. However, it must be noted that such a transformation is only a simplification since below the blending height the equilibrium layer may not cover the entire distance of the developing internal boundary layer IBL (see Figure 2.5).

For the case of a regional homogenous rural region, this procedure reduces to the application of a single logarithmic wind profile using suitable rural roughness parameters. In cases where the regional area includes multiple patches of different roughness, the downscaling procedure must account for effective roughness change above the blending height. More difficult cases arise when the local area is situated at the coastal or the built environment. These areas introduces significant complexities in the parameterisation of the surface roughness and are beyond this scope of the present study.

#### **2.6.5 Wind flow over complex orography**

Orography plays a significant role in resource assessment and siting of wind turbines and it determines whether wind turbines are capable of reaching their expected design lifetime or their early failures (Ragheb, 2016).

Obstacles such as ridges, trees, rock formations, hills and cliffs causes further modification to the wind flow that may not be considered in a simple boundary layer model. Adjustment of wind flows due to these obstacles results in speed-up and flow retardation at the crest and leeward side of a hill, along with other complex flow alterations. The flow modification in the case of a uniform, isolated hill is schematically shown in Figure 2.6. Considering the case of a

moderate slope ( $< 17^\circ$ ), see Figure 2.6 (a) the wind flow over a hill remains attached (Oke, 1987; Taylor and Lee, 1984). On the hand, when the wind flows over a fixed height above the ground level the intensity of the wind speed is greater at the crest than at the same height some distance upward the hill as shown in Figure 2.6 (b). This increase in speed is due to the compression of stream lines in the vertical direction (Oke, 1987) and a subsequent increase in the vertical wind gradient. However, in reality, the wind flow condition described in Figure 2.5 are significantly more complicated due to the topographical features of a hill which are rarely uniform.

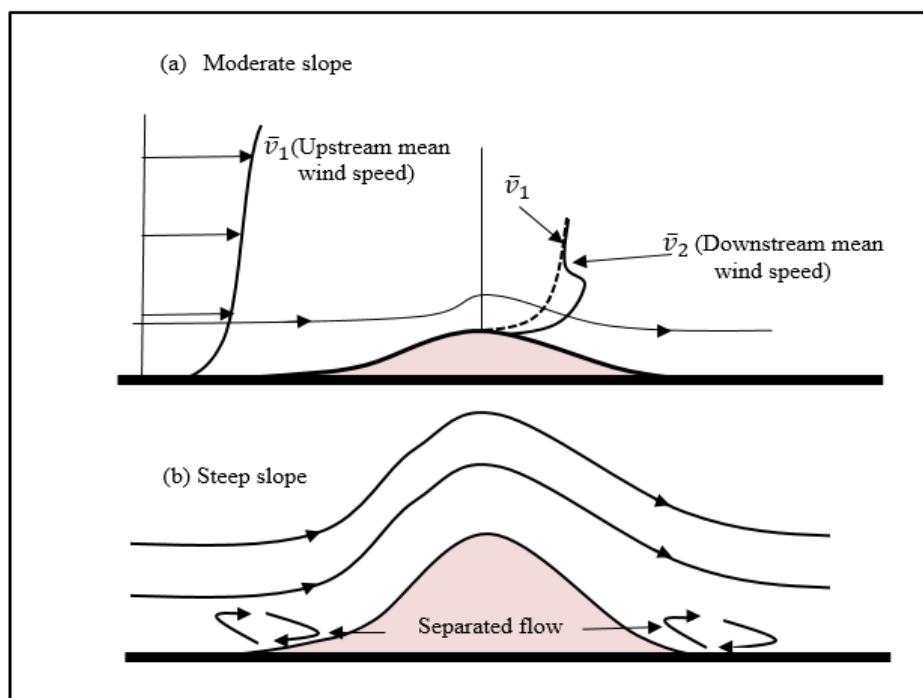


Figure 2.5: Wind flow over a hill with (a) moderate and (b) steep slope.

(Adapted from Taylor and Lee, 1984).

Such topography introduces complex flow phenomenon which are increasingly difficult to model using simple modelling techniques. A wide range of techniques, namely Wind Atlas Analysis and Application Program (WAsP) DTU (2013), Windsim and 3DWind (Jain, 2011) are available that considers the effect of orography on wind flows.

Complex orography at wind turbine sites can potentially complicate wind resource assessment based on the boundary layer meteorology and correlation approaches based on wind observations at correlated sites. For

the case of predicting the wind resource, the resolution of the input climatology will limit the size of the orographic features that can be resolved without the application of a detailed flow model. However, in the case of correlating to a reference climatology, complex orography may result in highly localised flow that is poorly correlated to nearby reference sites.

### **2.6.6 Summary of boundary layer approaches**

The science of wind flows close to the Earth's surface have been vigorously studied for many decades by several researchers, and in many simple situations these studies have revealed a deep understanding of the flow physics. Subject to certain limitations due to topographical features, the vertical wind profile can be modelled accurately by a logarithmic expression that accounts for the surface characteristics of the potential sites. At a point in the wind flow, known as a roughness change, an internal boundary layer (IBL) develops and the wind flow gradually adjusts to a new surface. This transition in the flow field entails that the logarithmic profile will be affected by upstream and downstream surfaces. Most often, multiple surface patches contribute to the changes in the surface roughness and this necessitates the use of blending methods to parameterise the effect of the overall surface above the blending height. Further complications are introduced by complex orography due to the nature of the wind flow in rugged terrain.

As will be seen in Chapter 3, wind resource assessment approach can be developed based on the scaling of a reference climatology using the principles of the boundary layer meteorology. However, a number of assumptions and simplifications are required in order to fully apply the approach for wind resource assessment.

## **2.7 Review of Vertical Axis Wind Turbines (VAWTs)**

The VAWT is a lift-based design, which implies that the aerodynamic torque is generated by the lift force of the blades. A clear visualisation of the schematic of a lift based turbine is shown in Figure 2.6. Each blade rotates around the turbine axis and possess a maximum lift only twice per revolution, thus resulting in a high torque and power output that is not found in horizontal axis wind turbines. The long blades of the vertical axis wind turbine causes a

natural frequency of vibration which must be avoided during operation in order not to break down the operation of the turbine.

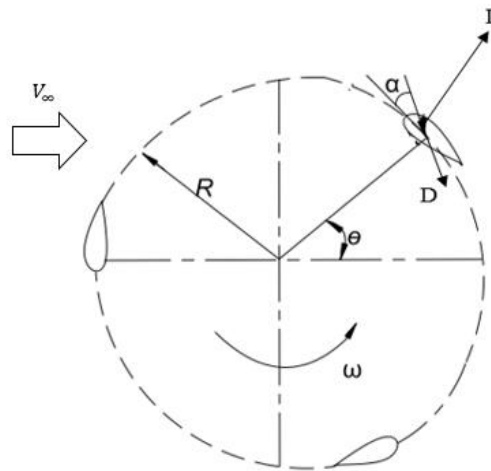


Figure 2.6: Plan view of a VAWT showing the lift  $L$ , drag  $D$ , and angle of attack  $\alpha$ , with freestream velocity  $V_\infty$  (Adopted from Sharpe, 1990).

There have been many designs of VAWTs which have attracted considerable research interest since the early 1970s and they can be broadly divided into two basic types, namely (i) Savonius type, and (ii) Darrieus type. These turbines were first patented in the 20<sup>th</sup> century and were then almost forgotten until the oil crisis of the early 1970s that stimulated a resurgence of interest in a wide range of renewable energy systems. A brief description of these turbines are given in the following sections.

### 2.7.1 Savonius VAWT

The Savonius-type turbine, shown in Figure 2.7, was invented in 1929 (Savonius, 1931). The Savonius rotor is a drag-driven turbine that consists of two half cylinders/cups fixed to a central shaft in opposing directions. Each cylinder/cup catches the wind and so turns the shaft, bringing the opposing cylinder/cup into the flow of the wind. This process is repeated, thus causing further rotation of the shaft, which completes a full rotational cycle. The turning of the shaft produces torque and this is used to drive a pump or small generator (Islam et al., 2008). Despite the fact that these rotors are easy to manufacture, they have a number of limitations. The Savonius rotors are bulky and heavy compared to other types of wind turbines with similar power output.

They require a large area of blade material per unit swept area and are generally associated with a low power coefficient  $C_p$  (Kirke, 1998).

Generally, the typical values of the maximum power coefficient  $C_p$  for other types of VAWT vary between 30 % and 45% (Ushiyama and Nagai, 1988) but the maximum attainable  $C_p$  for Savonius rotor does not exceed 25% according to a number of research studies (see for example Kirke, 1998).

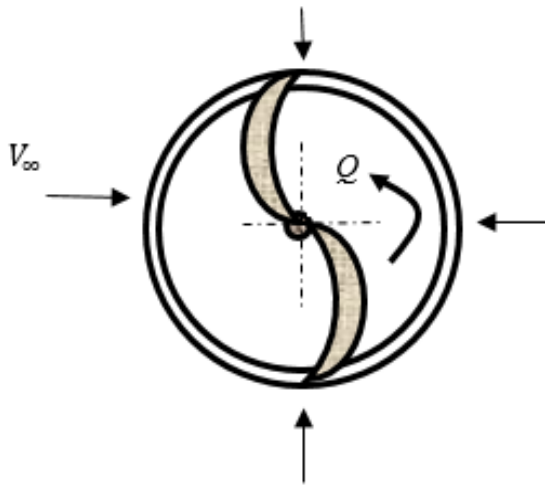


Figure 2.7: Sketch of Savonius-type VAWT. (Adapted from Boss, 2012).

Although some researchers have argued that the Savonius rotor can attain higher efficiency of up to 32%, there is no evidence in the literature to validate this claim. Therefore, it is concluded that the Savonius rotor is not efficient for electricity generation, and thus will not be considered further in this thesis, except as an auxiliary rotor to improve self-starting in a Darrieus rotor.

### 2.7.2 Darrieus VAWT

The modern Darrieus rotors are basically lift-based rotor which were first patented in 1931 (Darrieus, 1931) in the USA. The original design was fitted with curved blades of troposkein shape, which is similar to the shape of a flexible rope when twirled about a vertical axis. This kind of VAWT is also called the “eggbeater” as shown in Figure 2.8. The turbine consists of two or more aerofoil-shaped blades which are attached to a rotating vertical shaft. The wind flow around the aerofoil creates aerodynamic lift and generates torque  $Q$  which pulls the blade along. The troposkein shape, or eggbeater-

type, VAWT is a fixed pitch design which minimises the bending moments in the blade due to centripetal acceleration and were massively deployed in California, USA in the past decades.

However, the blade shape cannot completely eliminate the bending moments caused by the combination of aerodynamic, gravitational and inertial forces acting on the blade. There were also designs of the Darrieus rotor with straight blades (see for example Islam, et al., 2008; Patel and Kevat, 2013).

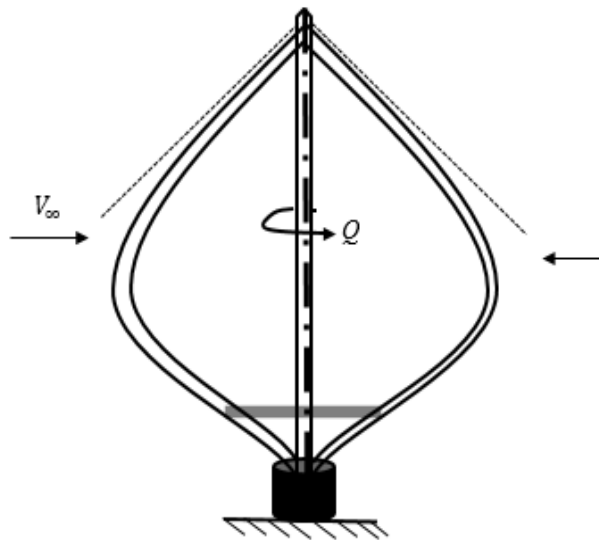


Figure 2.8: Sketch of the curved-blade (or “egg-beater” type) Darrieus VAWT (Adapted from Bos, 2012).

The straight-bladed design is very attractive for small-scale wind turbines due to its simple design. A wide range of experimental testing and theoretical models have been developed for predicting the performance of a straight-blade VAWTs (see for example, Howell et al., 2010; Dominy et al., 2007, Islam et al., 2007). However, whether the blades are curved or straight, the Darrieus VAWTs are haunted by several problems, including the inability to reliably self-start if they are of fixed pitch. Furthermore, the aerodynamics of the Darrieus rotor is very complex, which makes accurate performance prediction difficult. Several ways to improve the performance of a fixed-pitch VAWTs have been suggested in the literature and are reviewed in Section 2.8.

### **2.7.3 Advantages and disadvantages of VAWTs relative to HAWTs**

The advantages and disadvantages of VAWTs relative to the HAWTs are presented in the following sections.

#### **2.7.3.1 Yawning**

The major advantages of the VAWT are their ability to accept wind from any direction. This means that the turbine does not require the orientation of the rotor toward the wind direction. Therefore, complex yaw mechanism, which are inherent in conventional upwind HAWTs is not required. Consequently, there is no power loss when the rotor is adjusted to the wind direction. Yawning is a major problem, particularly with large-scale wind turbine which have large inertia, and in regions where the wind direction changes abruptly, such as in sites with uneven terrain. The absence of a yaw mechanism simplifies the turbine design. According to Hansen et al. (1990), the failures of yaw driven subsystems have been associated as being one of the major causes of HAWT downtime in California. Furthermore, they have revealed that smaller turbines with a free-yaw (passive) system also experience a wide range of issues, such as overloading due to the excessive yaw rate and poor alignment with the wind direction.

#### **2.7.3.2 Power transmission to the ground level and reduction of mechanical noise**

VAWTs are well suitable to drive vertical transmission shafts to the ground level so the drive train can be located at or below the ground level for ease of installation and maintenance, and where sound insulation can easily be fitted to minimise noise in the environment. In the case of a HAWTs, a bevel gear could drive a vertical shaft to the ground, but this could add to the overall cost of the turbine and this is rarely done in practice. However, there are a few exceptions. Clausen et al. (1992) described a HAWT with a bevel gear drive to a generator mounted with its shaft at the top of the tower to avoid slip rings (Kirke, 1998). Using these configurations, the reaction torque emanating from the vertical shaft tend to yaw the rotor out of the wind, thus necessitating a larger tail or a stronger yaw mechanism.

### **2.7.3.3 Blade design and manufacture**

One of the design requirements of a HAWTs is that it needs taper and twist before it can be manufactured. This complicates the shape of the turbine. If for instance the blades are to be made from fibreglass, the most common material, expensive machining operations are required to produce the original plug for the mould. However, for the case of VAWTs, the blades are untwisted and may be of uniform cross-section if the aspect ratio is large, thus making them easy to manufacture.

### **2.7.3.4 Aerodynamic noise**

Generally, the VAWTs tend to generate low aerodynamic noise because they operate at low tip speed ratios  $\lambda$  than do the HAWTs. As more small-scale wind turbines are being produced in recent years for various applications, noise is emerging as one of the major objections to wind turbine utilisation and so this point may be of important research interest. Although the HAWTs could be designed to operate at low tip speed ratios  $\lambda$  in order to improve the aerodynamic design of the blades in reducing the noise level.

### **2.7.3.5 Self-starting**

HAWTs tend to self-start under no load conditions, although some HAWTs have been reported as having starting difficulties when coupled to a load. Conversely, the Darrieus-type VAWTs may fail to self-start even with no load conditions, depending on the characteristics of the design parameters such as the aerofoil section and the range of Reynolds number in which they operates. This is one of the major limitations of the VAWT and is partly addressed in this thesis.

A number of studies have compared the VAWTs and HAWTs technologies to determine which is superior in terms of overall performance. The results are inconclusive-while the cost of energy for a HAWT may be less than that of a VAWT at a site with high positive wind shear and a prevailing wind direction, the cost of energy for a VAWT may be less at a site with low or negative wind shear or no prevailing wind direction. Furthermore, there are apparently not sufficient data in the public domain to address this question. FlowWind Cooperation in California, USA is the only company operating a significant



number of VAWTs, and these machines have been in operation for over 3 decades. Thus, comparing these turbines with newer HAWTs will not be a fair comparison, even if the HAWTs were operating in close proximity to the FlowWind turbines, which of course is not the case. Even if the VAWTs tends to produce less energy per unit swept area, if the cost of building them are cheaper, as claimed by FlowWind (Milborrow, 1995), they may produce a lower cost of energy. Each of these turbine models have strengths and weaknesses, and neither one is a clear winner in all situations.

#### **2.7.4 Vertical axis wind turbine design parameters**

The design parameters of a VAWT must be considered in terms of their influence on the overall performance, self-starting and other attributes as discussed in Section 2.7.3. The design parameters for a Darrieus VAWT performance are reviewed in the following sections.

##### **2.7.4.1 Number of blades**

The amount of power extracted by a wind turbine is strongly dependent on the wind velocity  $V$  and the swept area  $A$ . Wind turbines can function efficiently with a single blade, but a counterweight would be required to balance the mass of the blade and this counterweight would generate parasitic drag. Furthermore, in a single blade configuration, forward torque,  $Q$  is not produced at all blade positions and so a single blade turbine will not produce the necessary torque required for self-starting. Thus, a single bladed turbine is of no interest to this thesis. Although a number of designs have been implemented with two blades, three blades offer some distinctive advantages for VAWTs in that cyclic variations due to the aerodynamic forces on the blades are significantly reduced. The cyclic variations are not a major problem with the large-scale wind turbines since the 300 kW rated capacity VAWTs manufactured by Heidelberg Motor and the 100 kW rated capacity VAWT manufactured by VAWT Ltd in the UK have two blades. However, a number of studies have reported alarming shaking of the towers of small-scale VAWTs at certain operating conditions (see for example Storer, 1981 and Crookes, 1985). Islam et al. (2008) investigated the effects of the number of blades on the performance of small VAWTs. The results show that favourable load variations on the wind turbine may be achieved with more than three blades

although that will mean a higher manufacturing cost of the blades. Samaraweera et al. (2013) developed a theoretical model based on the momentum theory for small-scale wind turbines in stand-alone applications. They investigated the effects of the number of blades on the VAWT performance. It was found that an increase in the number of blades resulted in a significant improvement in the power coefficient of the turbine.

The other reason that influences the choice of number of blades is aesthetics. It is generally accepted that three-bladed turbines are less virtually disturbing than the one or two bladed designs. Modern VAWTs for small-scale applications normally contain three blades, which is an optimum number of blades (Hameed and Afaq, 2012).

Based on the above discussion, a three bladed design will be considered in this thesis.

#### **2.7.4.2 Flow Curvature Effects and chord to radius ratio ( $c/r$ )**

Performance prediction of a VAWT with blades of a given aerofoil section is complicated in that a blade moving in a curvilinear path behaves differently from the same blade moving in a straight line. Darrieus VAWTs operate in a circular motion and thereby encounter flow curvature if the chord/radius ( $c/r$ ) is high. This characteristic significantly affects the performance of the turbine (Pawsey, 2002; Migliore et al., 1980). Furthermore, at high tip speed ratios  $\lambda$ , the effect of the flow curvature increases (Mandal and Burton, 1994; Hirsch and Mandal, 1984). These aerodynamic challenges complicate the modelling of a VAWT.

#### **2.7.4.3 Solidity**

The solidity  $\sigma$  of a wind turbine is a measure of the ratio of the blade platform area  $A_b$  to the turbine swept area  $A_t$ . For a straight bladed VAWT, the most popular definition of solidity  $\sigma$  is given as follows:

$$\sigma = Nc/r \tag{2.27}$$

where  $N$  the number of blades is,  $c$  is the chord length and  $r$  is the radius of the blade.

This definition implies that the solidity of a wind turbine is a function of the number of blades and the size of the chord length, assuming that the rotor radius is held constant.

There is no clear definition of “high”, “medium” or “low” solidity, but certain types of VAWTs fall into one or other group. The Savonius rotor and the traditional fan windmill are good examples of high solidity rotors, that is, the blade area covers most or all of the swept area of the blade. As a general rule, high solidity rotors tend to operate at low  $\lambda$ , produce high starting torques and require more material but they are of less complicated construction than a low solidity rotor. These generalisations are further discussed in detail as follows.

The large-scale wind turbine technologies use low solidity rotors, primarily because they do not require as much material and are less expensive to construct per unit of power delivered, but also they have high  $\lambda$  and so require less step-up gearing to drive the generators (Kirke, 1998).

Between the extremes of high solidity ( $\sigma \approx 1$ ) and low solidity ( $\sigma \approx 0.1$ ), straight-blade VAWTs typically operate in the range 0.2 to 0.6 and can best be classified as medium solidity. Because low to medium solidity rotors are far more efficient and economical than the high solidity rotors, they are the logical choice for small-scale VAWTs development.

#### **2.7.4.4 Choice of an aerofoil section**

The selection of an appropriate aerofoil section can significantly improve the aerodynamic performance and self-starting characteristics of a wind turbine. The most commonly used aerofoil for VAWT research are the NACA four digit aerofoils such as NACA 0012, NACA 0015 and NACA 0018. These aerofoils were originally developed in the 1930s for the aircraft industries and have presumably been used for VAWT application due to the availability of their lift, drag and pitching moment coefficients see for example McCroskey (1987), thus making validation of the theoretical predictions easier.

Several studies have examined the choice of aerofoils section for VAWTs applications. For example, Migliorer and Fritschen (1982) investigated the performance of different aerofoil profiles and their effects on Darrieus turbines. They found that the NACA 6-series blades can produce a broader and flatter power curve while the peak power coefficient is comparable to the NACA 4-series. Further, they revealed that the energy yield can be improved by 17 to 27%.

A wide range of aerofoil were proposed in the 1990s by researchers from the Sandia national laboratories, and these aerofoils consists of three sections, namely SAND 0015/47, SAND0018/50, and SAND0021/50 (Klimas, 1984; Berg, 1990). It should be noted that the designation of these aerofoils are similar to those of NACA00xx family. A number was added after a slash to designate an aerofoil that supports laminar flow. They were originally designed to be natural laminar flow (NLF) aerofoils due to the requirement that they should exhibit low drag at their operating range. Although, the geometries of these aerofoils, along with a few performance characteristics were presented by Berg (1990), but no comprehensive information on their coordinates and performance are available in the public domain. On the other hand, Islam et al. (2007) investigated the performance of symmetrical and asymmetrical aerofoils on a VAWTs. They reported that the asymmetrical aerofoils (cambered) are superior to the conventional symmetrical NACA sections.

#### **2.7.4.4.1 Aerofoil performance data**

Aerofoil performance data required for small-scale VAWT applications is significantly different from those for large-scale applications. Since the blade is usually small and has to operate with a low cut in wind speed, the Reynolds number that it encounters are comparatively low. Furthermore, the small-scale turbines encounters a high incidence angle than any other wind turbine. For example, the horizontal-axis wind turbine blades experience incidence angles in the range  $0 \leq \theta \leq 180$ . On the other hand, the Darrieus wind turbine experiences all possible angles of incidence. At very low tip speed ratio  $\lambda$  the blade operates in a complete full cycle that ranges from  $0 \leq \theta \leq 360$  which reduces as the tip speed ratio  $\lambda$  increases.

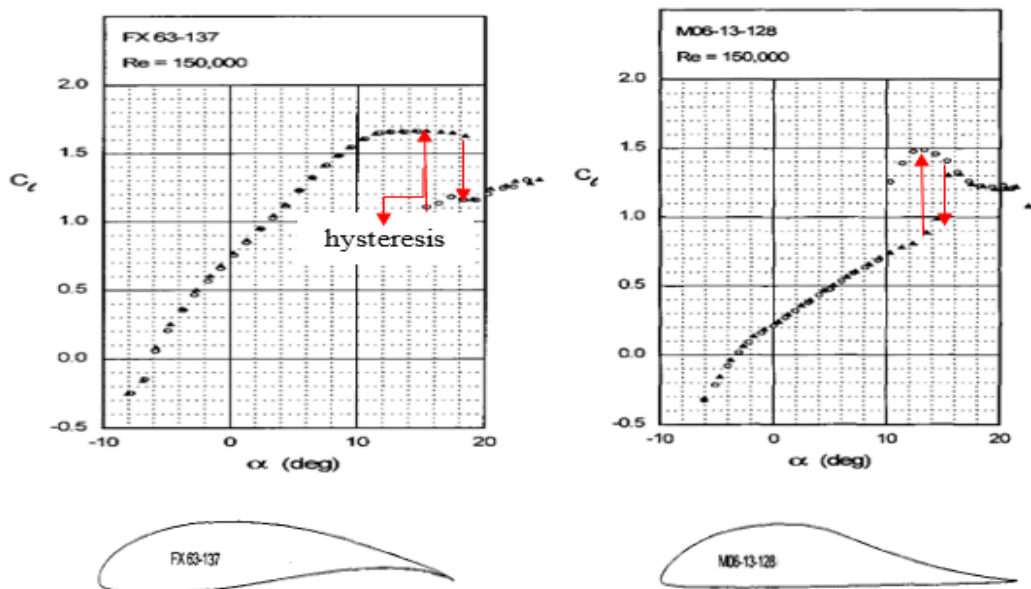
A comprehensive review of aerofoil performance data is conducted in this section. Special attention is focussed on the low-Reynolds aerofoils and high angle of attack test conditions in which the small-scale wind turbine operates.

#### **2.7.4.4.2 Low-Reynolds number performance tests**

One of the most comprehensive and reliable experimental data for use in low-speed aerofoil aerodynamics studies is that provided by the UIUC Applied

Aerodynamics Group by Selig et al. (1995). A wide range of aerofoil tests at low Reynolds number show that flow over an aerofoil is associated with laminar separation bubble. The presence of this separation causes a degradation in the aerofoil performance and ultimately affects its ability to reliably self-start.

The degradation is strongly dependent on two main factors, namely the Reynolds number and the geometry of the aerofoil section. According to the experimental investigations of Selig et al. (1995), the lift curve of most aerofoils does not follow a linear pattern and the slope is often lower than  $2\pi$  (which indicates that the increase in the lift force with respect to the incidence angle reduces) if the Reynolds number is low, normally less than 100,000. The hysteresis<sup>2</sup> behaviour at around the stall angle is strongly influenced by the geometry of the aerofoil. For example, while the FX 63-137 aerofoil section shows a hysteresis behaviour, the NACA 009 and SD8020 did not (Selig et al., 1995). On the other hand, high lift profiles, such as the M6-13-128, which has a concave pressure distribution exhibited a longer separation bubble than the aerofoil sections that use a convex pressure distribution. A stronger separation bubble is expected for aerofoil sections with a concave recovery distribution (see Figure 2.9).



<sup>2</sup> Hysteresis is an aerofoil aerodynamic characteristics that depends on the sense of change of the aerofoil angle of attack, near the aerofoil stall angle.

Figure 2.9: The effect of the laminar separation bubble on the hysteresis behaviour of different aerofoils (adapted from Selig et al., 1995).

#### 2.7.4.4.3 Aerofoil performance tests at high angles of attack

Small wind turbines usually encounter a high angle of attack during start-up. However, previous studies have been mostly focussed on the stall angle of the blades (see for example Abott et al., 1959; Selig et al., 1995).

Sheldahl and Klimas (1980) presented comprehensive experimental data for several NACA symmetric aerofoils for use in VAWT aerodynamic studies. Their data were broader in scope than those encountered for aircraft applications. They studied the NACA profile blades between  $0^\circ$  to  $180^\circ$  angles of attack, and the data for both increasing and decreasing incidence were taken to show comparisons of the aerofoils performance. These tests were conducted at the same Reynolds number that were usually encountered by the large scale wind turbine and it ranges between 400,000 and 9000,000. One classic example of such a test was performed on NACA 0012 and can be visualised in Figure 2.10. From this test, the aerodynamic lift curve exhibits a second-lift- peak behaviour at an angle of attack of about  $45^\circ$  while the maximum drag occurs at about  $90^\circ$ .

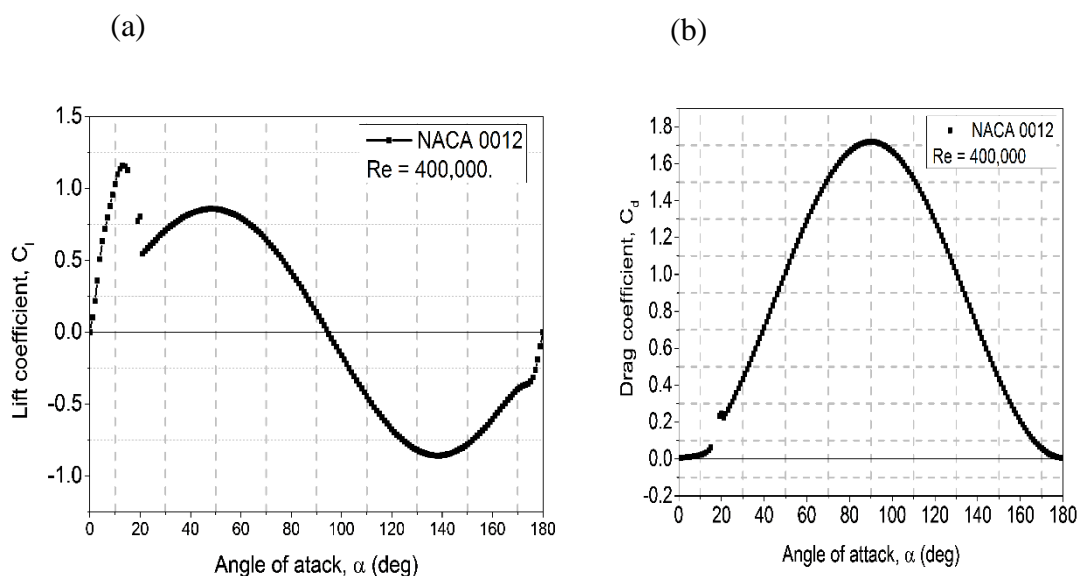


Figure 2.10: (a) Lift, and (b) drag coefficients of NACA 0012 as a function of the angles of attack (Adapted from Sheldahl and Klimas, 1981).

Timmer and van Rooij (2001) performed a test on two dedicated aerofoils for VAWTs applications, namely DU-96-W-180 and DU-97-W-300. The aerofoils were tested up to 90 degrees angles of attack at Reynolds of 700,000. Their results revealed that aerofoils exhibit different characteristics and that fully stalled and thicker aerofoils generate higher lift (see Figure 2.11).

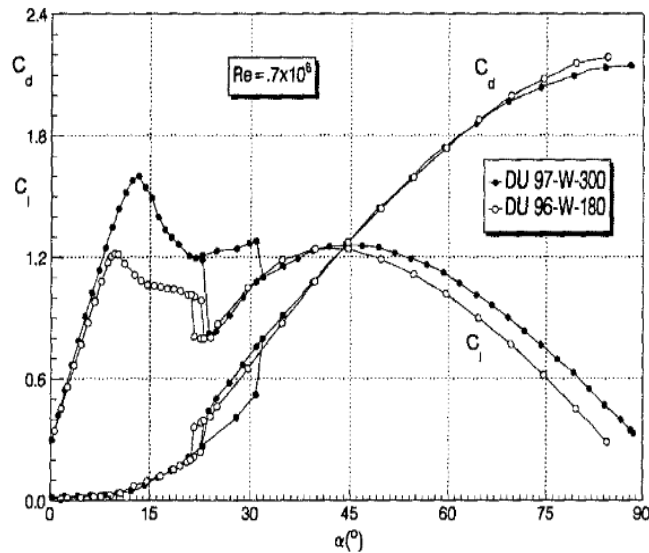


Figure 2.11: Lift and drag coefficients as a function of the angle of attack of two DU aerofoil sections (reproduced from Timmer, 2001).

#### 2.7.4.4.4 Estimation of Aerofoil performance data at high angle of attack

As noted above, small wind turbines operate at high inflow angles (360° range of angle of incidence), and since most of the available aerofoil polars (lift, drag and moment coefficients) are usually limited to small and medium angles of incidence (e.g. -20° to 20° angle of attack), estimation often has to be applied in order to extend to a wider range of angles of attack in which the small wind turbines operate. A wide range of approaches are available in the literature. Approaches based on the potential flow theory (such as those used in XFOIL) are only able to include viscous effects by semi-empirical models. Wind tunnel measurements are also complicated, due to the high blockage in the measurement section for high angles of attack. One possible way to overcome these complexities is to use aerofoil characteristics for normal operations and extrapolate them using the flat plate theory. This approach assumes that the aerofoil behave like a flat plate. The method is known as the Viterna method

(Viterna and Corrigan, 1981). However, experimental tests using high angles of attack on some aerofoils showed that aerofoils exhibit different characteristics even at stall regions (see for example, Ostowari and Naik, 1984; Timmer and van Rooij, 2001), thus casting doubts on the validity of the Viterna method. Furthermore, Spera (2008) developed a model to extract the lift and drag coefficients of both stalled and unstalled aerofoils. Using this model, he analysed a wide range of aerofoils specifically for lift based operations and wind tunnel test at high angles of attack in a Reynolds number that ranges from 250,000 to 2,000,000 in order to obtain the aerodynamic coefficients of the aerofoils. Although his results provide a useful starting point for analysis of small-scale wind turbine, it is questionable whether such analysis can be applied to other aerofoils or in cases where the Reynolds number fall outside this range, particularly at lower Reynolds number.

The above discussion indicates that although, a vast amount of experimental data is available, not all of them meet the required range of tests condition to fully investigate small-scale wind turbine performance and self-starting. Thus, further investigations on wind turbine aerofoils at suitable operating conditions are required.

## **2.8 Review of self-starting**

As noted in Section 1.4, the Darrieus VAWTs typically produce very little starting torque when conventional aerofoil sections are used and even when the turbine begins to move they do not accelerate beyond a range of tip speed ratios ( $0.7 < \lambda < 2.7$ ) where the power delivered by the turbine is significantly reduced (see Figure 1.2).

Self-starting is not a major concern in the large-scale wind industry where most research attention has been focused in recent years. This is because the large-scale wind turbines usually have a larger chord and higher Reynolds number than the small-scale turbines. Most aerofoil sections perform poorly at the range of Reynolds number encountered by small-scale VAWTs and the performance increases significantly when the chord length is increased. The vast majority of the previous research has been focused on the development of mathematical models for predicting the performance of VAWTs and these



models have been compared with the available experimental results, but little attention has been given on the problem of self-starting. Now the literature relating to self-starting is reviewed in the following subsections.

### 2.8.2 Reynolds number effects

The Reynolds number defined in Eqn. (2.28) has two main implications for aerofoil performance.

$$R_e = \frac{UL}{\nu} = \frac{\rho UL}{\mu} \quad (2.28)$$

where  $\nu = \frac{\mu}{\rho}$  is the kinematic viscosity,  $l$  is the length scale.

Firstly, the location of the transition point on the aerofoil moves forward when the Reynolds number is increased and secondly, the boundary layer thickness steadily increases at higher Reynolds number. This implies that a boundary layer can persist in stronger adverse pressure gradients before the onset of separation.

Generally, aerofoil performance decreases at low Reynolds number which considering the direct relationship with the wind speed is particularly relevant for self-starting. The influence of Reynolds number on the aerodynamics of NACA symmetric aerofoil can be as much as 60% (Jacobs and Sherman, 1937).

An important factor for small-scale wind turbine design is the low Reynolds range ( $<10^6$ ) in which they operate. Most studies in aerodynamics are undertaken for aircraft applications in which the Reynolds number lies above  $3 \times 10^6$ . Experimental data in this range of Reynolds number ( $Re=3 \times 10^6$ ) are not publicly available.

Several studies have examined the influence of Reynolds number on self-starting, e.g. Watson (1979) used a single streamtube model with NACA aerofoil data at  $Re = 40,000$ , and reported that the turbine did not self-start without a Savonius auxiliary rotor. Worasinchai et al. (2011) investigated the performance of several aerofoil sections at different Reynolds numbers and their results show that aerofoils are very sensitive to changing operating conditions. The lift produced by each of the aerofoil sections decreases significantly at low Reynolds number which affected the starting performance of the aerofoils.

From the above discussion, it is clear that one of the hindrance to a reliable self-starting is perhaps due to the performance degradation resulting from early laminar separation of the aerofoils at low Reynolds numbers which can potentially force the rotor to stall at most operating conditions. A situation where the vast portion of the blade trajectories reside in the post stall region and generates a net negative power coefficient or torque.

### 2.8.3. Savonius auxiliary rotor

Self-starting may be improved by a hybrid combination of Darrieus-Savonius rotor (see Figure 2.12). The combination of the two turbines is aimed at boosting the performance of the Darrieus rotor at low operating conditions. Several studies have examined the subject of this combination. For example, Gavalda et al. (1990) combined a Savonius rotor to a Darrieus rotor at a hub height 20 cm and with diameters 13 and 40 cm, respectively. Their result showed significant improvement in the starting torque of the VAWT. However, the peak power coefficient ( $C_p$ ) was significantly reduced due to the secondary rotor (Savonius rotor). This is because the outmost section of the rotor blades begin to produce opposing torque at tip speed ratio  $\lambda > 1$ . To forestall this occurrence, and increase the peak power performance, the Savonious rotor may either be disconnected after start-up, or kept from attaining a certain maximum value.

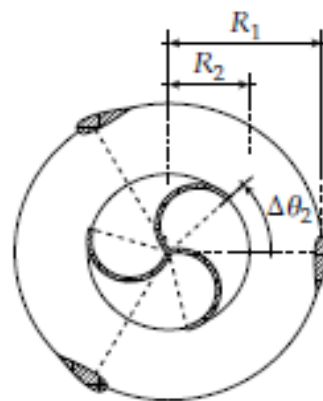


Figure 2.12: Schematic of a Darrieus-Savonius wind turbine where the two rotors have a phase difference of  $\Delta\theta_2$  (reproduced from Bos, 2012).

To achieve maximum efficiency of the hybrid structure, the Savonius rotor can be sized with reference to Figure 2.10 according to the following relations:

$$R_2 \leq R_1 \frac{\lambda_{2,rated}}{\lambda_{1,rated}} \quad (2.29)$$

in which  $\lambda_1$  and  $\lambda_2$  are the rated tip speed ratios of the primary rotor (Darrieus) and the secondary rotor (Savonius), respectively.

Since this equation limits the diameter of the secondary rotor, the only option to increase the torque output is to increase the height of the rotor. Wakui et al. (2005) performed an investigation of two different hybrid configurations of wind turbine where a Savonius rotor was linked with a troposkien-shaped Darrieus rotor. The rotors were analysed using the momentum model and tested in a wind tunnel. In the first case, where the secondary rotor was held inside the primary rotor, the turbine was able to reliably self-start but the performance was limited due to the interference from both rotors. In the second case, the two rotors are separated and still contribute to the total energy produced. Unfortunately, this separation added more complication to the design and required a thicker shaft to support the structure. Clearly, this will increase the moment of inertia, thus requiring more torque to bring the turbine to the operating speed at start-up.

From this discussion, it became clear that a Savonius auxiliary rotor can add a significant amount of torque at low speeds and consequently aids in the self-starting of a fixed-pitch turbine. However, there is a penalty to pay for this configuration. Firstly, adding an extra structure will ultimately increase the overall cost which will not be economical for small-scale wind turbines. Secondly, the tower will have to be stronger and therefore there will be a huge impact on the appearance of the configuration.

#### **2.8.4 Blade thickness**

The choice of suitable aerofoil section is vitally important for both the start-up and optimum performance of a VAWTs. Thick aerofoils tend to be more resistant to bending and can be used in high wind speeds. Generally, they have good stalling characteristics as they tend to delay stall and generate more torque over a wider operating range. According to Jacobs and Sherman (1937), aerofoils of at least 18% thickness tend to produce more lift at lower Reynolds number. An increase in thickness will ultimately increase the aerofoil drag which in turn increases the operating range of the turbine.

The effects of aerofoil thickness on self-starting of a Darrieus VAWT have been examined by many studies, for example, Kirke and Lazauskas (1991) investigated the effects of different blade sections on the aerodynamic performance using the NACA 00xx aerofoil profiles. Their results show that increasing the thickness leads to an increase in the performance of the VAWT at low tip speed ratios, although the analysis was performed at a constant Reynolds number of 200,000.

One major drawback of thicker aerofoils is the increase in the drag profile, which tends to be more significant at low angles of attack. In general, increasing the thickness beyond about 18% usually results in a loss in efficiency (Bos, 2012). This leads to a trade-off: thick aerofoil sections tend to increase the operating range of the angles of attack, thus resulting to a better performance at low  $\lambda$ , but this will lead to a higher zero-lift drag coefficient which will ultimately affect the performance at high tip speed ratios.

Furthermore, thicker aerofoil profiles tend to have higher suction peak followed by a strong adverse pressure gradient than the thin profiles. This is why thick profiles are significantly affected by bubble drag at low Reynolds numbers.

From this discussions, it is clear that the thick aerofoil sections tend to generate more lift and possess better stalling characteristics than the thin sections and thus could potentially be an ideal candidate to improve self-starting at low tip speed ratios  $\lambda$ . However, they tend to have a wider drag profile as well the potential to cause separation at the upper surface of the aerofoil, a term known as laminar separation bubbles<sup>3</sup>.

### **2.8.5 Cambered blades**

Early designs and development of wind turbines in the 1970s mostly used blades of symmetrical aerofoils from the US National Advisory Committee on Aeronautics (NACA), such as NACA 0012, NACA 0015, NCA 0018 sections. Although, these blade sections appear logical at first, it was later realised that they were unsuitable for self-starting applications. Cambered and specially-

---

<sup>3</sup> Laminar separation bubble is a phenomenon which occur at low Reynolds number and is caused by a strong adverse pressure gradient (pressure rise along the surface of the aerofoil), which makes the laminar bubble layer to separate from the upper surface of the aerofoil.

made aerofoils have been strongly advocated in the literature as an avenue to improve self-starting performance. These sections generally exhibit superior aerodynamic performance when compared with the conventional NACA symmetrical profiles. The net advantages of cambered aerofoils over the NACA symmetrical profiles are summarised as follows:

- (i) They possess high lift at low Reynolds numbers. The cambered blade sections produce higher lift at low Reynolds numbers than the symmetrical sections. With cambered aerofoils, the laminar boundary layer at low Reynolds numbers are more stable and resistant to transition. Also, the turbulent boundary layer for cambered aerofoils is weak and is able to tolerate only mild adverse pressure gradients (APGs). Therefore, the cambered aerofoils produce lift from high pressure on the lower surface of the aerofoil. In addition, they are less prone to separation, which causes the blade to stall.
- (ii) They exhibit larger stall angles. The stall angles of cambered aerofoil sections are higher than those of the symmetrical ones.
- (iii) Cambered aerofoils produce large negative pitching moments, unlike the symmetrical profiles. The large negative pitching moments indicate better aerodynamic performance (Kato et al., 1981). Despite these advantages, Cambered profiles perform poorly at negative angles of attack. Since a blade spends an equal amount of time at both the positive and negative incidence angles, the choice for symmetrical aerofoils appear more logical at first. However, because of the induction velocities, the apparent wind speed is significantly higher at the upwind pass of the blade ( $0^\circ \leq \theta \leq 180^\circ$ ), and since the power produced by a wind turbine is directly proportional to the cube of the wind velocity ( $P \propto V^3$ ), the higher performance of a cambered aerofoil might outweigh the large drag produced at the downwind pass.

At the start-up operation of small wind turbines, the performance of cambered and symmetrical blade sections is generally very prominent and some sections, specifically made to operate at low Reynolds number, have the ability to reliably self-start. This was investigated by Kirke (1998) by comparing

the performance of a NACA 0015 section with an S1210 blade<sup>4</sup> profile. However, when the  $Re$  is increased, this effect reduces and this results in a significant decrease in the performance of the turbine. This was investigated by Islam et al. (2007), who predicted the aerodynamic performance of five different cambered aerofoils in comparison with a symmetrical NACA 0015 section. The investigation revealed that, although the cambered aerofoil exhibits better aerodynamic performance during start up, the benefits of a thin and highly cambered aerofoil profile such as those of S1210, completely disappear at a later stage.

Kirke (1998) performed an evaluation of the fixed-pitch straight blade vertical axis wind turbine (SB-VAWT) and established that self-starting difficulty can be eliminated if the aerofoil possesses high lift and low drag at a Reynolds number between 80,000 and 150,000. Unfortunately, the conventionally used symmetrical profiles exhibit a contrary behaviour in this range of Reynolds number and are not capable of self-starting (Islam, Ting and Fartaj, 2007). However, cambered aerofoils with thin sections can generate a considerable amount of lift in the same range of Reynolds number which could be utilized to increase the self-starting performance of SB-VAWT. Based on this information, Kirke (1998) investigated the performance of a cambered fixed-pitch VAWT using computer simulations. The results from his simulations revealed an improved self-starting performance using cambered blades.

Despite the clear benefit of using cambered blades to enhance the self-starting performance, they have one inherent weakness, namely the force produced by a cambered blade tends to fluctuate frequently during operation, and this can induce unnecessary vibrations.

A number of studies have investigated the benefits of changing the blade camber, e.g. Baker (1983) studied the reason behind the lack of self-starting for a low solidity fixed-pitch straight-bladed VAWT by comparing the performance of a NACA 0012 blade with a Gö 420 and Worthmann FX63-137. The results showed that the Gö 420 possesses a superior performance compared to the NACA 0012 and FX63-137. Baker argued that the poor

---

<sup>4</sup> The aerofoil profile (S1210) was originally designed for aircraft propulsion particularly in a heavy lift flight completion (Selig, 1995).

performance of the FX63-137 could be a result of its large camber which can be unfavorable to its performance. Baker concluded that for optimum power extraction, the use of cambered aerofoils was favourable because of their profile which could increase the upstream power performance where most of the power generated by a VAWTs are produced. He argued that such aerofoils could help in self-starting because cambering enhances the performance curve to lower tip speed ratios. McIntosh (2008) performed a parametric study of thicker and cambered aerofoils using a method based on the vortex model. The study revealed that the thicker aerofoils enhance the maximum power coefficient. The study concluded that, thicker aerofoils exhibit better performance, especially in gusty conditions than cambered aerofoils.

Islam, Ting, and Fartaj (2007) noted that a large camber, or lack of it, will affect the initial start-up performance and ultimately hinder the ability of the turbine to go beyond the rated tip speed ratios. Tilman (2011) presented an improvement to VAWTs blades to aid the self-starting of an H-rotor VAWT using different aerofoil sections. The author concluded that a VAWT can achieve self-start through the use of cambered aerofoils at the low Reynolds numbers that are usually encountered by small-scale wind turbines.

More recently, Danao et al. (2012) presented results on the effects of thickness and camber on the VAWT performance. The results show that thinner symmetric sections produces higher maximum power coefficient while the cambered sections improve the performance of thick aerofoils.

Kunz and Kroo (2000) argued that the aft shift of maximum camber causes a less severe reduction in the lift past the unstalled region, higher attainable lift coefficients and high lift-drag ratios. They revealed that the aft cambered sections exhibit separation at lower angles of attack due to the deep stall adverse pressure gradient near the trailing edge, and the extent of the separation grows very slowly as the angle of attack increases. However, an experimental investigation by Selig et al. (1996) showed that the performance of cambered aerofoils decreases with an increase in the Reynolds numbers or higher cambers.

Moreover, Classens (2006) designed an aerofoil designated as DU 06-W-200 to comply with the Delft University of Technology aerofoil designation system. The main aim of his design was to investigate the aerodynamics of a VAWT

and to improve the NACA 0018 airfoil for the small-scale wind turbine application. However, the final result of his work produced a specially made cambered airfoil which is 20% thicker and contains 0.8% camber (Classens 2006). Classens compared the performance of the new airfoil with the conventional NACA 0018 and made the following conclusions: (i) The 20% thickness and the added 0.8% camber significantly increased the strength and performance of the blade with respect to a non-cambered airfoil; (ii) The DU 06-W-200 exhibited superior performance at positive angles of attack. However, at negative angles of attack, the performance of the DU 06-W-200 is the same as that of the NACA 0018; (iii) The DU 06-W-200 shows higher maximum lift coefficients for positive angles of attack, thus resulting in a wider drag bucket; (iv) The DU 06-W-200 is resistant to laminar flow separation and does not stall at low Reynolds numbers, and this is in contrast to the NACA 0018.

From these studies, one can argue that the use of cambered aerofoils offer a better prospect to alleviate the problem of self-starting, provided that the camber is not too large. However, cambered profiles tend to decrease the tangential force at a small angle of attack when symmetrical aerofoil are employed.

### **2.8.6 Rotor solidity**

Increasing the rotor solidity is a known strategy to increase the output torque and by extension the self-starting performance of a wind turbine. The rotor solidity,  $\sigma$ , given in Eqn. (2.27), describes what fraction of the swept area that the turbine sweeps through. A low rotor solidity implies that the blade has less area interface with the wind and therefore it has to depend on a high tip speed  $\lambda$  to cover the same swept area, thus producing less torque. Conversely, a rotor with a high solidity  $\sigma$  operate at a low tip speed ratios  $\lambda$  and produces more torque. Thus, machines requiring a high starting torque, such as pumps, are usually connected to a high solidity rotor. However, for electricity generation, low to medium solidity is often the preferred choice since a higher solidity reduces the difference between the rotor speed and the electrical frequency (Bos, 2012).

Therefore, according to the solidity definition in Eqn. (2.27), two strategies of increasing the rotor solidity of a turbine with the radius  $R$  are: (i) to increase



the number of blades, and (ii) increase the chord length. However, as noted in Section 2.7, departing from a three bladed design can be disadvantageous due to a number of reasons. Firstly, increasing the number of blades to be more than three will ultimately increase the overall cost of the turbine, the weight and the inertia. Secondly, an even number of blades will increase the cyclic variation because the aerodynamic forces generated by opposing blades will tend to peak in the same direction and phase. Finally, three bladed turbines are generally more aesthetically pleasing than one or an even number of blades (Stankovic et al., 2009).

On the other hand, increasing the chord length of the aerofoil will result in a corresponding increase in the blade weight. Furthermore, the Reynolds number increases when the chord length  $c$  increases, thus resulting to an improved performance of the aerofoil. However, when the blade is operating at a higher tip speed ratios  $\lambda$ , then the gain of having a larger Reynolds number due to a large chord can easily be lost when the blades are operating at a low tip speed ratio.

Several studies have examined the influence of rotor solidity on the VAWT performance, for example, Musgrove and May (1979) investigated the effect of rotor solidity on a VAWT. They revealed that a VAWT with a rotor solidity  $\sigma = 0.6$  and aspect ratio  $AR = 4$  produced large torque through the dead band, and this is unlike an earlier design with  $\sigma = 0.17$  and high aspect ratio  $AR$ . They attributed the improved self-starting performance of the later turbine to the increase in the rotor solidity and decrease in the aspect ratio.

Kirke (1998) investigated the effects of rotor solidities on the aerodynamic performance of an aerofoil and concluded that very high solidities are not desirable as they produce low power coefficients and a very narrow performance curve. Consul et al. (2009) studied the influence of solidity by varying the blade number on a tidal turbine using two and four blades. The results show that the power coefficient  $C_p$  increases from 0.43 for a solidity  $\sigma = 0.019$  to 0.53 for a solidity  $\sigma = 0.038$ . There was also a peak shift from the tip speed ratio  $\lambda = 6$  to  $\lambda = 4$  as the solidity  $\sigma$  increases. The authors argued that four bladed turbines cause larger impedance, which results in a reduction in the streamwise flow velocity between the lower and higher  $\sigma$  configurations. Lower flow velocities consequently reduce the maximum angle of incidence

perceived by the blades. This has significant effect on the blades stalling. At high tip speed ratios  $\lambda$ , the low incidence angle limits the power take off and this results in a lower power performance.

The effect of solidity was also examined by McIntosh (2008) using the free vortex model. His results revealed that the maximum power coefficient was attained for a medium value of solidity  $\sigma$  between 0.2-0.25 and a sharp drop in the maximum  $C_p$  for  $\sigma$  less than about 0.2. The author argued that the low  $\sigma$  produces a soft power curve with flat tops, low gradients and higher optimum tip speed ratios  $\lambda$ , while high solidity  $\sigma$  generate narrower power curves with lower optimum  $\lambda$ . Therefore it follows that the solidity  $\sigma$  dictates the rate between high and low performance turbines.

More recently, Li and Yan (2010) investigated the effects of the static and dynamic performance of solidity  $\sigma$  on straight bladed VAWTs. They argued that, for the static torque performance, increased solidity  $\sigma$  increases the average static torque coefficient in one rotational period of the VAWT, which could enhance the starting performance of the VAWT. For the rotational condition, they stated that medium solidity achieves maximum power at lower values of the tip speed ratios  $\lambda$ . However, for large values of the tip speed ratios  $\lambda$ , it was observed to decrease the power coefficient substantially. The study concluded that even for the same solidity, the different combinations of blade numbers and the chord affects the power performance of straight bladed turbines. More specifically, Koksai et al. (2004) and Islam et al. (2008) reported that the value of the solidity should be chosen between 0.1 - 0.24 for straight bladed small-scale VAWTs having three or more blades. Furthermore, they concluded that higher solidity turbines potentially affect the flow fields around the straight bladed turbines and thus results in an increase in the power performance but at the same time increases the torque production on the blade.

Clearly, from the above discussion, increasing the solidity will depend on three factors, namely, the number of blades, the chord length and the radius of the turbine. As an added caveat, an increase in the solidity would be more accurately described as an increase in the chord length. If the solidity is increased by reducing the radius rather than increasing the chord length, there is likely to be no significant improvement in the starting torque (Bos, 2012).

### 2.8.7 Leading/Trailing Edge

Another reliable approach to mitigate the problem of self-starting is to use aerofoils with a large leading edge<sup>5</sup> or sharp trailing edge<sup>6</sup>. Aerofoils with larger leading edge radii tend to exhibit higher performance for smaller-scale VAWTs (Islam, Ting, and Fartaj, 2007; Liang et al., 2014). This characteristic enhances the performance of the aerofoils as it tends to increase their lift-drag ratio, particularly at large angles of attack (Liang et al., 2014). However, using thick leading edges at low Reynolds numbers is often associated with high pressure peaks which has the tendency to affect the aerodynamic performance of the turbine. On the other hand, minimum drag coefficients of aerofoils can be reduced by having sharp trailing edges, as reported by Paraschavoui (2002). Moreover, Islam, Ting, and Fartaj (2007) revealed that a sharp trailing edge is desirable for self-starting. However, the manufacturing process of a sharp trailing edge is, in general, difficult and often associated with high costs. The main benefit in considering the increase in trailing edge thickness is that it assists in mitigating blade stall, and thereby resulting in the overall performance improvement of the aerofoils (Ahmed, 2012, Liang et al., 2014).

### 2.8.8 Variable pitch

Straight-bladed Darrieus VAWTs can be fitted with a blade pivot in order to control the variation of the angles of attack and improve the self-starting performance.

A wide range of researchers have proposed the use of a variable pitch VAWTs in order to delay the onset of stall, improve the angle of attack  $\alpha$  and potentially produce sufficient torque for low tip speed ratios  $\lambda$  (see for example Kentfield, 1978; Bayly and Kentfield, 1981, Nahas, 1993; Vanderberg and Dick, 1986, Chougule, 2014). The results from these studies revealed that the variable pitch design are more reliable in terms of self-starting performance than the fixed-pitch design, thus making them a

---

<sup>5</sup> Leading edge refers to a point at the front of the aerofoil that has maximum curvature (minimum radius).

<sup>6</sup> Trailing edge is the point of minimum curvature at the rear of the aerofoil.

particular choice for consideration in this present study. Although, self-starting as an avenue for performance is generally recognised in VAWTs, not much has been done to assess the performance of starting torque at low tip speed ratios.

There are basically two forms of variable pitch VAWTs, namely forced or active variable pitch and passive variable pitch (Lazauskas, 1992). The forced or active variable pitch system uses an external mechanism that forces the blade to pitch in a predetermined pitch regime. This system uses a simple eccentric drive and this results in a sinusoidal pitch variation. Other variations of the active variable pitch system senses the wind velocity, calculates the angle of attack and optimises the pitch angle as a function of the blade azimuthal position. In the following subsections brief reviews of each of the pitch systems are discussed.

#### **2.8.8.1 Active pitch systems**

The active variable pitch design may be defined as those systems in which the blade pitch is changed by means of an external mechanism such as actuators and cams to calculate an appropriate pitch angle regime.

Extensive work was performed on this type of turbine by McConnell (1979) and Meikle (1993) and from these studies it was shown that such a design is highly expensive and complicated which is not justifiable for small-scale decentralised wind turbine applications. A simpler form of the active variable pitch system was implemented in an original patent of a fixed-pitch blade by Darrieus (1931) in which the blades are actuated by means of a pushrods driven by a central cam, which produces a pre-set schedule of pitch variation (see Figure 2.13). Drees (1978) developed a similar design, known as a “Cycloturbine”, with the Pinson Energy Corporation.

The pitch variation is controlled by a central cam and pushrods. A small tail vane was used to orient the cam to the wind direction. Dress (1978) reported an improved self-starting and a high power coefficient of 0.45. Grylls et al. (1978) performed both theoretical and experimental investigation similar to those investigated by Dress. The theoretical analysis was based on the principle of the multiple streamtube model. Both studies revealed one of the shortcomings of such active designs, namely the amplitude of the pitch

variation is controlled by the cam and thus cannot change to suit the tip speed ratio. This deficiency limits the performance of the turbine to a narrow tip speed ratio  $\lambda$  band. High amplitudes ( $\pm 20^\circ$ ) of the pitch variation produces a significant starting torque up to  $\lambda = 1.5$ , which suddenly drops off as the tip speed ratio  $\lambda$  increases.

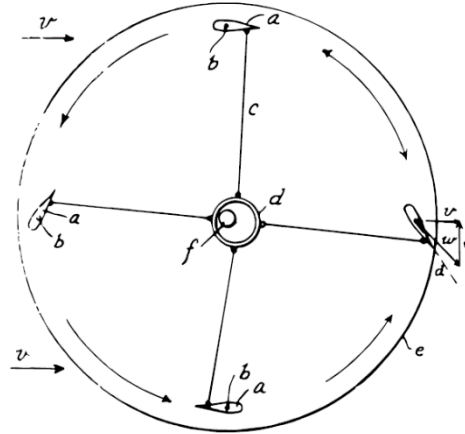


Figure 2.13: Schematic of the Darrieus cam driven design (Darrieus, 1931).

Conversely, a small amplitudes ( $\pm 5^\circ$ ) of the pitch variation produces high turbine efficiency while the starting torque is very low. One way to improve this limitation is to vary the cam profile with the turbine speed, however, to achieve this technically would significantly increase the overall cost of the system.

A further problem of high friction was reported on this design system by Grylls et al. (1978). These problems, along with the increase in the cost and complexity of the active variable-pitch design, are the main reason for the exclusive focus on the passive system in this current study.

### 2.8.8.2 Passive pitch systems

The idea of a passive variable pitch system was first conceived by Sicard (1977) who produced a patent where the blades are allowed to pivot about an axis in the chord line. The blades were balanced in such a way that their centre of mass lies radially outward of the pivot axis when the blade pitch is in a “zero-pitch” position. A schematic of this design is depicted in Figure 2.14.

Sicard (1977) did not mention any stopping mechanism to limit the pitch angle of the blades and so at a stationary position there is nothing to stop the blades

from turning, thus generating no thrust. Moreover, there was no mention of the experimental and theoretical performance of the blade.

Brenneman (1983) developed a similar VAWT to those of Sicard's which he called "inertial" type with an additional stopping mechanism to limit the pitch angle. Brenneman (1983) attached a second embodiment to the design, which he referred to as "elastic type".

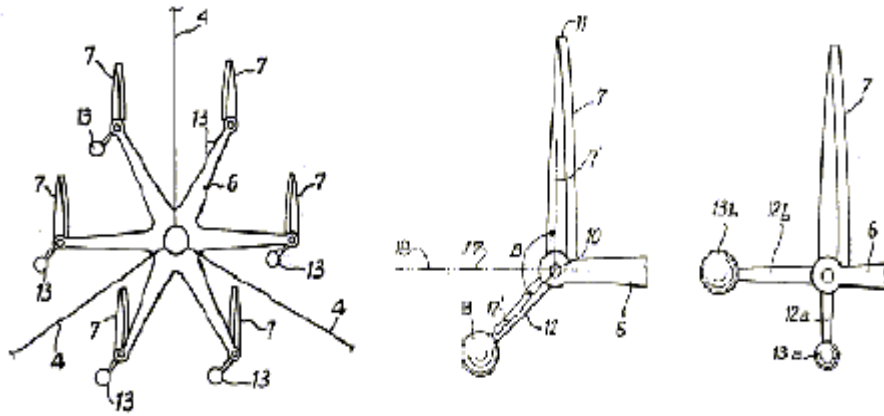


Figure 2.14: A schematic of the design patented by Sicard (1977).

The function of the elastic type is to balance the blades about the pivot axis using a steel rod or wire spring to return the blades to a stationary position as shown in Figure 2.15.

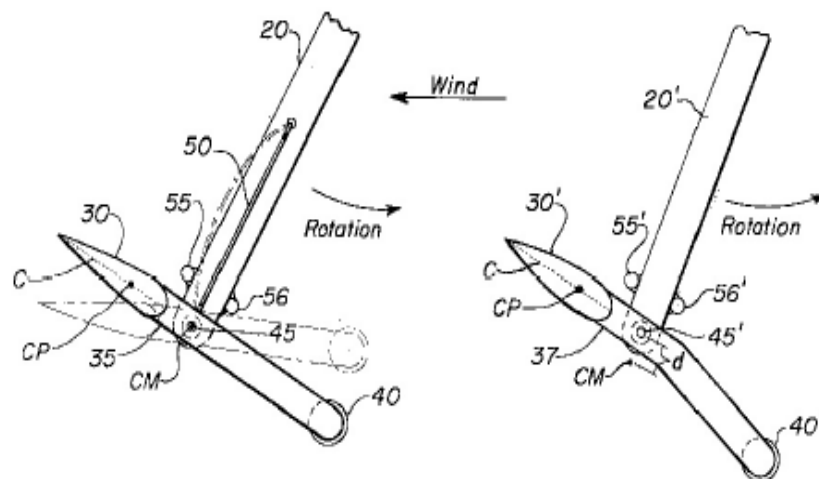


Figure 2.15: Schematics of the elastic (left) and inertial design patents (Reproduced from Brenneman, 1983).

The author claimed that the design is speed limiting since the natural frequency of the blade is fixed by the moment of inertia of the blade and the stiffness of the spring. This implies that when the rotational speed of the turbine exceeds the natural frequency, the blade motion becomes out of phase with the angle of attack variation, thus making the turbine lose thrust. Further, there was no mention of experimental testing on this design in the literature.

Evans (1978) proposed a design of a passive variable pitch in which the blades were pivoted at 1/3 chord location and balanced about the same location. The focus of the design was to pitch the blade in order to reduce the angle of attack and consequently reduce the rate at which the blade stalls. The design is based on the concept of a pitching moment, or the movement of the centre of pressure. Unfortunately, no experimental test data is available in the literature for this design and thus, it is unlikely if this concept will be successful. Furthermore, Evans proposed another design where the blades are allowed to pivot and the blades are interlinked by wires. The design was completed without a counterweight, but the blades mutually cancel out the tendency to flare outwards under the action of a centrifugal force. This means that the blades are not allowed to pitch freely without an external force and even it is unclear whether the pitching regime that was determined by the set of wires would produce an optimum pitch angle.

Another passive variable pitch design was implemented and patented by Liljegren (1984). In the patent shown in Figure 2.16, the blades were pivoted about the centre of mass, which is on the chord of the blade.

The design has two independent masses which regulates the pitch movement. Furthermore, springs were attached to the design that supports the restoring moment of the masses when the rotational speed is low. The aim of the design is to produce a diminishing pitch responses at high rotor speeds as well as to prevent the blade from pitching at running speeds. One major limitation of this design is the lack of experimental data to validate the design, although a similar concept was proposed by Kirke (1998) and it was reported to be largely successful.

Sharp (1982) developed a turbine in which the blades are made to lie radially outward of the pivot axis. The centre of mass on the chord of the balanced

blade is connected via a rocker arm to a hinge at the end of the support arm (see Figure 2.17). Sharp claimed that the design is superior to the one presented by Sicard (1977) because he used a lower moment of inertia which could potentially make the blade to be more responsive and fast moving.

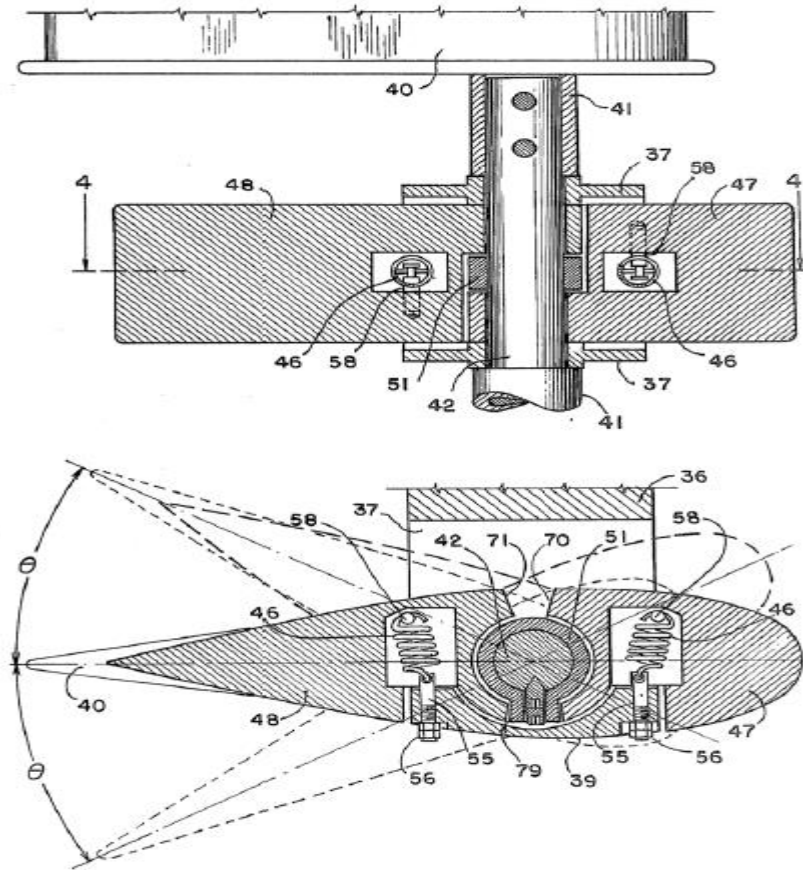


Figure 2.16: Schematic of the Liljegren passive variable pitch design (reproduced from Liljegren, 1984).

The location of the pivot axis off the chord implies that the blade no longer seeks zero angle of attack under a stationary position. The principle of operation of this turbine is much the same as that of Sincard, although Sharp did not present any mathematical analysis to back his claims.

Kirke (1998) performed an extensive evaluation of the self-starting performance of VAWTs as part of his PhD thesis. His work is the most comprehensive survey of previous active and passive variable pitch design found in the literature. Kirke investigated the prospects of variable pitch VAWTs as one of the avenues to improve the self-starting performance inherent in fixed-pitch VAWTs and focussed on a design of a mass stabilised



variable pitch system. His concept is depicted in Figure 2.18. Kirke's design is very similar to that presented by Liljegren (1984), although much simpler in construction and execution.

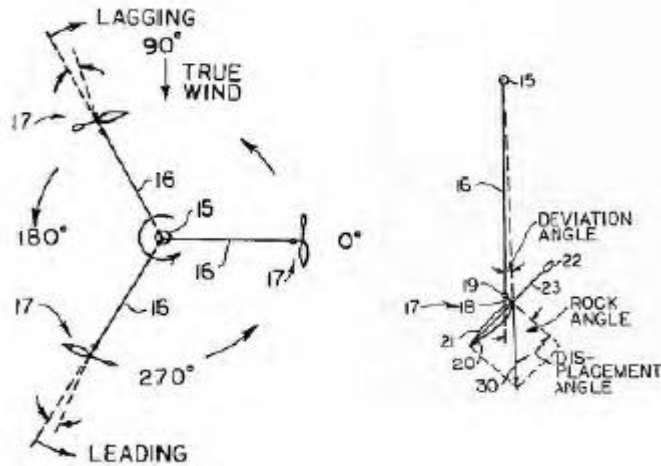


Figure 2.17: Schematic of the Sharp's design (reproduced from Sharp, 1982).

The design has a T-shaped stabiliser mass that is used to oppose the blade pitching outwards or inwards. Kirke did not use any spring to restore the masses at low speed. Unlike the Liljegren design, Kirke provided a means to modify the moment arms at which the two masses acted independently as well as the respective pitch limits. This enables the pitch responses to be biased in any direction. Also, the design has a point of restoring moment that must be exceeded by the aerodynamic moments acting on the blade before pitching can occur.

The Kirke (1998) design is an interesting concept because it tends to prevent small oscillations, particularly at high speeds that are generally associated with other design concepts and thus enables the turbine to function as a standard fixed-blade Darrieus turbine at high speeds.

In addition, Kirke developed a mathematical model based on the momentum model to test the performance of his turbine and validated it through a wind tunnel test. His results from both modelling and wind tunnel experiments reveals that the turbine achieved a reliable self-starting.

Although the Kirke (1998) passive design is quite promising and appears to have significantly increased the starting torque, the performance of the prototype rotor shows a maximum  $C_p$  value of less than a third of the predicted value (Kirke, 1998). Presumably, this was due to the uncertainties between the original design and the actual real-life model.

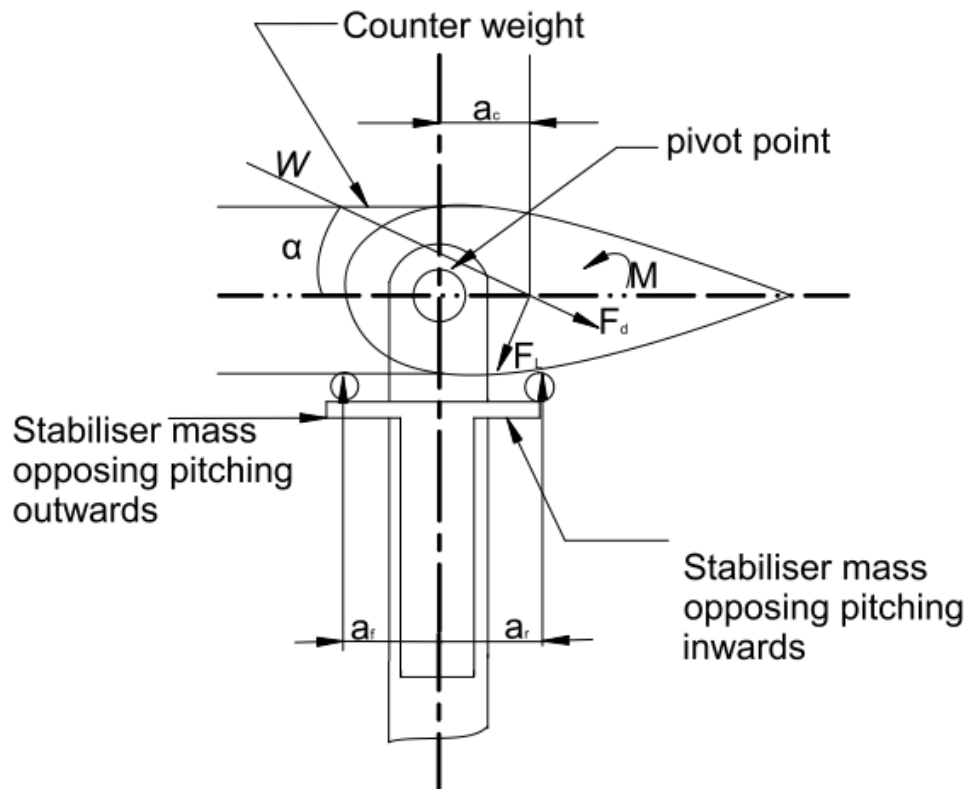


Figure 2.18: Schematic of the Kirke-Lazauskas initial design (Adapted from Kirke, 1998).

From these studies, it is clear that the variable pitch system gives a complete control over the cyclic variation of the angle of attack. However, they generally add extra complexities to the VAWTs and determining the optimal pitch system is increasingly more difficult, particularly in strong wind conditions.

## 2.9 Review of mathematical models for performance prediction

Several mathematical models have been developed for the prediction of VAWTs performance. The most studied and widely validated models are the momentum, vortex and cascade models. A review of these models is given in the following subsections.

### 2.9.1 Momentum Model

The Momentum Models are based on the calculation of the flow velocity through the turbine by equating the streamwise aerodynamic forces on the blades with the rate of change of momentum of air, which is equal to the overall change in the velocity times the mass flow rate. The major limitation of the Momentum Models is that they become inaccurate for high tip speed ratios  $\lambda$  and high solidities  $\sigma$  because the momentum equations are inadequate to calculate the aerodynamic forces generated by the blade (Paraschivoiu, 2002). Over the past decades, several approaches to wind turbine modelling have been attempted using the Momentum Models. The earliest use of the model for VAWT design was accomplished through the single streamtube model. The model was developed by Templin (1974) as the simplest prediction model for the calculation of the performance characteristics of a Darrieus-type VAWT (see Figure 2.19). Templin assumed that the entire turbine was enclosed within a single streamtube. The theory further assumed that the flow velocity is constant throughout the upstream and downstream side of the swept volume and is obtained by equating the streamwise drag with the change in axial momentum. The model was developed with the concept of the actuator disc theory (Glauert, 1947).

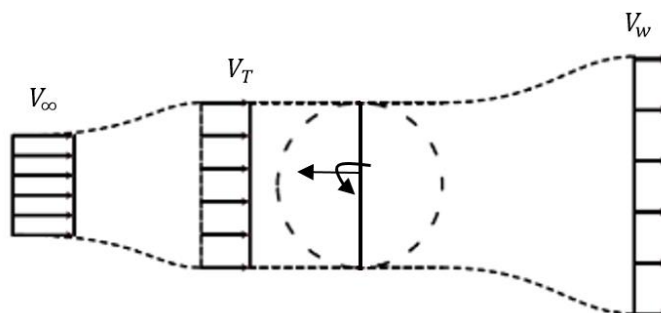


Figure 2.19: Schematic of Templin's single streamtube model (Adapted from Danao, 2012).

The major drawback of this model is the simplification of the interference factors that causes velocity induction. Although, the model is an acceptable approximation for lightly loaded turbines, the assumption break down at highly loaded or high solidity conditions. As the blade rotates, the force that exerted

on the fluid stream varies greatly due to the changing angle of attack. Reducing this variation into a single value causes the predictions to deviate significantly from the experimental data.

In order to account for this variations in the blade loading at different azimuthal positions, Strickland (1976) proposed an improvement to the Templin model by splitting the streamtube into multiple strips, each with a different actuator disc (see Figure 2.20). As such, the variation in the induced velocity across the swept area was taken into account for a more precise prediction of the blade loading. The Strickland model included lift and drag forces that results from the local angle of attack and experimental data. The modified model shows a significant improvement over the single streamtube model with less over estimation of the power performance, especially for highly loaded and high solidity VAWTs.

Prior to the Strickland model, Wilson and Lissaman (1974) and Muraca et al. (1975) proposed a multiple streamtube model. The model only considers the lift force in the calculation of the induced velocity in the blade loading and effectively assumed inviscid flow and uses the generated lift force instead of experimental data. The model is still an improvement over the single streamtube model and requires less computational cost as compared to the Strickland model. However, the model is still inadequate for the description of the flow field around a turbine and is only suitable for fast running lightly loaded VAWTs. Muraca et al. (1975) included the effect of the aerofoil geometry, support struts, blade aspect ratio, solidity and blade interference in their version of the multiple streamtube model. The authors derived a mathematical equation for the lift distribution on the plate with a variable angles of attack from both the leading and trailing edge sections of the flat plate. They revealed that the effect of the flow curvature on the performance characteristics is insignificant for a low chord to radius ratios. The limitations of their model led to the development of another multiple streamtube model by Sharpe (1977). The main idea behind the Sharpe model is similar to the Strickland's model but also considered the effect of the Reynolds number into the calculation. The Sharpe model was later improved by Read and Sharpe (1980) for the modelling of VAWTs.

The Sharpe model is strictly applicable to turbines with low solidity and having a high aspect ratio (AR). However, this model failed to accurately predict higher power coefficients ( $C_p$ ) as obtained experimentally. Although, the multiple streamtube model greatly improves the overall prediction of VAWTs, there is still an inherent flaw in the theory. For example, the blade loading in the downwind section of the blade was not accounted for, as the overall performance of the VAWT depends on both the upwind and downwind blade loadings.

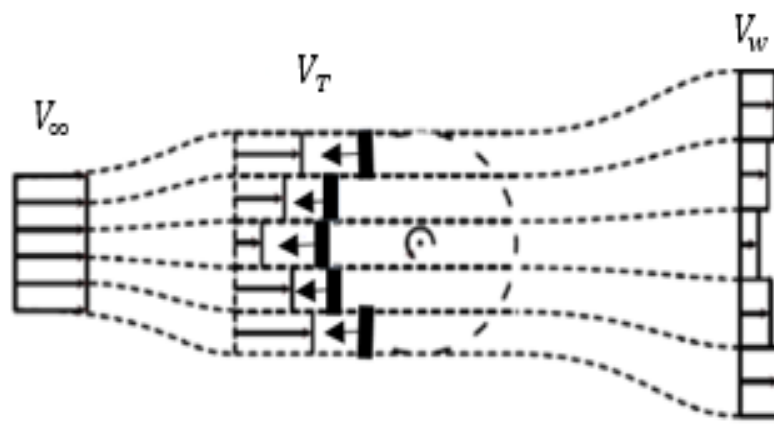


Figure 2.20: Schematic of Strickland's streamtube model (Adapted from Danao, 2012).

This major consideration was examined by Paraschivou (1981) by using the principles of the double actuator discs in tandem (see Figure 2.21), although the concept of the double actuator disc was first implemented by Lapin (1975). The Paraschivoiu concept accurately assessed the downwind and upwind forces on the blade as they rotate in the VAWT. Although, the Paraschivoiu model gives a more accurate prediction to both the single and multiple streamtube model, it is computationally more complex because a double iteration is required to account for the upwind and downwind passes of the VAWT. In a further refinement to this model, allowance was made to incorporate the dynamic stall (Paraschivou and Declaux, 1983) and flow curvature effects (Migliore et al., 1980; Hirsch and Mandal, 1984). Paraschivou (1983) provided more refinement to include strut parasitic drag, tower wake and different aerofoil sections.

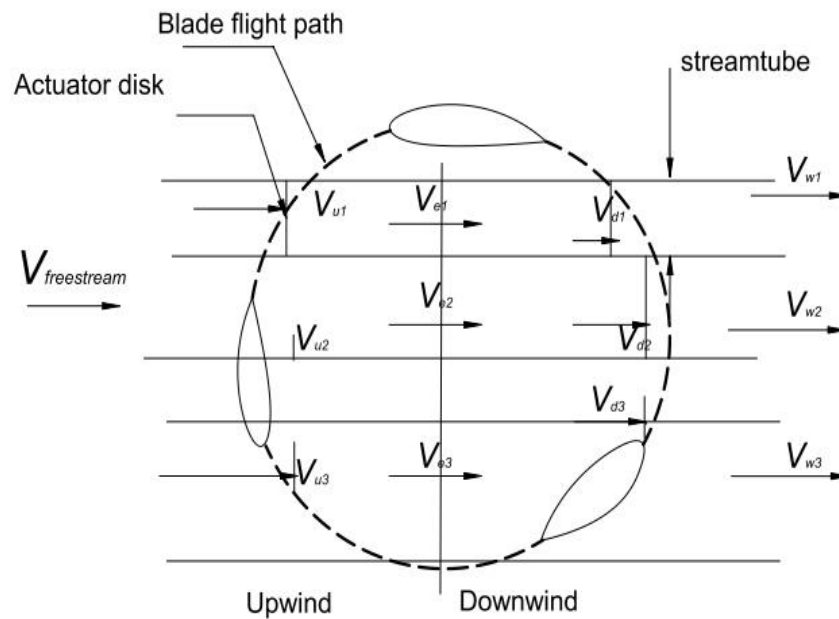


Figure 2.21: Schematic of the DMST model showing the induced velocities across the streamtubes.

### 2.9.2 Vortex Model

The Vortex Model is a potential flow model that was developed by Strickland (1979) based on the vorticity equation. A simple schematic of the vortex model associated with a blade element is shown in Figure 2.22.

In this model, the induced velocity generated by a single vortex filament in the flow field is computed from the Biot-Savart law (Currie, 1974), and the blade element is replaced by a lifting line which represents the flow field at a distance of more than one chord away from the aerofoil. Strickland utilised the model to predict the rotor performance of a VAWT. The findings revealed that the results are in agreement to those predicted by the momentum models. However, a large variation was observed when compared to the experimental data with a high solidity rotor.

Prior to the Strickland vortex model, Larsen (1975) had presented an earlier version of the vortex model which were followed by improved versions of the model by Fanucci and Walters (1976), Holme (1977) and Wilson (1980). Each of these models were represented in two-dimensional cases but were used to analyse three-dimensional problems which could not depict the real flow behaviour of the VAWT aerodynamics. A low angle of attack was also used in

the model, thus limiting the analysis of blade stall. These models like the streamtube models, were only suitable for lightly loaded rotors.

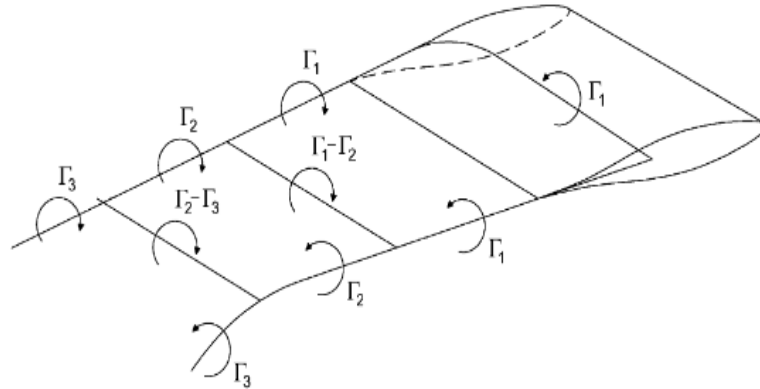


Figure 2.22: Schematic representation of a simple vortex model for a single blade element (reproduced from Islam et al., 2008).

With the resurgence of interest in VAWT, McIntosh and Babinsky (2009) presented a 2D swept vortex model that included blade sweep and unsteady wind conditions. The model was validated using force data from steady wind tunnel experiments in a full scale rotor and good agreement was observed in both swept and unswept configurations.

In contrast to the momentum models, the vortex model is capable of predicting the performance of VAWTs with higher solidities and at large tip speed ratios. Since this study does not involve high solidities and high tip speed ratios as will be seen in Chapter 5, the vortex model offers no significant benefit over the momentum models.

### 2.9.3 Cascade Model

The Cascade Model was proposed by Hirsch and Mandal (1987) using cascade principles, widely used in the design of turbomachinery for the analysis of VAWTs. The model assumes that the blade aerofoils are positioned in a plane surface (called the cascade) with the blade interspace equal to the turbine circumferential distance divided by the number of blades. The relationship between the wake velocity and free stream velocity is established by using the Bernoulli equation. The aerodynamic characteristics of each element of the blade are computed separately, for the upwind and downwind blade loadings. The instantaneous blade forces, as calculated by this model, show improved correlation in comparison to those calculated by

the conventional momentum models. Also, the model can predict the overall values of both the low and high solidity turbines reasonably well. However, the model requires a large computational time.

#### **2.9.4 Summary**

The prospects of small-scale Darrieus VAWTs for decentralised energy applications, particularly for power generation are quite promising but they have a major limitations. Self-starting was identified as one of the major limitations, but not much has been done to overcome this problem. A number of solution strategies have been proposed in the literature to alleviate the problem of self-starting in a fixed-pitch VAWTs and they include the use of the following:

- Cambered blades
- Thick aerofoil blades
- Variable pitch
- Leading and trailing edges
- Savonius auxiliary rotors
- High rotor solidity

However, little research has been performed to quantitatively assess whether these solutions actually produce sufficient starting torque required to overcome the drive train friction and the parasitic drag that causes the turbine blade to plunge into a “dead-band”.

From the preliminary analysis of the various design concepts at the beginning of this present research, it appears that the fixed-pitch VAWTs could be made to reliably self-start under some operating conditions. The Darrieus fixed-pitch VAWT is a promising concept because they are generally cheaper and simpler in construction, but due to the lack of adequate quantitative data, it is not clear if a Darrieus fixed-pitch turbine could be relied upon to produce enough starting torque to overcome the drive train friction and parasitic drag or whether the variable pitch VAWT concept could be ideal for self-starting improvement.

It was this lack of definitive data that stimulated the present investigation. If the problem of self-starting can only be alleviated by implementing expensive variable pitch designs, then it can be argued that the VAWTs



are unsuitable for decentralised application. However, if reliable self-starting can be achieved without the use of external mechanisms that increases the overall cost of the turbine, then it may be practicable and economical to use the small-scale wind turbine for decentralised power generation.

Furthermore, the number and variety of designs reviewed in this thesis show the need for a systematic approach to the problem. Most of the designs were presented with minimal theoretical basis in the patent and no supporting work has been reported in the literature. The most comprehensive existing work has been produced by Bayly (1981), Kirke (1998) and Pawsey (2002). It will be seen in Chapter 7 that a VAWT can achieve a high starting torque and reliably self-start by implementing a simple pitch system and suitable aerofoil section.

## **Chapter 3: Methodologies for Wind Resource Assessment**

This chapter describes the techniques employed in wind resource assessment for small-scale wind turbines. As discussed in the preceding chapters, wind flows are strongly dependant on both temporal and spatial variations that occur on different timescales. While such variability can theoretically be represented using long-term onsite measurements, or more advanced models such as mesoscale models and computational fluid dynamics (CFD) models, they are computationally expensive and are often not practicable for rapid deployment of small-scale wind turbines at potential sites. Thus, this chapter examines two cost effective approaches to wind resource assessment that is capable of predicting the long term wind resources. These approaches include the technique based on the boundary layer meteorology and data-driven approaches based on short-term onsite measurements at a target site.

The chapter is organised as follows: Section 3.1 describes the methodology based on the principles of boundary layer scaling methodology for predicting the wind resource. The implementation of the methodology is described in detail including the assumptions and limitations of the technique. Next, Sections 3.2 and 3.3 describe a data driven approach known as Hindcasting or Measure-Correlate-Predict for predicting the long-term wind resource using short-term measurements at a target site. The existing approaches are described with particular application to onsite measurements spanning a period of between 6 to 12 months.

### **3.1 The Boundary Layer Methodology**

Using regional climate information and local surface characteristics, a methodology can be developed to specifically predict the wind resource (mean wind speed and power density) at any given location near the Earth's surface. Although this prediction may not represent the complete characterisation of the site's wind conditions, it can be used as a starting point for predicting the wind resource at a particular location. The details of this method is given in Section 2.6 along with the simplifications that allow the technique to be deployed quickly without detailed knowledge of the sites characteristics.

A similar methodology was implemented by Weekes (2014) and Health et al. (2007). Weekes (2014) evaluated the wind resource potential at 32 UK sites using a modified boundary layer model and the results showed significant

prediction accuracy. Health et al. (2007) assessed the energy production of a micro-wind turbine installed in London. The model predicted the spatially averaged mean wind speed and also investigated the effects of building wind flows using a more advanced computational model. The study concluded with a recommendation for improvement of the model and appropriate siting guidelines for micro-wind turbines. Furthermore, the methodology has been used extensively by the UK Met Office, NOABL and the Carbon trust (Met Office, 2008) to provide estimates (1 km<sup>2</sup>) of the mean wind speeds across different geographical regions in the UK for small-scale wind energy, and this was extended to a wide range of UK sites.

The boundary layer method involves the calculation of the wind potential at a reference site near the top of the internal boundary layer which can then be downscaled using several stages so as to determine the mean wind speed at a potential turbine hub height. The difference stages of the methodology are briefly discussed in the following subsections.

### **3.1.1 Long-term reference climatology**

The climatological data obtained from the Modern Era Retrospective-Analysis for Research and Applications (MERRA) is used as a first input into the model. The dataset is hosted by the NASA global data assimilation database and contains historical measurements that extends from 1979 at all locations in the world at a height of 50 m above the ground level. This database has been used extensively in recent years for wind resource modelling due to the vast amount of data at any specific location in the world. MERRA consist of a spatial resolution of 1/2° latitude × 2/3° longitude × 72 vertical levels that extends through the stratosphere.

Since the reference climatology is given at 50 m height, it must be extrapolated to a higher height where the wind flow can be considered independent of the local flow. In the Met Office approach, a reference height of 200 m and a roughness length  $z_0 = 0.14$  m (representative of an open country) are used. This height signifies the height of the boundary layer over a rough surface and is usually determined as a function of the fetch<sup>7</sup> and surface roughness using

---

<sup>7</sup> Fetch refers to the distance measured in the upward wind direction.

expressions for boundary layer growth (Garratt, 1990; Elliot, 1958). However, implementing such a method is quite challenging since it requires estimates of significant roughness changes. Interestingly, the predicted wind speed close to the surface appears to be insensitive to this height provided an appropriate roughness value is used.

The extrapolation to the reference height is accomplished by scaling the logarithmic profile described in Section 2.6.2 according to the following expressions:

$$v_{ref} = v_{50} \frac{\ln(z_{ref}/z_0)}{\ln(\frac{10}{z_0})} \quad (3.1)$$

in which  $z_{ref}$  indicates the reference speed at 200 m,  $v_{ref}$  indicate the reference wind speed at this height and  $v_{50}$  is the wind speed at a height of 50 m as obtained from the NASA global database.

### 3.1.2 Wind speed at a blending height

After identifying the reference climatology as discussed above, the next stage in the methodology is to extrapolate this to a wind speed over a 1km grid square at the blending height as described in Section 2.6.4.1. This is obtained using a second logarithmic profile as follows (Best et al., 2008):

$$v_{bh} = v_{ref} \frac{\ln(z_{bh}-d_{eff}/z_{0eff})}{\ln[(z_{ref}-d_{eff})/z_{0eff}]} \quad (3.2)$$

in which  $v_{bh}$  indicate the wind speed at the blending height  $z_{bh}$ , and  $z_{0eff}$  and  $d_{eff}$  indicate the effective roughness and displacement lengths, respectively. To determine the effective roughness length  $z_{0eff}$  and effective displacement  $d_{eff}$ , the land cover over a grid square at the location of interest is used. The UK land cover data for various terrain types are obtained from the Centre of Ecology and Hydrology (CEH) (2007). After obtaining the values of the surface and displacement parameters, the values are substituted into Eqn. (3.2) to obtain the blending height mean wind speed  $v_{bh}$ .

### 3.1.3 Wind speed at a propose turbine hub height

The final step in the methodology is to downscale the wind speed at the blending height to the spatially averaged mean wind speed at the proposed

turbine hub height. This is achieved by further extrapolation of the logarithmic profile as follows:

$$v_{hh} = v_{bh} \frac{\ln(z_{hh}/z_0)}{\ln[(z_{bh})/z_0]} \quad (3.3)$$

in which  $z_{hh}$  and  $v_{hh}$  indicate the turbine hub height and the associated hub height of the mean wind speed, respectively.

The parameters  $z_{hh}$  and  $v_{hh}$  also depend on the local roughness and displacement values of the specific sites, thus, Eqn. (3.3) can be expressed as follows (Best et al., 2008):

$$v_{hh} = v_{bh} \frac{\ln(z_{hh}-d_{local}/z_{0local})}{\ln[(z_{bh}-d_{local})/z_{0local}]} \quad (3.4)$$

When the mean wind speed at a propose turbine hub height is predicted, a prediction can then be made using a suitable wind speed frequency distribution. The most validated and widely used distribution which has also been used by the Met Office is the Weibull distribution as described in Section 2.4.1. Using this distribution in combination with a suitable turbine manufacturer's power curve, the available energy at any given site can be computed.

### 3.1.2 Limitations of the methodology

The accuracy of the boundary layer scaling methodology is limited by the several simplifications and sources of uncertainty that are encountered at each stage of the implementation process. These uncertainties can combine to introduce large errors in the predicted wind resource, and summarised as follows:

- (i) The reference climatology as in any other reanalysis data, does not utilise real-time land surface observation; they reflect instead the time integration of the surface meteorological conditions (wind speeds, directions, etc.) by the land model component of MERRA and is thus subject to considerable uncertainty that is ultimately

propagated from the downscaling process and generalisation of the data sets.

- (ii) The aerodynamic parameters in the logarithmic profile are estimated based on the land cover in a local region of 1 km<sup>2</sup>. However, the considerations of boundary layer growth indicate that the mean wind speed is affected by upwind roughness over a much larger distance as described in Section 2.6.3.
- (iii) The boundary layer scaling method tends to predict only a temporally averaged mean wind speed, and therefore making power predictions will only be based on assumptions and simplification of the model. This is ultimately a limitation of the long term reference climatology which contains no information of the distribution of wind speeds.
- (iv) The extrapolation to a fixed internal boundary layer height of 200 m does not account for edge effects close to roughness boundaries which will ultimately affect the predicted wind resource.

These inherent uncertainties associated with the boundary layer scaling methodology implies that while the method is attractive, since it is relatively easy to implement, adequate care must be taken when using the approach to make site-specific wind resource predictions. Furthermore, these uncertainties offer opportunities for potential improvement to the analytical model. As will be seen in Chapter 4, some of these modifications are relatively easy to be incorporated into the model, while others are increasingly difficult to implement since they require the development of a more robust approach.

### **3.2 Hindcasting/Measure-Correlate-Predict (MCP) methodology**

As noted in the preceding section, the boundary layer scaling methodology is subject to considerable uncertainty and thus, is incapable of predicting the many complexities associated with real wind flows in the boundary layer. A more reliable alternative to the boundary layer scaling model is the approach known as Hindcasting or Measure-Correlate-Predict (MCP) where onsite data collection process forms part of the wind resource assessment. In the large-scale wind resource assessment, detailed wind data measurement are usually

carried out before any investment decision is taken. Generally, these measurements span between 1-3 years of onsite wind observations along with correlation to a long-term reference site using the MCP techniques (AWS & NREL, 1997, Jane, 2011). Although this may not be practical in the case of a small-scale wind assessment, a short time wind measurement program combined with correlations to a long term reference site can potentially provide a more robust wind resource assessment compared to the boundary layer method. Thus, a small number of research work has been undertaken in recent years to assess the validity of this technique in small-scale wind resource assessment. Therefore, this approach is ripe for further research. The MCP technique is schematically illustrated in Figure 3.1 and the principles of the implementation are summarised in the following steps:

- (i) **Take onsite measurement:** This step involve taking measurement of wind speeds at a target site for a short period of time, say up to 1 year, as close to the location and height of the proposed installation as possible.
- (ii) **Correlate** two sets of data: The measured data is correlated with long-term reference data sets for concurrent data period. If correlations are acceptable, then choose the reference data sets for the next step.
- (iii) **Predict estimate of long-term wind speed:** This step involve the prediction of the wind speed for historical period, which covers the duration of the reference time series wind speed. This is known as hindcasting.
- (iv) **Calculate net energy output and uncertainties:** The final step in the methodology is to convert the hindcast into an energy production estimates as well as predict the associated uncertainties in the predicted wind resource.

The main purpose of an MCP technique is to find a correlation between the short-term concurrent measurements at the reference and target sites, respectively. The aim of the correlation is to understand if the measurement data taken from a target site and the long-term reference data are similar over the measurement (concurrent) period. If the two data series are similar in terms of the wind speed distribution, then the wind regimes are similar, and

therefore a valid wind speed distribution and the long-term wind energy potential of the target site can be generated. It is important to note that the short-term, concurrent measurement period at the reference/target site is known as the “training period” since it is used to establish a correlation between the two sites.

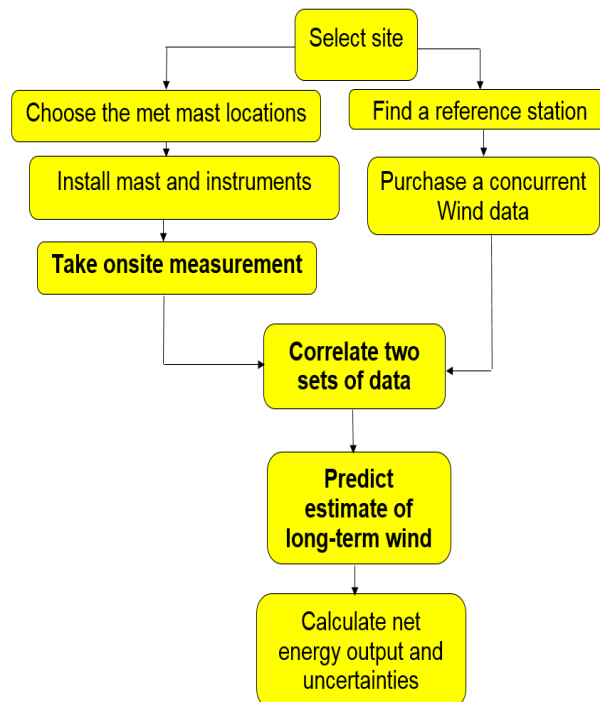


Figure 3.1: Schematic diagram of the Measure-Correlate-Predict process (Adapted from Jane, 2011).

There is a vast literature on MCP techniques which have been used in recent years including peer reviewed articles, technical reports and conference proceedings and several methods have been utilised to describe the relationship between the correlated variables which have contributed to the development of different MCP techniques as illustrated by an extensive review by Carta et al. (2013). In reviewing these techniques, attention is focused on the technique that includes the prediction of the distribution of the wind speeds over multiple years or the power rather than just the mean wind speed.

The following subsections provides an outline of the widely used MCP approaches. While this study is not intended to investigate all the approaches, special focus is given to the methods that have been validated and are already widely utilised in the wind industry as well as promising new techniques that



may be useful to the small-scale wind industry. Since there is a lack of reliable data for the use in MCP for short-term measurements, a brief review of the application of MCP to short term measurements periods is given in Section 3.8.

### **3.2.1 Determinants of the MCP methods**

It must be empathised that MCP techniques are based on a series of hypotheses which must be considered before it can be successfully implemented in the context of small-scale wind energy. A brief discussion of these techniques is given in the following subsections.

#### **3.2.1.1 Appropriate measurement protocol**

The MCP methods are based on the hypothesis that the reference and target sites climatology have been obtained in an appropriate manner that will guarantee their accuracy (Albers and Klug, 1999). Several wind speed measurements have an unacceptably low level of uncertainty and this is partly due to improper practices when selecting and mounting anemometers, choice of measuring site, or the height and duration of the measurement periods. Thus, it is important that a thorough check is made on the validity of the data before implementing an MCP analysis (Alkers and Klug, 1999, EWEA, 2009). Consequently, this hypothesis implies that the reference station data must satisfy the following requirements throughout the historical long-term period (Gerdes and Strack, 1999):

- (i) The station data must not have been affected by factors such as building constructions, installation of wind farms (Mina and Clive, 2012) or changes to the vegetation surrounding the wind masts that might affect reference and target wind data sets.
- (ii) The height and the location of the wind mast have not been subject to any form of modification during the measurement period.
- (iii) The reference site and the target site should have the same height above the ground.
- (iv) The wind data must be recorded using the same sets of instrumentation.

### **3.2.1.2 Knowledge of the pattern of seasonal variations in the concurrent data period**

The short-term period over which data is available for both the reference and target sites must be long enough (at least 10 years) to allow accurate seasonal information regarding the wind speed and direction. In general, the recommended practice is for the concurrent data period to be at least one year long (Taylor et al., 2004). These authors have investigated the long-term prediction variability of a wind resource with an MCP technique using data for 1, 3, 6, 12, 18 and 24 months. Their results revealed that one month of the data give rise to a high margin of uncertainty of between 6.5% - 12% for long-term wind speed estimations at the analysed sites. For the 3 and six months periods, they also observed a very high uncertainty of 4% for the six months period despite the existence of an inverse relationship between the uncertainty and data management period. However, once the data measurement period is extended to 12 months, a significant improvement in the uncertainty margin was observed (approximately 2%). In the 18 months period, few changes in the uncertainty margin was observed, but in the 24 month period, a much lower uncertainty margin was observed. They concluded that there is a significant seasonal influence on the quality of the long-term estimations. Consequently, they emphasised the importance of having at least 12 months or more measurements for the target site. Long-term predictions made with measurements taking less than one year at the target sites are full of large margin of errors (Oliver and Zarling, 2010).

### **3.2.1.3 Climate stability**

MCP techniques work on the assumption that the reference and target sites data sets are statistically stationary. This means that the effects of climate change are not considered and it is assumed that the wind conditions in the future will be similar to that of the past throughout the lifetime of the wind energy project. In reality, it is generally believed in the scientific literature that there will be a reduction in the temperature difference between the poles and the equator and that mid latitude winds will be altered as a result of global warming (Emeis, 2013).

### 3.2.1.4 Similar wind climate at the reference and target sites

This assumption is based on the notion that the reference site data are representative of the wind climate at the target site. If there is an appreciable difference in comparison of the target and reference sites or low coefficients of correlation, it is likely that this can lead to the rejection of the reference site for MCP methodologies unless special measures are applied to the data sets (Skibin, 1984; Jain, 2011).

The correlation is often determined by calculating the Pearson product-moment coefficient of linear correlation also known as the Pearson correlation coefficient,  $r$ . (Makridakis, Wheelwright and Hyndman, 1998)

The Pearson correlation coefficient measures the relationship between the wind speed recorded at reference and target sites during the concurrent period. The value is expressed as follows (Makridakis, Wheelwright and Hyndman, 1998):

$$r = \frac{\sum_{i=1}^n [(V_i)_t^{ST} - V_t^{\overline{ST}}] [(V_i)_r^{ST} - V_r^{\overline{ST}}]}{\sqrt{[\sum_{i=1}^n [(V_i)_t^{ST} - V_t^{\overline{ST}}]]^2 [\sum_{i=1}^n [(V_i)_r^{ST} - V_r^{\overline{ST}}]^2]}} \quad r = -1 \leq r \leq 1 \quad (3.5)$$

where  $(V_i)_r^{ST}$  and  $(V_i)_t^{ST}$  are the observed short-term wind speeds at the reference and target sites and  $V_r^{\overline{ST}}$  and  $V_t^{\overline{ST}}$  are the reference and target sites mean wind speeds, respectively.

Using this equation, the strength of the correlation coefficient can be determined. If the correlation is weak, the long term data from the reference station should be rejected or used with caution (Jain, 2011, EWEA, 2009).

No established criterion has been published in the literature regarding a correlation level below which the reference station data should not be utilised due to their unreliability (Jain, 2011). However, some rules of thumb have been proposed as a baseline in determining good and poor correlation coefficients. According to Langreder (2010), the coefficient of determination (Press et al. 1992),  $R^2$ , should not be lower than 70%.  $R^2$  is the square of the correlation between the predicted and actual values, in this case, the wind speed, and it can be expressed according to the following equation:

$$R^2 = \frac{\sum_{i=1}^n [(\hat{V}_i)^{ST} - V_i^{ST}]^2}{\sum_{i=1}^n [(V_i)^{ST} - V_i^{ST}]^2} \quad (3.6)$$

EWEA (2009) proposed a correlation coefficient,  $R^2$  of 70% and over for appropriate long-term and target site pair. Meanwhile, Bass (2009) warned that special care should be taken when dealing with values of the coefficient of correlation that exceed 0.7, and Jain (2011) stated that if the value of the correlation coefficient is 0.9 or higher then the correlation is considered as excellent. A comprehensive guide for an acceptable correlation between the climate conditions at two different sites is provided in Jain (2011). In an investigative study undertaken by Anderson (2004), the sites which were unsuitable for an MCP technique were rejected and excluded from further assessments.

Therefore, the choice of an MCP method is strongly dependent on the level of correlation. Overall, the correlation coefficient of 0.5 - 0.6 are considered to be very poor, while those that ranges from 0.6 - 0.7, 0.7 - 0.8, 0.8 - 0.9 and 0.9 - 0.10 are considered as poor, moderate, good and very good, respectively.

### 3.3 MCP models

Several MCP models have been developed for the assessment of the long term wind resource. The most widely used models are based on regression techniques, namely climatological reduction (Putman, 1948), linear regression, the variance ratio method (Rogers et al., 2005). Other MCP methods go beyond the regression approach, namely the Mortimer/matrix method (Moritmer, 1994) and the Weibull parameter scaling method (Thøgersen, et al., 2007). In addition, models based on Artificial neural networks (ANNs) (Sheppard, 2009), which determines the correlation as complex system has also been used in recent years in long term wind resource estimation. A comprehensive analysis of the different MCP approaches can be found in Rogers et al. (2005), Thøgersen, et al. (2007) and Sheppard (2009). The following subsections provide an overview of the MCP models considered in this thesis:

### 3.3.1 Climatological reduction

The first and earliest use of a long-term reference data in an MCP technique is the climatological adjustment by the method of ratios proposed by Putman (1948). This method involves estimating the long-term mean wind speed at the reference site based on the knowledge of its short-term mean wind speed. The expression used in the estimation is given as follows (Putman, 1948):

$$\hat{v}_{tar,j} = \left[ \frac{v_{mtar}^{-ST}}{v_{mref}^{-ST}} \right] v_{ref,j} \quad (3.6)$$

in which  $\hat{v}_{tar,j}$  and  $v_{ref,j}$  are the predicted target and observed reference sites wind speed,  $v_{mtar}^{-ST}$  and  $v_{mref}^{-ST}$  are the short-term mean wind speed observed at the target and reference sites, respectively.

The climatological reduction method can be used to predict the long-term time series of the wind data, and thus, the wind speed distribution at the target site. Several modification based on this method have been made, including those that use estimates of the variance at both the reference and target sites (see for example Justus et al., 1979). However, they do not differ significantly from the methods of linear regression.

### 3.3.2 Linear regression

The methods of linear regression are by far the most widely used in the wind industry due to its empirical success in predicting the long-term wind resource (Thøgersen et al., 2007). The method involves applying linear regression (LR) to the wind speed observations that has been binned into angular sectors according to the reference site wind conditions. The individual wind speeds at the target site are described according to the following expression (Carta et al., 2013):

$$v_{tar} = \alpha + \beta v_{ref} + \varepsilon \quad (3.7)$$

where  $v_{tar}$  is the observed wind speeds at the target site,  $v_{ref}$  is the observed wind speed at the reference site,  $\alpha$  and  $\beta$  are the regression coefficients (slope and intercept) obtained using a fit to the short-term measured data (training

data) and  $\varepsilon$  is an error term which represents the residual scatter. The regression coefficients  $(\alpha, \beta)$  could be determined by ordinary linear regression (OLR) (Landberg et al., 2003, Windographer, 2015). However, other methods such as the orthogonal regression and the quartile regression (QR) (Carta et al., 2013) can also be used.

The linear regression approach involves collecting data at the target site for a considerable period of time in order to determine the regression coefficients, which are assumed to be constant with time.

Now, assuming all the wind data are adequately represented by a linear fit, the mean wind speed prediction at the target site can be described by the following expressions (Derrick, 1992):

$$\hat{v}_{tar} = \alpha + \beta v_{ref} \quad (3.8)$$

The linear regression approach has been used extensively for wind resource assessment. For example, Bardsley and Manly (1983) used this method to derive estimators for the long-term mean wind speed and variance at a potential aerogenerator site. Their results revealed that while linear regression yields unbiased estimates of the mean wind speeds, the estimates of the variance are not unbiased. This issue highlights the importance of the residual scatter term  $\varepsilon$  in Eqn. (3.7) and it should be taken into account because it can lead to biased power predictions.

More recently, Rogers et al. (2006), as well as Perea and Amezcua (2011), have successfully used the linear regression approach as a basis of comparison against other MCP methods and the prediction results were validated using a wide range of error metrics.

### 3.3.3 Variance ratio (VR) method

The inherent uncertainty associated with the linear regression approach is corrected using the Variance Ratio method. Rogers et al. (2005) in an attempt to resolve this issue proposed the variance ratio method based on a simple linear regression approach by forcing the variance of the predicted wind speeds to be equal to the observed or measured wind, i.e.  $\sigma(\hat{v}) = \sigma(v)$ .

On using the method of least squares, the VR equation can be expressed as follows (Rogers et al., 2005):

$$\hat{v}_{tar} = \left[ v_{mtar} - \left[ \frac{\sigma_{tar}}{\sigma_{ref}} \right] v_{mref} \right] + \left[ \frac{\sigma_{tar}}{\sigma_{ref}} \right] v_{ref} \quad (3.9)$$

where  $\sigma_{tar}$  and  $\sigma_{ref}$  are the standard deviation about the mean wind speeds at the target ( $v_{mtar}$ ) and reference ( $v_{mref}$ ) sites, respectively.

Rogers et al. (2005) investigated the performance of the variance ratio model in terms of the predicted mean wind speeds, wind speed distribution parameters and the wind power at eight sites from different terrains. The results show a significant improvement over the linear regression approach, particularly for the parameters related to the wind speed distribution. The method has since been used in several MCP studies (see for example Perea et al., 2011; Jung et al., 2013).

### 3.3.4 Matrix method

This method was proposed by Mortimer (1994) based on the ratios of the binned wind speeds and it has been used extensively in a number of studies to assess the wind resources at different locations (see for example Rogers, Rogers and Manwell, 2005; Thøgersen, et al., 2007). As the name implies, this method is applied to a matrix of wind speed ranges and direction sectors from the reference time series data sets. The target site wind speeds are then predicted according to the following equation (Mortimer, 1994; Rogers et al., 2005):

$$\hat{v}_{tar} = (y + e)v_{mref} \quad (3.10)$$

in which  $y$  is the ratio of the wind speeds, and  $e$  is a random number drawn from a triangular distribution. It should be noted that while the linear regression, LR, and the variance ratio, VR, are linear approaches, the Matrix method is not. The addition of the  $e$  term in the equation allows for the residual scatter to be calculated. However, as noted by Derrick (1992), achieving a matrix of wind speed ranges and direction sectors from the reference time series can be a challenging undertaking. Although, interpolation methods can be used to achieve sufficient data matrix, it is likely that this will not be useful for short-term measurement periods. Consequently, this method may not be feasible in small-scale wind resource assessment.

### 3.3.5 Weibull parameter scaling

The Weibull parameter scaling involve the computation of the Weibull scale  $c$  and shaper  $k$  parameters for the wind speed in each of the 12 or 16 wind direction sectors for both the onsite measured data and the reference data. The advantage of this technique is that, it will match the nature of the wind at most locations, but it should be noted that this technique is not valid on locations with significant non-Weibull distributions as well as when the modification of the required Weibull parameters is very large.

The method is described by the following expressions (Thøgersen, et al., 2007):

$$\lambda_{site}^{long} = \lambda_{ref}^{long} \cdot (\lambda_{site}^{short} / \lambda_{ref}^{short}) \quad (3.11)$$

where  $\lambda$  is the distribution parameter under consideration, namely scale  $c$  or shape  $k$  parameter.

Using this approach the frequency of each sector can be computed according to the following equation (Thøgersen, et al. 2007):

$$f_{site,i}^{long} = \left[ \frac{f_{site,i}^{short}}{f_{ref,i}^{short}} \right] \times \frac{f_{ref,i}^{long}}{\sum_{i=1}^N \left[ \frac{f_{site,i}^{short}}{f_{ref,i}^{short}} \right] \times f_{ref,i}^{long}} \quad (3.12)$$

where  $f$  is the frequency,  $N$  is the number of sectors (typically 12 or 16), and  $i$  is the sector under consideration.

As a caveat, the Weibull scale MCP can be used only when the reference and observed data sets are primarily Weibull distributions, the scaling of the Weibull parameters is not very large and the sector-wise frequency of the onsite measurements and the reference data sets are similar.

### 3.3.6 Alternative regression models

In addition to the conventionally used MCP methods explored above, several other regression models have been developed for wind resource assessment in recent years.

Derek (1992) proposed an MCP model of the form  $\hat{v}_{tar} = \alpha(v_{ref})^\beta$  if  $\beta \neq 1$  and argued that it could be ideal to predict the long term wind speed. Clive



(2008) provided some theoretical background that underpins such a technique as well as analytical expressions for the power term  $\beta$  based on the assumption of the Weibull distribution of wind speed. Achberger, Ekstrom and Barring (2002) presented an MCP model based on linear regression of the orthogonal wind vector by transforming the time series wind speed data into eastern and northern components and applying linear regression into each of the components. The predicted components are then used to determine the resultant wind vector (wind speed and direction).

Achberger, Ekstrom and Barring (2002) also proposed a method known as vector correlation. The method is based on using a vector representation of the target and reference wind speeds to derive a relationship for the scaling and translation of the wind vector between the target and reference sites. These authors investigated the performance of the linear regression model of the orthogonal wind vectors, the vector correction and the standard linear regression methods using wind data from a single target site collected over a period of nine months. They concluded that the results do not present any significant prediction difference. More recently, Perea et al. (2011) investigated a regression approach known as the 'Weibull regression'. The method is based on a technique in which the correlated wind speed at the target and reference sites are assumed to be sampled from joint probability distribution. The output of this approach is a non-linear curve that can be used to predict the target wind speed using data observed from the reference site. However, investigation of the MCP approach using synthetic wind data does not present any significant improvement over the widely used linear regression and variance ratio methods.

### **3.3.7 Artificial Neural Networks (ANNs)**

These are computational based method inspired by animal central nervous systems, particularly the brain, which are capable of understanding machine language and recognising patterns in noisy or complex data. The ANNs involve a series of interconnected neurons organised into layers that can compute values from inputs based on the information provided through the network (Rojas, 1996). Basically, the main function of ANNs is to establish a relationship between the input and output data, given a training data sets of known inputs and outputs. That is, given a set of input training data sets, the

ANN is able to predict the output values. This system of ANN is similar to an MCP technique in which the short-term reference and target wind measurements are used to establish a relationship between two sites. Then using the long-term reference wind data sets, the long-term wind resource of the target site can be predicted. The main benefit of artificial neural networks in wind resource prediction are their ability to recognise non-linear relationships and can also use more than one long-term data sets (Zhang, 2015). However, it is difficult to conclude about the validity of this method to other MCP techniques due to lack of peer reviewed studies that considers short-term data. Further, artificial neural network algorithms, ANN, are generally difficult to implement.

### **3.4 Short-term measurement periods**

The measure-correlate-predict, MCP, techniques are essentially developed for large-scale wind assessment where a small error can have a huge financial loss due to the scale of the investment. Consequently, several studies have recommended the use of onsite measurement period of 1-3 years in order to reduce the uncertainties associated with implementing a successful MCP technique, see for example, Jain (2011) and Derek (1992). These studies provide a background to the potential of using MCP techniques in predicting the long-term wind conditions based on short-term measurements.

The first application of a training data period of less than 1 year in MCP analysis was reported by Barros and Estevan (1983). The authors used 13 weeks of measured data from 20 different stations which are 1000 km apart in the USA. The aim of the study was to predict the annual wind potential at one of the station by correlating it to the other stations using a method based on the principle component analysis. The results showed an average error of 5% in the mean wind speed and a 10% error in the mean wind power. However, Skibin (1984) criticised the results and argued that the use of different reference data over a very large area implies that the data sets experience a different climate to the target site. In addition, Skibin (1984) queried the validity of using short-term data and argued that such data will result in a misrepresentation of the wind resource.

These findings could be compared to some of the current problems facing the small-scale wind industry in recent years. However, in the present case, however, the challenge is not that a long-term measurement may be forfeited in preference to a short-term one but rather when no measurement was taken at all which could result in an unreliable prediction of the wind resource.

Another significant application of MCP approach to short-term training data was investigated by Oliver and Zarlring (2010). The authors examined the effect of measurement periods on the validity of MCP predictions using the linear regression method applied to a total of 14 sites across the USA. The results showed significant seasonal variability in the error observed for the long term predicted mean wind speed. The findings from this study reveals the importance of seasonal variability in the reference/target sites correlations. However, the results were obtained using the monthly mean wind speeds rather than the full distribution of the wind speeds necessary for predicting the wind power potential.

Therefore, there is a need for a more detailed study of the effect of using short term data from a single measurement point using reference data from multiple years to predict the wind speed distributions and associated parameters.

### **3.5 MCP uncertainties**

The uncertainties associated with the MCP approaches can originate from a number of sources: (i) the validity of the reference data sets, (ii) the chosen MCP method, (iii) the length of the reference and training data, and (iv) whether the relationship in the overlap period between the training data and reference data represents the long-term relationship of the wind data (Rogers, Rogers and Manwell, 2006). However, there is no direct approach in reducing the uncertainties associated with the MCP techniques and the information available in dealing with these uncertainties is also limited. Consequently, an attempt to reduce these uncertainties is the first option in carrying out an MCP method.

According to Bass et al. (2000), the uncertainties associated with predicting the long-term wind resource using an MCP is strongly dependent on the choice of the wind data, provided the correlation coefficient is greater than 80%. Thus, data validity is often the most influential factor in MCP uncertainty.

An investigation of the effects of training data length was carried out by Taylor et al. (2004). The study used a simple linear regression MCP method applied to three target sites using different training data length in order to estimate the mean wind speed over a 4 year period. The study revealed a strong reduction in the computed error when measurement period was increased to 1 year, after which, little or no change was observed in the measurement lengths. Rogers et al. (2006) also investigated the effects of training data length on a wide range of MCP techniques using data from 8 sites and concurrent data covering between 1.7 and 5 years. The study recommended a training data length of at least 9 months for a successful MCP analysis.

### **3.6 Summary of the methodologies for small-scale wind resource assessment**

A detailed, although not exhaustive, description of some of the widely used techniques for wind resource assessment has been given. While it is not possible to examine the validity of all the different techniques in this thesis, some of the techniques will be implemented based on their proven reliability in previous studies. These includes the technique based on the boundary layer meteorology and those based on data driven approach, namely linear regression, LR, and variance ratio, VR, techniques. These approaches have been used extensively for wind resource assessment. Thus, despite the limitations inherent in their implementation, they serve as a useful starting point for the implementation of a low cost wind resource assessment methodology in the context of small-scale wind energy.

These techniques along with their likely uncertainties will be evaluated in Chapters 4 and 5 using different range of measured wind data (training data). As discussed in **Section 3.2**, there is currently lack of reliable data into the use of MCP for short-training periods. Thus, the main aim of the present work is to assess the uncertainties associated with these techniques.

## **Chapter 4: Performance Evaluation of the Boundary Layer Methodology to Wind Resource Assessment**

### **4.1 Overview**

As described in Chapter 3, the boundary layer methodology was developed by the UK Meteorological Office to quantify the available wind resources for small-scale wind energy development in the UK (Best et al, 2008). In order to improve the prediction capacity, a number of corrections and simplifications were subsequently applied to the methodology based on the surface roughness parameters on a local and regional scale. These corrections resulted in a prediction of the spatial mean wind speed at a specific location and height, which could then be used in combination with an appropriate wind speed distribution to predict the wind resource potential. The methodology is a valuable starting point in the assessment of wind potentials for small-scale wind energy development.

The study described in this chapter is intended to achieve three goals: (i) to quantitatively assess the performance of the prediction methodology at specific locations, since this had not been previously investigated. (ii) to explore the avenues in which the methodology may be improved keeping in mind the principles that drove the original methodology, and (iii) to assess the inherent uncertainties associated with the method. These core aims are summarised as follows:

- (i) Prediction of the wind resource potential (wind speed and wind power density) by quantifying the errors between the predicted and measured values at four UK locations.
- (ii) Investigation into the choice of the Weibull shape parameter used to describe the wind speed distribution and recommendations for improving this choice in order to maximise energy production.
- (iii) Calculation of the error metrics in the predicted wind speed and wind power density due to the uncertainties in the simplification of the methodology.

Using this approach, the likely errors in the predicted wind speed and wind power density are computed. Further, based on the calculated errors, measures are suggested on the general applicability of the methodology to site-specific wind resource assessments.

This chapter is organised as follows: Section 4.2 describes the main methodology of the boundary layer scaling model, highlights potential improvements and describes a case study implementation at four sites. A comparison of the observed and predicted wind speeds, including an investigation to improve the implementation of the model, is given in Section 4.3. Section 4.4 describes the potential of the model as a site screening tool to assess viable wind turbine sites.

## **4.2 Methodology**

The methodology described in Section 3.1 was used as the basis for the current investigation. In order to evaluate the potential of the prediction methodology, a model is developed in Matlab. The model utilises the same principles as the original model described in the Met Office report (Best et al., 2008), however, two notable differences should be mentioned with regards to the estimation of the aerodynamic parameters and the source of the reference climatology used as inputs into the model. The surface roughness parameters were obtained from each specific site of interest, rather than from the closest ordnance survey grid square that was implemented in the original model and the reference data were obtained from the NASA's database known as the Modern-Era Retrospective Analysis for Research and Application (MERRA). It should be noted that the present method is better than the original method because it can be applied to a wide variety of sites due to the availability of Reanalysis data at every location of the world. Furthermore, it tends to produce less error when compared to the original methodology.

### **4.2.1 Potential modification to the original methodology**

As discussed in Section 3.1, a number of uncertainties were introduced at every stage of the methodology which may potentially reduce the accuracy of the final predicted wind resource. Thus, it is possible to modify the

methodology in order to reduce these uncertainties. These uncertainties emanated from the downscaling stages are shown in Figure 4.1. It should be noted that Stages I, II, III are the same with the original methodology and will not be discussed further.

The particular interest in the current work is focused on the uncertainties arising from the downscaling process in stage (IV) (see Figure 4.1) and the description of the uncertainty is described as follows:

Stage IV: The estimation of the aerodynamic parameters representative of the local region can be a challenging task. Assuming that the local region of interest is defined by say 100 m square surrounding the measurement site, the topographical features of the region can easily be determined from aerial photographs.

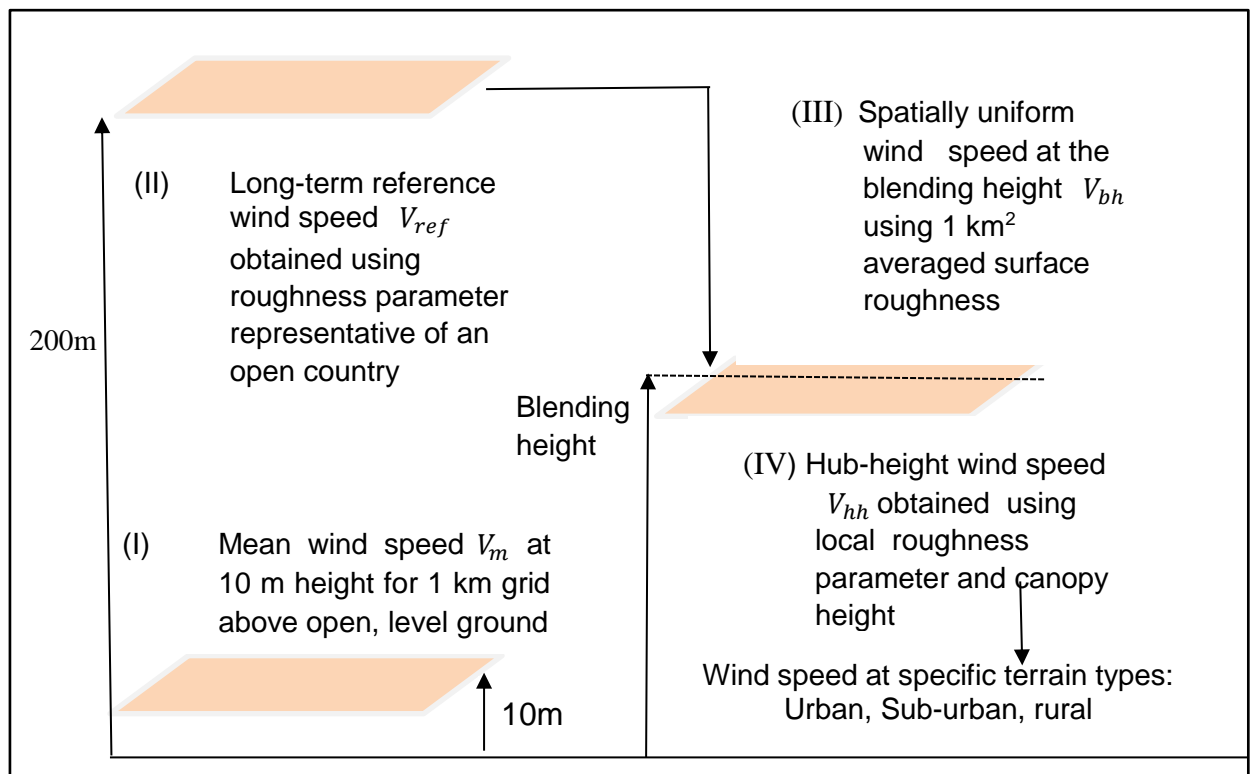


Figure 4.1: An illustration of the methodology used by the Met Office to predict the spatially averaged mean wind speed. The methodology begins with an input wind speed at 10 m height (I) and terminates in a predicted mean wind speed at a turbine hub height (IV) in any specific terrain (e.g. urban, sub-organ, coastal or rural location).

However, some studies such as those undertaken by Grimmond (1999), Ritter et al. (2014), etc. revealed that the estimation of the roughness parameters is site specific and can easily be computed for any particular location. Furthermore, the local values of the roughness parameters  $z_0$  and the displacement height  $d$ , as well as the transition point between a logarithmic and exponential wind speed profile, are calculated as a function of the canopy height<sup>8</sup>. Therefore, the estimated canopy height if any in the investigated sites will be of particular importance in the final downscaling of the mean wind speed. Additionally, the choice of the Weibull shape parameter used to represent the predicted wind speed distribution can significantly affect the final wind power prediction and thus methods to select an optimal choice should be investigated.

These factors were incorporated into a modified methodology and this is illustrated in Figure 4.2. It should be noted that the modified methodology is intended to predict only the spatially averaged mean wind speed which is then used with a Weibull distribution model to predict the wind power density. This approach is likely to be a reasonable approximation for well exposed locations. However, for wind turbines mounted close to high rise buildings or other obstructions, there may be significant deviations from this spatial average (Heath et al., 2007; Millward-Hopkins et al., 2011). These deviations will likely depend on a number of factors, namely the geometry of the obstructions, the prevailing wind direction and the turbine position on the building. In such cases, appropriate correction factors must be applied in order to accurately assess the wind resource. Unfortunately, these corrections are beyond the scope of the present model which is primarily concerned with a simple parameterisation of the local surface characteristics of the study area. However, previous studies have shown that the spatially averaged mean wind speed can be considered as a good approximation of the lower bound to the wind speed experienced at a potential wind turbine location (Millward-Hopkins et al., 2011).

---

<sup>8</sup> The canopy height is defined in the original methodology as the mean building height or the average height of the tallest buildings at any specific site.



The methodology may be summarised as follows:

**Stage 1:** Reanalysed data were obtained from a reference climatology (the Modern-Era Retrospective Analysis for Research and Application MERRA) for a specific location in Beighton, Sheffield, UK where this study is the primary focus in this thesis. Details of the data sets are provided in Section 4.2.4. A similar method has been used by Rose and Apt (2015); Kubik et al. (2013) and Zhang et al. (2015).

**Stage II:** The horizontal interpolation method developed by Ritter et al. (2014) was used in this stage to extract wind speed data from the closest unobserved location to the primary data collection site. The approach is based on the fact that every location lies within a rectangular area covered by the four nearest grid points. The wind speeds at these four points, i.e. the eastward and northward components  $u_h$  and  $v_h$  in 2m, 10 m and 50 m heights are interpolated from the turbine location weighted by their horizontal distance. This method assumes that the influence decreases with increasing distance. Given the short distances (maximum distance to the nearest grid point is about 26.22 miles/42.20 Km and the regular pattern of the MERRA grid, inverse distance weighting is a reasonable way forward.

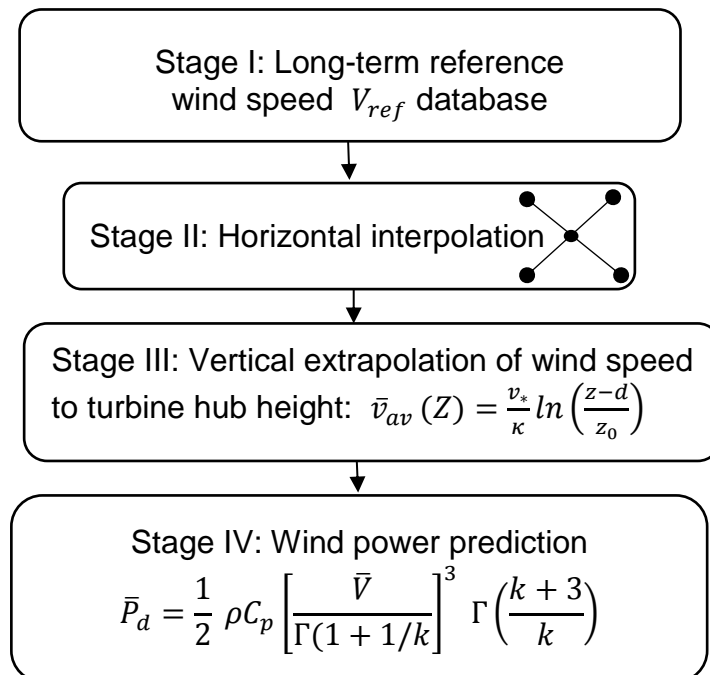


Figure 4.2: Modified methodology based on the boundary layer model used for the current investigation. This is referred to as Model A in this thesis.

However, other interpolation technique, namely Kriging, polynomial, or spline interpolation (Luo et al., 2008) may also be used.

After interpolation, the two components of the wind speed for each height are put together to obtain the absolute values of the wind speed using the following expressions (Ritter et al., 2014):

$$V_h = \sqrt{u_h^2 + v_h^2} \quad (4.1)$$

where  $h$  is 2, 10, and 50 m.

The wind direction  $\varphi V_h$  at this height can be obtained using the follows expression (Ritter et al., 2014):

$$\varphi V_h = \tan^{-1} \left( \frac{v_h}{u_h} \right) \quad (4.2)$$

Stage III: The vertical extrapolation is used to downscale the MERRA wind speed to a typical small scale wind turbine height. Hence, the extracted wind speeds at height  $h$  need to be extrapolated to a new hub height  $z$ . One extrapolation method is given by the power law (Brown et al., 1984; Kubik et al., 2013) as follows:

$$V_z = V_h \left( \frac{z}{z_h} \right)^\alpha \quad (4.3)$$

where  $V_z$  is the wind speed at some height above the ground  $Z$ ,  $V_h$  denotes a known wind speed at height  $Z_h$  and  $\alpha$  is the wind shear coefficient which depends on the stability of the atmosphere and can be derived empirically, but the results are very sensitive to the modelling accuracy and appropriate assumptions (Firtin et al., 2011). The power law approach gives a “reasonable first approximation” to wind resource modelling (Brown et al., 1984). However, the approach described in Eqn (2.23) and restated here for convenience is applied in this study, namely

$$\bar{v}_{av}(Z) = \frac{v_*}{\kappa} \ln \left( \frac{z-d}{z_0} \right) \quad (4.4)$$

where  $\bar{v}_{av}$  is the spatially averaged mean wind speed at height  $z$ ,  $v_*$  is the friction velocity,  $\kappa = \sim 0.41$  is the von Karman constant and,  $d$  and  $z_0$  are the displacement height and roughness length, respectively.

Using this equation, the wind speed at a proposed turbine hub height  $z$  can be predicted without detailed knowledge of the friction viscosity  $v_*$ , provided that the other variables in the equation are known. Thus, the only unknown variables are  $d$  and  $z_0$  which are collectively called the aerodynamic parameters and are of particular interest since they describe the characteristics of the surface roughness. The estimation of the aerodynamic parameters is given in the following subsection.

**Stage IV:** After the wind speed at a potential turbine hub height has been derived, the most important step is the conversion into produced energy. One way of achieving this step is to use a Weibull distribution model along with the predicted mean wind speed and applying a physical transformation, such as the wind power density  $\bar{P}_d$ , which was described in Section 2.4.1, but it is restated here for ease of reference as follows:

$$\bar{P}_d = \frac{1}{2} \rho C_p \left[ \frac{\bar{v}}{\Gamma(1+1/k)} \right]^3 \Gamma\left(\frac{k+3}{k}\right) \quad (4.5)$$

where  $\rho$  denotes the air density,  $C_p$  denotes the Betz limit ( $=16/27$ ), which describes the maximum theoretical energy a turbine can extract from the wind.

#### 4.2.2 Estimation of the local aerodynamic parameters

The estimation of the surface roughness parameters in stage III of Figure 4.2 is required in order to downscale the hub height of the observed wind speed to a new turbine hub height representative of a small-scale wind turbine. These parameters are obtained as a function of the mean height  $h_m$ , and frontal area density  $\lambda_f$ , of the roughness elements based on Raupach (1994) and expressed as follows (Best et al., 2008; Weekes, 2014):

$$\frac{d}{h_m} = 1 - \frac{1 - \exp\left(-\sqrt{15\lambda_f}\right)}{\sqrt{15\lambda_f}} \quad (4.6)$$

$$\frac{Z_0}{h_m} = \left(1 - \frac{d}{h_m}\right) \exp\left(-\frac{-\kappa}{\min(\sqrt{0.003+0.3\lambda_f}, 0.3)} + 0.193\right) \quad (4.7)$$

To obtain the values of the mean height  $h_m$ , and frontal area density  $\lambda_f$ , Grimmond and Oke (1999), the values recommended by Grimmond and Oke (1999), and shown in Table 4.1, are used.

It must be emphasised that this process of identifying the local site characteristics and relating the descriptions to the specific values of the aerodynamic parameters has a high degree of uncertainty and this has also been reported by Best et al. (2008) and Weekes (2014).

Using this principle, the local sites were identified and linked to the values of the roughness parameter in Table 4.1.

Table 4.1: Local terrain classification and associated mean height of the roughness elements  $h_m$ , and frontal area density  $\lambda_f$ . (Reproduced from Grimmond and Oke, 1999).

Terrain class	Description	$h_m$ (m)	$\lambda_f$	$\frac{Z_0}{h_m}$	$\frac{d}{h_m}$
Open countryside	Rural areas with little building	-	-	$Z_0=0.14$	$d_0 = 0$
Woodland	Mature trees	19.5	0.53	0.05	0.67
Urban low height and density	Small buildings and trees that are far apart	6	0.15	0.10	0.48
Urban medium height and density	Mixed height buildings of 2-4 stories and trees.	9	0.2	0.12	0.52
Urban high height and density	Closely spaced buildings of 4-6 stories and trees.	12	0.3	0.13	0.59
Urban very high height and density	Tall towers of various heights in dense urban areas	25	0.3	0.13	0.59

It should be noted that no site in the current study were identified as belonging to the urban category, although they are listed for completeness.

### 4.2.3 The Numerical Objective Analysis of the Boundary Layer (NOABL) – Microgeneration Certification Scheme (MCS) Method

For the UK, the NOABL-MCS method is the best practice guide currently recommended for small wind turbine installation. The method sets out the microgeneration installation standard (MCS, 2013) that must be met in order for small wind turbines to receive financial incentive via the Feed-in-Tariff. In the NOABL-MCS approach, the wind resource assessment involves a simple scaling of the NOABL 10 m wind speed using the following procedure:

- (i) The site is identified and categorised according to one of the terrains described in Table 4.1.
- (ii) Potential obstacles are identified both upwind and downwind of the site based on the prevailing wind direction.
- (iii) The height of the obstacles are used as a correction factor to the height of the turbine using the expression:  $hc = ht - 0.8ho$ , where  $hc$  represents the corrected turbine height,  $ht$  is the actual turbine height above the ground level and  $ho$  indicates the height of the highest obstacles within the site.
- (iv) The mean wind speed for a particular site is then obtained from a table of corrected NOABL 10 m wind speeds for heights between 1 and 100 m.

It should be noted that step (iv) of the NOABL approach is roughly an approximation of the logarithmic wind speed profile based on the local site conditions. While this approach provides corrections to the NOABL 10 m wind speeds, it is relatively simple when compared to the model described above. For example, the method only considers obstacles in the prevailing wind direction and no representation of the regional terrain is included. To highlight these issues, the NOABL- MCS prediction tool was used to extract wind speed data from the investigated sites and these values were compared with those of the present model.

#### **4.2.4 Terrain classification**

In order to assess the effect of a particular terrain on the prediction accuracy, sites were chosen in close proximity to the primary data collection point which is categorised as a rural location. Classification of the neighbouring sites was made from a subjective analysis of satellite images of a region covering several kilometres at the specific sites. In general, the terrain classification will match the local site category defined in Table 4.1. Details of all the sites investigated, including their geographical locations are described in the following subsections.

##### **4.2.4.1 Detailed site description**

Due to the variability of the wind and other local effects, only certain sites are suitable for small wind turbine installation. Therefore, six locations close to the primary data collection site were initially identified for investigation. However, after a preliminary screening of the sites wind resource, the mean wind speeds and the wind power density are compared against a predefined viable value for small-scale wind turbines based on a mean wind speed viability criterion of 4-5 m/s (AWS Scientific Inc. & NREL, 1997; Martin-Martínez, et al., 2012) and the power density based on the international electrochemical commission classification (IEC, 2008). If the predicted wind power density is below this value, the site is non-viable for wind turbine installation and are excluded from further analysis. The success achieved at this stage is investigated by comparing the predictions at the potential viable sites.

Using this criteria, four sites, namely Beighton, Ilkeston, Bilsthorpe and Colby were deemed viable and were further investigated to determine the available wind resource. The proposed sites are located in different counties in England and are characterised by a moderate relief with low hills and plains. Significant seasonal climatic variations could be observed with high temperatures in the summer season and very cold and sometimes snowy winters. In addition, the sites have low population density and the lands are state-owned and not declared as a natural reserve. Furthermore, the proposed sites are linked with good road access. Therefore, harnessing wind power in these locations does not pose any significant threat to the general population and wildlife. Figure 4.3 shows the approximate location map of the proposed sites in England. A brief description of the sites is given as follows:

**Beighton**

Beighton is the primary monitoring location considered in this study and is located in the eastern part of Sheffield, on the border with Rotherham and covers an area of approximately 5.7 km<sup>2</sup>. This location was chosen as the target site because it is the Europe's leading centre for novel research into low carbon technology and long term data for wind speed measurement are available. Beighton is located at 52.60 N and 1.48 E. The climate is moderated by prevailing southwest winds over the North Atlantic Ocean. The total population of Beighton in 2011 was 17,939 people (UK Census Data, 2011). Beighton is considered a strategic location in this study because it is relatively flat with low hills and is primarily a coal mining area.

**Ilkeston**

Ilkeston is a town in Derbyshire, England. It lies on the River Erewash. It is located South of Beighton at 53.000° N latitude and 1.333° W longitude. Its population as at 2001 census was 37,550 people. Ilkeston is a major location due to the many attractions such as traditionally coal mining, iron working and lace making.

**Bilsthorpe**

Bilsthorpe is located East of Beighton at 53.000 and N 0.667 W with an elevation of 121 m is a village in the Newark and Sherwood district of Nottinghamshire, England. As per the 2001 census its population was 3,076 people.



Figure 4.3: An approximate geographical location map of the study sites used to compare predicted and measured mean wind speeds studied sites. (Google Earth, 2015).

### **Colby**

Colby is an 8.34 km<sup>2</sup> village in the County of Norfolk located South East of Beighton at 52.500 N and 0.667 W. As per the 2001 census its population was 524 people. The strongest winds in Colby occurs in the winter months.

### **4.2.5 Metrological measurements**

To compare the predicted wind resource potentials with measurements from the proposed sites, a data collection methodology based on a quantitative and wind energy measurement network was developed. Since the current study is concerned with predicting the wind resource for a small-scale wind turbine, it



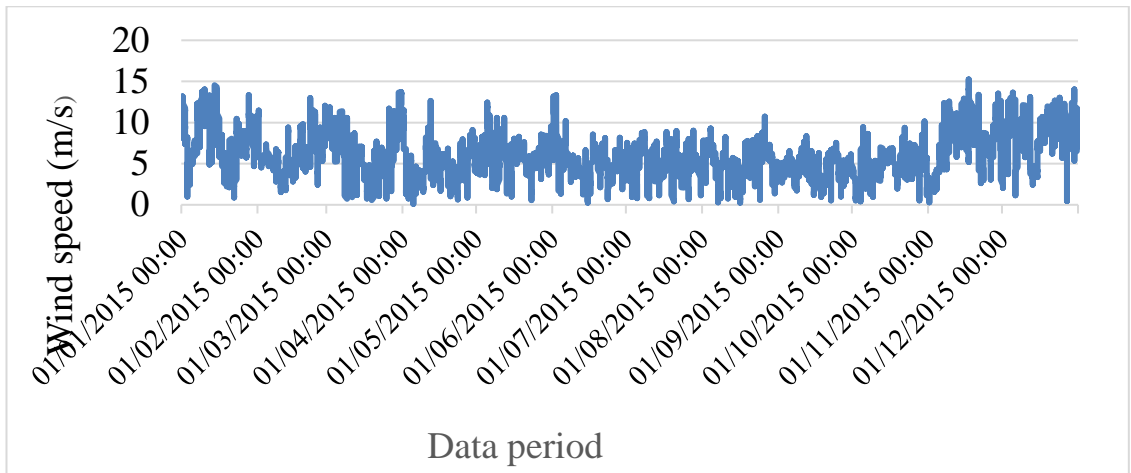
is necessary that the data used for validation and testing reflects the heights similar to small-scale wind turbines as listed in Table 2.1. From this table, it is clear that the typical hub heights for small wind turbines range between 10-35 m. At these heights, the local site features, such as the surface roughness, may have a significant impact on the wind flow. However, to ensure that the wind resource prediction is evaluated in realistic scenarios representative of small-scale wind turbine height, the data used for this study were obtained within this recommended range.

Two kinds of data, namely production data or wind speed data can be used to estimate the wind resource. Production data of nearby wind farms have the advantage that they reflect the true fluctuations and require no transformations, which might result to an estimation bias. Nevertheless, this approach involves making equal assumptions on the geographical and technical conditions of the region of interest. This approach has been criticised because of its unreliability (see for example Ritter et al., 2011) and it is unclear how it can be used to estimate the wind potential of an unobserved location. Another approach is to derive a wind energy index based on wind speed data, which are better available than the production datasets. The most commonly used data in wind resource assessment is weather station data because it objectively measures the actual wind speed at certain locations. However, using such data for this aim comes under criticism: the availability of weather station data is often limited; the historical data records might be incomplete; these datasets are often not located at realistic locations of wind turbine sites. In the UK, data is available through the Meteorological Office anemometer network which archives long-term surface wind speed measurements in the Met Office Data Archives System (MIDAS) (2012). However, this data requires more processing and further details to identify and are not usually available at all locations. An alternative dataset which has been used increasingly in wind resource assessment in recent years is re-analysis data, such as the Modern-Era Retrospective Analysis for Research and Applications (MERRA) provided by the National Aeronautics and Space Administration (NASA) Earth Observing System Distributed Information System (Carta et al., 2013; ESRU, 2015; Kubik et al., 2013; Green, 2014).

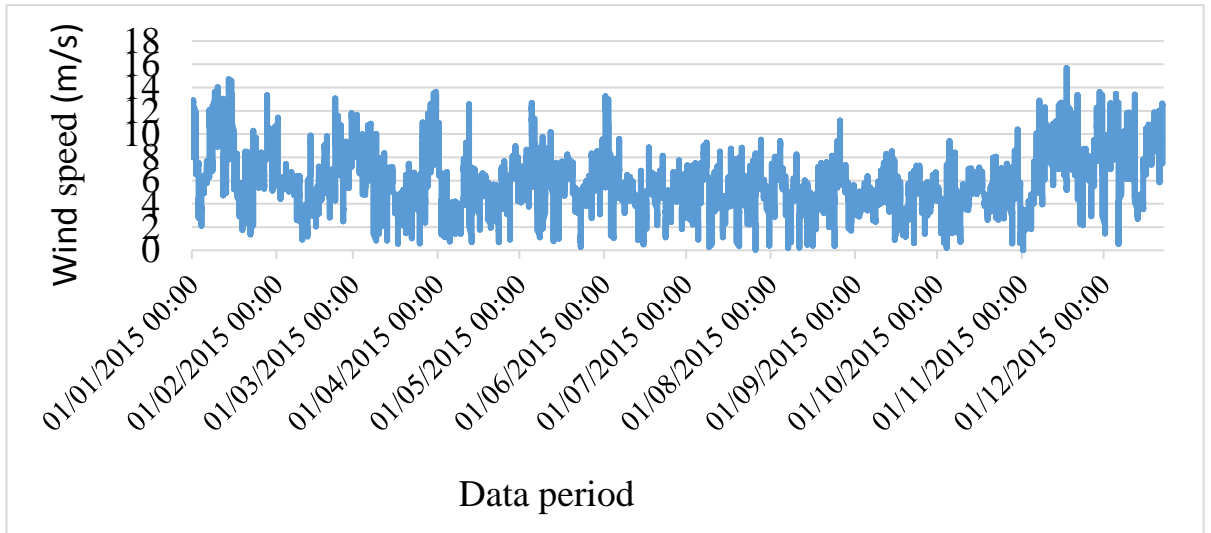
These datasets reconstruct the atmospheric state by integrating observation data with numerical models to produce high quality global synthesis of several climate variables such as conventional and satellite data (Rienecker et al., 2011). They are easily available at any location worldwide and they provide wind data at a high spatial resolution of  $1/2^\circ$  latitude and  $2/3^\circ$  longitude and on an hourly temporal resolution since 1979. Furthermore, MERRA re-analysis datasets typically produces good data quality that is not usually recorded with historical data sets, making it particularly attractive for wind resource applications (Brower, 2012). The wind recordings consist of a northward and eastward wind components at three different heights (2m, 10 m, 50 m above the ground), which are used to extract the wind speed and wind direction at a potential turbine hub height. There are other reanalysis data sources, namely NCEP/NCAR (National Centre for Environmental Prediction/National Centre for Atmospheric Research), ERA-Interim (European Centre for Medium-Range Weather Forecasts Re-Analysis, and CFSR (Climate Forecast System Reanalysis). However, there is no consensus so far on the superiority of one particular reanalysis model (Jimenez et al., 2012; Carvalho, et al., 2014). Thus, in this thesis, MERRA data was used to obtain wind speed and direction data at the nearest four locations to the primary data collection point.

To avoid seasonal bias, a minimum criterion of 95% data coverage over a period of 12 months was applied to the entire data sets to ensure representative mean wind speeds and directions that were obtained from the sites. Furthermore, to ensure consistency in the derived wind speeds and wind power density, all the observed data was converted to hourly means before being subjected to further analysis. The resulting wind speed and direction data at each site were checked for inaccurate readings before further analysis. The measured data at each site is thus representative of the one year wind speed over the period January 1, 2015 to December, 31 2015 as shown in Figure 4.4.

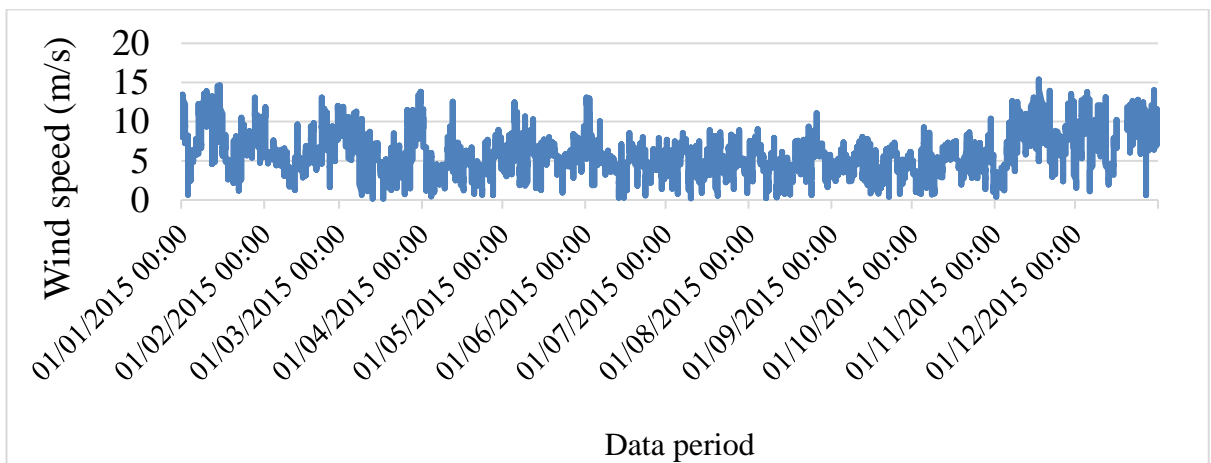
Figure 4.4 (a-d): Observed wind speed as a function of the month and time at each of the investigated sites. 00:00 (12 midnight) represents the beginning of the time step from each month and ends at 23.00 hours before a new month starts.



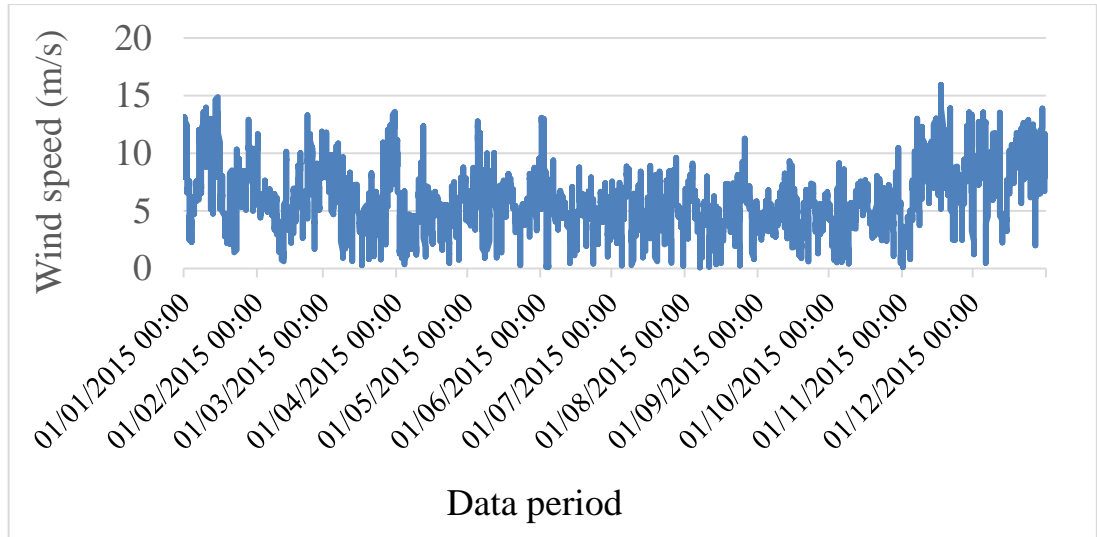
(a) Beighton site



(b) Ilkeston site



(c) Bilsthorpe site



(d) Corby site

Figure 4.4 (a-d) shows the average wind speeds variations, hour by hour and month by month, at a height 10 m for a 12 months period. It can be seen that the winter months (Dec. - Feb.) are windier than the other seasons. This sort of variability is typical in wind characteristics but more trends will be revealed in Section 4.3.

## 4.2.6 Error Metrics

On comparing the predicted wind resources with measurements at the proposed sites, three main errors were utilised to test the validity of the prediction methodology, namely the mean absolute error (MAE), the root mean square error (RMSE) and mean biased error (MBE). A brief review of these errors is given as follows:

### 4.2.6.1 Mean absolute error

The mean absolute error (MAE) is a measure of how closely a set of predicted values match the set of observed or true values. It is expressed according to the following equation:

$$\text{MAE} = \sum_{i=1}^n \frac{1}{n} |\hat{y}_{pred,i} - y_{obs,i}| \quad (4.8)$$

where  $n$  is the total number of samples in the data set,  $\hat{y}_{pred,i}$  is the predicted value,  $y_{obs}$  is the observed value.

### 4.2.6.2 Root mean square error (RMSE)

The root mean square error (RMSE) is given by the following expression:

$$\text{RMSE} = \sum_{i=1}^n \sqrt{\frac{1}{n} (\hat{y}_{pred} - y_{obs})^2} \quad (4.9)$$

#### 4.2.6.3 Mean biased error (MBE)

The mean bias error (MBE) is a measure of how closely a set of predicted values match the set of observed or true values. It is given as follows:

$$\text{MBE} = \sum_{i=1}^n \frac{1}{n} (\hat{y}_{pred} - y_{obs}) \quad (4.10)$$

#### 4.2.6.4 R squared test

The R squared ( $R^2$ ) or the Coefficient of Determination is a statistical measure of how close a data set are to the fitted regression line (Nadaei, 2014), and is most often seen as a number between 0 and 1. Therefore, in this thesis,  $R^2$  is used as a goodness of fit parameter which shows how closely the fitted Weibull distribution matches the measured wind speed data. Values of  $R^2$  approaching 1 indicates a good fit.

$R^2$  can be calculated using the following expressions (Nadaei, 2014):

$$R^2 = \frac{\sum_{i=1}^N (y_i - Z^*)^2 - \sum_{i=1}^N (x_i - y_i)^2}{\sum_{i=1}^N (y_i - Z^*)^2} \quad (4.11)$$

where  $y_i$  is the  $i$ th observed data (wind speed and power density),  $Z^*$  is the mean value of the observed data,  $x_i$  is the  $i$ th predicted data using Weibull distribution and  $N$  is the total number of observations.

### 4.3 Results and discussions

#### 4.3.1 Comparison of the observed wind speed with the predicted wind speed (data validation)

The quality of wind speeds are a determining factor for site selection when considering a location for wind turbine installation. Understanding the absolute wind speed at a potential wind turbine site before having to carry out an onsite measurement campaign reduces the high investment risks to developers during site selection and development. Thus, the performance of Model A is assessed by comparing the predicted wind speed with the wind speed output (observed) by MERRA. By this comparison, the relative differences of the two data sets can be determined.

It must be emphasised that the absolute wind speed is not necessarily a representative of the long-term mean wind speed at the investigated sites, but instead provides insight into the relative differences between the predicted wind speed and the MERRA data.

To reduce the effect of seasonal variability and uneven measurement periods as discussed earlier, a mean of the “monthly means” (MoMM) approach was used to reduce the length of the data as follows:

- (i) All data corresponding to a single month (i.e. 1st January to 31st January over a one-year period) was averaged to get a single wind speed average for the 12 months of the year.
- (ii) An overall average was calculated by weighting each month by the average number of days in that month.

Table 4.2 shows the results and the corresponding difference from each site between the predicted wind speed and the MERRA output. The results demonstrate that the MERRA wind speeds are slightly lower than the predicted wind speeds using Model A. On averaging across all sites, MERRA consistently under-predicts the overall wind speeds at all the investigated sites with an average error of about 0.42%.

Table 4.2: Comparison of the predicted absolute winds speed using Model A with MERRA wind speed at the height of 10 m.

Site Name	Predicted hourly wind speed using Model A (m/s)	Observed MERRA Hourly wind speed (m/s)	Difference
Beighton	6.037	6.036	0.01%
Ilkeston	5.653	5.643	0.17%
Bilsthorpe	5.978	5.914	1.07%
Corby	6.053	6.025	0.46%
<b>All</b>	<b>5.930</b>	<b>5.904</b>	<b>0.42%</b>

Furthermore, Figure 4.5 depicts the comparison of the predicted mean monthly wind speeds with the observed wind speed from MERRA for the full 12 month period (January-December 2015).

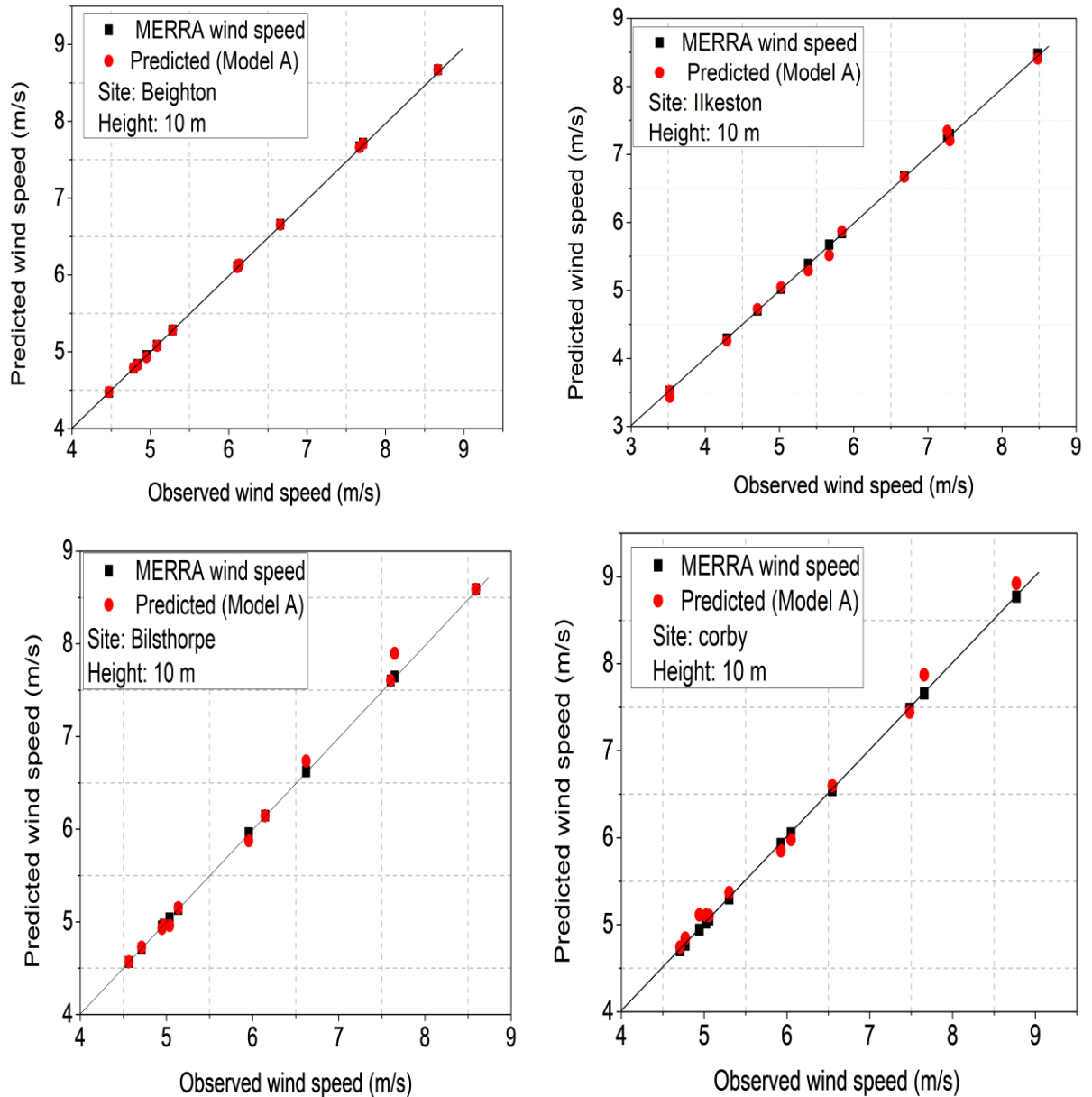


Figure 4.5: Comparison of predicted wind speed (red coloured symbol) versus observed wind speed (MERRA database). The solid line indicates a one-to-one relationship between the predicted and observed wind speeds.

Note that the original values of the MERRA wind speed were obtained at a height of 50 m and were downscaled to the appropriate turbine hub height representative of small-scale using the logarithmic profile for wind speed described in Equation (2.22) with no correction applied to the site characteristics (i.e. using the values of the aerodynamic parameters representative of open country as  $Z_0=0.14$  m and  $d = 0$ ).

The results show that the prediction made using Model A exhibited the general wind speed trend with the data observed from MERRA, although the scatter plot shows relatively low site specific errors in the predicted values, thus reflecting the uncertainty associated in the input parameters.

Furthermore, Figure 4.5 shows that the monthly predicted mean wind speed from the Beighton, Ilkeston, Bilsthorpe and Corby sites range from 4.8-8.6 m/s, 3.5-8.4 m/s, 4.4-8.4 m/s and 4.7-8.7 m/s, respectively. Also, it can be seen that the predicted wind speed using Model A is in close agreement with those obtained from the NASA Modern-Era Retrospective Analysis for Research and Applications (MERRA).

In Figure 4.6, the NOABL-MCS prediction is compared with the predicted wind speed at 10 m height.

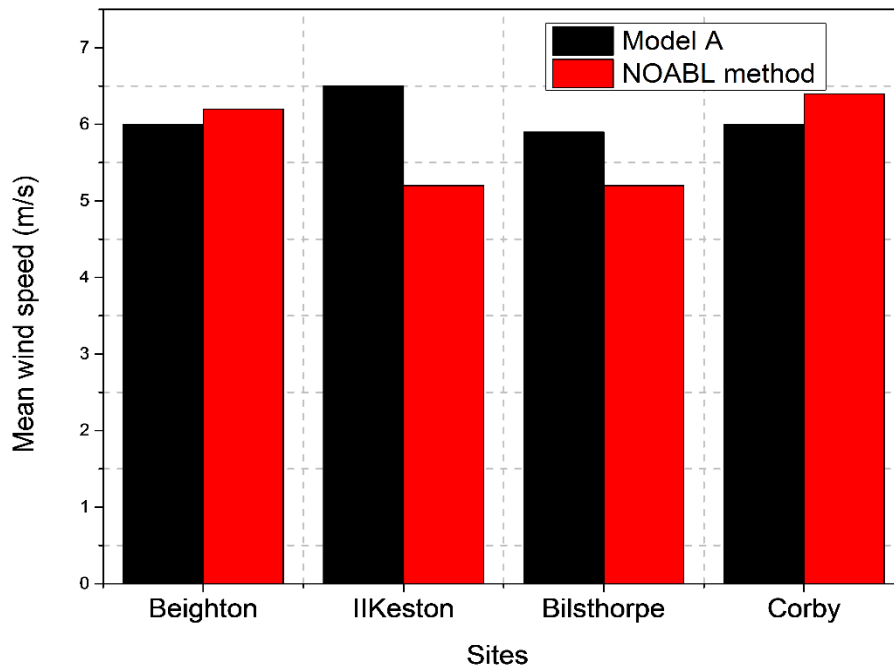


Figure 4.6: Predicted annual mean wind speed at all sites using Model A compared with a benchmark prediction obtained directly from the NOABL-MCS database at a hub height of 10 m.

The NOABL-MCS can be seen to show a similar trend for the general wind speed pattern across the sites. Overall, these results demonstrate that despite the site specific errors, the prediction made using the scaling model (Model A) is in good agreement with both the observed wind speed from MERRA and the output from the NOABL-MCS method.



The error metrics obtained for Model A at each specific site using the MERRA wind speed database as input is shown in Table 4.3. It can be seen that across all metrics, the errors are not too high. This is not surprising since all of these locations are in the rural sites. Generally, sites in rural locations tend to be well exposed and are less subject to abrupt changes in surface roughness or local perturbations due to buildings and hence they conform more closely to the idealised model described in Figure 4.1. Overall, the absolute error ranges from 0.01-0.80 m/s at the Beighton site, 0.02 - 0.65 m/s at Ilkeston and 0.03-0.79, 0.01-0.79 m/s at Corby, respectively.

Table 4.3: Error metrics associated with the predicted wind speed compared over four target sites using Model A.

Error metrics	Methodology	Beighton	Ilkeston	Bilsthorpe	Corby	All
MAE (m/s)	Model A (MERRA)	0.18	0.19	0.19	0.19	0.19
RMSE (m/s)	Model A (MERRA)	0.20	0.21	0.21	0.21	0.21
% Error	Model A (MERRA)	<b>10.76</b>	<b>10.03</b>	<b>10.75</b>	<b>10.75</b>	<b>10.57</b>

Further insight into the errors can be gained by analysing the residual errors in the predicted mean wind speed,  $\varepsilon_{\bar{v}}$ , defined by the following expression:

$$\varepsilon_{\bar{v}} = \bar{V}_{obs} - \bar{V}_{pred} \quad (4.12)$$

The distribution of the residual error is shown in Figure 4.7 for Model A using both MERRA and NOABL wind speed data as input. The results clearly show that the prediction made using the NOABL database have a small negative bias at the second and third sites (tendency to underestimate), while the predictions made using the wind speed from the MERRA database exhibits a positive bias at all the sites. This is presumably due to the positive bias in the NOABL reference database which has been previously reported by Best et al. (2008). Thus, due to the better performance of the observed wind speed from

the MERRA compared to the NOABL, the predictions that will follow subsequently will be made using only the MERRA database as input.

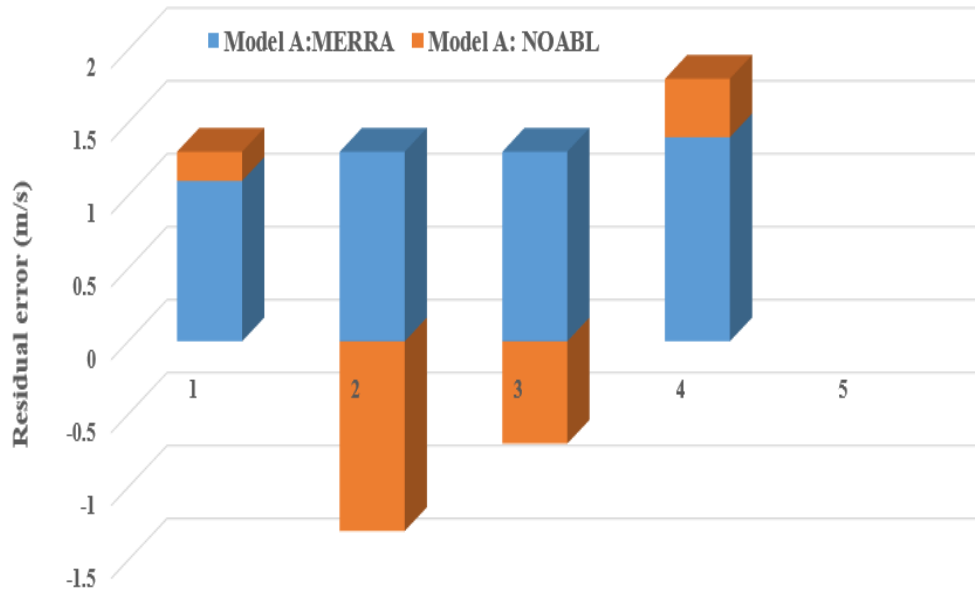
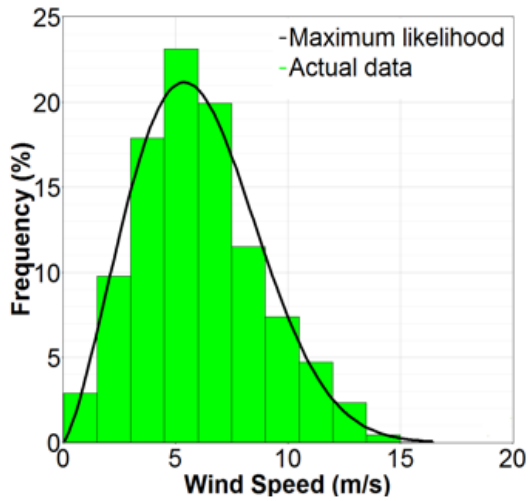


Figure 4.7: Distribution of the residual errors in the mean wind speed for different implementations of the prediction methodology at the 4 investigated sites.

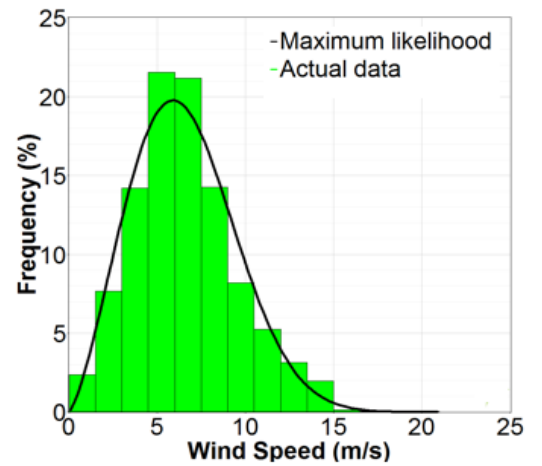
#### 4.3.2 Wind speed probability distribution and direction analysis

Wind speed probability distributions are used to characterise the wind speed observations at any location. The choice of this distribution is vitally important in wind resource analysis because wind power prediction is strongly dependant on the parameters of wind speed distribution. Selecting an appropriate distribution will ultimately reduce the uncertainties in the predicted wind power.

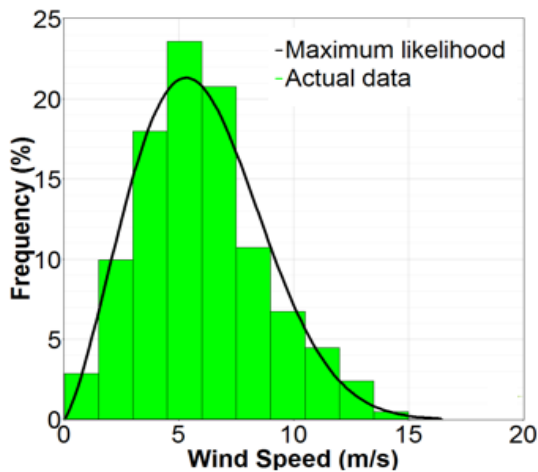
The probability distribution of the mean average wind speed across all sites at 10 m height has been estimated using the Maximum Likelihood Method (Section 2.4.1.1), and the results are shown in Figure 4.8.



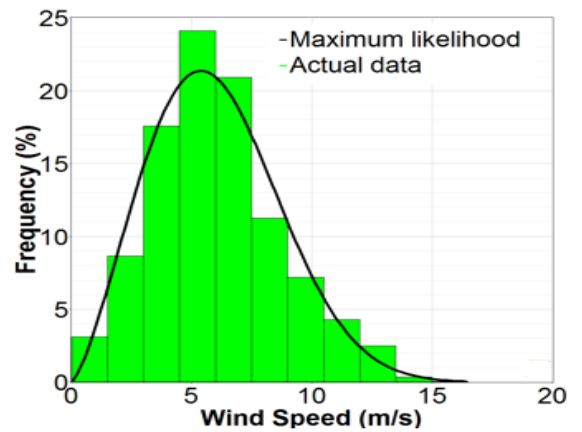
(a) Beighton site



(b) Ilkeston site



(c) Bilsthorpe



(d) Corby

Figure 4.8: Weibull probability distribution function calculated using the maximum likelihood method (Seguro and Lambert, 2000) and histogram of the actual wind speed data (green bars) for the 4 investigated sites.

The shape and size of the Weibull function is impressive. The probability distribution function is evenly distributed at all sites with very low probability of wind speed of less than 4 m/s. The results give an indication of finding high wind speeds in the range between 4-8 m/s which can be utilised for wind power production. The frequency distribution indicates that the maximum probability of average wind speed at all sites occurred at about 6-7 m/s.

Furthermore, these plots demonstrate that the data histograms very closely approximate the prediction made using the Weibull distribution.

On the other hand, wind direction plays an important role in the optimal positioning of a wind turbine in any given location. Wind rose plots for each of the investigated sites were created using the commercial code Windographer version 4 from the wind speed and direction data for 10 m height. The full cycle (360°) is divided into 16 sectors. Figure 4.9 shows the wind frequency distribution by direction, and they show that the predominant wind is available from the south-west direction. This means that the most energy are available in the south west direction.

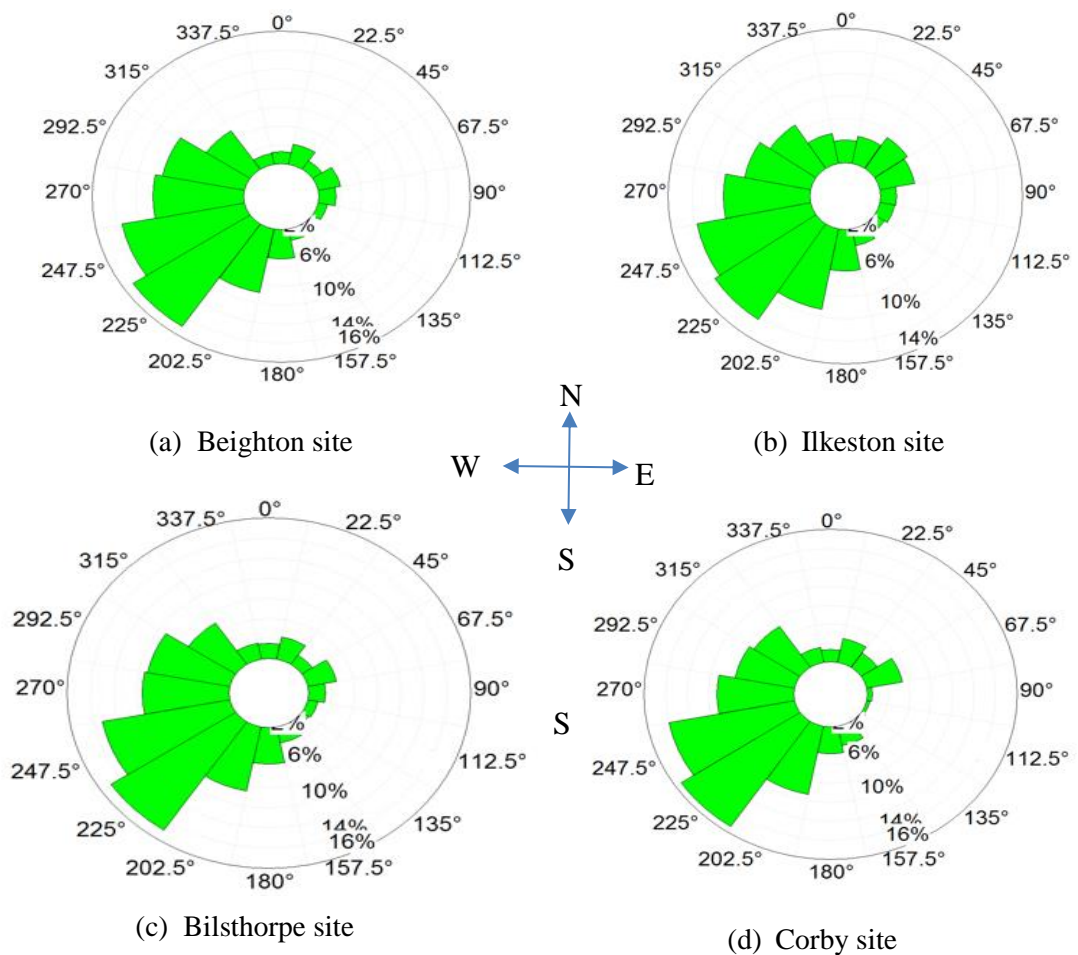


Figure 4.9: Wind rose plots showing the prevailing wind directions at the investigated sites.

These results is also consistent with the prevailing wind direction in most UK locations which was reported in the work of Aris (2013).

There are more variations in the direction and speed of the wind within each month of the year and this is shown for the Beighton site in **Appendix II**. Important observations about the wind distributions can be revealed when the data is visualised in this way.

### 4.3.3 Sensitivity to the Weibull shape parameter

Although an accurate estimate of the wind speed at any given site is the starting point in predicting the site wind resource, in cases where the onsite measurement campaign is not part of the resource assessment, some assumptions must also be made regarding the distribution of the wind speed at such sites. Typically, the Weibull two-parameter distribution is the preferred choice for this purpose since it has been shown to represent a wide range of wind regimes (see for example Jain, 2011, Manwell et al., 2008; Justus et al., 1976). The Weibull distribution is defined by a mean wind speed and a shape factor which describes the spread of the wind speeds about the mean. Due to the non-linear relationship between the wind speed and wind power, as described in Section 2.4.1, the value of the shape parameter  $k$  will ultimately affect the predicted power in the wind.

To evaluate the influence of the shape parameter on the predicted wind power, it is useful to express the Betz mean power density  $\bar{P}_d$ , in terms of the Weibull distribution parameters as follows (Jain, 2011; Manwell et al., 2009):

$$\bar{P}_d = 0.5 \left( \frac{16}{27} \right) \rho \left[ \frac{\bar{v}}{\Gamma(1+1/k_{obs})} \right]^3 \Gamma \left( \frac{k+3}{k} \right) \quad (4.13)$$

in which the factor  $\frac{16}{27}$  indicates the Betz limit,  $\rho$  is the air density and  $\Gamma$  is the gamma function.

A question worthy of investigation is the impact of the shape parameter on the predicted power density at each specific site. This equation can be used to investigate the sensitivity of the power density  $\bar{P}_d$  to the observed shape parameter  $k_{obs}$ .

The plot described by Eqn. (4.13) is depicted in Figure 4.10 for the values of the observed shape parameter  $k_{obs}$ . The result shows that the maximum power density is attained when the observed shape parameter is 3.5 at all sites, and thus it is possible to consider how accurately we must be able to

predict the wind power density based on the choice of the Weibull shape factor. For each of the 4 measurement sites, the maximum likelihood algorithm described in Section 2.4.1.1 was used to fit the Weibull distributions to the observed wind speed, thus resulting in a range of shape parameters,  $k_{obs} = 2.2 - 3.5$ .

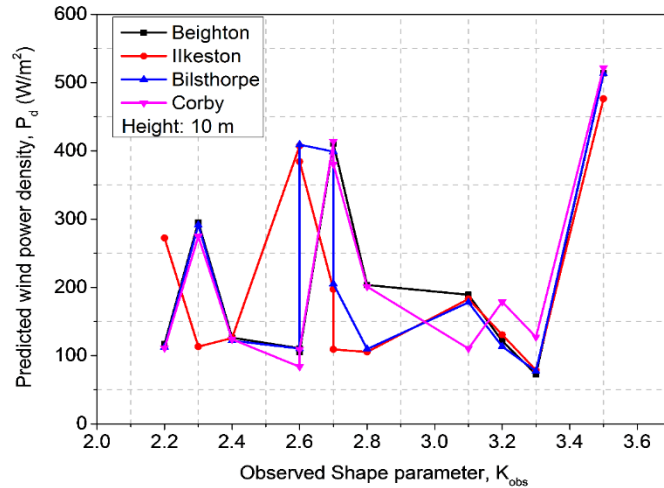


Figure 4.10: Predicted wind power density as a function of the shape parameter for the 4 investigated sites.

For these sites, the coefficient of correlation  $R^2$ , which indicates how a model fits the actual values or numerical prediction is shown in Figure 4.11. Overall, Figure 4.11 show that the values of  $R^2$  is close to 1.

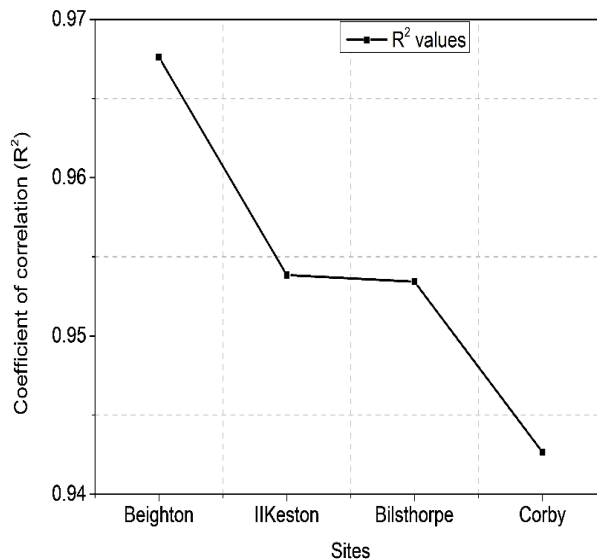


Figure 4.11: Error metrics using the coefficient of correlation ( $R^2$ ) to compare how the observed Weibull shape parameter fits the predicted wind power density.

Generally, the value of 1 for  $R^2$  indicates that 100% of the total variation in the fitted response can be explained in a linear relationship. Therefore, for value of  $R^2$  closer to 1 the better is the fit.

Errors arising from the predicted wind power density will usually result from the uncertainties in both the predicted wind speed  $\bar{V}_{pred}$  and the observed shape parameter  $k_{obs}$ . However, it is possible to calculate the relative magnitude of the fractional errors in the predicted power density resulting from these two error sources. In the case of uncertainties arising from the predicted wind speed  $\bar{V}_{pred}$ , the errors in the predicted wind power density  $\bar{P}_d$  will be a function of the observed wind speed  $\bar{V}_{obs}$ .

Given that the observed values of the shape parameter range from  $k_{obs} = 2.2 - 3.5$ , we can consider the best approach to predict the mean power density based on the choice of the shape parameter.

Figure 4.12 shows the comparison of the observed wind power density at all sites using the modifications suggested in this methodology.

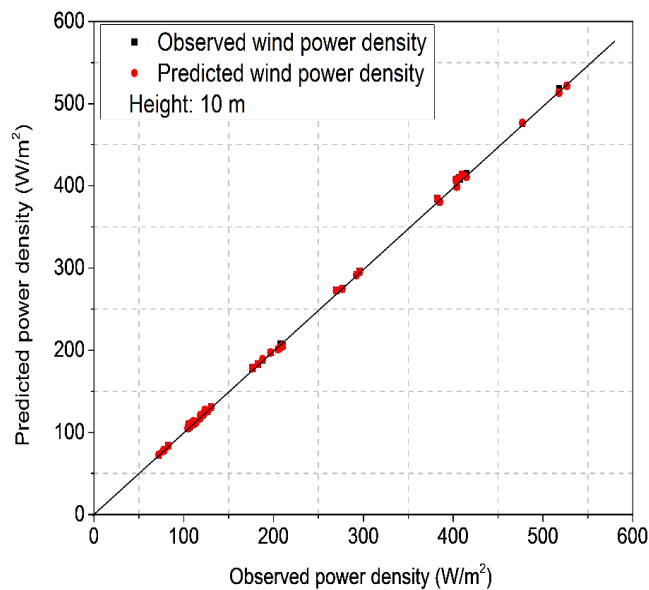


Figure 4.12: Comparison of the observed and predicted wind power density at all 4 sites. The solid line represents a one-to-one relationship.

The results revealed that across all sites, the predicted wind power density is within the same bound as the observed wind power density, thus indicating that the uncertainties in the predicted wind speed and the observed shape

parameter will not have a significant impact on the prediction of the power density.

This does not mean that improvements in the observed wind speed  $\bar{V}_{obs}$  and the shape parameter  $k_{obs}$  will not increase the accuracy of the predicted wind power density  $\bar{P}_d$ , rather, it is an indication of the relative contribution of these error sources to the predicted wind power density  $\bar{P}_d$ .

A question worthy to be asked is how can an optimum value of the observed shape parameter  $k_{obs}$  be chosen in order to accurately calculate the wind power density.

Since the plot shown in Figure 4.10 is not a linear relationship, the mean value of the observed shape parameter  $k_{obs}$  is not necessarily equal to the optimum value. Hence it is possible to calculate an optimum value, known as an assumed shape parameter  $k_{ass}$ , that will results in maximising the wind power density and reducing the errors to the lowest minimum when combined at all sites.

For instance, given a set of observed values  $k_{obs}$ , across  $n$  sites and an assumed constant shape parameter  $k_{ass}$ , used to evaluate the wind power density at the  $n^{th}$  site, the combined fractional error in the predicted power density  $\bar{P}_d$  at all sites,  $\varepsilon_{\bar{P}_d}(k_{ass})$  is given according to the following expressions (Weekes, 2014):

$$\varepsilon_{\bar{P}_d}(k_{ass}) = \sum_i \left[ 1 - \frac{\Gamma(1+1/k_{ass})}{\Gamma(1+1/k_{obs,n})} \right]^3 \frac{\Gamma(1+3/k_{obs,n})}{\Gamma(1+3/k_{ass})} \quad (4.12)$$

This equation can be solved iteratively with respect to the assumed shape parameter,  $k_{ass}$ , to find an optimum value given a set of observed values of the shape parameters  $k_{obs}$ . In the present case of the 4 sites investigated in this study, the optimum value for  $k_{ass}$  is 2.6, which is also very close to the mean values of the observed shape parameter  $k_{obs}$ .

It is important to note that the above discussion is based on the assumption that the datasets are accurately represented by a Weibull probability distribution. This was found to be true for the 4 four sites investigated in this study as represented in Figure 4.8. Therefore, in the absence of no contrary



site specific information, the assumption of the Weibull distribution appears to be justified.

#### 4.3.4 Overall performance of the prediction methodology

Generally, the validity of a wind resource prediction methodology may be assessed by its ability to accurately predict the available wind power, as tested by comparison with actual measurements. In the present study, measured wind speeds were collected across the 4 sites for a period of one year to account for monthly variability in the wind speed patterns. Hence, in order to calculate the observed wind power density  $\bar{P}_d$ , a Weibull probability distribution was fitted to the actual measurements from each site using the maximum likelihood method described in Section 2.4.1.1. and the extracted values of the observed shape parameter ( $k_{obs}$ ) was used along with the mean wind speed calculated to the wind power density using Eqn. (4.5).

The error metrics described in Section 4.2.5 are then used to investigate the success of the performance methodology. Table 4.4 compares the calculated wind power density with the associated errors at each site.

Table 4.4: Predicted wind power density with associated errors across all the 4 sites investigated at a hub height of 10 m using Model A.

Sites	$\bar{P}_d$ (W/m <sup>2</sup> ) observed	$\bar{P}_d$ (W/m <sup>2</sup> ) calculated	$R^2$	MAE	MBE	% Error
Beighton	223.3	222.9	0.96	1.41	-0.85	<b>17</b>
Ilkeston	179.4	178.9	0.95	1.31	-1.3	<b>27</b>
Bilsthorpe	217.8	217.0	0.95	1.39	-1.3	<b>36</b>
Corby	220.0	219.5	0.94	1.40	-1.4	<b>22</b>
<b>All (average)</b>			<b>0.95</b>	<b>1.37</b>	<b>-1.2</b>	<b>25</b>

These results in Table 4.4 show that the model predicted the wind power density with reasonably accuracy. Also, Table 4.4 includes the mean bias error (MBE) and % Error. These errors are useful indicators as to whether the predicted wind power density is over-or underestimated. At all the sites, the

MBE and % errors show the directions of the error bias and it demonstrates that the model slightly under-predicted the wind power density.

Figure 4.11 compares the distribution of the annual errors in the predicted wind power density. This is a useful guide to the likely errors in the predicted value of the power density using this methodology. Furthermore, the error metrics across all sites are compared in Table 4.3 and Figure 4.7. On average, this error shows a clear improvement of Model A when using data from the MERRA database as compared to the NOABL database.

It is important to note that due to the cubic relationship between the wind power and wind speed, over-estimation of the predicted mean wind speed ( $\hat{V}_{pred}$ ) will significantly affect the predicted wind power density ( $\bar{p}_d$ ) than under-estimates of the same magnitude. Thus, the reduced errors observed in the predicted wind speed  $\hat{V}_{pred}$  does not automatically translate to reduced errors in the predicted wind power density  $\bar{p}_d$ . This effect can be seen in Table 4.3 across all the sites where Model A performs better in terms of the predicted wind speed using the MERRA data as input into the model. However, the errors in the predicted mean wind speed can result in the error in the predicted power density  $\bar{p}_d$  as shown in Figure 4.9. This highlights the need for caution when using such a model to assess the potential of a site for wind turbine installation. However, in spite of this, the overall predictions as compared to the actual data demonstrates that with even relatively simple changes, a consistent improvement can be achieved in the predicted wind resource.

#### **4.4 Boundary layer prediction methodology as a site screening tool**

One approach to maximise the implementation of the prediction methodology at multiple sites is to apply the tool to screen for viable sites for potential wind turbine installation using a pre-defined viability criterion. The sites that exceed this set criterion would be judged worthy of further investigation using either direct onsite measurements or an advanced computational approach.

To define a viability criterion, two main factors must be considered, namely environmental viability (ability of the turbine to produce sufficient energy and repay its embedded carbon) and financial viability (ability of the turbine to

produce energy economically and repay the investment cost). These two factors will greatly depend on the cost and type of the turbine as well as the availability of government support incentives (Feed-in Tariffs). In the case of small-scale wind turbine installations, different studies (see for example, Millward-Hokpins et al., 2013; Sobol 1967) have used a mean wind speed viability criterion of 4-5 m/s to screen for viable wind turbine sites.

Furthermore, while the minimum wind speed criterion is a useful starting point to screen for potential sites, the available wind power will depend on the distribution of wind speed and the mean wind speed at a proposed site. Thus, it will make sense to express the viability criterion in terms of the minimum wind power density. Now, assuming a site has been modelled using a Weibull distribution, which is the case in the present study, the mean Betz power in the wind can be computed using Equation (4.13). If a 4 m/s minimum wind speed criterion and a Weibull shape parameter  $k$  representative of typical UK site ( $k = 1.9$ ) are substituted in Eqn. (4.13), this will result to a viability criterion of power density  $\bar{p}_d \geq 47 \text{ W/m}^2$ .

The meaning of this number ( $\bar{p}_d \geq 47 \text{ W/m}^2$ ) can be demonstrated by doing a simple power calculation. Assuming 60% of the available Betz wind power can be converted to electrical power (this may not be practicable in real life due to friction and blade tip losses and efficiency will depend on the wind speed and turbine design), for a small-scale wind turbine with a blade diameter of 1.5 m, the average power production by the turbine  $P = 0.5\rho v^3 C_p$  equates to 40 W and an annual energy production  $AEP = 0.5\rho v^3 \eta$  equates to 179 kWh. For the case of a large wind turbine with a diameter of 10 m, the power produced equates to 1822 W and an annual energy production of 7984 kWh. In the preceding analysis, this minimum power density criterion is applied to screen for viable wind turbine sites.

To investigate the site screening process, we aim to identify sites which may be potentially unsuitable based on the defined viability criterion of power density  $\bar{p}_d \geq 47 \text{ W/m}^2$ .

Figure 4.13 depicts the observed wind power density at all 10 sites along with the error bars which represent the uncertainties in the prediction.

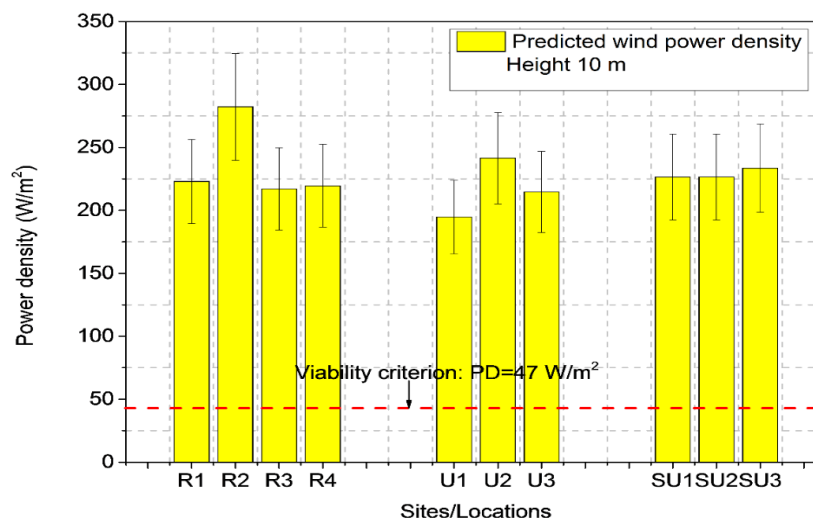


Figure 4.13: Mean annual wind power density predicted at 10 sites with the uncertainties associated with each site prediction (bars). The dotted red line represents a viability criterion in which the sites are judged viable or not.

The sites were specifically selected to reflect three general terrain categories, namely urban (3 sites), sub-urban (3 sites) and rural site (4).

Table 4.5: Summary of the sites used to compare predicted and measured wind power density. The sites are defined by the letter in the parenthesis as Rural, Urban and Sub-Urban.

Site name/location	Long (deg)	Latitude (deg)	Height (m)	Wind speed (m/s)	Data (yrs)
Beighton (R1)	52.60	1.48	10	5.8	5
Ilkeston (R2)	53.00	1.33	10	5.4	5
Bilsthorpe (R3)	53.00	0.67	10	5.6	5
Corby (R4)	52.5	0.67	10	5.5	5
Manchester (U1)	53.47	-2.25	10	3.2	5
London (U2)	51.46	0.10	10	2.5	5
Leeds (U3)	53.78	-1.54	10	2.9	5
West Sussex (SU1)	50.83	-0.59	10	2.2	5
Rochdale (SU2)	53.60	-2.18	10	2.2	5
Oxford (SU3)	51.96	-1.55	10	3.2	5

These sites were categorised based on the analysis of satellite images of an area covering several kilometres centred at the test site and the terrain

classification falls under the local site condition defined in Table 4.1. The full details of these sites are given in **Table 4.5**.

The results show that the power density at all sites exceeded the viability criterion of  $\bar{p}_d \geq 47 \text{ W/m}^2$  and are thus judged viable for small scale wind turbine installation. Furthermore, the result indicate that for the hub heights considered in this study, the highest wind resource tend to be in the rural site (R2) as compared to the urban and sub-urban sites. The uncertainties associated with the prediction represent approximately +/- 12 W/m<sup>2</sup>. These uncertainties tend to be higher in the urban sites than the rural sites in line with the error metrics ( $R^2$ ) in **Table 4.6**.

Furthermore as a benchmark, the wind power density predicted using the NOABL methodology are compared with the observed and predicted wind power density in Table 4.5.

Table 4.6: Comparison of observed and predicted viability for the 10 sites based on a criterion of  $\bar{p}_d \geq 47 \text{ W/m}^2$ . Tick depict viable sites, and crosses depict non- viable sites. Correct prediction are highlighted in green, and incorrect predictions are in red.

Site	Coefficient of correlation ( $R^2$ )	Observed value	Predicted value (present model)	NOABL-MCS method
Beighton (R1)	0.96	✓	✓	✓
Ilkeston (R2)	0.96	✓	✓	✓
Bilsthorpe (R3)	0.95	✓	✓	✓
Corby (R4)	0.94	✓	✓	✓
Manchester (U1)	0.85	✓	✓	✓
London (U2)	0.85	✓	✓	x
Leeds (U3)	0.87	✓	✓	✓
West Sussex (SU1)	0.85	✓	✓	x
Rochdale (SU2)	0.84	✓	✓	x
Oxford (SU3)	0.84	✓	✓	x

The tick indicate that a site passes the viability criterion while crosses indicate it fails. Correct predictions are highlighted in green, while incorrect predictions are highlighted are in red.

These results (Table 4.6) show that the boundary layer scaling model predicted the variability correctly in all 10 sites as compared to the observed values. In screening for potential viable sites, it is important that promising sites are not excluded from further investigation based on an incorrect viability prediction, shown by the red crosses in Table 4.6.

This is a promising result given that the boundary layer methodology does not require onsite wind measurements.

On the other hand, the NOABL method makes accurate viability predictions in 8 out of the 10 cases investigated and incorrectly excludes 2 viable sites. These results demonstrate that the boundary layer model can be a very useful tool when used in a site screening process to select potential small-scale wind turbine sites and can add significant value to site screening compared to the NOABL-MCS approach.

#### **4.5 Conclusions**

This chapter investigated the ability of a modified boundary layer scaling model to estimate the wind energy resource potentials at an unobserved location. The choice of this model is driven by cost and its wide applicability to a wide range of atmospheric conditions, and the successful use for resource analysis at other locations.

The model results were compared to wind speed measurements obtained from MERRA at four locations. The results were validated against observations using reliable and traditional error metrics, namely RMSE, MAE, % error and bias and the distribution of the residuals. Annual and monthly variations of wind speed, wind speed frequency histograms, and wind roses have shed further light onto the validity of the model. Averaged across all sites, the mean absolute error and % error in the predicted wind speed were found to be 0.18 m/s and 10.57%, respectively. These results are very encouraging and give us the confidence in being able to produce an accurate wind resource assessment.

Based on the success achieved in predicting the wind speed, the methodology was extended to predict the wind power density  $\bar{p}_d$  at each of the investigated

sites using the Weibull distribution along with the observed Weibull shape parameters  $k_{obs}$ . An expression was derived to describe the fractional error in the power density resulting from the use of an assumed shape parameter  $k_{ass}$  to predict the wind power density and the impact of this error in relation to the errors in the predicted wind speed  $\bar{V}_{pred}$  was evaluated. Using the values of the observed Weibull shape parameter  $k_{obs}$  obtained from the investigated sites, this expression was evaluated in order to obtain an optimum value of an assumed shape parameter  $k_{ass} = 2.6$  which maximises the wind power density  $\bar{p}_d$ .

Furthermore, the overall performance of the prediction methodology in predicting the wind resource was investigated by predicting the wind power density at each site and the results were further compared to the values obtained from MERRA. The coefficient of determination  $R^2$ , mean absolute error (MAE), mean biased error (MBE) and the % error were found to be 0.95, 1.37, -1.2, and 0.25%, respectively. These errors clearly demonstrate that while the methodology has limitations, improvements can be achieved with relatively simple modifications to the original methodology.

In addition, the methodology was extended to screen for viable wind turbine sites using a predefined viability power density criterion. Ten sites were used as case studies and the predictions obtained at these sites were compared to the measured values. As a benchmark, these predictions were also compared with those obtained using the NOABL-MCS method. The results show that the present model predicted variability is correct at ten sites which also agrees with the observed values. However, two of the sites were excluded as non-viable sites using the NOABL-MCS method. These predictions demonstrate that the present model can be a useful tool when used as a site screening tool to identify viable sites.

Due to the huge cost and timescales associated with the onsite measurement approach of wind resource assessment, semi-empirical and low cost models such as the model presented in this chapter can be a useful tool to quickly assess the wind resource potential of any location in the World at no cost before analysing the site's wind energy potential in greater detail by means of site specific onsite measurements. However, it is important to be aware of the potential limitations inherent in such a model. Given the uncertainties

associated with the methodology as demonstrated in the magnitude of the average errors in the predicted wind speed and wind power density, such models are better applied to identify potential viable sites against a defined viability criterion. Using this approach, potential viable sites can then be identified and supplemented with onsite measurements in order to reduce huge investment risks. However, since long-term wind measurement approaches are unlikely to be adopted in small-scale wind resource assessments due to the timescales and costs, there is need for the development of methods that can relate short-term measurement periods to yield a long-term resource characterisation of approximately 20 years. These methods, such as those based on hindcasting or measure-correlate-predict (MCP), are explored in the following Chapter.



## Chapter 5 Data Driven Measure-Correlate-Predict Approaches to Wind Resource Assessment

### 5.1 Overview

In Chapter 4, an estimate of the temporary variability of the wind conditions at four locations were determined using a physical modelling approach based on the boundary layer scaling model. These estimates were made from an input reference wind speed recording typically made during a relatively short period (1 year) that is not representative of the long-term wind conditions at the sites. Long-term correction of the wind conditions is therefore needed in order to estimate the expected long-term wind climate at the measurement site.

An illustration of the approach adopted in the long-term correction of the onsite wind measurements is given in Figure 5.1. The bullet points represent important factors that requires special caution in evaluating the uncertainty in the estimated long-term wind resources.

The two main input parameters necessary for the long-term correction process are the short-term onsite measurement taken from a target site and a historical long-term data from a representative location. How well the short-term onsite measurement represent the site's long-term wind climate is largely dependent on the accuracy and timescale of the measurements (box 1 in Figure 5.1). In the context of small-scale wind turbines, the onsite measurement period is often taken for a period of one year in order to capture the seasonal variability of the site wind conditions (Jain, 2011). However, the longer-term variability is not captured. Hence, it is essential to evaluate the long-term time series that is believed to be representative of the long-term wind conditions at the measurement site.

It should be noted that the long-term data representativeness, along with its characteristics, is an important factor that should be calculated (box 2 in Figure 5.1). The term representativeness indicate how well the long-term data represents the long-term wind conditions at the measurement site. In addition, this dataset describe the variations in the local climatic conditions, and will not be affected by changes due to the modification in the methodology or the measurement system used in the data collection process.

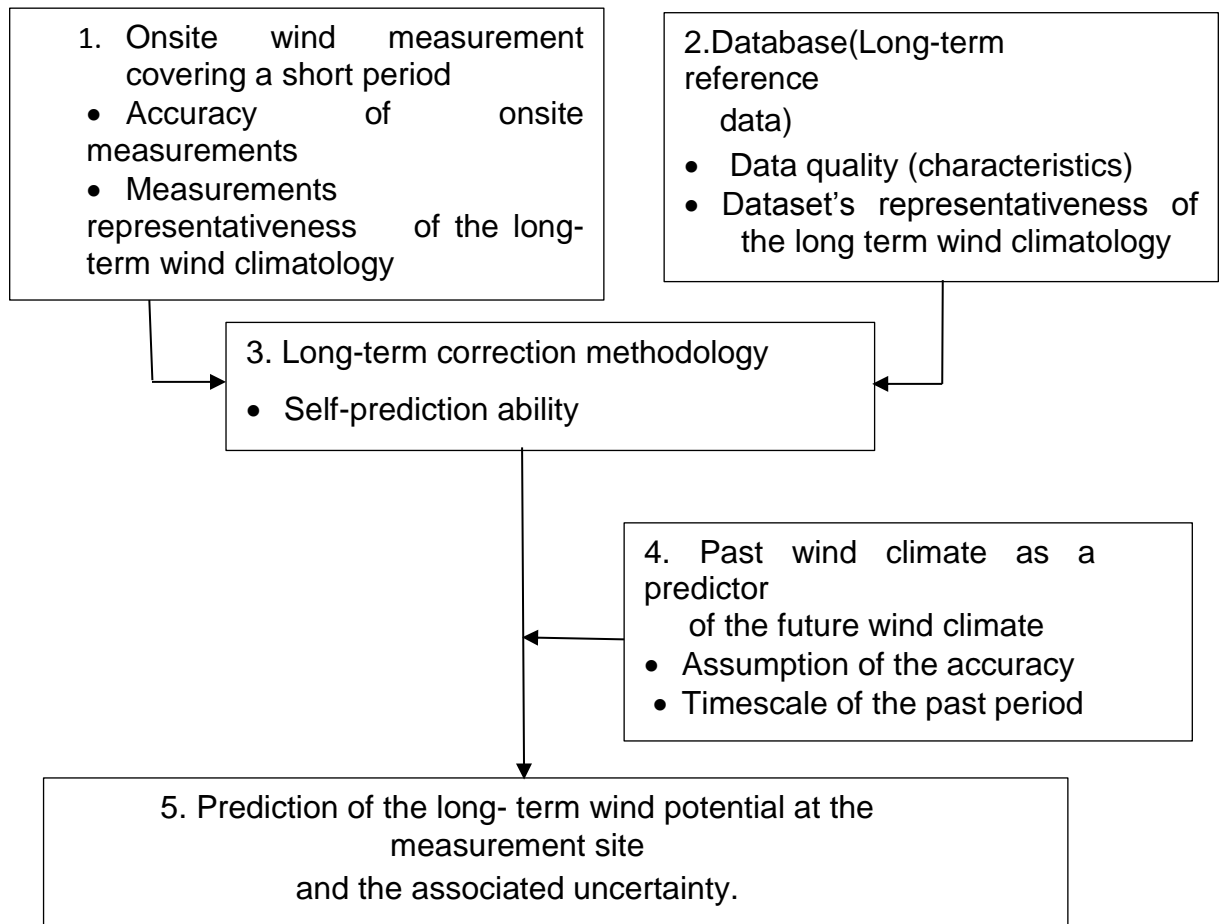


Figure 5.1: A workflow diagram illustrating the process involved in the long-term correction of onsite wind measurements. The bullet points represent parameters of high relevance for the evaluation of the uncertainty in the overall long-term corrected wind resource.

Based on the above reasons, the evaluation of the spatial and temporary characteristics of the long-term wind conditions cannot be overemphasised. Once these data series have been established, a long-term correction methodology is applied in order to obtain an appropriate description of the long-term wind conditions at the measurement site. However, the accuracy of a chosen methodology is dictated by its self-prediction ability. That is, its ability to accurately predict the long term wind conditions (box 3).

The long-term or future wind climate at the measurement site is unknown. Therefore, an assumption is made that the past is a predictor of the future wind climate, i.e. the statistical properties of the future and past wind condition

are assumed to be the same. However, the accuracy of this assumption is very crucial since it will be used to determine the long-term wind condition and shall therefore be evaluated. Furthermore, the timescale of the future wind condition in which the energy production estimate will be made should be calculated (box 4 in Figure 5.1). Typically, the timescale is usually the lifetime of the wind turbine, i.e., when the investment costs will be recouped. This is usually 15-20 years for most wind turbines (Lileo et al., 2013, Nadaei, 2014). The long-term correction methodology used here is the measure-correlate-predict (MCP) approaches discussed in Section 3.2. However, the MCP approaches have received little attention in small-scale wind resource assessment where short-term measurements may be used to provide corrections to seasonal variability of wind conditions. While conducting a long-term wind measurement is clearly needed in order to reduce prediction uncertainty, the focus of the present work is to establish the possibility of applying the MCP technique to a short-term training data between 3-12 months. The aim is to determine whether wind resource assessment driven by short-term measurements can be useful for the small-scale wind industry. However, using this approach should not be seen as a substitute for long-term wind measurements, which has a higher prediction accuracy but rather as a measure to increase the value of short-term measurements in locations where long-term onsite measurements are not available.

As discussed in Section 3.4, although a limited amount of research has been undertaken that investigated the effect of small measurement periods on MCP performance, there is need for a more detailed study in this regard, particularly using a single measurement point along with reference data from multiple years to predict the wind resource potentials. Many studies were evaluated based on a relatively short data record (between 1-3 months) and the MCP performances were judged using just the mean wind speed rather than the parameters related to the full wind speed distribution.

The contribution of the work presented in this chapter is an evaluation of measure-correlate-predict performance using a short-term training period at a site specific location. Two MCP approaches were investigated using different measurement lengths and the error metrics were used to quantify the average errors in the predicted wind resource.

The main objectives of this study are as follows:

- (i) Development of a technique to account for the uncertainty associated with different MCP approaches using onsite measurement.
- (ii) To examine the performance of two linear MCP techniques using short-term measurement. It should be noted that the scope of the present work is limited to linear MCP models. Non-linear models were not examined in the present work.
- (iii) To assess the uncertainty in the estimated wind resource and highlight relevant issues of using short-term onsite measurement for wind resource prediction.
- (iv) An assessment of the expected energy production and economic evaluation at the target site for potential wind energy development.

This chapter is structured as follows: Firstly, a brief description of the core methodology used to predict the long-term wind resource is given. Next, the evaluation set up, data quality control measures, choice of long-term data set, correlation relationship between the target and reference sites and the uncertainties associated with measure-correlate-predict (MCP) approaches are described. Further, an evaluation of the performance of the MCP approaches is presented, including the effects of seasonal changes on the predicted wind resource. This is followed by a comparison of the error metrics between the MCP approaches and the boundary layer model described in Chapter 4. Finally, an energy production estimate as well as economic feasibility of installing a small-scale wind turbine is given and overall conclusions are drawn.

## 5.2 Methodology

The methodology implemented in this chapter has four main steps.

Step 1: To begin with, a data collection window is built spanning a period of 12 months which is shifted in steps of one month throughout the 12 month period. The dataset covered by this collection window is referred to as the training period. The remaining data not covered by this window is designated as the long-term reference data which cover a period of 15 years. The dataset was expressed as a function  $f_{x,y}(x,y)$ , where  $x=$

$\{x_1 \dots \dots \dots x_n\}$  the wind speeds at the reference site and  $y$  is the wind speed at the target site.

Step 2: The training data are decomposed into D1, D2, D3, and D4 with each containing 3, 6, 9 and 12 months of data, respectively. These datasets represents the short-term data and are used to obtain the regression parameters for the MCP approaches. The experimental set up of the data collection process is presented in **Appendix II**.

Step 3: The MCP approaches are then applied to the long-term reference data spanning a period of 15 years in order to predict a concurrent time series of wind resource at the target site. This is referred to as the long-term wind resource extrapolated from the short-term onsite measurement.

Step 4: The uncertainties (see Section 5.2.4) at each stage of the data collection are calculated by comparing the predicted values with the observed values over the entire data collection window.

The methodology implies choosing an appropriate MCP model. After some preliminary iterations, a simple and straight forward choice is the linear regression (LR) and variance ratio approaches.

### **5.2.1 Evaluation of the MCP techniques**

The MCP techniques highlighted above are described in Section 3.3.2 (linear regression), and Section 3.3.3 (variance ratio method). The approaches were applied sector wise to the dataset which was binned according to the wind direction at the reference sites. This approach was employed in the present work because it accounts for the directional dependence of the upwind roughness which was also reported by the work of Weekes and Tomlin (2013) to have a significant effect on the scaling between the reference and target wind speeds. With regards to recommendations from previous studies (see for example Derrick, 1992; Woods and Watson, 1997), the angular bins were divided into  $30^\circ$  resulting in a 12 directional regression sectors for each target/reference site pair.

### **5.2.2 Choice of long-term data sites**

Locating high quality, nearby reference wind datasets of sufficient length, appropriate height and resolution is often a challenging endeavour. The UK

Met office owns and operate a Met Office Data Archive System (MIDAS) for the purpose of aviation and weather observation systems. However, these datasets are not publicly available and require further processing and quality control before they can be extracted for wind power predictions. It should be noted that the choice of reference long-term datasets is driven by the availability of concurrent, long-term dataset as well as the proximity to the target site. For this reasons, MERRA datasets described in Section 4.2.4 were examined to determine their suitability as a reference site.

Table 5.1 provides a summary of each location. Ultimately the MERRA reference dataset (RF4) was determined to provide the best correlation with the monitoring site and was subsequently used to make the long-term prediction.

Table 5.1: Summary of the target and reference sites: the PACT site, Beighton is at position (N53.60°, W2.18°). Column 3-6 show the locations of the reference sites in which long-term data are available.

Variables	Target site	Reference sites			
		RF1	RF2	RF3	RF4
Latitude	N53.60°	N54.00°	N54.00°	N53.50°	N53.50°
Longitude	W2.18°	W2.67°	W2.00°	W2.67°	W2.00°
Distance from Target site (miles)	0	81.10	70.10	91.30	47.70
Begin data	1/1/2015	1/1/2000	1/1/2000	1/1/2000	1/1/2000
End data	31/12/2015	31/12/2015	31/12/2015	31/12/2015	31/12/2015
Height (m)	10	10	10	10	10
Avg wind speed (m/s)	N/A	5.74	5.87	5.75	5.74
Avg wind speed (monitor period) (m/s)	6.036	5.75	5.06	5.41	5.90

Furthermore, Table 5.1 indicates that the average wind speed at the target site is slightly higher than three of the reference sites (RF1, RF2 and RF3). Only at the fourth reference site (RF4), which also doubles as the closest to the target site is the average wind speed almost the same as those at the target site. The reference dataset extends from 2000-2015.

Table 5.2 provides a summary of the wind dataset for this reference site (RF4) for the period January 1, 2000-December 31, 2015. As shown, the mean wind

speed over the 16-years reference period is 5.64 m/s. The mean at 10 m height is 5.9 m/s for the period of interest, January 1, 2015- December 31, 2015, concurrent with the data at the PACT Beighton site (target site). Therefore, the target site data should be correspondingly adjusted to reflect the expected annual wind speeds on a long term basis.

The long term mean wind speed data for the MERRA reference dataset (RF4) is shown graphically in Figure 5.2 by the horizontal blue line. The annual mean wind speeds at the reference site (RF4) can be seen graphically in the black curved line. The mean wind speed of the monitoring period of interest, January 1, 2015-December 31, 2015 is shown in the green line. Overall, the results represents a wind year slightly above the average wind year.

Table 5.2: MERRA reference (RF4) long-term wind data at 10 m (Jan 1, 2015- Dec 31, 2015).

Year	Possible records	Valid records	Recovery rate	Mean	Min	Max	Weibull k	Weibull c
2000	8,784	8,784	100%	5.82	0.15	15.80	2.36	6.38
2001	8,760	8,760	100%	5.44	0.01	17.40	2.45	6.14
2002	8,760	8,760	100%	5.66	0.04	18.50	2.43	6.13
2003	8,760	8,760	100%	5.41	0.05	15.90	2.44	6.10
2004	8,784	8,784	100%	5.61	0.04	15.10	2.32	6.33
2005	8,760	8,760	100%	5.65	0.01	14.94	2.44	6.39
2006	8,760	8,760	100%	5.64	0.13	13.00	2.30	6.36
2007	8,760	8,760	100%	5.71	0.07	15.00	2.36	6.44
2008	8,784	8,784	100%	6.00	0.04	15.70	2.46	6.76
2009	8,760	8,760	100%	5.68	0.02	15.50	2.46	6.40
2010	8,760	8,760	100%	5.07	0.12	14.30	2.47	5.71
2011	8,760	8,760	100%	5.81	0.18	15.00	2.45	6.55
2012	8,784	8,784	100%	5.51	0.07	14.80	2.39	6.22
2013	8,760	8,760	100%	5.72	0.08	15.00	2.44	6.45
2014	8,760	8,760	100%	5.64	0.09	15.80	2.29	6.37
2015	8,760	8,760	100%	5.94	0.04	14.00	2.30	6.70
All data	219,256	219,256	100%	5.64	0.08	14.30	2.35	6.35
MoMM <sup>9</sup>				5.64				

<sup>9</sup> MoMM indicate Mean of monthly mean

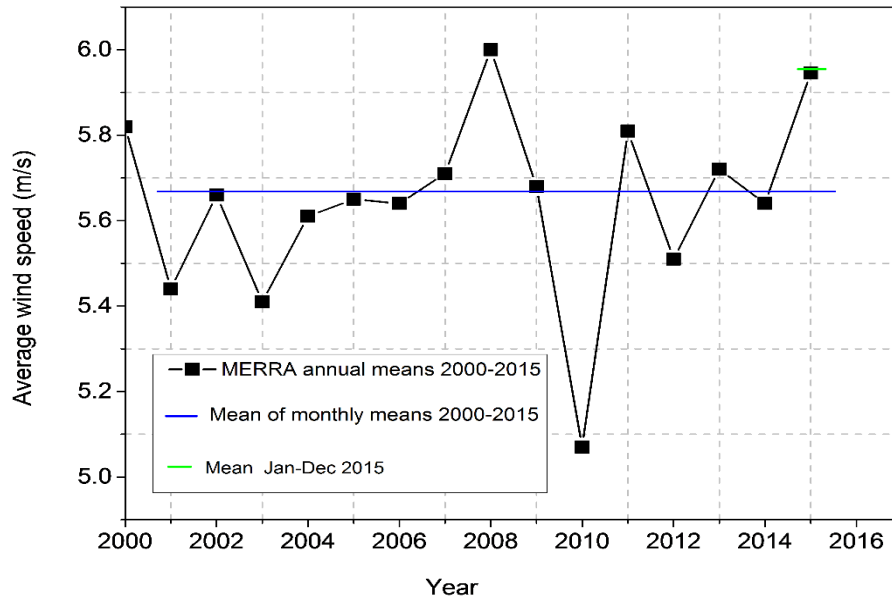


Figure 5.2: Long-term and short-term mean wind speeds for the MERRA reference (RF4) dataset.

### 5.2.3 Correlation of the target site (PACT, Beighton) wind speed to the MERRA reference (RF4) wind speed

The wind speed data collected from the target site (PACT Beighton) in the period between January 1, 2015 to December 31, 2015 was compared to the reference sites wind speed during the same period in order to determine the degree of correlation between the target site and each of the four reference sites. To reduce uncertainties due to shear, the MERRA reference dataset was correlated to 50 m wind speed at the PACT target site using the commercial software Windographer. Using a time step of 60 mins, the coefficient of determination  $R^2$  (i.e. correlation factor) was calculated between the PACT site and each of the four reference sites. The results are presented in Table 5.3.

From these results, it can be seen that the correlation is highest with RF4 which is a suitable candidate for a reference site. Consequently, the RF4 dataset (Table 5.1) was used to create the synthetic long-term data using the MCP approaches outlined in Section 5.2.1.



Table 5.3: Coefficient of correlations for the PACT (target) and Reference sites.

Site pair	Coefficient of correlation ( $R^2$ )
PACT site (50 m) to MERRA RF1 (50 m)	0.83
PACT site (50 m) to MERRA RF2 (50 m)	0.86
PACT site (50 m) to MERRA RF3 (50 m)	0.88
PACT site (50 m) to MERRA RF4 (50 m)	0.94

#### 5.2.4 Uncertainties associated with the different MCP methods

The MCP approaches outlined in Section 5.2 were used to make predictions of the future wind resource at the target site over a period of 15 years. From this time series result, a number of parameters related to the wind resource were extracted. The most important of these parameters includes the predicted mean wind speed  $\bar{u}_{pred}$  and the mean wind power density  $\bar{p}_d$  described in Section 2.4.1, Eqn. (2.6). Furthermore, the Weibull parameters (predicted using the method of maximum likelihood) are of special interest in wind resource analysis because they provide valuable information regarding the form of the predicted wind speed distribution and the standard deviation of the predicted wind speed  $\sigma$  defined as follows:

$$\sigma = \sqrt{\frac{1}{N-1} \sum_{i=1}^N (u_{i,pred} - \bar{u}_{pred})^2} \quad (5.1)$$

in which  $u_{i,pred}$  is the  $i^{th}$  wind speed prediction,  $\bar{u}_{pred}$  is the long-term mean wind speed prediction and  $N$  is the total number of instantaneous wind speed predictions. The standard deviation  $\sigma$  is an important wind resource parameter because, unlike the Weibull parameters which are estimated by fitting a Weibull distribution to the wind data series,  $\sigma$  is a measure of the spread of the wind speed about the mean without the knowledge of any wind speed distribution. The uncertainties associated with the predictions were assessed quantitatively using the mean absolute percentage error (% error). The

performance analysis was based on the fact that the reference datasets fulfil the following criteria:

- (i) More than 2 years of data.
- (ii) Good data coverage exceeding 85%
- (iii) Hourly correlation coefficient between the target and reference site larger than 80%.

The technique used is illustrated in Figure 5.3 and is described as follows:

Candidate site: Short-term (Year: 2015) period

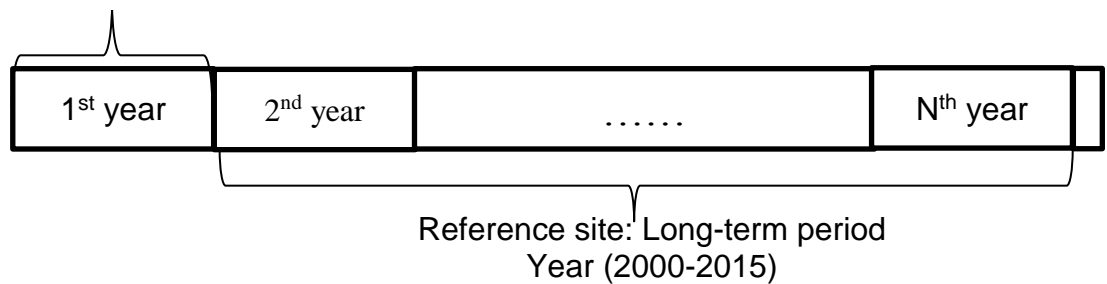


Figure 5.3: Illustration of the method used to test the prediction capacity of the different MCP approaches.

- (i) The first year of the measurement period indicates the short-term period.
- (ii) The long-term period is defined as the maximum number (N) of the complete years in which data is available.
- (iii) The data measured during the short-term and long-term periods are known as the site short-term and long-term data, respectively.
- (iv) The reference dataset was chosen from the MERRA database whose relationship to the site long-term data shows the highest correlation coefficient (calculated hourly).
- (v) The reference data corresponding to the long-term period designated as the reference long-term data.
- (vi) The site short-term and the reference long-term data are given as input into the MCP models described in Section 5.2.1., in order to estimate the mean wind speed at the site during the long-term period, i.e. estimated  $\bar{u}_{pred}$ .
- (vii) The error in the estimate of the long-term corrected mean wind speed (prediction error) is evaluated using the following error metrics:

$$\text{Prediction error} = \sum_j \left( \frac{|\bar{u}_{obs,j} - \bar{u}_{pred,j}|}{\bar{u}_{obs,j}} \times 100 \right) / n \quad (5.2)$$

$$\text{MAE} = \sum_j \bar{u}_{obs,j} - \bar{u}_{pred,j} / n \quad (5.3)$$

$$\text{MBE} = \sum_j \bar{u}_{pred,j} - \bar{u}_{obs,j} / n \quad (5.4)$$

where  $j$  denotes the  $j^{th}$  site,  $\bar{u}_{obs,j}$  and  $\bar{u}_{pred,j}$  are the long-term observed and predicted mean wind speeds, respectively and  $n$  is the total number of target sites. Using the approach described above, the uncertainty across the short-term (training period)/long-term periods were estimated.

### 5.3 Results and discussion

#### 5.3.1 Comparison of linear MCP approaches with measured wind speed data

Figure 5.4 shows the results of the correlation of the monitoring site to the reference site using the MCP methods described by Eqns. (3.8) and (3.9). To increase the correlation, the wind speeds were divided into 12 directional regression sectors, and a separate equation was created for each sector. The correlation was evaluated using a time step of 4 hours while a 1 hour average was used to create the synthetic data.

The linear correlation equation, shown by the trend line (line of best fit), for long-term to short-term data for the year of collected data at PACT site and for the direction sector  $135^\circ$ - $165^\circ$  is evaluated according to Eqn. (3.8) and restated here for ease of reference as follows:

$$\hat{v}_{tar} = \alpha + \beta v_{ref} \quad (5.5)$$

where  $\hat{v}_{tar}$  is the expected wind speed at 10 m is,  $\alpha$  is the intercept,  $\beta$  is the slope of the correlation trend line,  $v_{ref}$  is the reference wind speed (RF4) downscaled to 10 m.

It should be noted that the direction sector  $135^\circ$ - $165^\circ$  was chosen for illustration purpose only. The correlation for all the other sectors is given in Table 5.5.

The best fit slope and intercepts and their corresponding correlation coefficients for each of the 12 directional sectors are given in Table 5.5.

On inspecting Figure 5.5 and Table 5.5, it is clear that the accuracy in the wind speed prediction is similar in both methods since they only differ in the prediction phase. However, the overall correlation coefficient is slightly higher with the linear regression method (Table 5.3).

Each set of correlation equations relate the wind speeds dataset obtained at 50 m and downscale to 10 m from MERRA (RF4) to the target site wind speed at 10 m during the concurrent period. It should be noted that since the resultant annual energy of a wind turbine varies considerably with real time wind condition, the hourly correlation was chosen in this analysis in order to improve the overall accuracy of the prediction.

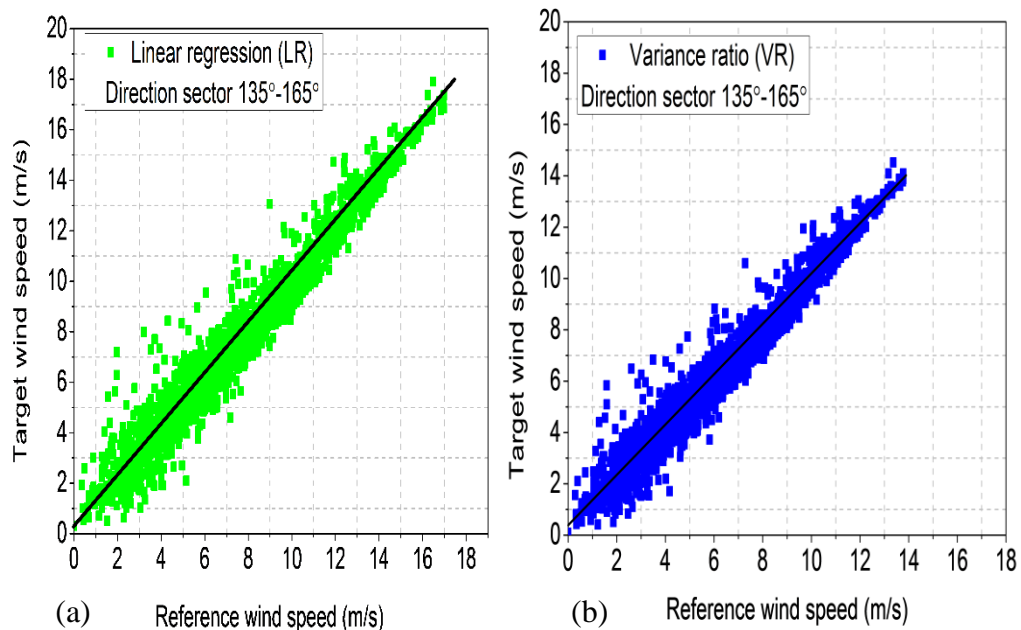


Figure 5.4: Target and reference site wind speeds for a single directional sector (135°- 165°) from the reference/target site pair. Prediction was made using wind observation over 12 months training data along with 16 years wind observation using (a) the linear regression, and (b) variance ratio MCP approaches. The solid line represents the correlation trend line (line of best fit). The dots show the observed or predicted scatter.

Furthermore, Figure 5.5 shows a comparison between the measured wind speed and the predicted wind speed. The results show a strong agreement

between the measured data and the predictions made using the MCP approaches.

Table 5.4 presents the overall statistical result for the “raw” 10-minute measured data at the target site, the processed 1 hour site data and 1 hour synthesised data spanning a period of 16 years using linear regression and variance ratio MCP methods, respectively. Clearly from these results, averaging the 10 minute data into 1-hour data did not present any variation to the mean wind speed and the Weibull parameters,  $k$  and  $c$  which remained at 6.03 m/s, 2.348 and 6.812 m/s, respectively. On the other hand, the predicted mean wind speed using the same MCP methods are obtained as 5.749 m/s and 5.739 m/s, respectively. This drop in the predicted wind speed is expected because it was shown in Table 5.2 that the monitoring period wind speeds is slightly higher than the long-term wind speeds. The predicted Weibull  $k$  and  $c$  using linear regression are variance ratio methods are 2.506 and 2.415, and 6.481 and 6.471 m/s, respectively.

Table 5.5: Correlation between the target site (PACT, Beighton) and the MERRA reference site (RF4).

Linear regression (LR)				Variance ratio (VR)			
Sector	Intercept	slope	R <sup>2</sup>	Sector	Intercept	slope	R <sup>2</sup>
345°-15°	0.487	1.021	0.904	345°-15°	0.282	1.074	0.901
15°-45°	1.003	0.895	0.811	15°-45°	0.611	0.994	0.801
45° - 75°	1.242	0.796	0.871	45° - 75°	1.004	0.854	0.866
75° - 105°	0.919	0.802	0.746	75° - 105°	0.406	0.929	0.728
105° - 135°	0.736	0.829	0.920	105° - 135°	0.568	0.865	0.918
135° - 165°	0.011	0.978	0.954	135° - 165°	-0.107	1.001	0.954
165° - 195°	0.058	1.002	0.961	165° - 195°	-0.062	1.022	0.961
195° - 225°	-0.028	1.031	0.9	195° - 225°	-0.150	1.048	0.968
225° - 255°	0.026	1.004	0.968	225° - 255°	-0.131	1.026	0.958
255° - 285°	0.061	0.972	0.958	255° - 285°	-0.113	0.998	0.949
285° - 315°	0.184	0.974	0.897	285° - 315°	-0.117	1.028	0.894
315° - 345°	0.031	1.020	0.903	315° - 345°	-0.212	1.074	0.900
<b>All</b>			<b>0.922</b>	<b>All</b>			<b>0.920</b>

Figure 5.6 shows a comparison of the wind rose for the measured and MCP predicted data. As can be seen from this result, both the measured and predicted wind direction show more of the wind coming from the south west direction and a smaller proportion from northeast. This is also consistent with the wind direction predicted using the MERRA data in Section 4.3.2.

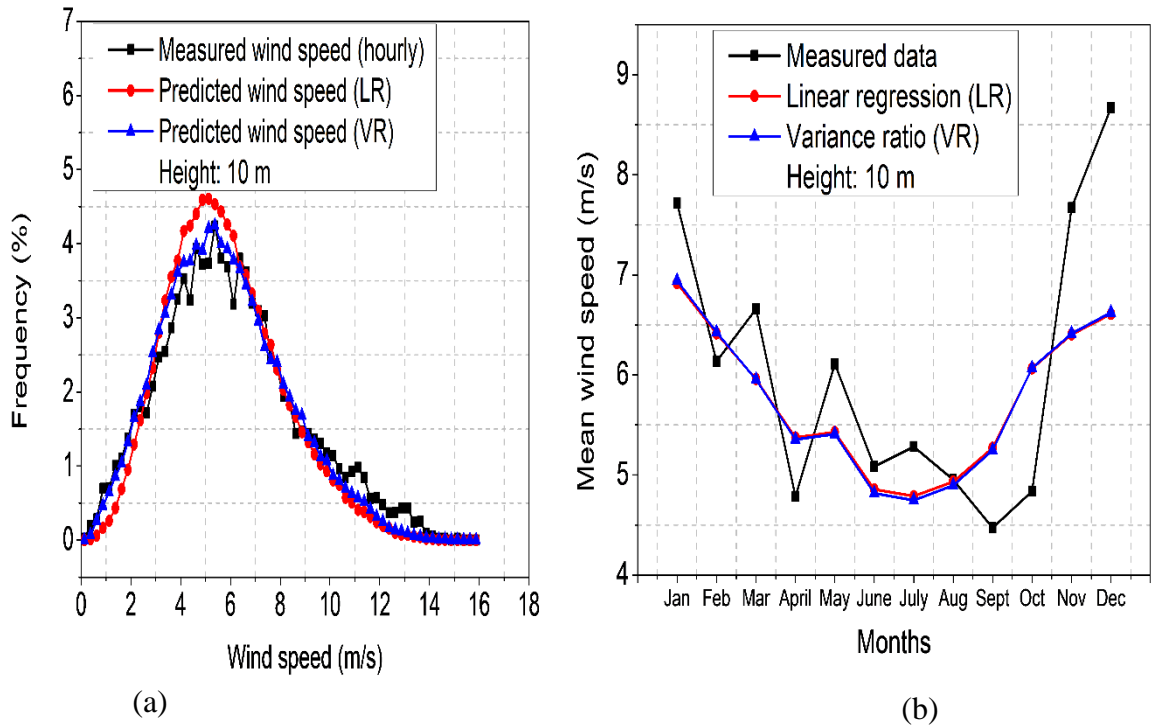


Figure 5.5: Comparison of the measured and the predicted wind speed using linear regression (LR) and Variance ratio (VR) MCP approaches, (a) wind speed frequency distribution (b) monthly mean wind speed profile at the target site.

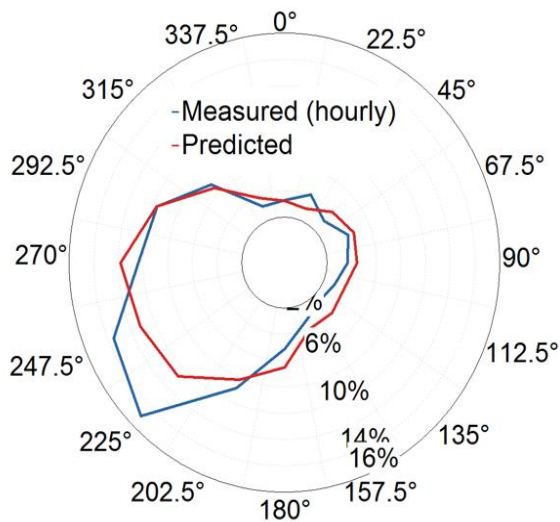


Figure 5.6: Measured and predicted wind frequency roses at 10 m using the method of linear regression (LR).

Table 5.5: Comparison of the values for measured and predicted wind resource spanning 16 years at the PACT site, Beighton.

Property	Measured data (Target site) 10 mins	Measured data (hourly)	Long-term data (LR method)	Long-term data (VR method)
Start time	01/01/2015 00:00	01/01/2015 00:00	01/01/2000 04:00	01/01/2000 04:00
End time	31/12/2015 00:00	31/12/2015 00:00	31/12/2015 00:00	31/12/2015 00:00
Duration	12 months	12 months	16 years	16 years
Time step	10 minutes	60 minutes	60 minutes	60 minutes
Time step used	52,560	8,760	140,255	140,255
Time step -direction	52,560	8,760	140,255	140,255
Mean speed @10 m	6.036 m/s	6.036 m/s	5.749 m/s	5.739 m/s
MoMM speed @10m	6.036 m/s	6.036m/s	5.749 m/s	5.739 m/s
Min. speed @10 m	0.105 m/s	0.105 m/s	0.105 m/s	0.095 m/s
Max. speed @ 10 m	15.247 m/s	15.247 m/s	15.575 m/s	15.911 m/s
Weibull k @10 m	2.348	2.348	2.506	2.415
Weibull c @ 10 m	6.812 m/s	6.812 m/s	6.481 m/s	6.474 m/s
Mean power density @10 m	223 W/m <sup>2</sup>	224 W/m <sup>2</sup>	183 W/m <sup>2</sup>	187 W/m <sup>2</sup>
Mesan direction. @ 10m	245.0°	245.0°	245.0°	244.5°

### 5.3.2 Adjustment to the target site wind speed data

The analysis described above resulted in a new long-term data set representing the expected wind speeds during a 16-year period, 2000-2015, at the target site. These datasets consist of wind speeds and directions at 10 m height above the ground.

Furthermore, it is necessary to estimate the wind resource at a typical turbine height representative of small-scale, i.e. 10-35 m. This can be achieved using either the power law or the log law extrapolation equation described in Eqn. (2.22). In the present case, however, the log law profile was used because it results in a slightly more conservative wind speed estimate when extrapolating

to higher heights. Since wind shear<sup>10</sup> tends to decrease with height, extrapolating the wind speed and direction at 10 m will potentially result in an overestimate. Using the slightly more conservative log law profile somewhat compensates for this. Consequently, the surface roughness values by direction and time of the day from the period of interest at the target site, were applied to the 10 m predicted dataset with the end result being a 16- year data set at multiple heights between 10 m and 35 m that can be used for energy production estimates for a variety of wind turbines and hub heights. Table 5.6 shows a comparison of the measured short-term data and the projected long-term data at the target site. In addition, Table 5.6 shows the variance in the long-term data.

Table 5.6: Comparison of short-term to long-term predicted wind speed at the target site at six heights commonly used for small-scale wind energy installation. LR and VR represents linear regression and variance ratio, respectively.

Data source	Height (m)	Short-term PACT site mean wind speed	Long-term PACT site MCP algorithm		Adjustment to long term mean wind speed (%)	
			LR	VR	LR	VR
Measured	10	6.03	5.74	5.73	-4.75	-5.23
extrapolated	15	6.39	6.08	6.06	-5.06	-5.44
extrapolated	20	6.64	6.32	6.30	-5.06	-5.39
extrapolated	25	6.83	6.50	6.48	-5.13	-5.40
Extrapolated	30	6.99	6.65	6.64	-5.11	-5.27
Extrapolated	35	7.13	6.78	6.76	-5.16	-5.47

---

<sup>10</sup> Wind shear refers to the difference in wind speed or direction over a relatively short distance in the atmosphere.



Overall, the long-term mean wind speed of 5.74 m/s at 10 m shows that this site has a good wind resource for small-scale wind energy utilisation. However, the wind resource at 15 m to 35 m appears to be somewhat better.

### 5.3.3 The added value of the Measure-Correlate-Predict (MCP) method

As noted above, the main purpose of using the MCP technique in wind resource assessment is to provide a correction to the long-term wind resource. Thus, it is necessary to estimate the added value of correlating to a long-term reference site. In the absence of an MCP, onsite wind measurement could be used to predict estimates of wind speed  $\bar{v}$  and power density  $\bar{p}_d$ . However, due to seasonal variability, making such a prediction with onsite measurements of less than 12 months would be subject to considerable error. Figure 5.7 shows the mean absolute errors in the predicted wind speed  $\bar{v}$  calculated using Eqn. (5.3).

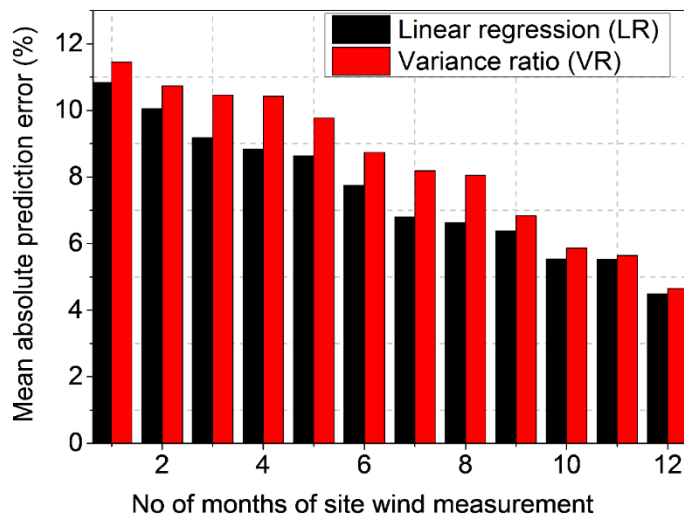


Figure 5.7: Mean absolute prediction error as a function of the measurement period length based on the linear regression (LR) and variance ratio (VR) MCP approaches.

The mean absolute error is seen to strongly decrease with the increase in the measurement period (concurrent period) length from 1-12 months. For example, when the measurement period is increased from 2 months to 10 months, the prediction error reduced from about 10% to 5.8% using the best performing MCP approach. While this study is concerned with a fixed 12

months of onsite measurement period, Figure 5.7 demonstrates that the error increases when using a training period of less than 12 months.

The added value of an MCP approach is particularly evident for short training periods where direct onsite wind observations are subject to large seasonal variability. However, when the training period is increased to a minimum of 12 months, direct onsite measurements become more representative of the long-term wind resource. This result clearly demonstrates the likely uncertainties when the onsite measurement period is less than the minimum recommended 12 months for small-scale wind energy.

### 5.3.4 Overall error statistics

The error metrics for the MCP approaches are summarised in **Table 5.7**. In addition, the error metrics obtained using the previously discussed boundary layer model are included and are discussed further in Section 5.3.9.

Table 5.7: Direct comparison of the error metrics at the target predicted using linear regression (LR), variance ratio (VR) MCP approaches and the boundary layer (BL) model discussed in Chapter 4.

Error metrics	Method	Wind speed $\bar{v}$	Power density $\bar{p}_d$
MAE (%)	BL model	18.90	17.00
	LR MCP model	7.20	12.90
	VR MCP model	7.90	14.40
MBE (%)	BL model	-18.9	-0.85
	LR MCP model	<0.01	-0.70
	VR MCP model	<-0.01	-0.80

The results show that the absolute error obtained in the estimate of the long-term mean wind speed and power density is, on average, 7.2% to 12.9%, respectively using the best performing MCP methods. It must be noted that the individual predictions can exhibit larger or lower errors depending on the length of the measurement period as demonstrated in Figure 5.7.

Furthermore, the results indicates that no clear difference between the two MCP approaches in the predicted wind speed. However, in terms of the wind

power density, the linear regression approach produces the least error. Overall, the largest errors are observed for the variance ratio (VR) method. The mean bias error (MBE) indicate the degree to which the MCP approaches overestimate or underestimate the wind speed and power density. Table 5.7 shows that both the linear regression (LP) and variance ratio (VR) approaches have a very low bias in the predicted wind speed  $\bar{v}$ , and power density  $\bar{p}_d$  which indicates the tendency to slightly underestimate these parameters. Further insight can be gained by considering the distribution of the residual errors at the site. The residual percentage errors  $\varepsilon\%$  in the predicted mean wind speed at any site can be evaluated as follows:

$$\varepsilon\% = \left[ \frac{\bar{v}_{obs} - \bar{v}_{pred}}{\bar{v}_{obs}} \right] \times 100 \quad (5.6)$$

where  $\bar{v}_{obs}$  and  $\bar{v}_{pred}$  are the observed and predicted mean wind speeds, respectively.

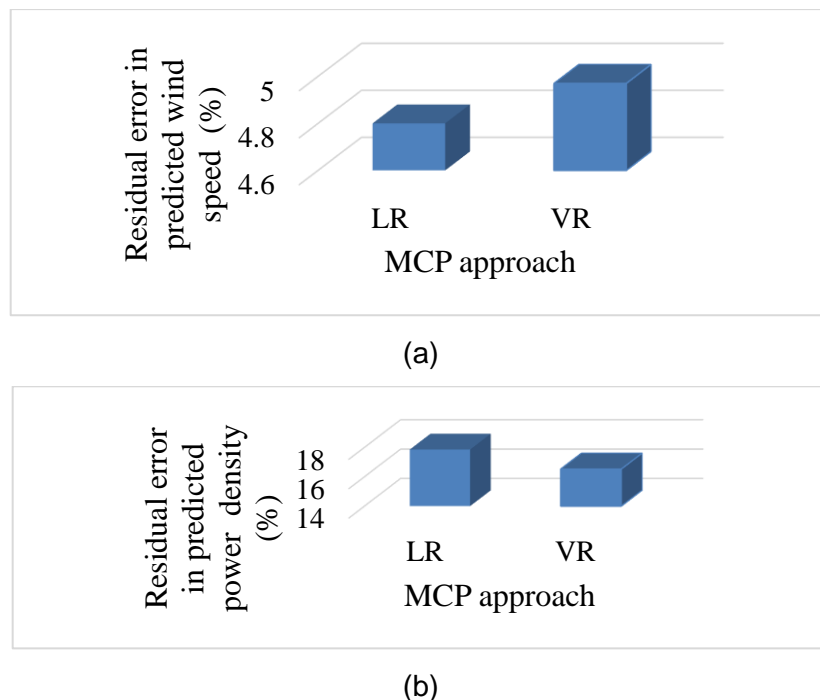


Figure 5.8: Residual percentage error distribution at the target (measurement) site: (a) predicted mean wind speed, and (b) predicted wind power density.

Note that a positive residual error  $\varepsilon\%$  indicates the tendency to underestimate. Similar expressions may be obtained for the wind power density.

Figure 5.8 shows the error distribution at the target site for a 12 months training period.

The pattern of the error distributions are both similar (positively skewed), thus exhibiting the tendency to underestimate. However, for the case of the power density, which is perhaps the most important parameter given that the aim is to predict the wind energy resource, the linear regression method exhibits a strong tendency to underestimate. It is likely that while the LR results in very low bias in the predicted wind speed, it tends to underestimate the standard deviation  $\sigma$  and Weibull shape factor  $k$  (not shown here) resulting in a narrower wind speed distribution which ultimately leads to a large underestimate of the wind power density  $\bar{p}_d$ .

### **5.3.5 Seasonal characteristics and variations in the percentage error of the predicted wind resource**

Because the MCP approaches described in this study were evaluated using a training data of 12 months, it is necessary to analyse the effects of seasonal variations with regards to the error estimates. Note that while the error metrics above provided robust statistics, they do not give any information as to how the magnitude and sign of the errors may differ with a particular measurement season. Obtaining such information is vitally important in making a more accurate estimate of the likely error given a specific measurement season. Furthermore, such information will help to determine if prediction error can be minimised by choosing an optimum season in which to conduct onsite measurement.

To analyse these sensitivities, the average error statistics were decomposed into seasonal averages.

Figure 5.9 depicts the percentage error of the wind speed and wind power density as a function of the seasons. The vertical lines represent the training periods corresponding to the seasons of autumn (Sept-Nov), winter (Dec-Feb), spring (Mar-May) and summer (June-Aug).

These results show a clear variation in the predicted errors using the linear regression (LR) and variance ratio (VR) MCP approaches. It can be seen that the largest errors for the predicted wind speed and wind power density occur in the summer and autumn seasons, respectively, while the smallest errors were observed in the winter season for both parameters. These results show

that on average, large reductions in the error of the predicted wind power density can be achieved through choosing optimum seasons in which to obtain onsite measurements.

Using the method of linear regression (LR), the best season to conduct onsite measurement results in a %error in power density  $\bar{p}_d$  of  $\sim 5.4\%$ , compared to  $\sim 30.3\%$  for the worst season. Similarly, for the variance ratio (VR) method, the best season results in a %error in power density  $\bar{p}_d$  of  $\sim 5.5\%$ , compared to  $\sim 30.4\%$  for the worst.

These variations demonstrate that the regression parameters obtained from the training data varies seasonally according to the weather patterns. If a particular set of the training data is characterised by a high frequency in the typical weather patterns, the obtained values of the regression parameters will not be a representative of the long-term reference/target site pair and this will ultimately result in errors in the predicted long-term wind resource. For instance, since the MCP approach implemented in this study is based on a sector wise method, it is expected that the measurement periods that include wind directions that populate each of the  $30^\circ$  angular sectors will result in improved long-term predictions.

Furthermore, the periods with low wind speed will be subject to variability due to local site conditions as described in Section 2.6, and this could lead to decoupling between reference and target sites, particularly when they are separated by a large distance.

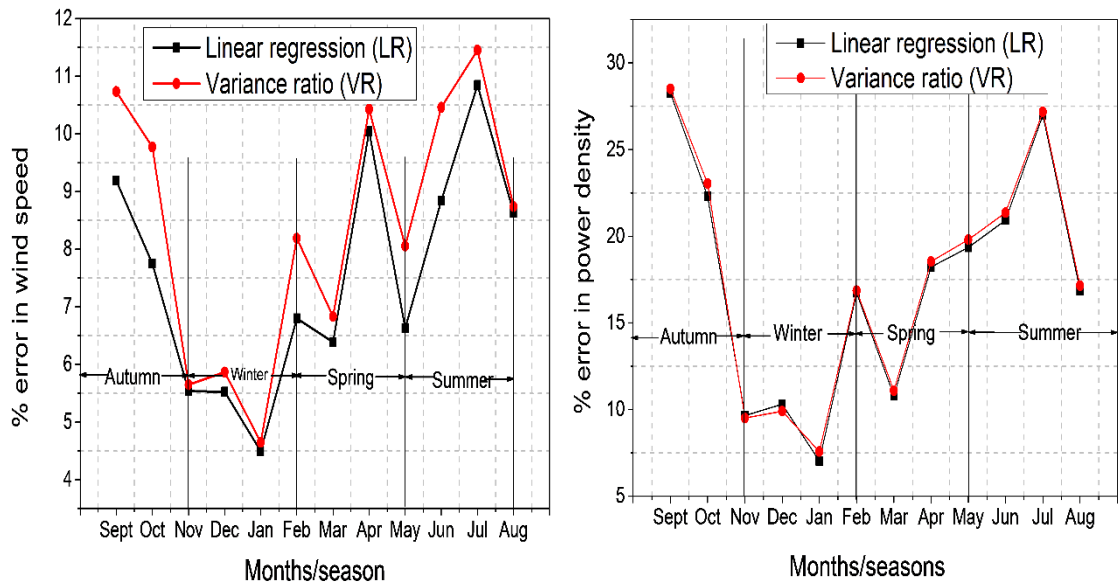


Figure 5.9: Variation of the %error in the predicted wind speed and power density as a function of the seasons. The vertical lines represents the seasons of autumn (Sept-Nov), winter (Dec-Feb), spring (Mar-May) and summer (June-Aug).

### 5.3.6 Seasonal variations in the mean bias error

As discussed in Section 5.3.2, the mean bias error indicates whether a particular wind resource parameter is over or underestimated. Thus, it is important to identify the seasons of the year that will result in over or underestimates of the wind resource in order to take appropriate measurement precautions that will maximise the available wind resource. Figure 5.10 shows the seasonal variation for the case of the predicted wind speed. It can be seen that, for both MCP approaches, measurements taken during the autumn period and the start of winter are more likely to result in overestimates of the long-term wind speed, particularly when using the variance ratio MCP approach.

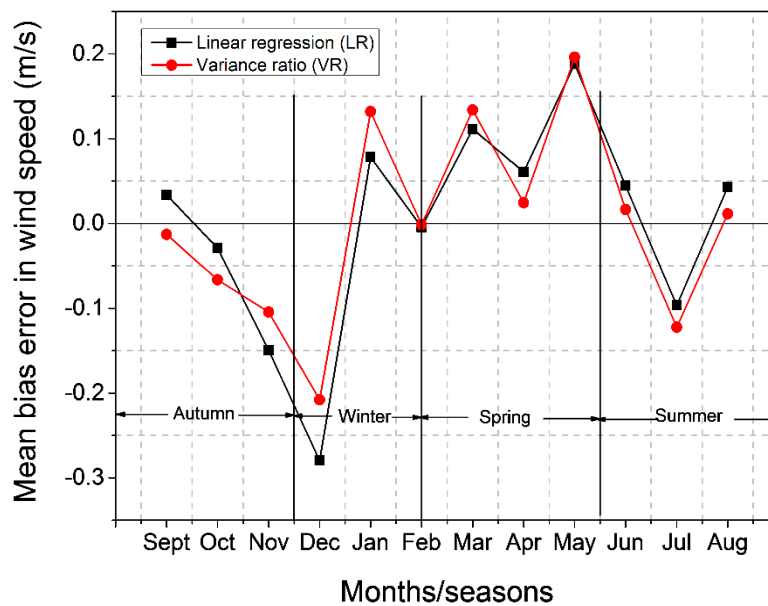


Figure 5.10: Seasonal variation of the mean bias error in the predicted wind speed using two MCP approaches at the target site. The vertical lines represent the seasons of autumn (Sept-Nov), winter (Dec-Feb), spring (Mar-May) and summer (June-Aug).

### 5.3.7 Summary of seasonal effects

The results presented above show that on average, significant improvements in the accuracy of the predicted long-term wind resource, based on short-term measurements can be achieved by choosing optimum seasons in which to conduct measurements. Furthermore, the results provide information regarding the sign of the bias error at any specific season and the MCP method used. While these results are potentially relevant in predicting the long-term wind resource from short-term measurements, it is important to note the following factors:

- (i) The results are the average statistics of a single site and year and thus individual predictions in any given year may differ from these trends.
- (ii) These results may vary significantly for urban and coastal sites that experience the same climatic conditions and in particular non-UK sites that experience different climatic conditions.
- (iii) Since the present study is based on a single measurement site, it may not be appropriate to generalise the results to all UK sites.

### 5.3.8 Comparison between boundary layer scaling model and data-driven MCP approach

Since undertaking an onsite wind measurements, even for a very short period of time requires additional time and cost, but it is important to investigate the impact of a data-driven MCP approach, based on a short-term measurement on the prediction accuracy of a wind resource compared to a semi-empirical modelling approach described in Chapter 4. Note that the target site used in this chapter is a subset of the sites used in the evaluation of the boundary layer model in Chapter 4. Therefore, it is possible to compare the performance of the two approaches for the investigated site. Table 5.7 show a direct comparison of the error metrics for the boundary layer model and two MCP approaches, namely linear regression and variance ratio. As described in Chapter 4, the predicted wind resource using the boundary layer model is based on the modifications suggested in Section 4.2.1. It should be noted that the error statistics presented in this chapter for the boundary layer model is based on a single site which is smaller than the 4 sites in Chapter 4. This is because the site used in the current chapter boost of modern measurement equipment and is currently one of Europe's leading centres into low carbon technology unlike the other three sites in Chapter 4 where there is no measurement equipment.

The results presented in Table 5.8 indicates that the predictions made using the MCP approaches results in a clear improvement in all the error metrics. For example, using the linear regression (LR) and variance ratio (VR) compared to the boundary layer (BL) model reduces the average mean absolute error (MAE) in the predicted wind power density  $\bar{p}_d$  from 17.0 % to 12.9% and 14.4%, respectively and the MBE from -0.85% to -0.70% to -0.80%, respectively.

Despite the uncertainties associated with the boundary layer approach, it is still of significant value since it can easily be implemented without any huge financial investment. However, the results based on the data-driven approach show that the additional time and investment required for the onsite measurement campaign, along with MCP analysis, is well justified in cases where developers and investors require more confidence in the predicted wind resource, even when the measurements are taken for only a few months.



## 5.4 Energy production estimates

Annual energy production estimates of five different wind turbines were made using the long-term dataset created for the target site. An overall energy production loss factor of 15% was assumed in the calculations in line with previous studies, see for example Jimenez (2013). The wind turbines belong to different manufacturers and the rated power varies between 1 kW to 55 kW, which are considered as small scale-wind turbines. The 1 kW, 1.3 kW, 2.50 kW, 15 kW and 55 kW wind turbines cut in wind speeds are 3.5, 4.0, 2.5, 2.5 and 2.0 m/s, respectively, and the cut out wind speed are 25,18,20,20 and 20 m/s, respectively.

Table 5.8: Specifications of the analysed wind turbines, including the output mean hub height wind speed (AWE, 2013; ECI, 2013; BWPC, 2013; EWPC, 2013).

Turbine model	Rated Power (kW)	Hub height (m)	Rotor diameter (m)	Mean hub height wind speed (m/s)	Turbine cost (\$)
Raum	1.30	10	2.90	5.17	4,500
Proven	2.50	10	3.50	5.17	6,500
Proven	15.0	10	9.00	5.17	25,000
Bergey XL.1	1.00	10	2.50	5.17	3,450
Endurance G3120	55.00	10	19.2	5.17	168,000

The average power output from a wind turbine may be calculated as follows (Ahmed and Sharma, 2015):

$$\bar{P}_{w\ ave} = \frac{1}{N} \sum_{i=1}^N P_w(v_i) \quad (5.7)$$

in which  $P_w(v_i)$  is the gross power output (without losses) defined by the turbine power curve and  $N$  is the number of recorded observations.

Hence, the mean annual net energy output in kWh/yr. can be expressed as follows (Ahmed and Sharma, 2015):

$$E_{net, \ annual} = \bar{P}_{w\ net} (\Delta t) \quad (5.8)$$

The specifications of the wind turbines are presented in Table 5.8.

Figure 5.12 shows the annual energy production and the corresponding capacity factors at the target site.

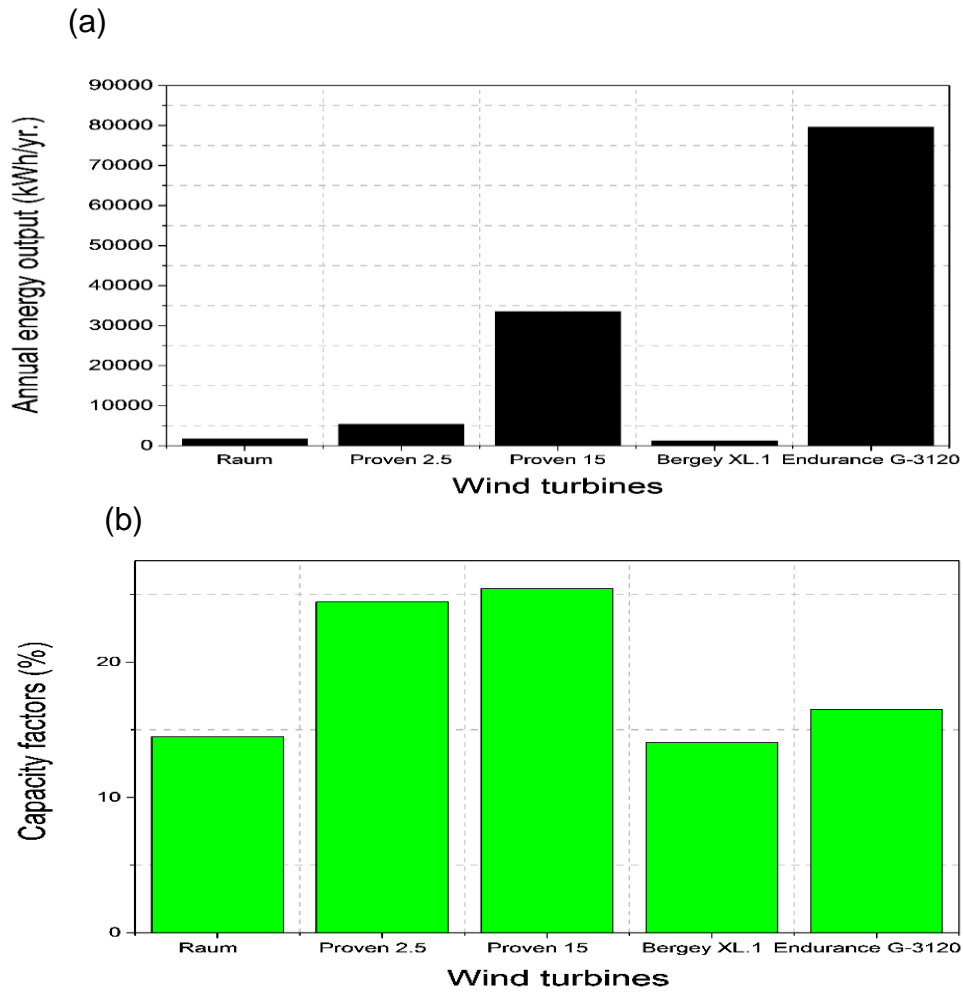


Figure 5.12: Output of individual wind turbines, (a) annual energy production, and (b) the corresponding capacity factors at the PACT measurement site Beighton.

The capacity factor represents the energy production output of a wind turbine and is generally affected by the wind characteristics and the turbine efficiency. It can be seen that the highest and lowest values of the capacity factor were calculated as 25.46% and 14.06% using the Proven 15 kW and Bergey 1 kW wind turbines, respectively.

On the other hand, the energy production estimates indicate that the Endurance wind turbine with a rated power of 55 kW exhibited the highest amount of energy. For this configuration, the highest annual energy production reaches 79,568 kW h.

Overall, the Endurance 55 kW and Proven 15 kW configurations produce the highest annual energy output at the target site. Thus, in terms of the energy production and capacity factors, the Endurance 55 kW and Proven 15 kW wind turbine is considered as the best choice wind turbine for the site wind resource. However, the optimal siting of a wind turbine is strongly dependent on its economic performance. Hence, the economic assessment of the turbines were investigated in order to identify most cost effective and profitable wind turbines option.

## 5.5 Economic evaluation

The economic analysis of installing any of the above wind turbines at the target site is evaluated based on the present value of the cost (PVC) method as follows (Gökçek et al., 2007; Ahmed, 2012; Belabes et al., 2015):

$$PVC = C_I + C_{OMR} \left( \frac{1+i}{r-i} \right) \times \left[ 1 - \left( \frac{1+i}{1+r} \right)^t \right] - S \left( \frac{1+i}{1+r} \right)^t \quad (5.9)$$

in which  $PVC$  is the current investment made throughout the life span of the system, and it includes investment costs for the turbines  $C_I$ , the operation, maintenance and repair cost  $C_{OMR}$ , the inflation rate  $i$ , the yearly interest rate  $r$ , which corresponds to the operator's yearly profit, the salvage cost at the last year of use  $S$ , and the economic lifetime of the turbine  $t$ .

The operation, maintenance and repair cost are computed according to the following expression (Nedaei et al., 2014):

$$C_{OMR} = \frac{C_I}{t \times 4} \quad (5.10)$$

After computing the PVC value, the cost per kilo (kW h) watt of energy may be computed as follows (Nedaei et al., 2014):

$$Cost \text{ of } kW h = \frac{PVC}{AEP}, \frac{\$}{kWh} \quad (5.11)$$

To implement the PVC method, the following assumptions were made:

- (i) The economic lifespan ( $t$ ) of the machine as designed by the manufacturers is 20 years.

- (ii) The inflation rate ( $i$ ) and discount rate ( $r$ ) were assumed as 15% and 10%, respectively based on the recommendation of Nedaei et al. (2014).
- (iii) Due to the many costs associated with wind energy project, it is ideal to consider the operation and maintenance costs as a fraction of the capital cost of the system. Hence, it is logical to assign 1.5–6% of the system cost for yearly repair and maintenance in line with previous studies (see for example, Nedaei et al., 2014).
- (iv) All the sites are located outside the urban terrain. Hence, most of the costs involved in the installation are always higher than normal, when compared with the cost of installing a turbine in an urban terrain. Major installations always have to be carried out at sites located in rural regions. Because of this, the scrap value ( $S$ ) was taken as 10% of the cost of the turbine.

Figure 5.13 shows the relationship between the cost of the wind energy and the individual turbines. The results indicate that the cost of wind energy is significantly reduced with the increase in the rated power of the turbines. For example, installing a Bergey wind turbine with a rated power of 1 kW, the cost per kilo watt of electricity at the target site is calculated as \$5.55 which is significantly higher than the UK average, while the cost for an Endurance wind turbine is calculated as \$0.08.

The current UK Feed-in Tariff for electricity generated by a wind turbine with rated capacity of less than 100 kilo watts is about \$8.53 p/kWh ( ~ 0.12 \$/kWh) (Renewable UK, 2013). General speaking, a site below the viability criterion (see Section 4.4) and a high cost of energy will not be economically viable to install a wind turbine. Based on the current cost of energy at this target site and without any financial incentives such as the Feed-in Tariff, the only economical viable wind turbine option is the Endurance wind turbine with a rated power of 55 kW.

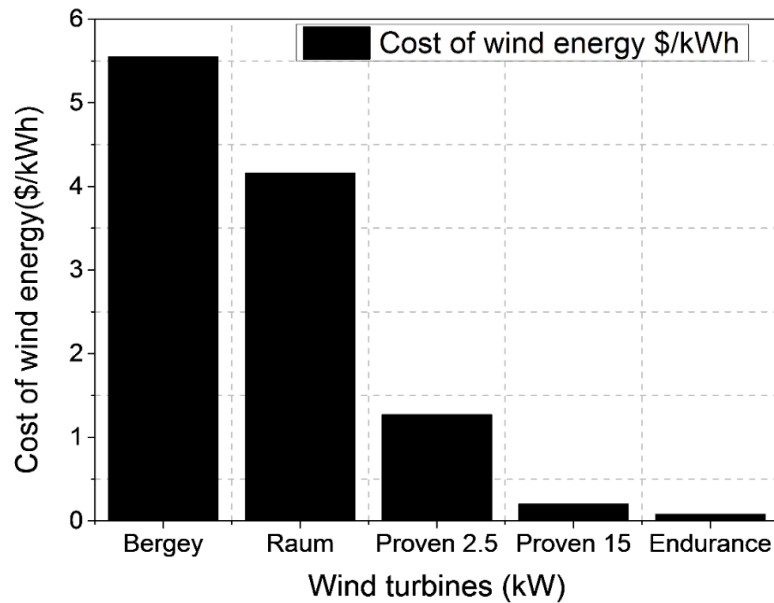


Figure 5.13: Cost of electricity as a function of the wind turbines at the target site.

## 5.6 Summary

This chapter examines the feasibility of a data-driven MCP approach in predicting the long-term wind resource at a specific target site using short-term onsite measurement at various months. The results revealed that while short-term data may be subject to seasonal variations, the approach can provide a reliable estimate of the long-term wind resources and thus can be a useful tool for wind resource assessment in the small-scale wind industry.

Two MCP approaches, namely linear regression (LR) and variance ratio (VR), were compared for the predictions and the results obtained show that both approaches predicted the mean wind speed and power density with reasonable accuracy. In general, the absolute error obtained in the estimate of the long-term mean wind speed and power density is, on the average, 7.2% to 12.9%. Furthermore, the results demonstrate that no clear difference between the two MCP approaches in the predicted wind speed. However, in terms of the wind power density, both approaches showed a slight bias. Further analysis in the residual error revealed that the predictions made using the MCP approaches are positively skewed, thus indicating the tendency to underestimate the predicted parameters. However, the linear regression

approach tends to exhibit a stronger tendency to underestimate the wind power density.

Further insight into the seasonal variations revealed the sensitivities in which the onsite wind data were obtained. The results show a clear seasonal variations in the signs of the predicted errors. The lowest prediction error occurred when using the training data acquired during the winter or spring season, while the highest error occurred when using summer and autumn training data. Overall, the results show that choosing an optimum measurement season can significantly reduce the error in the predicted wind power density from 30.3% to 5.4 % using the best performing MCP approach. A comparison was made using the error metrics between the data-driven MCP approach and the boundary layer method presented in Chapter 4. The results clearly indicate a significant improvement in the predicted long-term wind resource using the MCP approach. The results show that the best performing MCP approach resulted in an absolute error in the mean wind speed and power density of 7.2% and 12.9% in contrast to 18.9% and 17% using the boundary layer model. However, it must be emphasised that these errors indicate the average errors over a specific site and training season and may vary considerably from one location to another.

Based on the success achieved in predicting the long-term wind resource, energy production estimates and economic feasibility of installing a wind turbine at the target site were made using five different wind turbines. Unfortunately, the site does not look promising for small-scale wind energy considering the current price per kilo watt of energy for small-scale wind generated electricity in the UK except for the Endurance wind turbine model with a rated power of 55 kW. What this means is that it will be difficult for any wind project less than 55 kW capacity to be economically viable in this site without some sort of grant or subsidy.

The following chapter will consider the aerodynamic design of a small-scale wind turbine model based on the site's wind resource. Measures to improve the performance of the turbine concept, particularly self-starting are evaluated.

## Chapter 6 The Design of a Small-Scale Wind Turbine

As discussed in Sections 1.4, one of the objectives of this thesis is to design a small-scale vertical axis wind turbine with self-starting capabilities. Here, the emphasis is on a particular rotor: the Darrieus vertical axis wind turbine with straight blade which was first developed in the USA by Darrieus (1931).

The interest in Darrieus turbines was reinvented by engineers at the National Research Council of Canada during the 1970s energy crisis that resulted in substantial petroleum shortages as well as high prices. At that time, most commercially available turbines for the production of electricity were inefficient due to their cost and complexities arising from the designs. This led to the search for simpler and less expensive machines. The result was a Darrieus-type turbine with the ability to extract wind energy from any direction.

In this chapter, the case of a Darrieus rotor is introduced in Section 6.1. Next, a list of design requirements that drove the original design, and which should naturally apply to any solution including the main aim of this chapter is restated in **Section 6.2**. Finally, the modelling strategy for the start-up conditions including the generation and processing of viscous aerofoil data and the important assumptions and simplifications are presented in Section 6.3.

### 6.1 Darrieus-type VAWT

The first performance data for the Darrieus-type turbine with its original blades were reported by Sheldahl and Blackwell (1977) at the Sandia National Laboratory. Each of the original blades consisted of three segments: a circular arc located near the turbine equator with a 0.19 m chord of NACA 0012 aerofoil section, and two straight sections attach to the circular arc to the central column of the turbine.

The solidity,  $\sigma$ , of the turbine was calculated to be 0.26. It was found that the aerofoil section was detrimental to the turbine performance and that the blades should have the aerofoil section from hub-to-hub. With that in mind, the design was revised and the aerofoil section was changed to NACA 0015 and thus was presumably due to its favourable stall characteristics. The revised design had a chord length of 0.1524m and was designed to operate at a constant rotational speed by connecting the turbine shaft through a 2-

stage timing belt drive to the induction motor/generator operator at 150 rpm. This connection to an induction motor clearly indicates the turbine is not self-starting and that the machine is started by relying on an external mechanism to bring the turbine up to an operating speed.

## 6.2 Design requirements

In order to successfully achieve any modification to the Darrieus rotor, they have to comply with several requirements that drove the original design. These requirements are briefly discussed as follows:

- Performance. The turbine is expected to perform well in different ranges of wind speed. Preferably, the maximum attainable (peak) performance in the power coefficient versus tip speed ratio curve ( $C_p - \lambda$ ) should be as broad as possible. In addition, an improvement to the self-starting performance should not compromise the power output of the turbine.
- Noise emissions. The turbine is expected to be quiet during operation. In the UK, the noise emitted by wind turbines is limited by regulations and a fixed limit of 43 dB is recommended for night-time (DOE, 2007). This is based on a sleep disturbance with an allowance for attenuation through an open window.
- Safety. There should be no safety risks during the operation of the turbine.
- Capital cost. The modifications to the turbine should not add extra cost to the purchase price so as not to deter customer.
- Attractive. It is expected that any modification to the rotor should not make it unattractive. However, the aesthetics quality of the turbine is very subjective and thus difficult to define<sup>11</sup>.

As stated earlier, there is currently a lack of reliable performance data regarding the performance of small-scale wind turbines with self-starting capabilities. Hence a major aim of the present work is to modify the aerodynamic design of a Darrieus-type VAWT in order to make it self-start at low tip speed ratios while honouring the requirements that drove the original design and without compromising the overall power output.

---

<sup>11</sup> Stankovic et al. (2009) provided an example of an aesthetic wind turbine with a smooth, streamlined modern-looking shape, while a turbine of low aesthetic quality appears crude and industrial.



This encompasses the elimination of the regions of negative power from the power coefficient versus the tip speed ratio ( $C_p - \lambda$ ) curve by improving the torque produced at low tip speed ratios. The following sections examine the modelling approaches to achieve this task.

### **6.3 Modelling approaches of the VAWTs self-starting**

A well-known strategy to model a vertical axis wind turbine rotor is to use aerofoil data for an average Reynolds number to assume completely inviscid flow conditions. Generally, the errors arising from such assumptions are acceptable for high tip speed ratios or high Reynolds numbers. Modelling of start-up condition for a small-scale rotor, such as the Darrieus turbine, is completely opposite. The blade regularly encounters static stall due to complex flow phenomenon, particularly at low tip speed ratios. Thus, the variations in the blade chordal Reynolds number becomes increasingly important. The next section examines the modelling approaches used in this thesis for start-up conditions.

#### **6.3.1 Viscous aerofoil data**

An important aspect in the modelling of self-starting behaviour of VAWTs is to predict how the blade behaves under different design conditions. This can be achieved in several steps, which are discussed in the following section.

##### **6.3.1.1 XFOIL**

There are a wide variety of computational tools for the simulation of the performance of aerofoil sections. The selection of a suitable tool strongly depends on the scope of the investigation as well as the available computational time and resources. In this thesis, the open source numerical simulation code XFOIL (Drela, 1989) is used. XFOIL is a viscous aerodynamic tool for the design and simulation of aerofoils. The basic theory of the code is based on a simple linear-vorticity stream function panel method with an explicit Kutta condition closure equation system. To achieve good compressible flow predictions then a Karman-Tsien compressibility correction model is integrated into the program (Drela and Giles, 1989). Different computational models, such as CFD, are too time consuming to be considered for use within the scope of this work.

### 6.3.1.2 Validity of XFOIL predictions

A design tool, such as XFOIL/ XFLRS, is simply a representation of the real life situation. However, the accuracy of prediction tends to diminish at very low Reynolds numbers. For example, laminar separation bubbles can be a great source of error when they are present over parts of the aerofoil modelled with the panel method code. Another issue of concern is the uncertainty associated with the prediction of the free stream turbulence level and the setting of an appropriate amplification factor (**see Section 3.4.1.2**). In addition, the drag coefficient in XFOIL is computed from the wake momentum thickness downstream of the aerofoil using the Squire-Young formula (Drela, 1995). When separation occurs at the trailing edge of the aerofoil, the assumption that justifies this method breaks down and large uncertainties can be expected. However, the panel methods code are developed to operate at moderate angles of attack simulation ranges, therefore, the wake trajectory problem is not critical for the aerofoil computation accuracy at low angles of attack (Drela and Giles, 1986).

### 6.3.1.3 High angles of attack

Despite being a convenient design tool, XFOIL tends not to converge at lower Reynolds numbers ( $< 10^5$ ) and close to separation. This ultimately limits the boundary of application to the range between plus and minus the static stall angle. To demonstrate the prediction capacity of XFOIL at higher angles of attack, the results of two aerofoil section are compared with a wind tunnel experiment of Abbott and Doenhoff (1949). These aerofoils include a turbulent profile, namely NACA 4418 and a laminar profile NACA 64-218 and the results are shown in Figures 6.1 and 6.2. The results indicate a good agreement between experimental data and those obtained using XFOIL, see Figure 6.1. However, for the case of the turbulent profile, XFOIL tends to slightly over estimate the lift as compared the experimental data (see Figure 6.1). Consequently, XFOIL produces a higher maximum lift coefficient  $C_{lmax}$ . Thus, at higher Reynolds number, XFOIL has some difficulty in accurately predicting turbulent profiles accurately.

Conversely, for the case of the laminar profile, a strong agreement was observed between XFOIL and the Experimental data over the whole range of

aerofoil. The results exhibit the same behaviour, except at the point where the angle of attack,  $\alpha > 10^\circ$  see Figure 6.2.

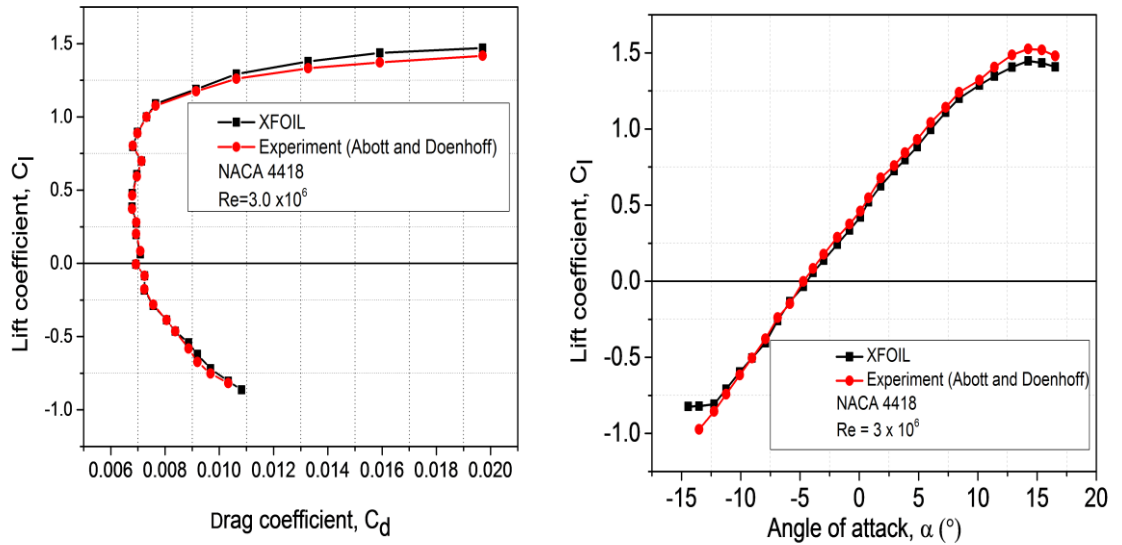


Figure 6.1: Comparison of NACA 4418 aerofoil characteristics with wind tunnel experiments at a Reynolds number,  $Re = 3000000$ .

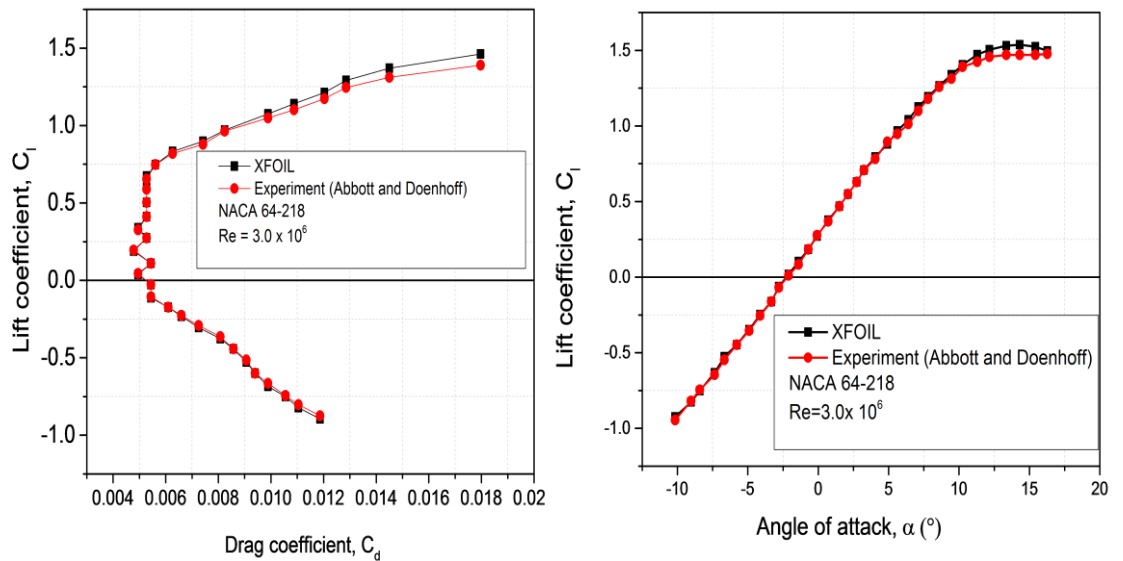


Figure 6.2: Comparison of NACA 64-218 aerofoil characteristics with wind tunnel experiment at a Reynolds number,  $Re = 3000000$ .

Therefore, XFOIL accurately predicted the behaviour of NACA 64-218 with reasonable accuracy and is thus a suitable aerofoil design tool.

### 6.3.1.3 Turbulence level

The VAWT tends to generate high turbulence, particularly at the downwind pass of the rotor. These perturbations could be of high scale so that they can

impact on the boundary layer and possibly stabilise it. This can be accounted for in XFOIL by setting a suitable critical amplification factor for the  $e^n$  model,  $N_{crit}$ , which enables free transition to be predicted over the aerofoil using the Tollmien-Schlichting wave disturbances (Drela, 1995). Some examples of turbulence level that follows from this code are given in the user manual (see Table 6.1) and its effect on the lift curve of the NACA 0018 aerofoil section is depicted in Figure 6.3.

Table 6.1: Typical turbulence values of  $N_{crit}$  for various scenarios as listed in the XFOIL user manual (Drela, 1995).

Situation	$N_{crit}$	Turbulence level
Sail plane	12-14	0.009-0.020%
Motorglider	11-13	0.013-0.030%
Clean wind tunnel	10-12	0.020-0.046%
Average wind tunnel	9	0.070%
Dirty wind tunnel	4-8	0.106-0.563%

Clearly, the effects can be quite significant on the overall performance of the aerofoil. A similar analogy was illustrated by Paraschavoui (2002) to limit the application of dynamic stall models to regions of low turbulence bounds in the range  $15^\circ \leq \theta \leq 135^\circ$  - the point where all vorticity is shed at the extremes. Based on this, the rotor plane is split into an upwind region of relatively low turbulence ( $N_{crit} = 9$ ), ranging from  $15^\circ$  to  $135^\circ$ , and in the downwind region of high turbulence ( $N_{crit} = 4$ ) for the remaining angles.

The  $e^n$  model is regarded as the most widely used transition model in the field of aerofoil aerodynamics (White, 2005) as well as in the field of wind energy (Hansen, 2008). For high inflow turbulence levels, or highly distributed 3D roughness effects, other transition effects occur, namely by pass transition and this cannot be predicted using the  $e^n$  model (Drela and Giles, 1989). VAWT applications include highly turbulent flows but in the absence of a more robust transition model with reasonable computational cost, the  $e^n$  model was and is still regarded as the most popular transition model.

More advanced transition models have been developed in recent years and their use is expected to gain more popularity an examples of such a model is

the  $k - kl - \omega$  model developed by Walters and Cokljat (2008) for RANS solvers, which was implemented in the Open FOAM™ code. However, this version of the transition model was not implemented in this thesis.

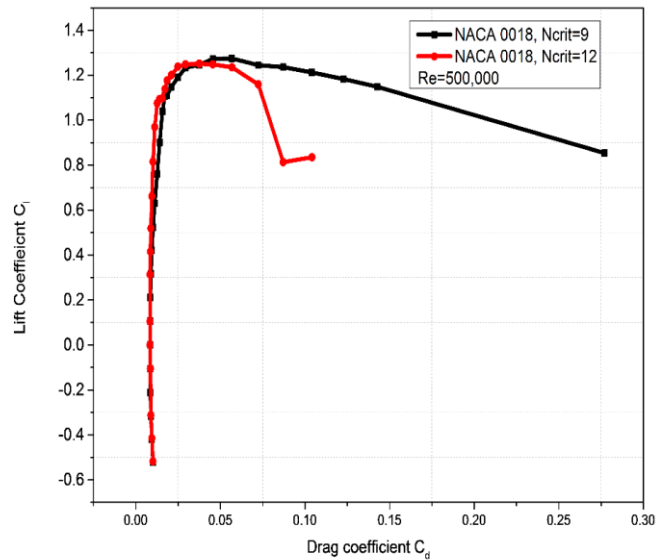


Figure 6.3: Performance prediction of a NACA 0018 profile at 0.070% and 0.046% turbulence levels.

Overall, XFOIL is a powerful and flexible design and simulation code that has been widely used for the analysis of low Reynolds number aerofoils by leading wind turbine research organisations, including NREL and Risoe (Dahl and Fuglsang, 1998), SWIP (European Commission, 2013). The current version of the code, the open source code XFLRS, is integrated within the Qblade software to design or import aerofoil geometries, generate or import measured aerofoil performance coefficients for rotor simulations and manage the aerofoil database. The benefits of employing the current version are the large number of experimental and numerical validations and the high quality of the simulated aerofoil coefficients. Also, the aerofoil lift and drag coefficients can be extrapolated using either the Montgomery or the Viterna-corrigan post stall model (Marten et al., 2013). However, the program being a panel method code has some inherent limitations, such as its inability to handle large flow separation, unsteady flow conditions etc.

## 6.4 Wind turbine simulations

The BEM theories were first developed in the 1930s and are still being widely utilised in recent years for wind turbine simulations. A detailed description of the theories underpinning the Blade Element momentum method (BEM) and the blade element theory was given by Hansen (2008) and Paraschavoui (1981). Therefore, in the following paragraph we do not describe the method in detail, but rather present a description of one of the simulation algorithms, its assumptions and limitations. Based on the work of Paraschavoui (1981) and Hansen (2008), an open source code based on the Double Multiple Stream Tube Model, namely Qblade was developed by Marten et al. (2010). The vertical axis wind turbine (VAWT) simulation algorithm in Qblade is based on the blade element theory (to compute the local blade forces) coupled with a multiple streamtube momentum balance (to account for the global flow field) over two vertical axis wind turbine rotor discs. The prediction tool allows for a rapid development of the aerodynamic rotor shape, based on a comparison of different rotor designs. The code has been widely validated against experimental and field data, and their computational efficiency and robustness are the reasons why they are widely used in wind turbine industry and research.

### 6.4.1 The Double Multiple Streamtube Algorithm

The vertical axis wind turbine (VAWT) tool in Qblade is an implementation of the Double-Multiple Streamtube Model algorithm, based on the concept of Paraschavoiu (1981). The turbine is modelled as two actuator rotor discs in tandem, see Figure 6.4, one for the upstream half-cycle and one for the downstream half –cycle during one rotation. The rotor blade is discretised into an arbitrary, user specified, number of streamtubes, the circular path of each streamtube is divided into  $5^\circ$ , as recommended by Parashavoui (1981). Each of the streamtubes is recognised by the angle  $\theta$ , defined as the angle between the direction of the free stream velocity and the position of the streamtube in the rotor. The model assumes that the wind velocity experiences a deceleration near the rotor, and if the front and rear parts of the turbine are represented by two discs in tandem, then the flow velocity will be decelerated twice, once for the upstream and the second for the downstream half-cycle.

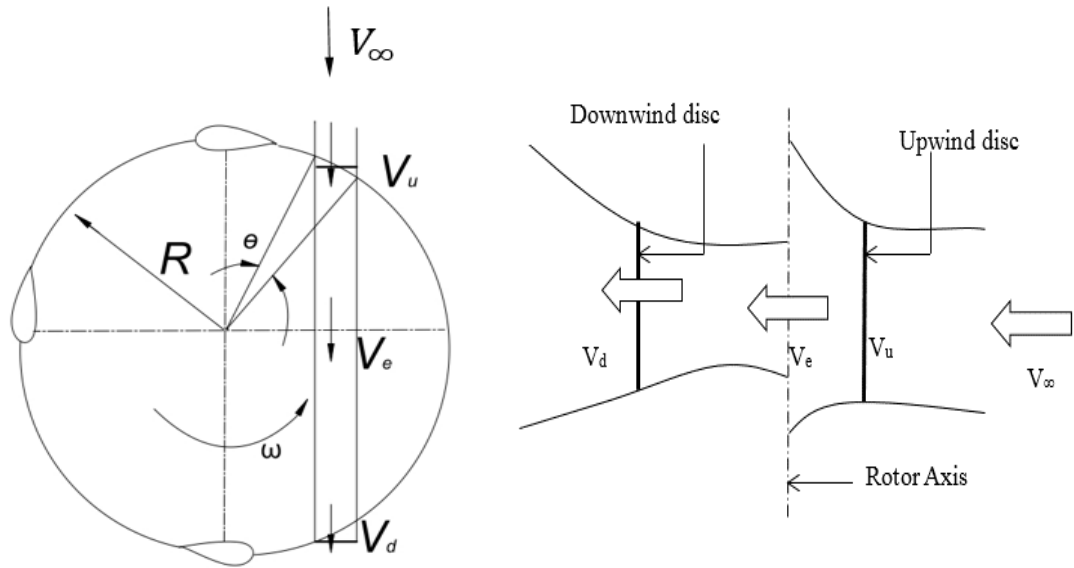


Figure 6.4: Illustration of the Doubles Multiple Streamtube Model with actuator discs and velocity vectors at the upstream, equilibrium and downstream cycles of the actuator disc (Adapted from Newman, 1983; Paraschavoui, 1981).

The calculation of the induced velocity is described as follows (Paraschivoiu, 1981):

For the upstream half cycle, the induced velocity at the rotor is given as follows:

$$V_u = V_\infty a_u \quad (6.1)$$

where  $V_u$  is the upstream induced velocity,  $V_\infty$  is the free stream velocity and  $a_u$  is the upstream interference factor.

The induced velocity in the equilibrium plane is given by:

$$V_e = V_\infty \left( 2 \frac{V_u}{V_\infty} - 1 \right) = V_\infty (2a_u - 1)$$

(6.2)

Similarly, for the downstream half cycle, the induced velocity is expressed as follows:

$$V_d = V_e a_d \quad (6.3)$$

where  $V_d$  is the downstream induced velocity and  $a_d$  is the downstream interference factor.

Under these conditions, the streamtube induced velocity is calculated by a double iteration, one for each part of the rotor.

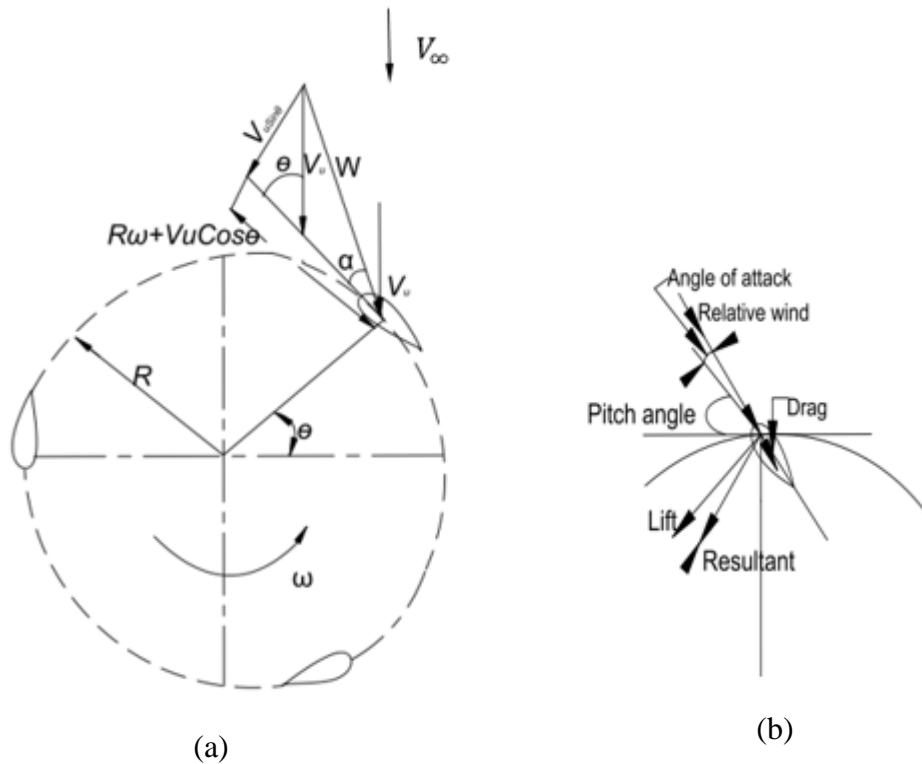


Figure 6.5: (a) Plan view of the DMST showing velocity triangle to determine the relative velocity. (b) A single blade illustrating the concept of pitching.

#### 6.4.1.1 Upstream half-cycle of the rotor

For the upstream half cycle of the rotor, the local resultant air velocity or relative velocity, is computed according to the following expression:

$$W_u = \sqrt{V_u^2 [(\lambda - \sin^2 \theta)^2 + \cos^2 \theta]} \quad (6.4)$$

where  $W_u$  is the upstream relative velocity and  $\lambda$  is the tip speed ratio given as follows:

$$\lambda = \frac{R\omega}{V} \quad (6.5)$$

The definition of the angles, force and the velocity vectors at the equatorial plane of the rotor are given in **Figure 6.5**.



The local angle of attack, as a function of the tip speed ratio is given as follows:

$$\alpha = \sin^{-1} \left[ \frac{\cos\theta \cos\alpha - (\lambda - \sin\theta) \sin\alpha}{\sqrt{(\lambda - \sin\theta)^2 + \cos^2\theta}} \right] \quad (6.5a)$$

For a pitch blade, the pitch angle is included in Eqn. (6.5a) as follows:

$$\alpha = \sin^{-1} \left[ \frac{\cos\theta \cos\alpha - (\lambda - \sin\theta) \sin\alpha}{\sqrt{(\lambda - \sin\theta)^2 + \cos^2\theta}} \right] - \gamma \quad (6.5b)$$

Then, using a combination of the blade element momentum theory and the momentum equation at each streamtube and by equating the vertical variation of the induced drag coefficient of the rotor, the following expression is obtained:

$$F_{up} = \frac{Nc}{8\pi R} \int_{-\pi/2}^{\pi/2} \left( C_n \frac{\cos\theta}{|\cos\theta|} - C_t \frac{\sin\theta}{|\cos\theta|} \right) \left( \frac{W_u}{V} \right)^2 d\theta \quad (6.6)$$

where  $F_{up}$  is the function that characterises the upwind conditions,  $C_n$  and  $C_t$  are the normal and tangential force coefficients defined in Eqns. (3.14) and (3.15).

The aerodynamic coefficients ( $C_l, C_d$ ) are obtained from experimental data using both the local Reynolds number and the local angle of attack.

A blade Reynolds number can be defined as follows:

$$Re_b = V_c / \nu \sqrt{(\lambda - \sin\theta)^2 + \cos^2\theta} \quad (6.7)$$

where  $c$  is the aerofoil chord and  $\nu$  is the kinetic viscosity.

For a given rotor geometry, rotational speed and free stream velocity, a first set of calculations from equations (6.1) to (6.7) is obtained by assuming the initial interference factor  $a_u=1$ . Then, the new value of  $a_u$  is used to repeat the procedure until the initial and final values are within some level of prescribed tolerance. The procedure is repeated for each streamtube position and once the upstream induced velocity has been calculated, then the procedure is repeated for the downstream half cycle by interchanging the upstream induced velocity  $V_u$  by the downstream induced velocity  $V_d$ .

### 6.4.1.2 Upstream blade force and performance

The streamwise blade forces acting on the blade such as the normal and tangential force may be evaluated for each streamtube as a function of the blade azimuthal angle. Half rotor torque, power and drag are resolved by averaging the contributions from each streamtube for the upstream half cycle of the rotor.

For each blade in the upwind cycle, the non-dimensional force coefficients as a function of the blade azimuthal angle are expressed as follows (Paraschavoui, 1981):

$$F_n(\theta) = \left(\frac{cH}{S}\right) \int_{-1}^1 C_n \left(\frac{W_u}{V_\infty}\right)^2 d\zeta \quad (6.8)$$

$$F_t(\theta) = \left(\frac{cH}{S}\right) \int_{-1}^1 C_t \left(\frac{W_u}{V_\infty}\right)^2 d\zeta \quad (6.9)$$

where  $F_n$  and  $F_t$  represent the normal and tangential forces,  $\zeta = z/H$  is the height ratio between the upwind and downwind half-cycle of the rotor and  $S$  is the swept area of the rotor.

The torque produced by the blade is then obtained at the center of each blade element as follows (Paraschavoui, 1981):

$$T_{up}(\theta) = \frac{1}{2} \rho c R H \int_{-1}^1 C_t W_u^2 \quad (6.10)$$

The average half-cycle of the torque produced by  $N/2$  of the  $N$  blades is given by:

$$T_{up}(\theta) = \frac{N}{2} \int_{-\pi/2}^{\pi/2} T_{up}(\theta) d\theta \quad (6.11)$$

then, the average torque coefficient is given by the expression as follows (Paraschavoui, 1981):

$$\bar{C}_{q1} = \frac{NcH}{2\pi S} \int_{-\pi/2}^{\pi/2} \int_{-1}^1 C_t \left( \frac{W_u}{V_\infty} \right)^2 d\zeta d\theta \quad (6.12)$$

and then the upstream cycle power coefficient is given according to the following equation (Paraschavoui, 1981):

$$C_{pu} = \frac{R\omega}{V_\infty} \bar{C}_{qav1} = \lambda \bar{C}_{qav1} \quad (6.13)$$

#### 6.4.1.3 Downstream half-cycle of the rotor

Similarly, for the downstream half-cycle of the rotor, the blade relative velocity is given as follows:

$$W_d = \sqrt{V_d^2 [(\lambda_d - \sin^2\theta)^2 + \cos^2\theta]} \quad (6.14)$$

where  $\lambda_d = \frac{\omega R}{V_d}$ ,

The angle of attack is evaluated using Eqn. (6.5) where  $\lambda$  is replaced by  $\lambda_d$ , and the subscript  $d$  represents the downwind cycle.

Using the same analogy for the upstream cycle, the equilibrium equation given by Eqn. (6.2) is used as input into the downstream half-cycle at each streamtube. Thus, the computation process is initialised by  $a_d = a_u$ .

The expression that contains the downstream interference factor becomes (Paraschavoui, 1981):

$$F_{dw} a_d = \pi(1 - a_d) \quad (6.15)$$

$$F_{dw} = \frac{Nc}{8\pi R} \int_{\pi/2}^{3\pi/2} \left( C_{nd} \frac{\cos\theta}{|\cos\theta|} - C_{td} \frac{\sin\theta}{|\cos\theta|} \right) \left( \frac{W_{ud}}{V_d} \right)^2 d\theta \quad (6.16)$$

#### 6.4.1.4 Downstream blade forces and performance

The normal and tangential force coefficients for the downstream blade as a function of the azimuthal angle  $\theta$  are given as follows (Paraschavoui, 1981):

$$F_{nd}(\theta) = \left( \frac{cH}{S} \right) \int_{-1}^1 C_{nd} \left( \frac{W_u}{V_\infty} \right)^2 d\zeta \quad (6.17)$$

$$F_{td}(\theta) = \left(\frac{cH}{s}\right) \int_{-1}^1 C_{td} \left(\frac{W_u}{V_\infty}\right)^2 d\zeta \quad (6.18)$$

The torque produced by the downstream blade is computed as follows (Paraschavoui, 1981):

$$T_d(\theta) = \frac{1}{2} \rho c R H \int_{-1}^1 C_{td} W_{ud} d\zeta \quad (6.19)$$

the average half-rotor torque is expressed as follows (Paraschavoui, 1981):

$$\bar{T}_d = \frac{N/2}{\pi} \int_{\pi/2}^{3\pi/2} T_d(\theta) d\theta \quad (6.20)$$

and the average torque coefficient is given as follows:

$$\bar{C}_{q2} = \frac{NcH}{2\pi s} \int_{\pi/2}^{3\pi/2} \int_{-1}^1 C_{td} \left(\frac{W_{ud}}{V_\infty}\right)^2 d\zeta d\theta \quad (6.21)$$

The effective power coefficient  $C_{pt}$  of the VAWT is the sum of both the upstream and downstream cycles, given as follows:

$$C_{pt} = C_{pd} + C_{pu} \quad (6.22)$$

### 6.4.2 Summary

The aim of the simulation program is the possibility to design and analyse 2D aerofoils for use in the self-starting improvement of a small-scale vertical axis wind turbine. Low cost and short calculation time are essential to incorporate the simulation program into the aerofoil design process. CFD and vortex models are too time consuming to use for this purpose. Therefore the choice of the model to use is a momentum based Double Multiple Streamtube model which is incorporated into the Qblade simulation code. This code provides the functionality for pitch angle and rotational speed controllers, geometry export and it serves as a powerful tool to compare different blade designs and their

performance and to investigate all the design variables along the rotor, see **Chapter 7**.

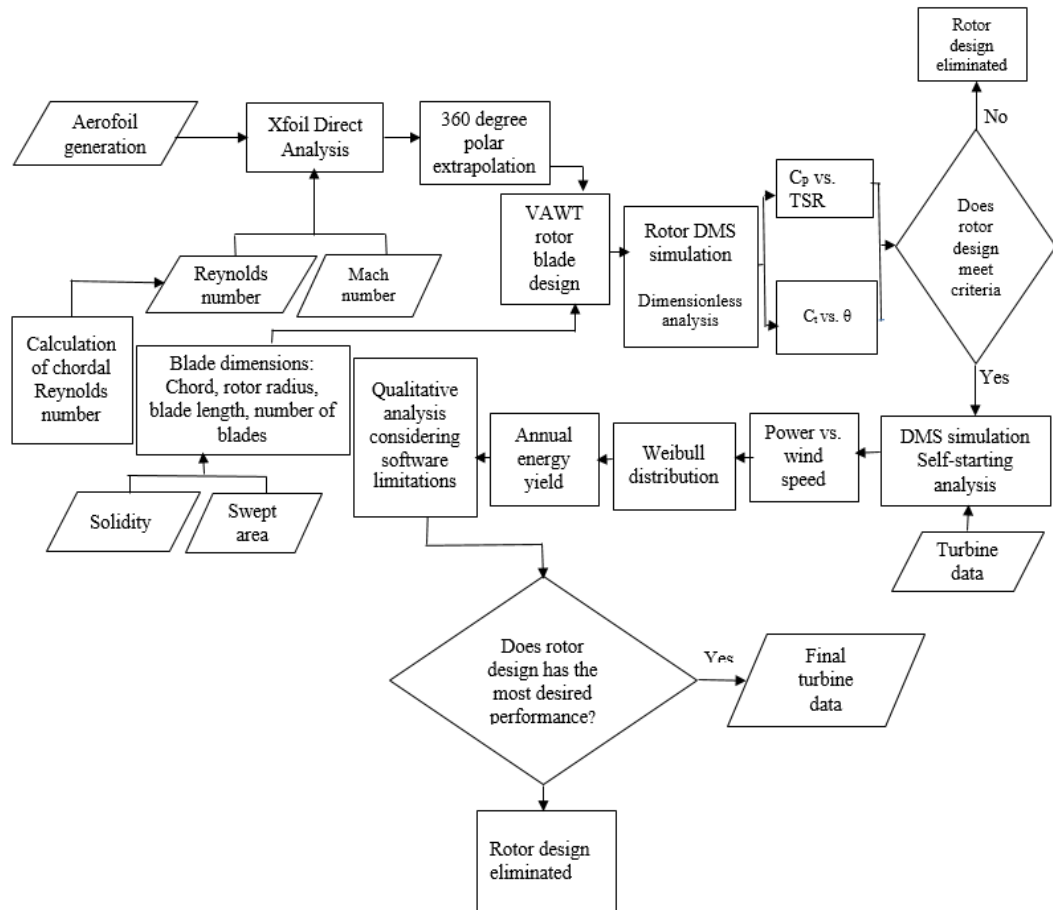


Figure 6.6: Simulation sequence and data flow.

To summarise, the following assumptions and simplifications have been employed and they are valid for all the wind turbine simulation approaches based on this method.

- The aerofoil performance is estimated using steady state aerodynamic data from XFOIL up to an appropriate point of stall. It should be noted the prediction for the post stall region can be a great source of error for low tip speed ratios. This is one of the major limitations of the panel method code.
- The induction velocities through the turbine are obtained from a 2D vortex panel method under the assumption of inviscid, incompressible flow. All 3D effects including swept flow are completely neglected.

However, in reality, the induction velocities is fluctuating in time and space.

- The turbulence at the downwind half of the rotor is taken into account by dividing the blade trajectories into different parts where each part corresponds to a different critical amplification factor. Working with XFOIL also implies that the transition mode is a free transition and not an other mechanism.
- The rotational effects, are accounted for only with respect to the velocity distribution along the rotor blade. All the other rotational induced effects such as Coriolis and centrifugal forces, are ignored.

Figure 6.6 show the sequence of workflow employed for the simulation.

## Chapter 7: Evaluation of a Darrieus VAWT with self-starting capabilities

### 7.1 Overview

As discussed in Sections 1.4 and 2.8.1, the Darrieus vertical axes suffers from one major drawback and this is their inability to reliably self-start under some operating conditions and this has limited their application in small-scale decentralised power generation. Unless the turbines are designed to overcome this problem, and reliably self-start by accelerating beyond the regions of negative torques, they may be unsuitable for small-scale power generation.

A wide range of solution strategies to improve self-starting have been reviewed in Sections 2.8.2-2.8.8, and from these reviews a number of conclusions can be drawn as follows:

- (i) Self-starting may be improved with the use of a Darrieus-Savonius hybrid rotor;
- (ii) A number of modelling strategies, such as increasing the Reynolds number, using cambered aerofoils, rotor solidity, and thickness appear to improve the self-starting performance of a fixed-pitch VAWT
- (iii) Variable pitch mechanism can be used to completely control the blade angle of attack from stalling at low tip speed ratios, and ultimately results in high starting torque. However, implementing such a design is inherently complex and expensive in the context of small-scale wind energy.

Although, these solution strategies provide a guide to some possible areas of investigation, it is generally difficult to implement some of the solution strategies due to lack of quantitative data as noted in Section 2.7.4.4.1. Thus, the following questions are posed:

- (i) Can the conventional fixed-pitch VAWT be redesigned to incorporate self-starting with acceptable cost and efficiency?
- (ii) Is it possible to design a low cost small-scale VAWT capable of self-starting?

In order to answer these questions it is important to have the following:

- (i) Reliable lift and drag coefficients data of suitable aerofoils at different range of angles of attack and Reynolds numbers.
- (ii) A design proposal which can reliably predict the performance of both the fixed and pitch VAWTs under some nominated conditions

Although a number of studies have investigated the performance of a fixed-pitch VAWT, only a few of these studies have considered the concept of self-starting in small-scale scale wind energy. Thus, the work presented in this Chapter is intended to identify the variables and equations governing self-starting and goes on to predict the performance of a small-scale wind turbine under some nominated conditions.

Specifically, the main objectives of the work presented in this Chapter are as follows:

- (i) Identify the variables that affect self-starting in a VAWT.
- (ii) Evaluation of the aerofoil profiles for self-starting of a small-scale VAWT through a critical examination of their salient aerodynamic features.
- (iii) Design and performance assessment of a small-scale VAWT with self-starting capabilities.

The chapter is structured as follows: Section 7.2 describes the variables and the basic equations governing the torque and power output of a vertical axis wind turbine, including the variation of the tangential force coefficient with the angle of attack and the influence of Reynolds number on self-starting. Section 7.3 present some important design choices to be considered. Then, Sections 7.4 and 7.5 deal with the evaluation and discussion of existing aerofoils for VAWTs. Sections 7.6 and 7.7 present the design choices leading to the design proposals. Finally, Section 7.8 presents a summary of the design outcomes.

## **7.2 Variables and equations governing the performance of a vertical axis wind turbine (VAWT)**

In order to develop strategies to overcome self-starting, an understanding of why they produce little torque at low tip speed ratios or at a stationary position is required. Section 7.2.1 sets out the equation for the tangential force coefficient  $C_t$  acting on the aerodynamic centre of a blade cross-section. The



$C_t$  can be calculated if the values of the dimensionless lift and drag coefficients as well as functions of the angle of attack  $\alpha$  for a particular aerofoil section are known, and thus, it is possible to predict the torque output of a stationary VAWT. This will provide some understanding into the factors that affects reliable self-starting but does not indicate whether a VAWT can accelerate beyond the region of negative torque where it starts to do useful work, because, according to Figure 1.3 minimum torque generally occurs at a range of tip speed ratios  $\lambda$  between 0.7 and 2.7.

Furthermore, the tangential force coefficient, torque and power produced by a blade element connected to a spinning rotor can be calculated as a function of the blade azimuthal position  $\theta$ , tip speed ratio  $\lambda$ , and the blade pitch angle  $\gamma$ . This procedure, deepens the understanding of the factors that influence the torque behaviour when the rotor is spinning at low tip speed ratio  $\lambda$  and provides more insight into the actual torque and power at these operating conditions, but it does not show two important trends in the VAWTs operation. These are as follows:

- (i) Generally, the downstream velocity that a VAWTs experiences during rotation is lower than the upstream velocity and the total free stream wind felt by the blade is less than the vector difference of the free stream velocity and the blade velocity.
- (ii) Because about 90% of the energy extracted by a wind turbine occurs at the upstream half cycle, the actual wind experienced by the blade downstream will be less compared to their upstream pass.

Therefore, because of this upstream/downstream difference in the wind velocity, it is vitally important to use a suitable aerodynamic model that adequately accounts for the velocity differences at both the upstream and downstream passes. Existing models which account for this interactions have been reviewed in Section 2.9, and the model considered for the present analysis is described in Section 6.4.1.

### **7.2.1 Variation of tangential coefficient with the angle of attack**

Consider a blade element at a stationary position showing the dimensionless lift and drag coefficients along with the blade relative velocity and a

corresponding angle of attack, see Figure 7.1. The contribution to the total torque acting on the blade can be expressed by decomposing the lift and drag coefficients into tangential force coefficients as follows:

$$C_t = C_l \sin \alpha - C_d \cos \alpha \quad (7.1)$$

where  $C_t$  is the tangential force coefficient which determines whether an aerofoil generates a positive or negative torque.  $C_l$  and  $C_d$  are the lift and drag coefficients and are functions of  $\alpha$ , Reynolds number and the aerofoil section used.

It should be noted that when the rotor is at a stationary position, Eqn. (6.5a) reduces to  $\alpha = 0$ .

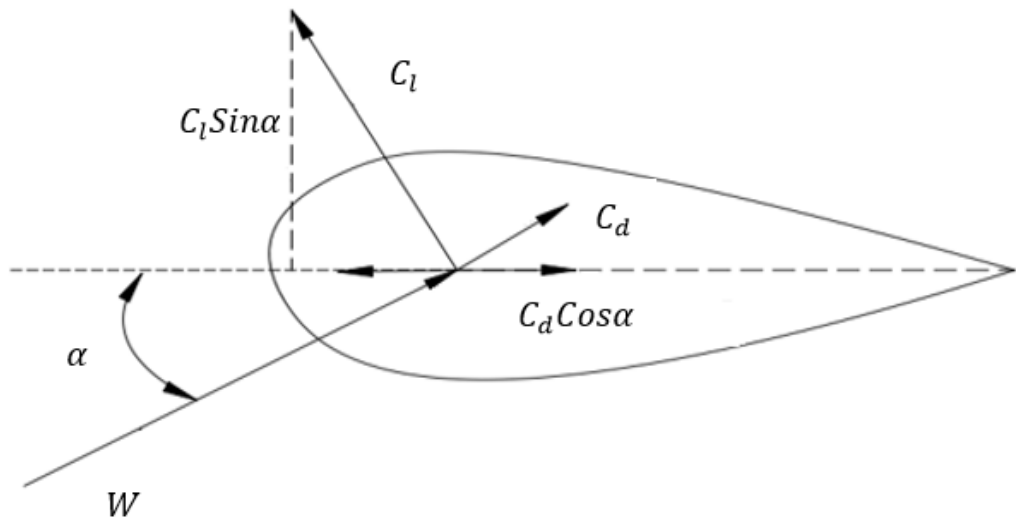


Figure 7.1 Schematic of a blade element showing the components of the lift and drag coefficients contributing to the tangential force coefficient.

To demonstrate the behaviour of a rotor at a stationary position, consider the case of a two-dimensional NACA 0018 blade. Using Eqn. (7.1) and experimental data from Sheldahl and Klimas (1981), the forward tangential force coefficient at a Reynolds number of 80,000 is plotted in Figure 7.2 and can be seen that a large drop in the tangential force coefficient  $C_t$  occurs at the point of leading-edge separation caused by the sudden loss in lift and increase in drag. This results in a post stall region of negative tangential force

coefficient, followed by a high angle of attack region of positive  $C_t$ . Although, some regions of negative tangential force exist, the net torque over a complete cycle is definitely positive. This should allow this hypothetical layout to accelerate from a stationary position.

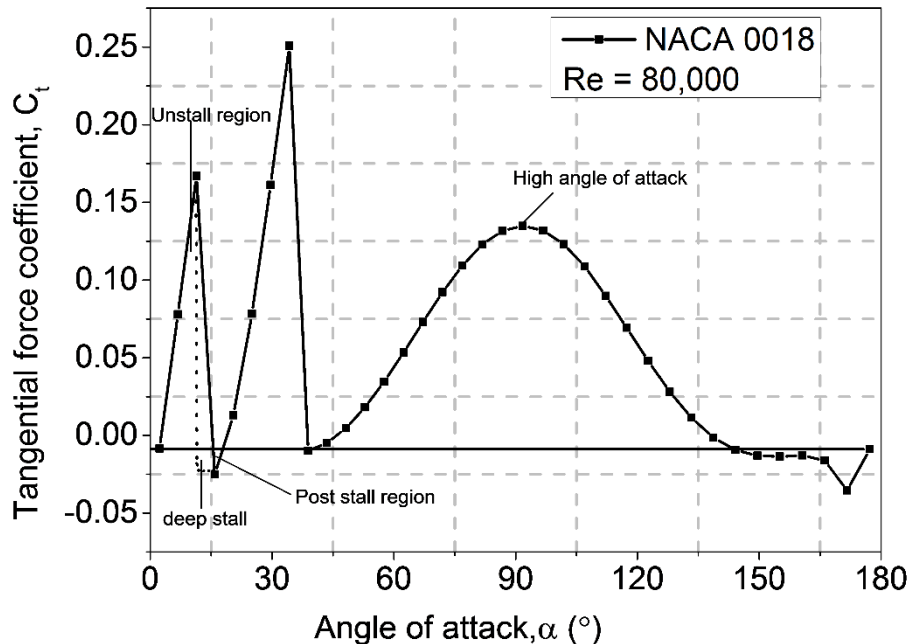


Figure 7.2: Tangential force coefficient as a function of the angle of attack for a single NACA 0018 aerofoil at rest ( $\lambda=0$ ) based on the formula given in Eqn. (7.1) and experimental data from Sheldahl and Klimas (1981).

### 7.2.2 Variation of torque with blade azimuthal position and tip speed ratio

As shown in the previous subsection, the tangential force coefficient  $C_t$  can easily be evaluated if the aerodynamic coefficients ( $C_l$ ,  $C_d$ ) and the angle of attack  $\alpha$  are known. The variations of  $C_t$  with  $\alpha$  shown in Fig. 7.2 indicates whether or not the net torque for a given blade is positive or negative. However, it does not indicate the actual magnitude of the torque when the turbine is in motion. Further, it does not give an indication of the values of the torque at each position of the blade or the average value over the complete turbine rotation. To calculate the torque at a specific azimuthal position, the following steps are required:

- (i) The forces acting on the blade (lift, drag and tangential forces) must be calculated from the corresponding dimensionless aerodynamic coefficients ( $C_l$ ,  $C_d$ ) and thrust coefficients.
- (ii) The angle of attack  $\alpha$  and the relative velocity must be expressed as a function of the wind velocity  $V$ , rotational speed of the turbine  $\omega$ , and the blade azimuthal position  $\theta$ .

The aerodynamic forces produced by a blade on a fixed-pitch VAWT are given as follows:

$$F_l = C_l(0.5\rho AV_{rel}^2) \quad (7.2)$$

$$F_d = C_d(0.5\rho AV_{rel}^2) \quad (7.3)$$

$$F_t = 0.5\rho AV_{rel}^2 C_t \quad (7.4)$$

in which  $F_l$ ,  $F_d$ ,  $F_t$  are the lift, drag and tangential forces,  $\rho$ ,  $A$  and  $W$  indicate the air density, blade platform area and relative velocity of the blade, respectively.

The torque produced by the blade as a result of these forces is given as follows:

$$T = F_t R = 0.5\rho AV_{rel}^2 C_t R \quad (7.5)$$

where  $T$  is the torque and  $R$  is the radius.

For an aerofoil with a straight blade, the angle of attack  $\alpha$  and relative velocity  $W$  are seen to be functions of the blade azimuthal position  $\theta$ , the induced velocity  $V_u$  and  $\omega R$ , see Figure 6.5(a).

The magnitude and direction of the induced velocity  $V_u$  varies significantly with  $\theta$  due to the extraction of power by the blades, thus  $V_u$  is always less on the downwind cycle than the upwind cycle. However, when the blade is at a static position or accelerating at low  $\lambda$ , the turbine produces a very small power and in that condition it might be ideal to assume that the induced  $V_u$  is uniform at both the upwind and downwind cycle and is equal to the free stream

velocity  $V_\infty$ , so that the tip speed ratio  $\lambda$  is independent of the azimuthal position  $\theta$ . Thus, the angle of attack becomes a function of  $\theta$  and  $\lambda$ . Therefore, when there is no inflow induction into the turbine, the angle of attack can be computed according to the following expressions:

$$\alpha = \tan^{-1}(V_u \sin\theta / (\omega R + V_u \cos\theta)) = \tan^{-1}(\sin\theta / (\lambda + \cos\theta)) \quad (7.6)$$

Equation (7.6) indicates that, apart from the dependence on the azimuthal position,  $\theta$ , the angle of attack variation of a blade element is strongly determined by the tip speed ratio,  $\lambda$ . This dependence is better illustrated in Figure 1, but for convenience it is repeated as Figure 7.3 at several values of the tip speed ratio  $\lambda$  for the ease of reference.

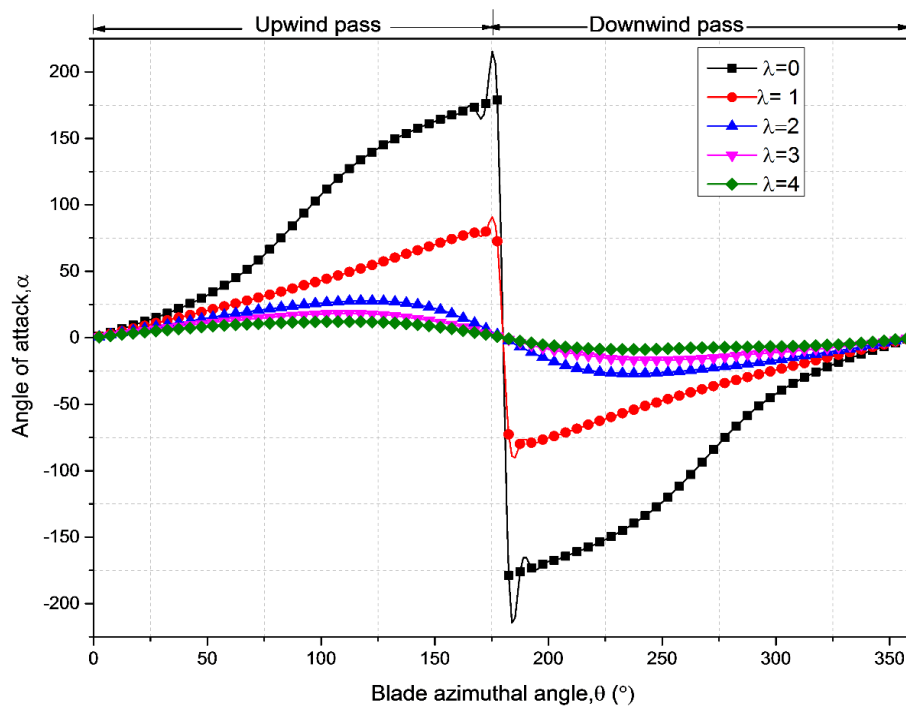


Figure 7.3: Angle of attack variation as a function the azimuthal position and tip speed ratio experienced by a blade under different conditions.

At  $\lambda = 0$ , the blade experiences only wind speed and its angle of attack varies linearly with the azimuthal position. Consequently, when the turbine is at a stationary position, it has to cope with a wide range of angles of attack ( $-180^\circ \leq \alpha \leq 180^\circ$ ) and up to  $\lambda = 1$ . It is only when  $\lambda > 1$  that the blade experiences a head wind at every azimuthal position (making  $\alpha$  drop to zero at  $\theta = 180^\circ$ ).

The assumption made to derive Eqn. (7.6) can never hold in real life situations. Nevertheless, the tip speed ratio remains an essential parameter that governs the behaviour of a VAWT. In real situation, the downwind half of the rotor is strongly affected by the vorticity due to the upwind pass.

Furthermore, from Figure 6.5 (a), the relative velocity  $W$  can be expressed as follows:

$$W = \sqrt{(V_u \sin\theta)^2 + (\omega R + V_u \cos\theta)^2} = V_u \sqrt{(\sin^2\theta + (\lambda + \cos\theta)^2)} \quad (7.7)$$

where  $\lambda = \omega R / V_u$

The torque acting on the blade can then be calculated as a function of  $\theta$  and  $\lambda$  and assuming constant wind flow through the turbine and provided the aerodynamic coefficients data ( $C_l, C_d$ ) are available for a particular aerofoil as a function of  $\alpha$ . **Figure 7.4** depicts the torque,  $T$  as a function of  $\theta$  for a tip speed ratio  $\lambda=1.5$ .

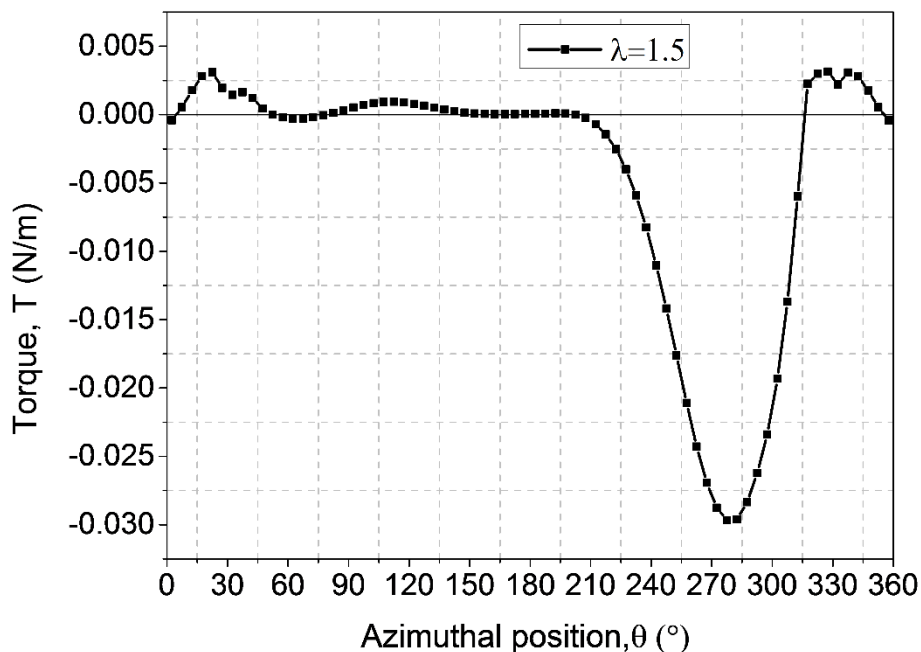


Figure 7.4: Torque,  $T$  as a function of azimuthal positions and tip speed ratio for NACA 0018 section blades at  $Re = 80,000$ .

For this Reynolds number, the positive peaks are smaller and the negative troughs are greater. The net effect of this trend is shown in Figure 7.5 in which the power and torque coefficient is plotted as a function of the tip speed ratio. This plot indicates that a typical small-scale Darrieus turbine with a fixed-blade utilising NACA 0018 blades of 0.2 m chord may not be able to achieve passive start-up at a wind speed of 5m/s.

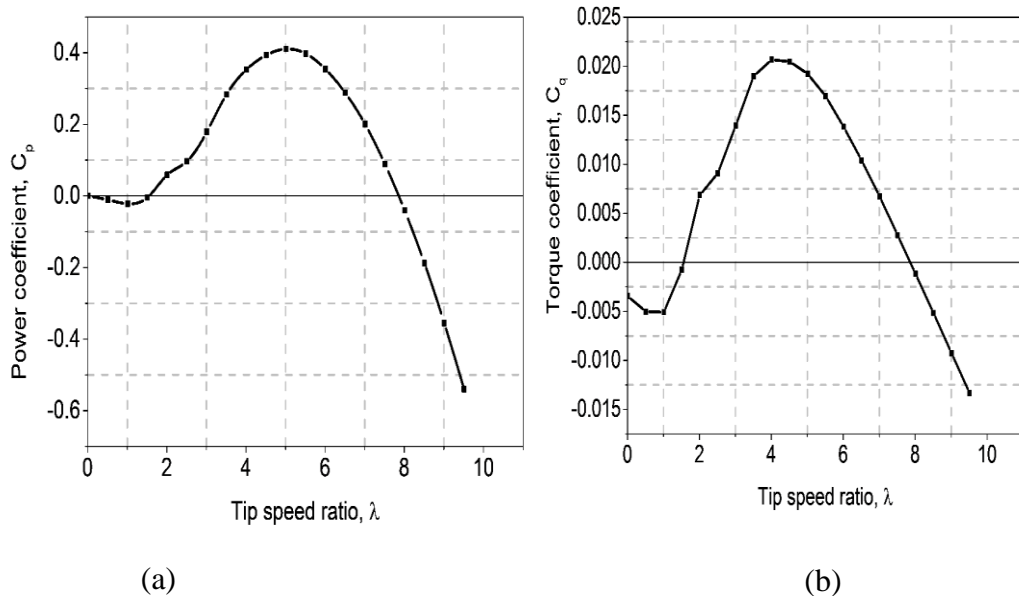


Figure 7.5: (a) Power coefficient, (b) Torque coefficient as a function of tip speed ratios for NACA 0018 section blades at a wind speed 5 m/s.

### 7.2.3 Power output and Torque coefficient

The power produced by a wind turbine is the product of the torque and its rotational speed and is expressed as follows:

$$P = T\omega \quad (7.8)$$

It should be noted that the power produced by a wind turbine is usually expressed in terms of its coefficient of performance  $C_p$ , which indicates the amount of power intercepted by the turbine as follows:

$$C_p = P/0.5\rho AV^3 \quad (7.9)$$

The corresponding torque coefficient is given as follows:

$$C_q = C_p/\lambda = T/[(0.5\rho AV^2)R] \quad (7.10)$$

### 7.2.4 The influence of Reynolds number

As noted in Section 2.8.2, the aerofoil performance is strongly affected by the Reynolds number. This is illustrated for NACA 0018 blade at  $Re = 500,000$ ;  $360,000$ ;  $80,000$  and  $50,000$ , respectively. Figure 7.6 shows the predictions for four Reynolds numbers. In this data, the design stall angle of attack ( $\alpha_{\text{stall}}$ ) ranges from 8 to 17 degrees. These results show that the aerofoil is very sensitive to changes in the Reynolds numbers.

Furthermore, the results indicate that the generation of lift and drag can significantly drop by the choice of a Reynolds number which will clearly affect the self-starting performance of the aerofoil.

In line with the findings of many researchers, the above discussion reveals that there is a band of negative torque, often known as the dead-band, in the operating range  $0.5 \leq \lambda \leq 1.5$ .

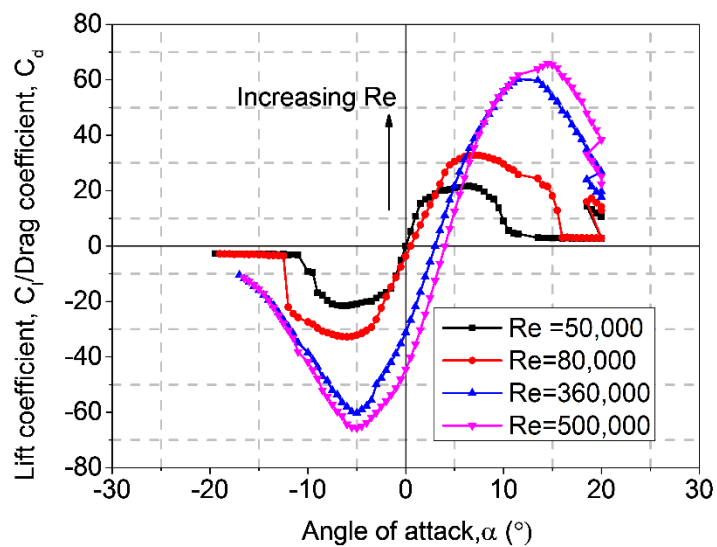


Figure 7.6: The predicted lift and drag coefficient as a function of angle of attack at several Reynolds number for the NACA 0018 aerofoil.

The main reason behind the dead-band is the combination of small-scale and the light wind conditions which lead to low Reynolds numbers, often less than  $10^5$ . The lift production and stall behaviour of the aerofoil at this low Reynolds number is severely aggravated, thus resulting in a low starting torque. The net



effect of these operating conditions is evaluated numerically and plotted in Figures 7.5 (a) and 7.5 (b). The results show that at the point of cut-in, the power and torque coefficient is completely negative, thus indicating that a typical small-scale VAWT with fixed NACA 0018 blades does not achieve passive start-up. Therefore it is necessary to investigate other avenues to achieve self-start. This is treated in the following sections.

### **7.3 Conceptual design**

Some of the solution strategies to improve self-starting in Section 7.1 can be bundled into a new blade design. Therefore, this section is intended to set out the design choices leading to one or more proposals of improving the self-starting performance in small-scale VAWTs.

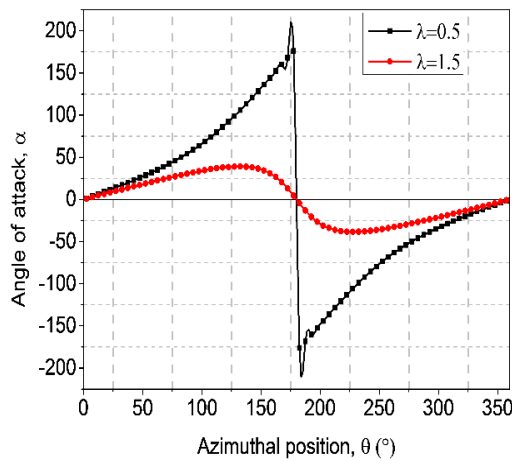
#### **7.3.1 Design considerations**

The design of a VAWT is actually a compromise between different design options, concerning the parameters of operation of the system and its components. This implies that the appropriate selection should be made between the different options, taking into account their characteristics and their influence on other components of the system. For instance, the rotational speed of the turbine should be selected based on the aerodynamic performance criteria in order to avoid possible static and dynamic problems. For the purpose of this design, the most important parameters are perhaps the angle of attack and the chordal Reynolds number in which the blades operate.

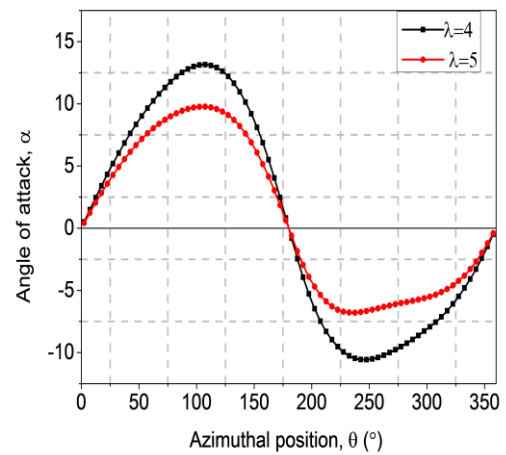
#### **7.3.2 Design conditions**

The operation of small wind turbines at low tip speed ratios and light wind speed implies that the Reynolds number regime and the angle of attack is highly sensitive to unstable region with high probability of separation. This situation makes it difficult to choose a specific design point. Instead, there is a wide range of design considerations at which the design is expected to perform well.

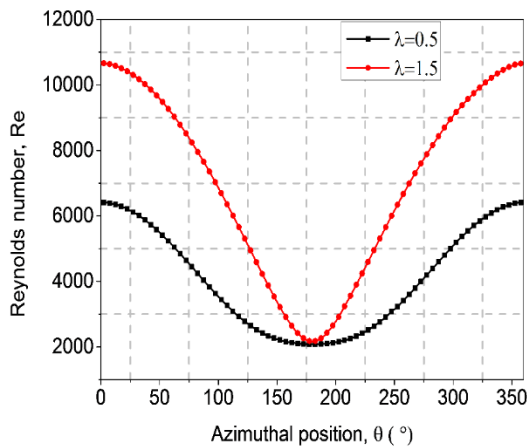
Improving self-starting performance focuses on increasing the lift at a high angle of attack (maximising the term  $C_l \sin \alpha$  in Eqn. (7.1), narrowing the post stall region, etc. On the other hand, maximising the power coefficient  $C_{pmax}$  at the rated wind speed focuses on decreasing the drag (minimising the term  $C_d \cos \alpha$  in Eqn. (7.1) and avoiding dynamic stall. Based on these conditions, two design points can be identified, shown in Figure 7.7 (a-d), namely the region of negative power coefficient  $C_p$  between the operating range  $0.5 \leq \lambda \leq 1.5$  and the maximum  $C_p$  at the operating range  $4 \leq \lambda \leq 5$ .



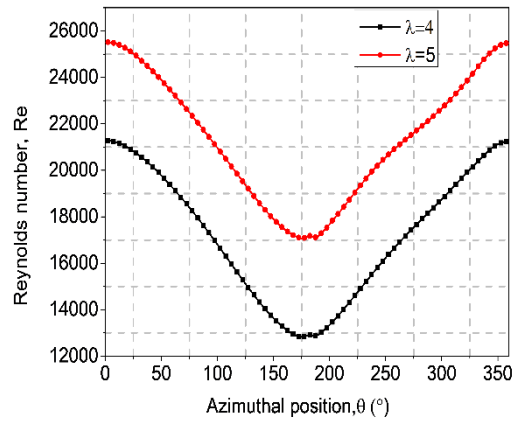
(a): Predicted angle of attack at  $\lambda = 0.5 - 1.5$  (wind speed,  $V = 5$  m/s).



(b): Predicted angle of attack at  $\lambda = 4 - 5$  (wind speed,  $V = 5$  m/s).



(c): Variation of Reynolds number as a function of azimuthal position at  $\lambda = 0.5 - 1.5$  (wind speed,  $V = 5$  m/s).



(d): Variation of Reynolds number as a function of azimuthal position at  $\lambda = 0.5 - 1.5$  (wind speed,  $V = 5$  m/s).

Figure 7.7: Predicted performance of a small-scale VAWT utilising the NACA 0018 blade showing the operating conditions during start-up.

### 7.3.3 Aerofoil profile features

An optimum aerofoil profile is expected to possess some desirable characteristics which were conveniently identified by Islam et al. (2007):

- (i) Stall characteristics. In order to minimise the separation that results in blade stalling, it is important to ensure that the stall angle of the aerofoil for a fixed-pitch turbine is moderately large, particularly for low tip speed ratios that are usually encountered by straight bladed vertical axis wind turbines. A high stall angle, along with a high maximum lift coefficient  $C_{lmax}$ , enables the blade to generate a high starting torque during operation. For self-starting performance, it is therefore vitally important to evaluate aerofoil characteristics at low Reynolds number where performance is severely affected.
- (ii) Performance. Aerofoil performance is assessed by the lift-drag ratio which refers to the amount of lift generated by an aerofoil compared to its drag. The overall efficiency of an aerofoil is estimated by the level of the lift-drag ratio. Aerofoils with a higher  $C_l/C_d$  ratio over a wide range of  $\alpha$  generally possess higher aerodynamic and start-up performance by increasing the tangential force coefficient  $C_t$ . This also implies that the minimum amount of drag, and the zero-lift-drag coefficient  $C_{d0}$  should be as low as possible.
- (iii) Pitching moment. The pitching moment is defined as the point on the chord line of the aerofoil at which the pitching moment coefficient does not change significantly over the range of angles of attack  $\alpha$ . Preferably, the aerofoil pitching moment should pitch nose-down (negative direction) in order to enhance the starting torque<sup>12</sup>.
- (iv) Drag polars. Generally, aerofoils exhibit the lowest drag over a narrow range of angles of attack, called the “drag bucket”.

---

<sup>12</sup> The main role of a pitching moment is not clearly understood. At the time of writing this thesis, there are arguments that the resultant pitching moment (normal force on the blade) does not increase starting torque. Consequently, attention is focussed on the tangential force.

Aerofoil for start-up should possess a wide drag bucket which invariably increases its efficiency.

In addition to the above characteristics, Islam et al. (2007) concluded that the optimum aerofoil should possess the following geometric features:

- (i) Camber. Cambered aerofoil sections exhibit superior aerodynamic performance and tend to provide lift at low Reynolds numbers, are less prone to roughness, possess a large stall angle and exhibit stronger negative pitching moments.
- (ii) Thickness. Aerofoils with thicker blade shapes possess some known advantages for small-scale SB-VAWT, including improved performance, increase starting torque and increase the width of the drag bucket.

Several studies have shown that aerofoils with greater thickness are favourable for improving the self-starting ability of SB-VAWT. However, the negative aspect of increasing the thickness should also be considered. Sato and Sunada (1995) argued that there was a limit to the benefits of using very thick aerofoils at low Reynolds numbers. They revealed that airfoils with up to 28.5% thickness may not produce any valuable lift at low Reynolds numbers. Moreover, increasing the thickness beyond 18% is usually accompanied by a loss in the efficiency of the aerofoil section. Therefore, care must be taken when increasing aerofoil thickness beyond 20%.

- (iii) Large leading-trailing edge radius. Aerofoils with larger leading edge radii tend to exhibit higher performance for smaller scale SB-VAWT. This characteristic enhances the performance of the aerofoils as it tends to increase their lift-drag ratio, particularly at large angles of attack (Liang et al., 2014). However, using thick leading edges at low Reynolds numbers is often associated with high pressure peaks which could affect aerodynamic performance.

Furthermore, sharp trailing edges reduce the minimum drag coefficients of aerofoils and raise the lift-drag ratio. However, the manufacturing process of sharp trailing edges is generally difficult

and often associated with high costs particularly for small chord lengths. In addition, sharp trailing-edge thickness assists to mitigate blade stalling, thereby resulting in generation of more torque at start-up as well increase the overall performance of aerofoils (Ahmed, 2012, Liang et al., 2014).

### 7.3.4 Design Philosophy

In order to increase the starting torque for a fixed-pitch turbine, there are a number of factors to consider. One of the most important, perhaps, is to delay the point of the leading-edge separation on the aerofoil. This will be appropriate for start-up since it tends to decrease the post-region (see for example, Figure 7.2). Furthermore, at higher tip speed ratios, the aerofoil traverses frequently in and out of the dynamic stall region and a wide linear lift regime is desirable in order to reduce the effects of hysteresis. Leishman (2006) investigated the self-starting behaviour of a combination of NACA 0012 and HH-02 and SC1093 rotorcraft aerofoil and revealed that most of the static behaviour of these aerofoils also applied to the dynamic range. This implies that designing for a high static lift also means that dynamic stall is delayed to higher angles of attack.

Another viable option is to reduce the violent movement of laminar separation bubbles<sup>13</sup>. It may be possible to attempt a transition ramp, however, it is not certain if natural transition would occur at all during start-up. This is because critical amplitudes may not be attained before the trailing-edge is reached. This implies that the lower amplification factors,  $N_{crit}$  encountered in the downwind cycle at the bottom of the aerofoil will cause instabilities to grow much faster. Therefore, different methods are required for both upwind and downwind cycles.

There are several design approaches available for aerofoils. The most straight forward approach is by changing the specifications of an existing aerofoil

---

<sup>13</sup> Laminar separation bubble is a phenomenon that are usually encountered by low Reynolds number aerofoils as a result of a strong pressure rise along the surface of the aerofoil, in which a laminar boundary layer separates and undergoes transition to turbulent and subsequently reattaches as a turbulent layer.

profile. A more advanced approach is the surface speed design routine in the XFOIL/ RFOIL which revolves around modifying an existing profile or designing a new one and can be an effective approach in reducing bubble drag that results in blade stalling. Therefore, a choice was made to work with an advance design routine in XFOIL which was introduced in Chapter 6 (see figure 6.3). The current version of the code, XFLRS, is integrated within the Qblade code to aid in the design, import and the analysis of different aerofoil geometries and rotor simulations based on the double multiple streamtube model. One of the main benefits of using the new version of the code is the flexibility to extrapolate the lift and drag coefficients to  $360^\circ$  blade rotation using either the Montgomery or the Viterna-corrigan post stall models. However, because the code was developed using a potential flow model, it does not converge for very high angles of attack (Marten et al., 2013).








#### **7.4 Evaluation of Aerofoils for self-starting**

A wide variety of aerofoils were generated in XFOIL that maximizes the lift to drag  $C_l/C_d$  or the tangential force coefficient during a complete cycle. In order to select the prospective candidate aerofoils, the following series of aerofoil database were explored: (i) UICC database for aerofoils with low Reynolds numbers; (ii) NACA symmetrical and asymmetrical aerofoils; (iii) Eppler low Reynolds number aerofoils; (iv) NASA NLF aerofoils; and (v) Worthmann FX series aerofoils.

The selection criteria was based on the desirable aerodynamic features discussed in Section 7.3.4. For the present case, only the experimental data sets for the low speed application, which are often known as low Reynolds number aerofoils or low speed data sets. After a preliminary assessment of the candidate aerofoils, seven prospective airfoils were shortlisted for initial assessment and comparison with the conventionally used symmetrical NACA 0018 airfoil. Table 7.1 summaries the sources of the experimental data for the prospective aerofoils.

The aerofoils were analyzed based on the following specifications: Number of blades = 3, wind velocity = 5 m/s, turbine diameter = 2m, rotational speed= 18.5 rpm and chord length= 0.3m. This results in a blade Reynolds number of 383,200.

Table 7.1: Selected prospective aerofoils based on the availability of experimental data.

Airfoil Name	Airfoil geometry	Source of Exp. Data	Remarks
NACA 4415		Rodrigues et al. (1988)	NACA asymmetrical airfoil
E 193		Selig et al. (1995)	Eppler low Re asymmetrical airfoil
S 1210		Selig et al. (1995)	High lift low Re number asymmetrical airfoil
S 1223		Selig et al. (1995)	High lift low Re number asymmetrical airfoil
S 8037		Lyon et al. (2014)	Low Re asymmetrical airfoil
SG 6040		Lyon et al. (2014)	Giguere wind turbine low Re asymmetrical airfoil
DU06-W-200		Classens (2006)	TU Delft Airfoil

#### 7.4.1 Comparison of XFOIL results with published experimental data

Before XFOIL was used to predict the performance of the above listed aerofoils, the code was compared with the available experimental results to demonstrate the validity of XFOIL predictions. These include the experimental data from Sheldahl and Klimas (1981); Trimmer (2008) and Bianchini et al. (2016). A default value of 9 for  $N_{crit}$ , used in transition prediction was conservatively used. For performance comparisons, a Reynolds number equal to  $3.0 \times 10^5$  was designated in line with the experimental data and is comparable to blade Reynolds number in a typical operating range of a small scale VAWT. Figures 7.8 depicts the lift,  $C_l$  and drag  $C_d$  coefficients as a function of angles of attack,  $\alpha$  for NACA 0018 aerofoil section.

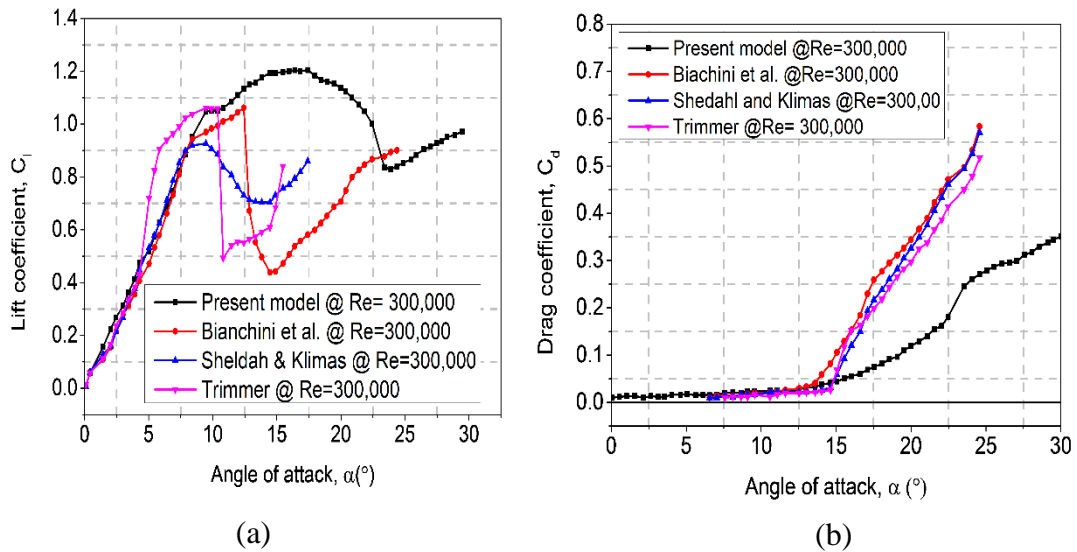


Figure 7.8: Performance comparison of the NACA 0018 aerofoil with the available experimental data: (a) Lift as a function of the angle of attack, (b) Drag as a function of the angle of attack, at a Reynolds number = 300,000.

In Figure 7.8 (a), the results show good agreement between the present study and the experiments in most of the lift curves, except in the stall region, where the stall angles are slightly different at this operating condition. For example, the stall angle for Bianchini et al. (2016) Sheldahl and Klimas (1981), and Timmer (2008) occurred at approximately 12, 8 and 11 degrees, respectively, while the present model stalled at an angle of 16 degrees. The stall angle is particularly difficult to predict accurately due to a number of factors, such as the aerofoil surface finish and 3D effects. Similarly, in Figure 7.7 (b) the present model matches very well with the experimental data, particularly up to approximately 12 degrees. After 12 degrees, XFOIL uses internal correlations to extrapolate the lift and drag coefficients and its accuracy is considerably reduced for the prediction of the lift and drag.

It should be noted that the XFOIL prediction beyond 12 degrees angle of attack is significantly different from the famous data of Sheldahl and Klimas (1981). This was also reported by Du et al. (2014) and confirms a general underestimation of the lift coefficient. This data set has been frequently used in the past in most blade element momentum (BEM) simulations due to the availability of their lift, drag and moment coefficients to validate theoretical



prediction with no proper evaluation of the validity of the data. Using such a data, particularly for the NACA 0018, therefore, requires extreme caution as it is extrapolated from experimental data for thinner aerofoil sections. The aerofoil section thickness has a significant impact on the performance, especially at the stall region, thus reducing the validity of the extrapolation at this region.

## 7.5 Results and discussion

### 7.5.1 Comparison of the performance of selected asymmetrical aerofoils

Figure 7.9 show the variation of the blade tangential force coefficient  $C_t$  as a function of the blade azimuthal positions for seven asymmetrical airfoils in comparison with representative symmetrical aerofoils NACA 0018. The angles of attack  $\alpha$  range between  $-20^\circ \leq \alpha \leq 30^\circ$  and a critical amplification factor  $N_{crit} = 9$  was used in line with previous studies.

For a straight bladed VAWT, the tangential force coefficient  $C_t$  indicates the potential of the airfoil to self-start the turbine, i.e. if the tangential force coefficient  $C_t$  is positive, the blade tends to produce a forward tangential or thrust force. The instantaneous torque produced by the blade can then be evaluated when the thrust force is multiplied by the radius (R). It can be seen from Figure 7.9 that the  $C_t$  values for all the asymmetrical aerofoils, namely S 1210 and S 1223, SG 6040, NACA 4415, S 8037 and DU 06-W-200 are more superior to the conventional NACA 0018 at  $Re = 383,200$  for  $0 \leq \theta \leq 90$ . It should be note that this typical operation range is highly susceptible to leading edge separation that results in blade stalling

Further, the results show the tangential force coefficient for the E 193 aerofoil is less than the conventional NACA 0018 and is therefore excluded from further analysis. These results confirm the assertion by Kirke (1998) that a fixed-pitch SB-VAWT using certain airfoils and at low Reynolds numbers should reliably self-start.

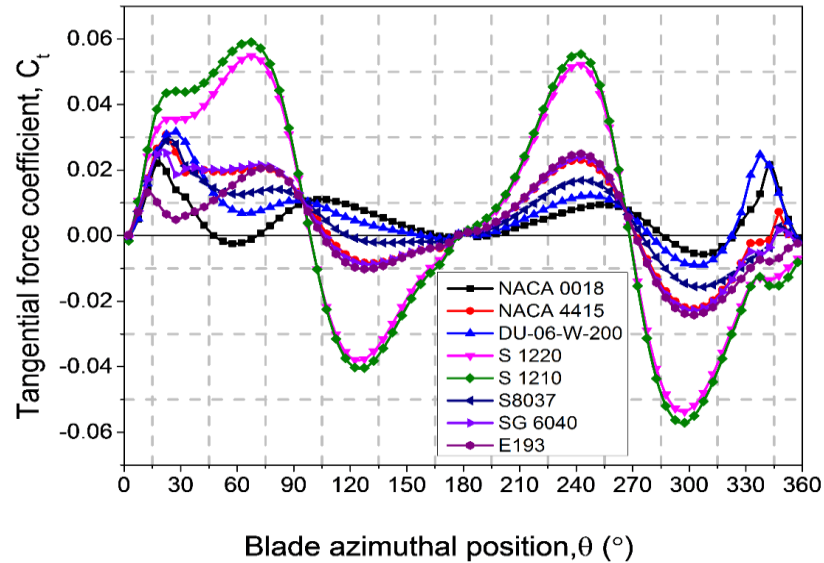


Figure 7.9: Tangential force coefficient  $C_t$  as a function of the blade azimuthal position  $\theta$  for the investigated aerofoils at  $Re=383,200$ ,  $N_{crit} = 9$ .

### 7.5.2 Stall characteristics

At low tip speed ratio  $\lambda$ , the behaviour of lift and drag coefficients in the post stall region have serious consequences for a fixed-pitch VAWT and their lack of starting torque is partly due to the cyclical variation in the blade angle of attack  $\alpha$  with the azimuthal position  $\theta$ . Thus, the stall blades generally tend to contribute negatively to the driving torque so that the net work output per revolution may be negative for some values of  $\lambda$ .

Therefore, if the stall angle is increased at low tip speed ratios  $\lambda$ , the starting torque will be improved as the blades are stalled at a smaller proportion of their travel path. Consequently, a large stall angle of the aerofoil sections for a fixed-pitch VAWT is desirable in the low Reynolds number range typically encountered by small-scale VAWTs in order to reduce the separation that occurs at low tip speed ratios.

Figure 7.10 show a typical variation of the lift coefficient  $C_l$  with the angle of attack  $\alpha$  for the prospective aerofoil sections in comparison with the conventional NACA 0018 at a Reynolds number 383,200.

It is clear from Figure 7.9 that the DU06-W-200 is the most superior aerofoil in this case with a stall angle  $\approx 18^\circ$ . This is followed by S 8037, NACA 4415,

S1210, S1223, SG 6040 and NACA 0018 with stall angles of  $\approx 13.7^\circ$ ,  $14.70^\circ$ ,  $13.0^\circ$ ,  $13.0^\circ$ ,  $14.0^\circ$ , and  $10.0^\circ$ , respectively.

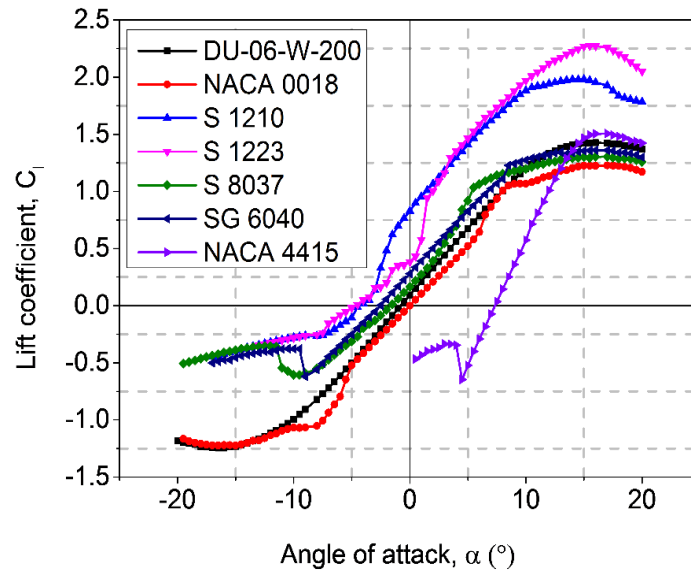


Figure 7.10: Lift coefficient  $C_l$  as a function of the angle of attack for the prospective aerofoils at  $Re=383,200$ ,  $N_{crit} = 9$ .

These results show that the values of  $\alpha_{stall}$  for all asymmetrical airfoils are higher than for the NACA 0018 at this Reynolds number. This indicates their superiority in the positive angles of incidence where about 90 or 95% of the power of a typical wind turbine is extracted. However, at the negative angles of incidence, the NACA 0018 and DU06-W-200 show superior performance over all the other asymmetrical airfoils at the same operating conditions. This is expected because airfoils encounter negative incidences in the downstream section of the straight-bladed (SB) VAWT where a lesser amount of power is extracted (Kirke, 1998).

Furthermore, the amount of torque that an airfoil generates in the pre-stall region depends on the maximum available lift from the airfoil, i.e. if the airfoil has a higher maximum lift coefficient, then more torque is expected to be generated, which consequently improves the starting torque of the turbine. Therefore, high lift  $C_l$  and high stall angle  $\alpha_{stall}$  are desirable airfoil features for a self-starting SB-VAWT. It is evident from Figure 7.9 that the maximum lift coefficients  $C_l$  for all the investigated asymmetrical airfoils are higher than for the symmetrical NACA 0018 airfoil.

### 7.5.3 Drag polar

Generally, aerofoils tend to exhibit the lowest drag over a narrow range of angles of attack, called the “drag bucket”, and the position of the drag bucket is strongly influenced by the shape of the aerofoil.

Several studies, including Klimas (1985) and Islam et al. (2007), have revealed that a wide drag bucket increases the performance of VAWTs.

It was also confirmed by Classens (2006) that an increased width of the drag bucket enhances the performance of a VAWT over a large range of angles of attack. Figure 7.11 depicts a typical drag polar curve for the prospective aerofoils. It can be seen that the width of the drag bucket for the DU-06-W-200 is the largest among the analysed aerofoils and is similar to that of the NACA 0018. The drag polars of all the other asymmetrical aerofoils are similar in shape and tend to increase towards the positive lift coefficient.

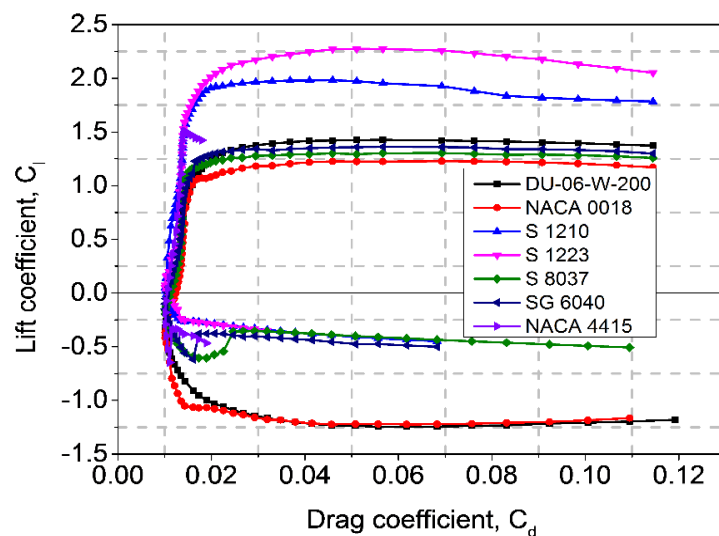


Figure 7.11: Lift coefficient  $C_l$  as a function of the drag coefficient for the prospective aerofoils at  $Re=383,200$ ,  $N_{crit} = 9$ .

### 7.5.4 Lift-Drag Ratio

The lift-drag ratio  $C_l/C_d$  refers to the amount of lift generated by an airfoil compared to its drag and it demonstrates the overall efficiency of an airfoil. Aerofoils with a higher  $C_l/C_d$  ratio over a wide range of  $\alpha$  generally possess higher aerodynamic performance as they tend to increase the tangential force coefficient  $C_t$ .

Figure 7.12 depicts a typical performance curve of the prospective aerofoils in comparison with the NACA 0018.

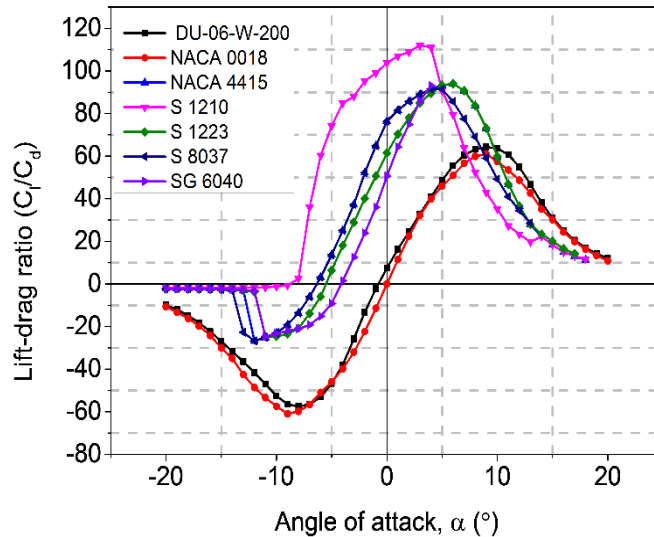


Figure 7.12: Comparison of the lift-drag ratio of the prospective aerofoils in comparison with the NACA 0018 at different angles of attack at  $Re = 383,200$ ,  $N_{crit} = 9$ .

The results indicate that all the asymmetrical airfoils exhibit higher  $C_l/C_d$  than the NACA 0018. Specifically, the results show that the S 1210 possesses the highest  $C_l/C_d$  over a wide range of  $\alpha$ , particularly at positive angles of incidence. At the same time, at negative angles of incidence the NACA 0018 and DU06-W-200 could be seen as the aerofoils with the highest  $C_l/C_d$  ratios. However, the contribution of the positive angles of incidence to the overall power generated by the wind turbine is much higher than those of the negative angles of incidence.

### 7.5.5 Pitching Moment

The pitching moment is defined as the point on the chord line of the airfoil at which the pitching moment coefficient does not change significantly over the range of angles of attack  $\alpha$ . The nature of the airfoil pitching moment affects its efficiency (Kato et al., 1981).

Figure 7.13 compares the performance of the investigated airfoils with the NACA 0018. Due to the shape of the NACA 0018, a change in angles of attack  $\alpha$  does not present much change to the pitching moment.

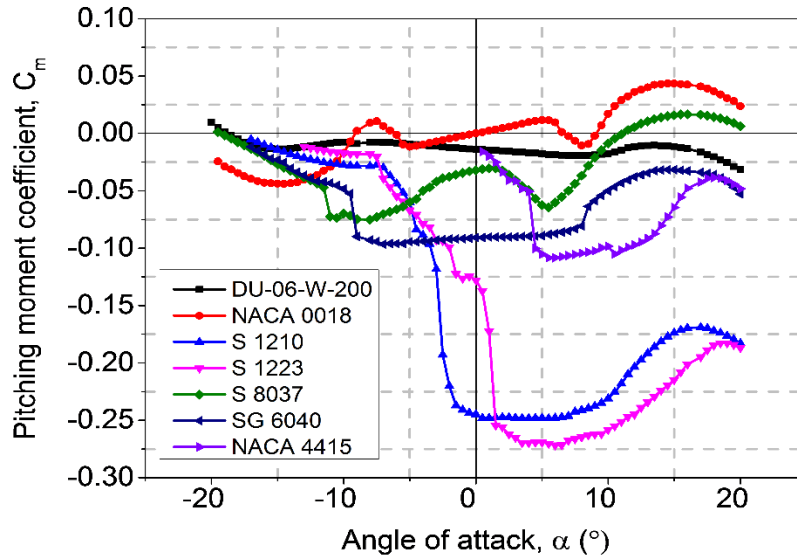


Figure 7.13: Comparison of the aerofoil pitching moment coefficient as a function of the angle of attack of the prospective aerofoils at  $Re = 383,200$ ,  $N_{crit} = 9$ .

This is due to the fact that all the distributed forces on the airfoil surface increase in the same proportion. However, for cambered aerofoils, the moment's distributed forces are non-zero even when the total lift force is zero. Furthermore, the results show that the pitching moment coefficient for the asymmetrical airfoils tends to become more negative as the angle of attack increases. Generally, cambered airfoils supported at the aerodynamic centre pitch nose-down (negative direction) and possess superior aerodynamic performance compared to airfoils that pitch nose-up (positive direction).

### 7.5.6 Drag Coefficient

For improved start-up performance, aerofoils are expected to have a minimum amount of drag, and the minimum lift-drag coefficient  $C_{d0}$  should be as low as possible (Islam et al., 2007). The  $C_{d0}$  represent the value of the drag coefficient when the lift is zero. Figure 7.14 depicts the performance curve of the prospective aerofoils showing the  $C_{d0}$  values. The results indicate that the DU06-W-200 and NACA 0018 exhibit the lowest possible  $C_{d0}$ . However, as noted earlier, symmetrical aerofoils are severely affected by roughness, which could impede their aerodynamic performance.

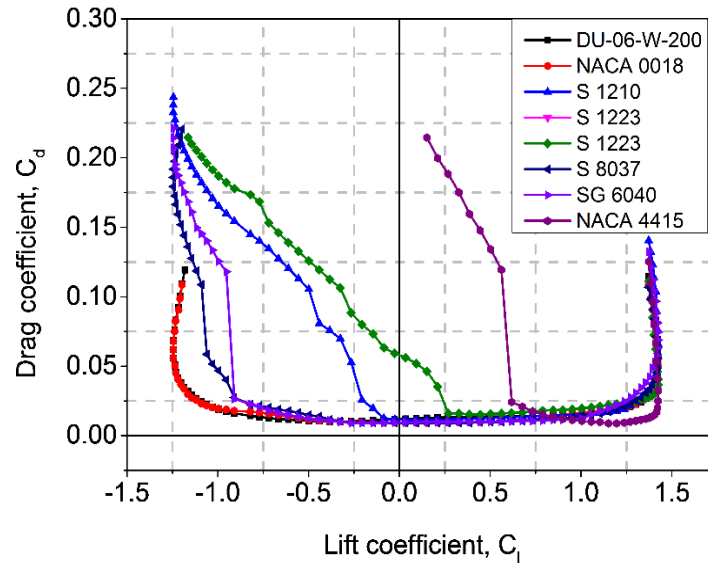


Figure 7.14: Comparison of drag coefficients as a function of the lift coefficients of the prospective aerofoils at  $Re = 383,200$ ,  $N_{crit} = 9$ .

### 7.5.7 Overall comparison of the aerofoil performance

Table 7.2 shows a summary of all the desirable features of the prospective aerofoils for an overall comparison and rating (shown in parentheses). These results indicate that some of the aerofoils exhibit superior aerodynamic performance compared to others. However, no particular aerofoil exhibits all the desirable characteristics. For example, in Table 7.2, row 2, the DU06-W-200 exhibit the most superior performance in terms of the stall angle and is rated (1) in parenthesis.

Aerofoils with high stall ratings tend to delay the onset of stall at low Reynolds numbers. In row 3, the S 1223 produces the highest maximum lift coefficient at low Reynolds number and positive angles of incidence in comparison to all the other aerofoils under investigation. This implies that the aerofoil will be less susceptible to separation, which results in blade stalling. Similarly, in row 4, the DU06-W-200 and NACA 0018 could be seen as the airfoils that exhibit the best minimum drag value. However, Islam, Ting and Fartaj (2007) have shown that the symmetrical airfoils, in particular NACA 0018, are very sensitive to roughness, which could affect their self-starting performance. Cambered airfoils, on the other hand, are not severely sensitive to roughness. Furthermore, in row 5, the DU06-W-200 could be seen as the aerofoil with the

largest drag bucket, and in row 6, the S 1210 exhibit the highest maximum efficiency and is rated 1. Finally, in row 7, the S 1223 possesses the best characteristics in terms of the large negative pitching moment.

Table 7.2: Ratings of the investigated airfoils based on the desirable aerodynamic characteristics.

Aerofoil section	Stall angle	$(C_l)_{\max}$	$C_{d_0}$	Drag bucket	$(C_l/C_d)_{\max}$	$(C_m)_{\min}$
DU-06-W-200	18.00° (1)	1.23 (5)	0.010 (1)	Large (1)	62.00 (4)	-0.16 (3)
NACA 0018	10.00°	1.20 (7)	0.015 (1)	Large (1)	62.00 (4)	-0.04 (6)
S 1210	13.00° (5)	1.98 (6)	0.012 (3)	Medium (2)	112.00 (1)	-0.25 (2)
S 1223	13.00° (5)	2.27 (1)	0.016 (5)	Medium (2)	91.18 (5)	-0.27 (1)
S 8037	16.70° (2)	1.30 (4)	0.011 (2)	Medium (2)	93.37 (3)	-0.10 (5)
SG 6040	14.00° (4)	1.36 (3)	0.012 (3)	Medium (2)	91.00 (6)	-0.14 (3)
NACA 4415	14.70° (3)	1.46 (2)	0.015 (4)	Medium (2)	94.00 (2)	-0.13 (4)

- $(C_l)_{\max}$  = maximum lift coefficient;  $C_{d_0}$  = minimum drag coefficient;  $(C_l/C_d)_{\max}$  = maximum lift-drag ratio;  $(C_m)_{\min}$  = minimum pitching moment coefficient.

The main goal of this comparison is to identify the desirable aerofoil features for self-starting at low wind conditions. Clearly, Table 2 shows that no particular aerofoil possess all the desirable characteristics to improve the start-up performance. Further analysis of the torque performance will reveal the aerofoils with the highest starting torque at low tip speed ratios  $\lambda$ .

Figure 7.15 depicts the torque performance over a full blade rotation at a wind speed 5 m/s and rotational speed  $\omega = 15 \text{ rpm}$ .



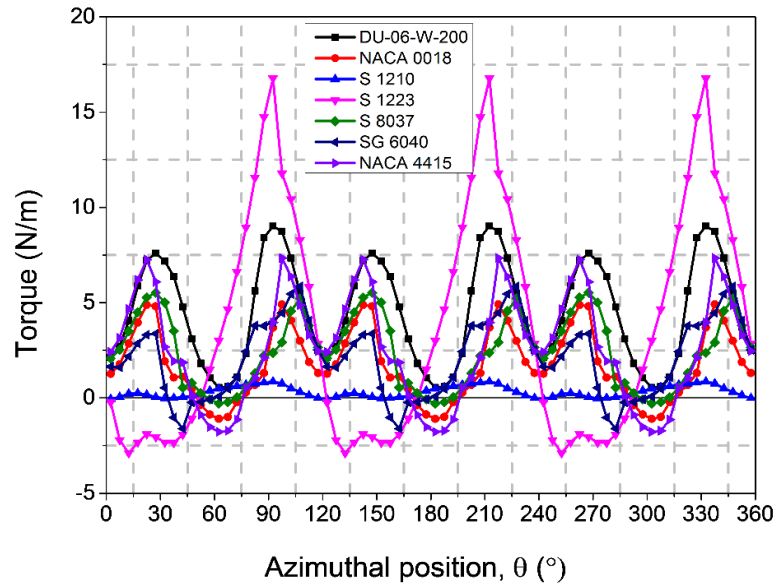


Figure 7.15: Torque output as a function of blade azimuthal position for the prospective aerofoils at a wind speed 5 m/s, rotational speed 18.5 rpm.

Two of the aerofoils, namely DU06-W-200 and S 1210, exhibit positive torque throughout the full blade rotation. Considering the DU06-W-200 blade, the torque increases with the increase of the rotor angle from  $\theta = 0^\circ$  to  $\theta = 30^\circ$  and then decreases to  $\theta = 65^\circ$ . Again, the rotor torque increases with the increase of the rotor angle up to  $\theta = 95^\circ$ . Between  $\theta = 95^\circ$  to  $\theta = 120^\circ$ , the rotor torque decreases. From  $\theta = 90^\circ$  to  $\theta = 150^\circ$ , the torque rises and then falls smoothly to a rotor angle of  $\theta = 180^\circ$ . Again, a further increase was observed from  $\theta = 180^\circ$  to  $\theta = 210^\circ$  before decreasing at  $\theta = 210^\circ$ . Between  $\theta = 240^\circ$  and  $\theta = 270^\circ$ , the torque increases and decreases at  $\theta = 300^\circ$ . Finally, from  $\theta = 300^\circ$  the torque increases up to  $\theta = 330^\circ$  and falls sharply to  $\theta = 360^\circ$ . Therefore, the positive torque is produced for the full rotational angle of the rotor. Similarly, the S 1210 exhibit the same torque behaviour throughout the full rotational cycle. However, the maximum torque produced by the S 1210 is smaller than that of the DU 06-W-200. For the other airfoils, the nature of the curve is opposite to that of the DU06-W-200 and S 1210. The difference is that the value of the torque is both positive and negative. Also, the results show that the torque for the DU06-W-200 is higher than that of the S 1210 and the other investigated aerofoils.

## 7.6 Aerofoil design

A comparison of the different aerofoil profiles above has shown that the DU-06-W-200 is the most promising aerofoil to improve the self-starting performance due to its low drag, wide drag bucket and the torque output. In this section, the DU-06-W-200 concept will be used as a basis to investigate the desirable geometric features, namely thickness and camber and the influence on the self-starting performance.

### 7.6.1 Thickness

The effect of thickness on the self-starting performance has already been discussed in Section 2.8.8. From the viewpoint of low Reynolds-number aerodynamics, thinner aerofoils are desirable in terms of performance since they tend to reduce the leading-edge suction peak. However, increasing aerofoil thickness increases the structural strength of the aerofoil. Figure 7.16 shows the lift coefficient as a function of the drag coefficients for the original DU-06-W-200 aerofoil.

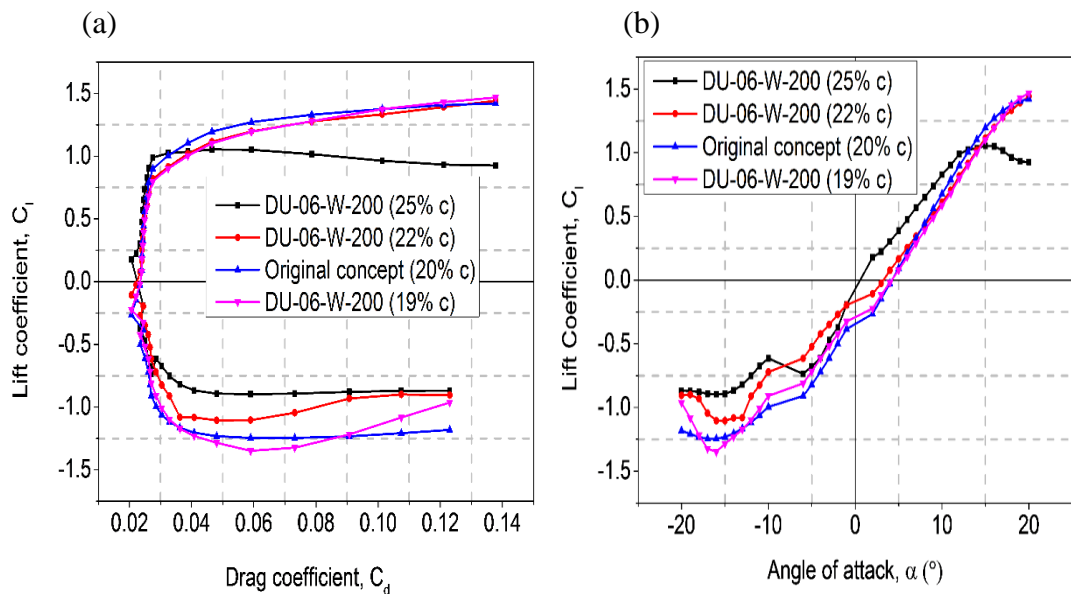


Figure 7.16: (a) Lift coefficient as a function of drag coefficients, and (b) lift coefficients as a function of the angles of attack showing the several variations in the thickness of the original DU-06-W-200 at  $Re = 383,200$ .

The results demonstrate the effect of scaling the thickness from 19% $c$  to 25% $c$ . The reduction in the drag bucket from the original concept up to 22%

chord is only small. However, increasing the thickness to 25% chord, results in a corresponding increase in the zero lift drag and a reduction in the drag bucket.

The effect of increasing the thickness on self-starting performance is depicted in Figure 7.17. It can be seen that the increase in the thickness results in a greater penalty in the maximum power coefficient,  $C_{pmax}$ . The maximum power coefficient is attained at  $C_{pmax} = 46\%$  using a thickness of 19%.

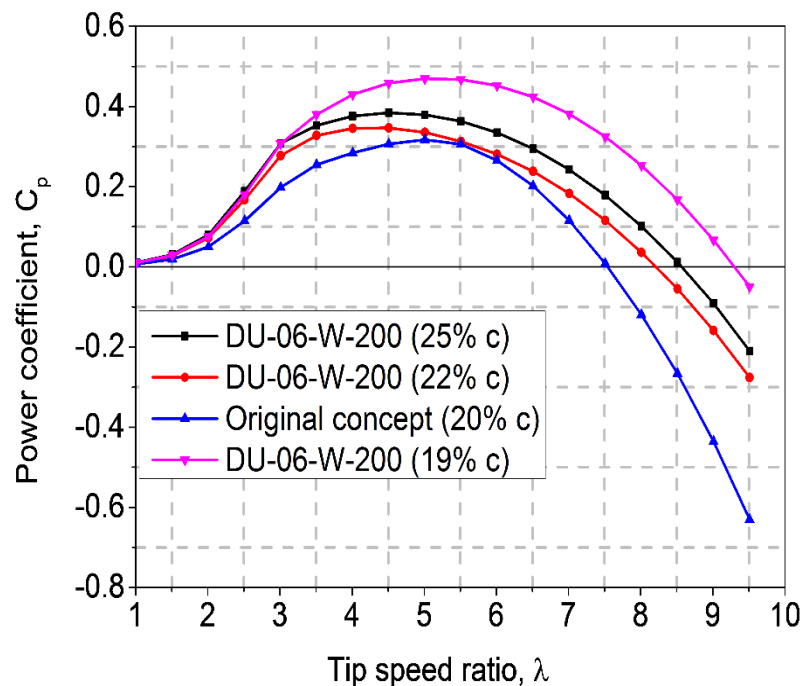


Figure 7.17: Power coefficient as a function of tip speed ratios for DU-06-W-200 profiles with different thicknesses and  $Re = 383, 200$ .

Figure 7.17 shows the power coefficient as a function of the tip speed ratios for the different thicknesses of the aerofoil and confirms what was noted by Classens (2006) during the design of the original concept, namely the maximum performance is attained when the thickness was increased to 18% chord, but increasing the thickness provides higher structural strength in turn for an acceptable loss in performance. These results, particularly at low tip speed ratios (start-up conditions), demonstrates what can be expected from a low Reynolds number operation: very low thickness are required for an aerofoil to be able to compensate for the drag in the post stall region. Although it seems that increasing the thickness to 25% chord has a slight advantage at

start-up, but with a penalty at the maximum attainable power coefficient. Clearly, Figure 7.17 shows a thickness of 19% chord appears to be a viable option to replace the original concept DU-06-W-200 (20%) for start-up operation.

### 7.6.2 Fixed pitch

Setting the aerofoil at a fixed pitch angle,  $\gamma$  as shown in Figure 7.18, can be used to reduce the angle of attack variation and ultimately assist in avoiding the blade from stalling.

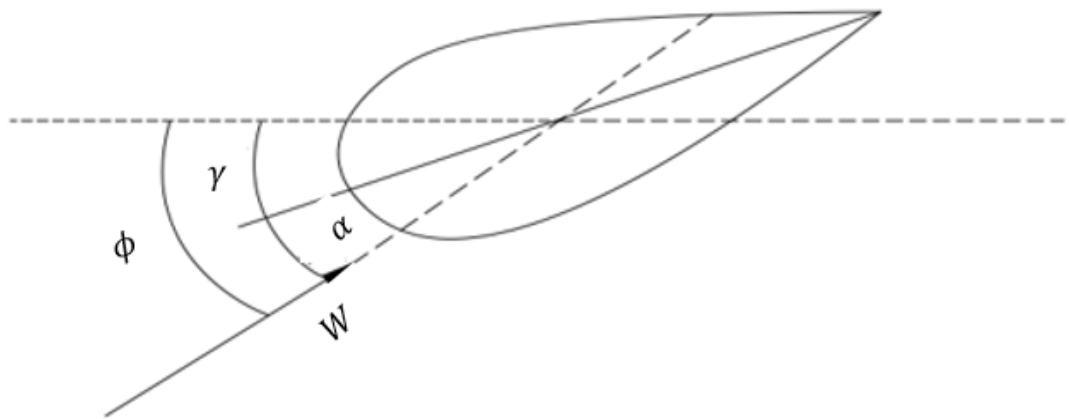


Figure 7.18: Schematic of an aerofoil section set under a fixed pitched angle. From the configuration shown in Figure 7.18, positive values of the pitch angle  $\gamma$  tend to decrease the angle of attack and therefore increase the stall angle of the aerofoil. The angle of attack based on this configuration is expressed as follows:

$$\alpha = \phi - \gamma \quad (7.11)$$

in which  $\phi$  is the inflow angle. The blade tangential force coefficient, given by Eqn. (7.1), can then be expressed as follows:

$$C_t = C_l \sin \phi - C_d \cos \phi \quad (7.12)$$

Aiming at the effects of the blade pitch angle on the self-starting and power generation, a 2D simulation of a three bladed VAWT with straight blades were performed in Qblade and the results are shown in Figure 7.19. The simulation

has been carried out for pre-set pitch angles  $\gamma = -4^\circ, -3^\circ, -2^\circ, -1^\circ, 0^\circ, 1^\circ, 2^\circ, 3^\circ, 4^\circ$  and a wind speed  $V = 5$  m/s.

The results suggest that pitching out of dynamic stall can significantly enhance the dead-band region (see Figure 7.5a) and the maximum power coefficient  $C_{pmax}$  of the wind turbine. At  $\gamma = -4^\circ$ , the  $C_p$  increases with an increase in the tip speed ratio,  $\lambda$  until  $\lambda \approx 1.8$  and then decreases. The maximum power coefficient  $C_{pmax}$  is obtained with the case  $\gamma = 4^\circ$ , compared to the case  $\gamma = -4^\circ$ , where the minimum power coefficient was obtained. The start-up performance and maximum efficiency of the turbine at  $\gamma = 4^\circ$ , is better than at all other pitch angles and at all tip speed ratios  $\lambda$ . This is in line with the results reported by Boss (2012). To gain more understanding of this behaviour, the torque characteristics of the blade at  $\gamma = 4^\circ$  are investigated.

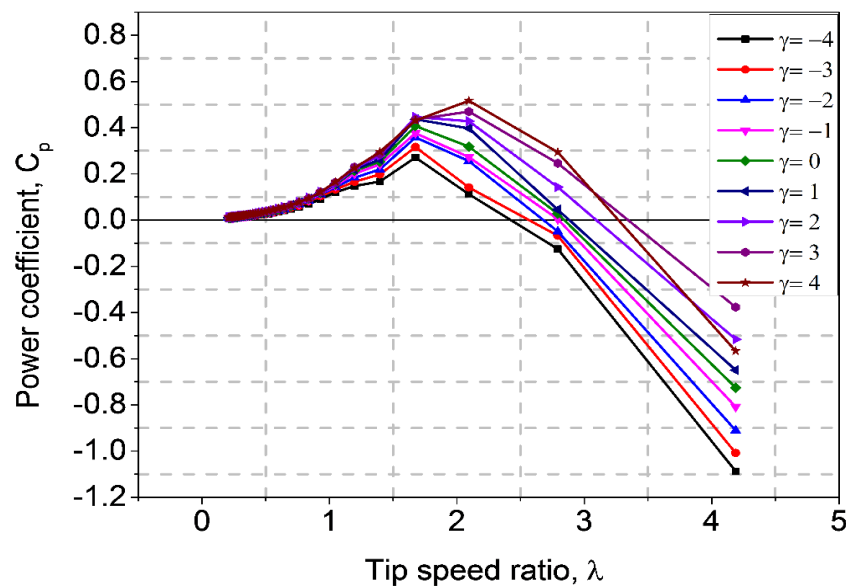


Figure 7.19: Predicted power coefficient as a function of the tip speed ratios for the DU-06-200 (19% chord) aerofoil as a function of the pitch angles and wind speed 5 m/s.

From Figure 7.20a, it can be seen that for a wider range of azimuthal angles, the blade torque experiences a different torque. The maximum torque for the wind speeds 5, 7 and 9 m/s are obtained close to  $90^\circ$  when the blade is in upwind cycle where about 90-95% of the power of the turbine is extracted. It should be noted that the net torque for the full blade rotation is mostly positive

(Figure 7.20b) for both toe in (positive pitch) and toe out (negative pitch) angles, thus indicating that pitching can significantly eliminate the band of negative torque that hinders effective start-up performance compared to the case presented in Figure 7.4 where the net torque on the blade is negative.

Since the aim of pitching the blade is to achieve a reliable self-start (passive start-up), the above analysis shows that setting the transformed DU-06-W-20 at a pitch angle  $\gamma = 4^\circ$  tends to outperform all other pre-set pitch values. Based on this observation, along with the torque characteristics of the turbine, it is sufficient to understand the effect of pitch angle on start-up performance.

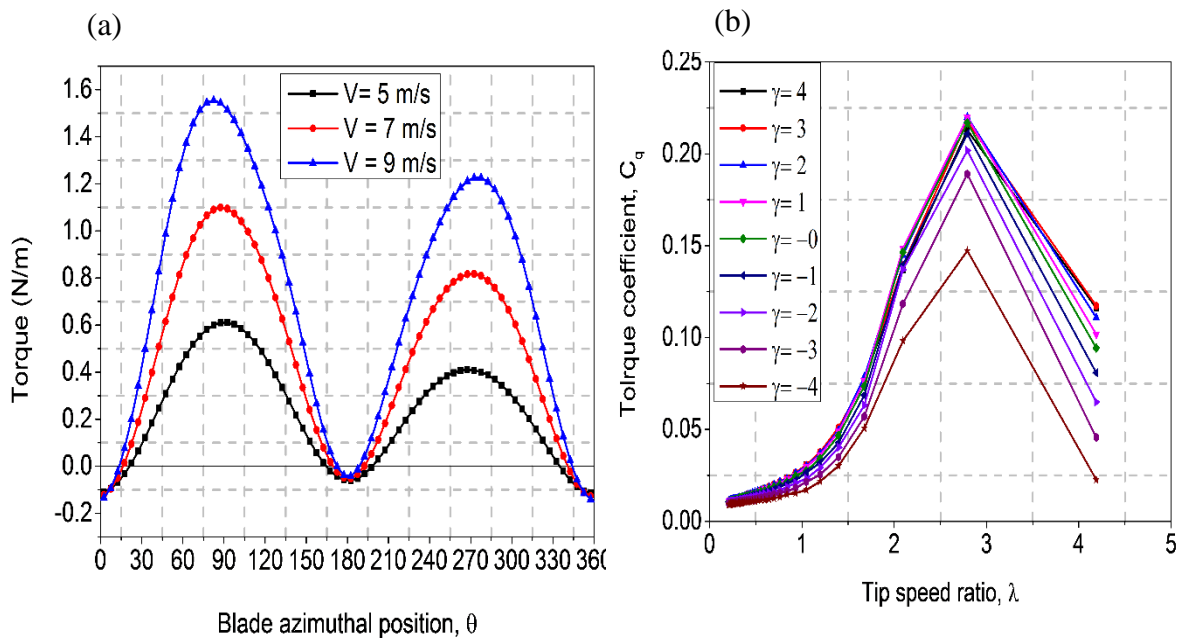


Figure 7.20: (a) Torque as a function of the blade azimuthal position for a three bladed DU-06-W-200 (19% c) for wind speeds 5 m/s, 7 m/s, 9 m/s at a pre-set pitch angle  $\gamma = 4^\circ$  and Reynolds number 383,200; (b) Torque coefficient as a function of the tip speed ratio for various pitch angles at the same operating conditions.

### 7.6.3 Solidity

As discussed in Section 2.8.6, rotor solidity is an extremely important parameter for improving the self-starting performance of a VAWT. The Rotor solidity defined in Eqn. (2.27), was varied by considering different chord lengths between 0.03 m and 0.33 m, resulting in a range of solidity values

from 0.1 to 1.0 in line with previous studies, see for example McIntosh (2008) and Aslam et al. (2012). The main performance parameter considered are the power coefficient and the produced power.

Figure 7.21 shows the results obtained by varying the rotor solidities on the turbine performance. For a cut in wind speed  $V=5$  m/s, there are clear advantages in increasing the rotor solidity, particularly at the design point of interest (low tip speed ratios), provided an appropriate pitch angle is chosen. The results show that increasing the rotor solidities decreases the optimal tip speed ratio. For example, with a solidity in the range  $0.1 \leq \sigma \leq 1$ , the DU-06-W-600 set at a pitch angle  $\gamma = 4^\circ$  appears to significantly improve the region of the dead-band which affects the self-starting. However, in an ideal operation of a small scale wind turbine, a low value of solidity is usually preferred to keep the blade from stalling. Therefore, setting the blade at a pitch angle  $\gamma = 4^\circ$ , and a solidity in the range  $0.1 \leq \sigma \leq 0.3$  tends to be the best choice for maximum and start-up performance of the turbine.

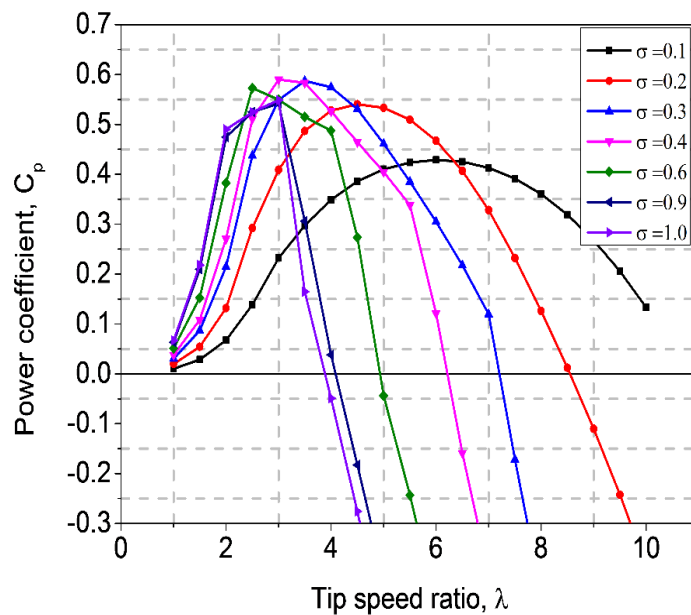


Figure 7.21: Predicted power coefficient for the DU-06-W-200 as a function of the pitch angle  $\gamma = 4^\circ$  for different solidities.

Furthermore, the simulations were extended to investigate the combined effect of solidity, wind speed and rotational speeds. In line with previous studies for small-scale wind turbines, a wind speed ranging from 5 up to 13 m/s, with a step of 2 m/s was considered for the simulation.

The wind turbine was assumed to be coupled with a variable speed generator, capable of varying the rotational speed in a range between 50 and 450 rpm in order to find an optimum value to maximise the power production. The results for a chord lengths 0.03, 0.06 and 0.10 m, representing solidity values 0.1, 0.2 and 0.3, respectively, are shown in Figure 7.22.

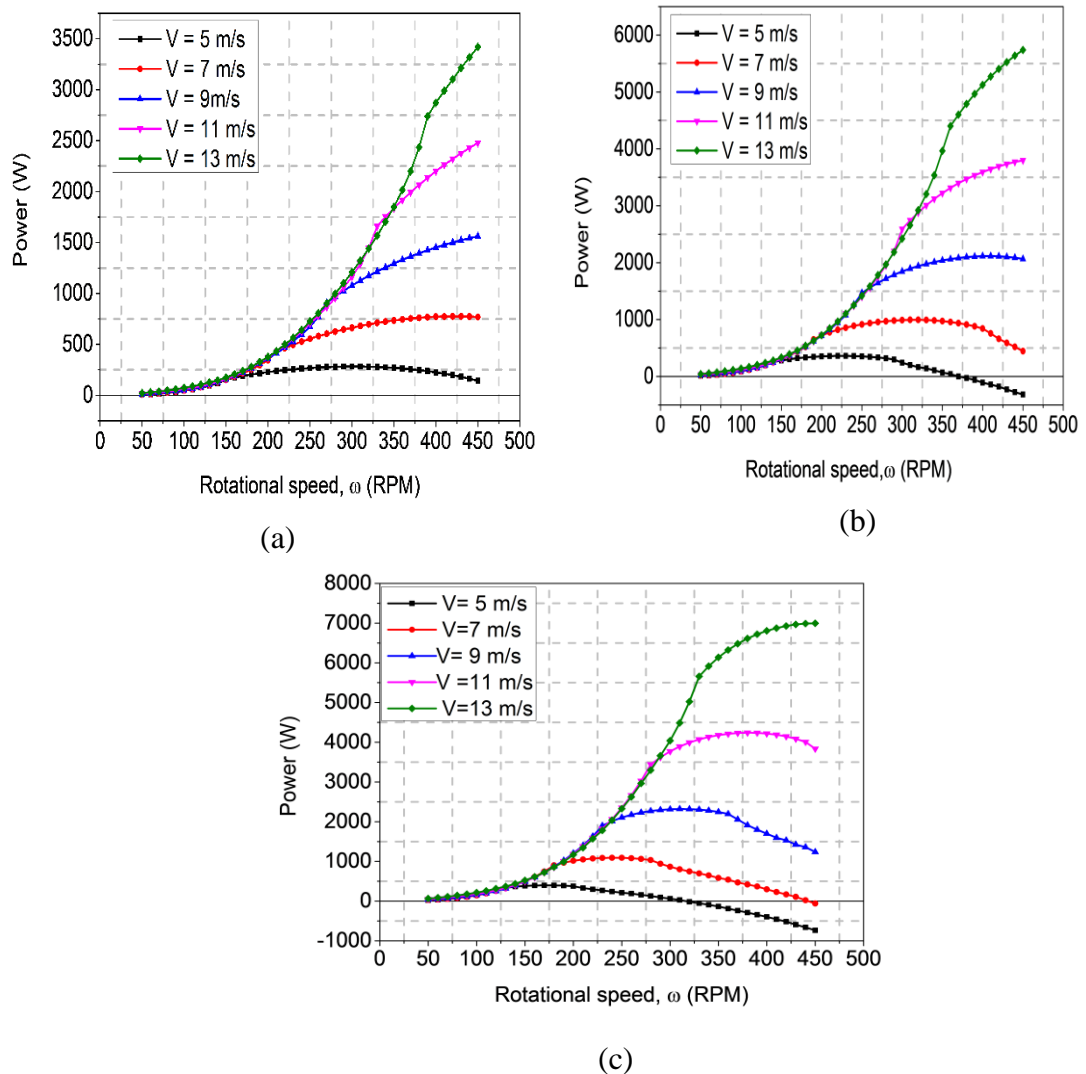


Figure 7.22: Predicted power as a function of the rotor rotational speed with respect to wind speed and pitch angle  $\gamma = 4^\circ$ ; (a) chord length  $c = 0.03\text{m}$  ( $\sigma = 0.1$ ), (b)  $c = 0.06\text{m}$  ( $\sigma = 0.2$ ) and  $c = 0.10\text{m}$  ( $\sigma = 0.3$ ).

These results indicate that higher solidity requires lower rotational speed to obtain the maximum amount of power produced for a wind speed range between 5 to 11 m/s. After 11 m/s the maximum amount of power is attained at a higher rotational speed, i.e. at a solidity of 0.3, the maximum power was obtained at about 150 rpm, 280 rpm, 320 rpm and 430 rpm for the wind speeds



5, 7, 9, 11, and 13 m/s, respectively. Moreover, a slight reduction in the rotor efficiency with an increase of rotor solidity can be observed for low wind speeds between 5 to 9.5 m/s as shown in Figure 7.23.

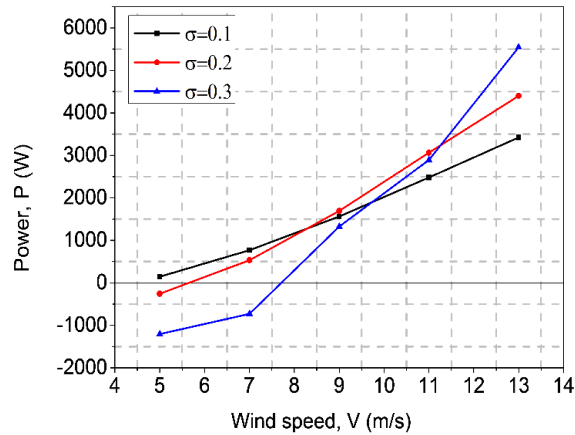


Figure 7.23: Predicted maximum power as a function of both wind speed and rotor solidity.

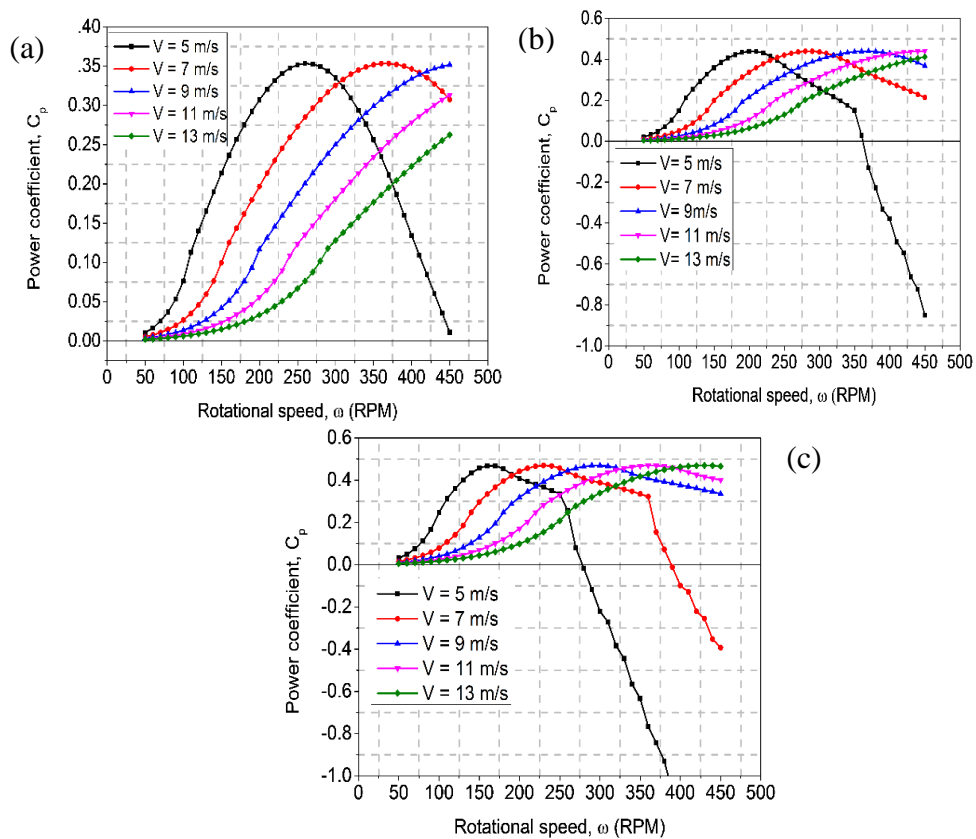


Figure 7.24: Power coefficient as a function of both rotor rotational speed and wind speed, (a) chord length  $c = 0.03\text{m}$  ( $\sigma = 0.1$ ), (b)  $c = 0.06\text{m}$  ( $\sigma = 0.2$ ) and  $c = 0.1\text{m}$  ( $\sigma = 0.3$ ).

From the comparisons between Figure 7.22 (a-c), it can be observed that for low solidity the power curve appears to be flat close to its maximum output. This allows the turbine to achieve initial start-up since the rotational speed can easily be adjusted. This is more visible through the power coefficient,  $C_p$  as a functions of rotational speed,  $\omega$  curve shown in Figure 7.24.

#### 7.6.4 Final design

The initial design with a fixed symmetrical NACA 0018 blade is not capable of self-starting due to the fact that the angle of attack is above the stall angle which results in low lift and high drag and makes the tangential force coefficient  $C_t$  negative.

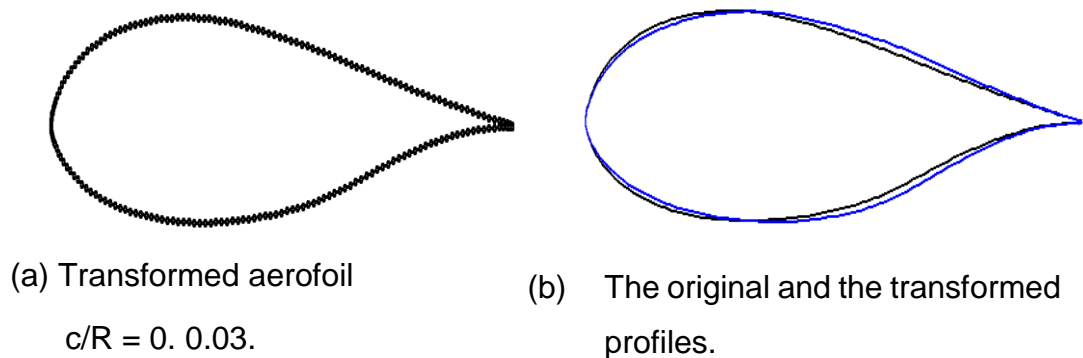


Figure 7.25: Schematic of the investigated aerofoils. (a) Final shape of the transformed aerofoil section. (b) The original and the transformed profiles. The blue represents the original aerofoil shape while the black represents the transformed aerofoil.

The final design, see Figure 7.25 is based on a standard DU-06-W-200 transformed so that its camber line follows an arc of a cycle such that the ratio of the aerofoil's chord to cycle radius  $c/R$  ratio is 0.03. This is referred to as the present design to avoid confusion between the two aerofoils. This configuration appears to significantly improve the start-up performance.

The final design yields the following design configurations:

- (i) Self-starting performance: transformed DU-06-W-200  $c/R = 0.03$ ; thickness = 19.6%  $c$  (upper surface) and maximum  $x - pos = 30.90\% c$ , solidity  $\sigma = 0.10$ ,  $\gamma = 0^\circ$ .
- (ii) Maximum power: solidity  $\sigma = 0.20$ ,  $\gamma = 4^\circ$ .

## **7.7 Design proposal**

The initial design process presented in Section 7.5 revealed that none of the XFOIL generated aerofoils possess all the desirable features to facilitate passive start-up. The results, which are in line with previous studies, revealed that a small VAWT fitted with a conventional NACA 0018 requires the designer to focus on avenues of reducing the blade angle of attack. The design process aimed to improve the start-up performance in the previous sections led to two main design configurations, namely the design for improved start-up and the design for the maximum power production.

In the following sections, the design proposals are presented in greater detail.

### **7.7.1 Improved start-up performance**

Designing for start-up performance is aimed at achieving self-starting at a projected cut in wind speed. The final design is based on the transformed aerofoil section DU-06-W-200. In order to boost the starting torque, a low solidity  $\sigma = 0.10$  and pre-set pitch angle  $\gamma = 0^\circ$  were selected. The torque comparison and performance prediction at a wind speed 5 m/s, between the fixed blade (NACA 0018) and the pre-set pitch of the present design, shown in Figures 7.26 and 7.27 demonstrates that self-starting can be achieved. It is clear from Figure 7.24 that the produced torque for the pre-set pitch configuration is high enough to facilitate passive start-up whereas this is not possible with the fixed pitch case where the produced torque is mostly negative. The resultant effect of the present design on the VAWT is shown in Figure 7.27.

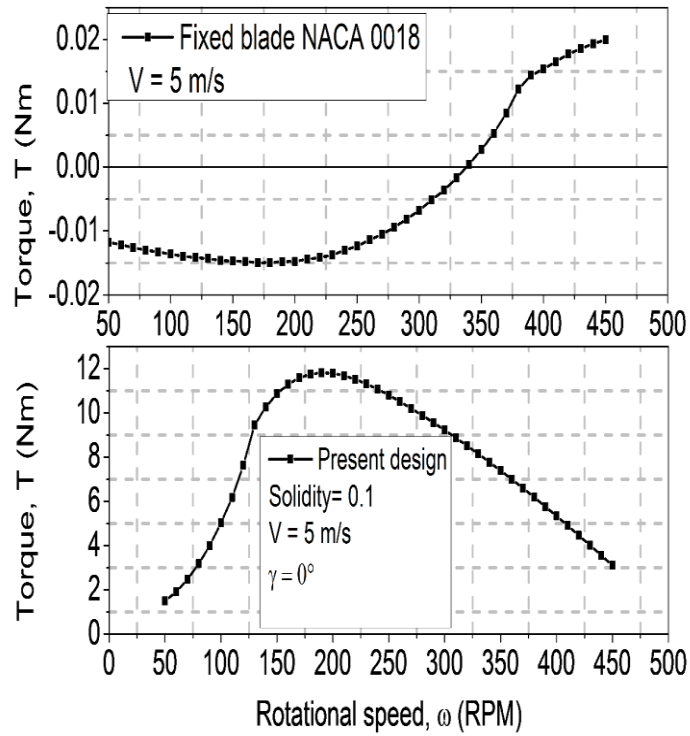


Figure 7.26: The torque as a function of the rotational speed for the fixed of NACA 0018, and the pre-set pitched-blade for the DU-06-W-200 rotors.

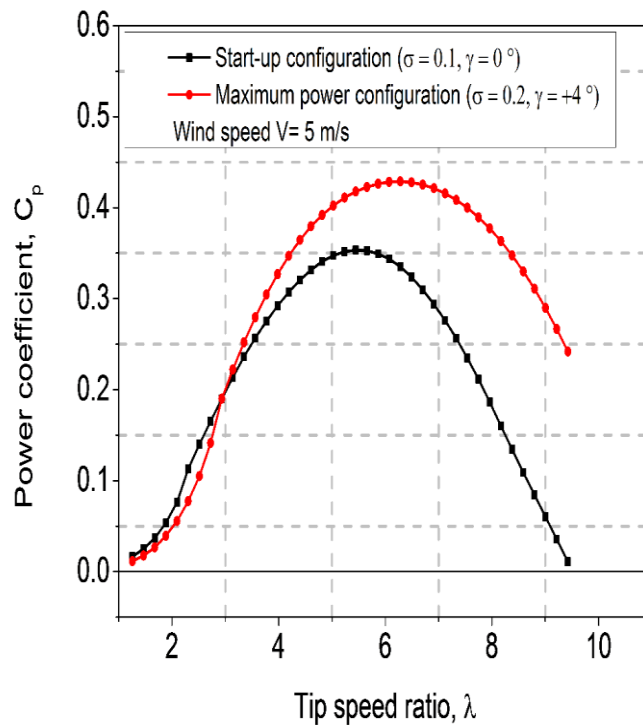


Figure 7.27: Predicted performance of start-up and maximum power configuration at a cut in wind speed of 5 m/s.

### 7.7.2 Maximum power performance

The configuration for the maximum power performance was designed by keeping the aerofoil and most of the design parameters the same from the start-up configuration. Only the chord length and solidity were adjusted in order to increase the stall angle of attack at low tip speed ratios and ultimately increase the overall performance of the turbine. This configuration is particularly suitable for the condition at the rated wind speed. The result is a power curve, see Figure 7.28, which shows a significant improvement from the previous configuration.

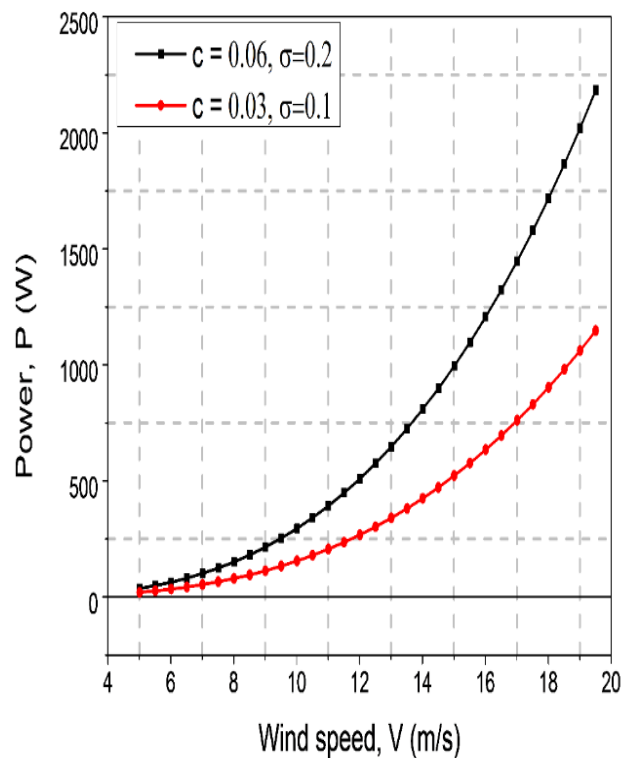


Figure 7.28: Predicted power as a function of the wind speed and the rotor solidity for start-up ( $c = 0.03\text{m}, \sigma = 0.1$ ), and maximum power configurations ( $c = 0.06\text{ m}, \sigma = 0.2$ ).

However, it should be noted that the enhancement is at the cost of performance at the nominal operating conditions.

Table 7.3 summarises the main characteristics for the start-up and maximum power configuration.

Table 7.3: Characteristics for improved start-up and maximum power configuration.

Operating conditions	Start-up configuration	Maximum power
Aerofoil geometry	Transformed DU-06-W-200 (19% chord)	Transformed DU-06-W-200 (19% chord)
Pitch angle	0°	+4°
Upper transition	0.074	0.074
Lower transition	0.929	0.929
Rotor solidity	0.1	0.2
Number of blade	3	3
Chord length (m)	0.03	0.06
Rotational speed min	50	50
Rotational speed max	450	450
Turbine max height (m)	4.5	4.5
Diameter (m)	2	2
Rotor swept area (m <sup>2</sup> )	9	9
Maximum $C_p$	0.35	0.41
Rated power (kW)	1.2	2.2

### 7.7.3 Comparison with NACA 0018 and the original DU-06-W-200

The calculated  $c_p$  as a function of the tip speed ratios for the DU-06-W-200, NACA 0018 and the transformed aerofoil are visualised in Figure 7.29.

A minimum wind speed 5 m/s based on the site wind resource in Chapter 5 m/s was used for the simulation. The shaded region indicate where the transformed aerofoil outperforms the NACA 0018 and the original DU-06-W-200. The results indicate that the blade operating with the transformed aerofoil provides a much higher power coefficient at low tip speed ratios.

It should be noted that the NACA 0018 has a large deep (dead-band) of negative power coefficient  $C_p$ , which prevents the turbine to reliably self-start. This implies that extra energy is required to bring the turbine to an operating speed during the start-up operation.

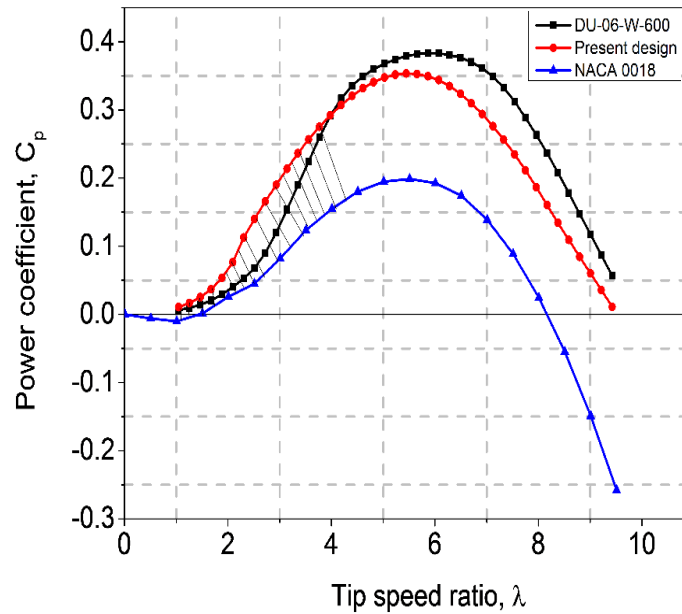


Figure 7.29: Power coefficient as a function of the tip speed ratio for the hypothetical three bladed rotor with chord length  $c = 0.03$ ,  $R = 1$  and wind speed = 5 m/s using either the DU-06-W-200, the present design (transformed DU-06-W-200) or the NACA 0018 aerofoil.

The reverse is the case when using either the old DU-06-W-200 or the transformed aerofoil where the turbine is capable of self-starting at low values of the tip speed ratios. For example, the  $C_{pmax}$  for the transformed aerofoil, the DU-06-W-200 and the NACA 0018 at  $\lambda = 3$ , are approximately 22%, 15% and 7%, respectively. However, at higher tip speed ratios the results indicate that the DU-06-W-200 outperforms the transformed aerofoil. This is presumably due to a high  $c/R$  ratio of the aerofoil profile. This clearly demonstrates a significant improvement over the conventional NACA 0018 aerofoil.

The transformed aerofoil has 1.6% thickness which is expected to provide higher structural strength. This means that the rotor can operate at high wind

speeds. Furthermore, the performance of the transformed aerofoil is significantly higher at low tip speed ratios. This implies that the aerofoil is capable of operating at lower rotational speeds while still producing adequate power. This is particularly beneficial since the aerodynamic forces on the blade will be substantially reduced, thus eliminating the dangers of failure.

## 7.8 Summary

The main aim of this chapter was to examine the self-starting performance of a small-scale Darrieus turbine and to find cost effective and suitable solution strategies that could be used to improve the performance of the turbine at low tip speed ratios.

To achieve this aim, a start-up analysis was performed in order to identify the problems and variables that hinders the turbine from reliable self-start. It became clear that the combinations of small chord lengths, low tip speed ratios and wind speeds lead to low Reynolds number well below  $10^5$ . This low-range Reynolds number results in undesirable complex flow characteristics that influence the stalling behaviour of the turbine, thus resulting in a deep negative power curve ( $C_p$ -  $\lambda$  curve). The solution to this problem generally have to do with improving the aerofoil performance at low Reynolds numbers ( $< 10^5$ ), or finding other cost effective strategies of increasing the starting torque. Bearing this in mind, seven potential aerofoils configurations were generated in XFOIL along with the conventional symmetrical aerofoil NACA 0018.

A computational analysis based on the potential flow model was used to simulate the performance of these aerofoils based on an operating chordal length 0.3m and an average wind speed (5 m/s) based on the resource assessment in Chapter 5. The results indicate that the traditionally used NACA 0018 aerofoil lacks the desirable aerodynamic characteristics suitable for improving the self-starting problem of straight bladed VAWTs. Hence the need for a low-speed asymmetrical aerofoil that possesses high lift and low drag. Further, the results indicate that no particular aerofoil exhibits all the desirable characteristics for self-starting. However, two aerofoils, namely the DU-06-W-200 and S 1210 showed exceptional aerodynamic performance. In particular, the DU06-W-200 exhibited a higher starting torque and was subjected to



further re-design. This lead to two design proposals, namely design for start-up ( $\lambda \approx 0.5 - 1.5$ ) and maximum power production ( $\lambda \approx 3 - 5$ ). The design process involved the modification of the original DU-06-W-200 aerofoil shape and evaluating its performance. Furthermore, two main design parameters, namely the pitch angle  $\gamma$  and rotor solidity  $\sigma$  tend to significantly affect the conditions in which the transformed aerofoils have to operate and are incorporated into the final design. The final design was optimised by adjusting the camber and thickness and the performance are then compared with the conventional NACA 0018 aerofoil and the original design. The important point in the design process and some final thoughts will be disused in Chapter 8.

## **Chapter 8: Overall conclusions and suggestions for future research**

The potential for the production of renewable energy through small-scale wind turbines has increased globally in recent years due to the desire to decarbonise the electricity sector and the need to diversify fuel sources to enhance energy security. In the UK, the small-scale wind industry is growing at a fast rate and it is mainly driven by a good wind resource and financial incentives under the Feed-in Tariff system. However, in order to maximise electricity production and carbon savings, as well as increase the confidence in the technology, it is important to utilise systematic approaches in assessing the wind resource for potential wind turbine sites. Although robust and advanced assessment approaches are usually utilised in the large-scale industries, these approaches are often associated with high cost and longer timescales and thus may not be economical in the context of small-scale wind industry. Hence, there is an urgent need for cost effective approaches that are capable of accurately assessing the available wind resources for potential installation of small-scale wind turbines.

While the research into large-scale wind resource assessment has received tremendous attention over the years, there is little research performed on small-scale wind resource assessment and installations. A good number of researchers have focussed on analytical models using either scaling or fluid flow approaches to evaluate the wind flow over buildings and rough surfaces. Undoubtedly, these studies have significantly contributed to new developments but there has been a need to assess the accuracy of analytical models in predicting the wind resource in different terrains.

Furthermore, there has been a lack of research on data-driven wind resource assessment, particularly with regards to short measurement periods for small-scale wind energy despite their promising prospects to accurately predict the long-term wind resource of potential sites. In addition, site specific wind turbine designs that incorporate self-starting capabilities have received very little attention in the context of small-scale wind energy.

The work described in this thesis is focused on finding solutions to these issues by considering two main approaches to small-scale wind resource

assessment, namely (i) an analytical model based on the principles of the boundary layer meteorology, and (ii) a Measure-Correlate-Predict (MCP) approach based on short-term onsite measurements to predict the long-term wind resource.

The main aim of this thesis is to develop a cost effective methodology that is capable of predicting the wind resource with reasonable accuracy and to gain a deep understanding of the likely uncertainties associated with the analytical model and those based on the onsite-data measurements.

Chapter 4 of this thesis focuses on a performance evaluation of the methodology based on a modified boundary layer scaling model using long-term reference data from four sites. However, due to the uncertainties associated with the methodology, as demonstrated in the magnitude of the average errors in the predicted wind resource, it was suggested that such models are better applied to identify potential viable sites for further investigations. Chapter 5 explores the potentials of obtaining a better prediction based on a data-driven, Measure-Correlate-Predict (MCP) approach at a specific target site using short-term measurements. The results revealed that while the short-term onsite measurements may be subject to seasonal variations, the approach tends to provide more reliable estimates of the long-term wind resource. Direct comparison of the results obtained with the boundary layer approach shows significant improvement in the predicted wind resource using the MCP approach. Based on the success achieved in predicting the wind resource, energy production estimates and economic feasibility of installing a small-scale wind turbine were made. The promising results led to the design of small-scale wind turbine at the target site. Finally, in Chapters 6 and 7, a double multiple streamtube model, along with a 2D panel model was applied to evaluate the performance of small-scale turbines incorporating self-starting capabilities. Based on the performance results, a design proposal to improve the self-starting and maximum performance of small-scale vertical axis wind turbines were bundled into an aerofoil design. The results show a significant improvement over similar design with symmetrical aerofoils. Overall, these results offer a cost effective choice to small-scale wind energy developers to assess the available wind resource, along with the knowledge of the uncertainties associated with each method.

In addition, the results from the design show that self-starting and maximum performance at low tip speed ratios of a small-scale VAWT can be significantly improved using a combination of a cambered aerofoil, pitch angle and suitable solidity.

## **8.1 Research outcomes**

### **8.1.1 Boundary layer model**

A modified analytical model based on the principle of the boundary layer meteorology, originally developed by the UK Meteorological Office, was evaluated in Chapter 4 in terms of its feasibility to predict the wind resource potentials (spatially averaged mean wind speed and wind power density). This methodology is promising because it can be implemented using surface roughness parameters at a reference climatology without necessarily conducting an expensive onsite measurement campaign or without a detailed knowledge of the site specifications. The methodology can be used to quickly assess the wind resource potential of multiple sites at any geographical location. However, the results from four potential wind turbine sites show large site specific errors and this is mainly due to the choice of the input data, namely the choice of the local aerodynamic parameter and the Weibull shape factor, thus highlighting topics for further investigations of the prediction methodology. Despite these uncertainties, the methodology tends to be particularly useful when applied to screen for viable sites using a predefined viability criterion. Using this approach will ensure that time and money are not wasted on non-viable sites. As a benchmark, the methodology was compared with a currently used NOABL-MCS approach applied at ten potential sites to screen for viability. The results show that the methodology outperformed the NOABL-MCS approach.

### **8.1.2 MCP approaches**

The limitations and uncertainties associated with the boundary layer methodology led to the evaluation of a data-driven Measure-Correlate-Predict techniques in Chapter 5. This approach utilises short-term onsite measurement periods obtained from a specific site. Two linear MCP approaches, namely linear regression and variance ratio were assessed in

terms of their feasibility to predict the wind resource over a 15 years period using 12 months onsite measurements and long term correlation to a reference climatology. The results obtained using the data-driven MCP approaches showed significant improvements in the accuracy of the predicted wind resource compared to the boundary layer approach. Furthermore, the implemented MCP approaches shows that no clear differences in the predicted wind speeds. However, the linear regression approach resulted in a more accurate prediction of the wind power density compared to the variance ratio and boundary layer approaches, respectively. Seasonal variabilities in the reference and target sites were observed to have a strong influence on the magnitudes and directions of the predicted errors with the most accurate predictions obtained when onsite measurements were acquired during the winter or spring seasons. A significant improvement in the error of the predicted wind power density of 24.9% was observed using these seasons to conduct onsite measurements. These results clearly demonstrate that even with very short onsite measurements that significant improvements can be added to the wind resource assessment technique, thus justifying the additional time and resources during the measurement campaign periods.

## **8.2 Design for self-starting improvement**

Based on the successful prediction of the long-term wind resource, as characterised by the mean wind speeds, distribution of the wind speeds and the wind power density, a small-scale wind turbine was designed for the purpose of facilitating a passive start-up in Chapters 6 and 7. The major findings can be found in the following subsections.

### **8.2.1 Failure to achieve self-starting**

The inability of a small-scale fixed-pitch VAWT to achieve self-starting is due to the combination of several factors which are summarised as follows:

- In a given range of tip speed ratios,  $1 \leq \lambda \leq 1.7$ , the blade encounters a wide range of angles of attack,  $\alpha$ . As a result of this, the aerofoils are frequently pushed far beyond the point of stall. The resulting tangential force coefficient,  $C_t$  is mainly negative over the operational cycle of the turbine thus leading to a net negative torque. The net effect of this

behaviour results in a dip in the power curve (power coefficient,  $C_p$  vs tip speed ratio,), often known in the literature as the dead-band.

- The term small-scale implies the combination of small chord lengths and low or intermediate wind speeds which ultimately results in low Reynolds numbers well below  $10^5$ . Unfortunately, the conventional symmetrical aerofoils that are widely used for VAWT applications perform poorly in this range of Reynolds number. Specifically, the aerofoil performance at this Reynolds number severely decreases the lift-drag ratio,  $C_l/C_d$  and consequently lowers the aerofoil stall angle.

### 8.2.2 Summary of ways to achieve self-starting

Generally, any solution aimed at eliminating the self-starting problem will mostly focus on improving the aerofoil performance at low Reynolds numbers ( $Re < 10^5$ ) or exploring any other viable option of increasing the torque. Section 2.8 discusses several solution strategies to self-starting performance. Some of these strategies are worth highlighting again.

- A Savonius auxiliary rotor can add a significant amount of torque at low tip speed ratios and consequently aids in the self-starting of a fixed pitch turbine. However, there is a penalty to pay for this configuration. Firstly, adding an extra structure ultimately increases the overall cost of the turbine as well as adds more complexity to the structure of the turbine. Secondly, the tower will have to be stronger and there will be a huge impact on the appearance of the configuration. Perhaps, the most important consideration in this sort of configuration is the possibility of combining the tip speed ratios of the two rotors. For example, the maximum power coefficient,  $C_p$  for a Savonius rotor is usually attained at a tip speed ratios,  $\lambda \approx 0.7-0.8$ , whereas the dead-band region of typical VAWTs often occurs in the range  $1 \leq \lambda \leq 1.7$ . In this situation, combining the two rotors may lead to an inefficient design.
- Using cambered aerofoil profiles with low minimum drag ( $C_{do}$ ) such as the DU-06-W-200 at low values of  $Re$  tends to improve the performance of the turbine inside the dead-band region. This option, with appropriate thicknesses and solidities, appears to offer the best

combination of acceptable self-starting torque and maximum power performance with simplicity and low cost.

- Implementing a pitch-system is perhaps one of the most effective approaches to eliminate self-starting problems. This systems reduces the angle of attack and prevents the blade from stalling.

### **8.2.3 Design proposals for an efficient and economical self-starting of a small-scale VAWT**

In chapter 7, a wide range of cambered aerofoils were generated and compared with a widely used symmetrical aerofoil NACA 0018 using a 2D panel method code. After a detailed evaluation of these aerofoils, it became clear that the symmetrical section performs poorly at low Re and the cambered sections, particularly the DU-06-W-200 possess exceptional starting characteristics and are to be preferred for small-scale VAWTs. During the design process, several important features revealed the key requirements for an efficient and economical self-starting of a small Darrieus VAWTs. These factors are discussed as follows:

- A 2D panel model code XFOIL is a suitable tool for aerofoil design that have to satisfy many different design requirements. For a self-starting turbine, the rotor solidity and the pitch angle tends to strongly affect the conditions in which the aerofoils operate and these were included in the final design process.
- A new transformed DU-06-W-200 aerofoil was generated to accomplish two main design configurations: design for start-up and design for maximum power performance. Both design configurations were scaled to a thickness,  $t = 19\%c$ .
- Setting the aerofoil under a pre-set pitch angle was found to greatly improve the power coefficient and self-starting performance and this is verified in Section 7.6.2.
- The start-up configuration was achieved using the transformed DU-06-W-200 aerofoil with the following specifications:  $c/R=0.03$ ,  $t = 19.6\%c$  (upper surface) and maximum  $x - pos=30.9 \%c$ , respectively. In addition, a low solidity  $\sigma = 0.1$  and a zero pre-set pitch angle,  $\gamma$  appears to give the best performance. Higher

solidities tend to result in a power coefficient higher than the Betz limit.

- Performance predications based on this configuration revealed that a small wind turbine of 2 m diameter with 3 blades of 0.03 m chord would reliably self-start in 5 m/s and achieve a maximum power coefficient,  $C_{pmax}$  0.35 (see Section 7.7.1).
- The configuration for maximum power was achieved using the same specifications as the start-up but with a solidity,  $\sigma = 0.2$  and pitch angle  $\gamma = 4^\circ$ . For this case, the maximum power coefficient was attained at  $C_{pmax} = 0.43$ , but also showed good performance at rated tip speed ratios (see Section 7.7.1).

#### **8.2.4 A cautionary note**

The goal of this thesis is two fold: (i) To develop cost effective and indirect methods capable of predicting the long-term wind resource without necessarily undertaking long-term measurement campaigns. This choice was largely motivated by the fact that undertaking such measurements in recent years has proved to be increasingly time consuming and expensive, and may not be easily realisable except in cases where huge investments are to be made. The systematic application of these methods, applied with the full knowledge of their limitations and risks, is certainly better than excluding potential wind turbine sites. However, it should be borne in mind that wind resource assessment based on these methods is subject to uncertainties in the long-term measurement campaigns techniques. Furthermore, they tend to result in bias and must be applied with extreme caution. It should be emphasised that these methods are not a substitute to direct long-term measurement campaigns, if such a campaign is financially feasible. Rather, they are intended to provide valuable site characterisation where direct onsite measurements are practically impossible due to the impact on the total investment costs.

(ii) Design a Darrieus-type small-scale VAWT based on the site's wind resource (i.e. the maximum attainable wind speed based on the site wind resource assessment was used as an input into the analytical model) that allows the turbine to reliably self-starting at low tip speed ratios. This is



motivated by the fact that the Darrieus turbines have higher power potential than the horizontal axis wind turbines and their increasing demand in recent years for small-scale and domestic energy production. However, they suffer from one major drawback, and this is their inability to self-start. If, as has been argued by a large number of researchers, they require an external mechanism to bring them to an operating speed, then much of their advantage is lost. During the design process, it became clear that achieving self-starting entails that some of the design choices are complicated and hence have to be dropped. Presumably, the most effective solution to achieve self-starting are:

- Variable-pitch design: This design, if implemented correctly will give complete control of the blade angle of attacks. However, designing such a system is relatively complex but not impossible, and therefore more expensive in the context of small-scale wind turbines.
- Hybrid configuration of the Darrieus-Savonius rotor: The combination of Darrieus and Savonius rotors certainly exhibits high starting torque and power coefficient at low speeds, but such design poses a threat to the essential aesthetics and it is often difficult to combine the tip speed ratios of the two rotors. In addition, this configuration tends to increase the mass moment of inertia, and consequently restricts the rotational acceleration of the turbine.
- High solidity rotors: Using high solidity rotors clearly results in a significant increase in the Reynolds number and the torque at low operating speeds. However, the blade regularly encounters stall.

Based on the above discussion, it was decided to redesign an existing aerofoil that has shown significant improved self-starting characteristics by setting appropriate design parameters such as solidity, thickness and pitch angles. The design results showed that self-starting can be achieved in a small-scale VAWT. Still, without comparison to actual real-life cases, the improvements at low tip speed ratios remains merely an estimation. This implies that the design proposals presented in this thesis for start-up operations is not fully guaranteed to reliably self-start in real life situations.

## **8.3 Limitations and recommendations for further research opportunities**

Throughout the body of this thesis, several limitations and a number of additional research opportunities were identified. These are discussed in the following sections.

### **8.3.1 Boundary layer model**

The boundary layer model implemented in Chapter 4 has several limitations which are related to the restriction that such an approach should be capable of rapid application at multiple sites without detailed knowledge of the site information.

The problem with such a method is that the surface roughness parameters must be deduced from the regional land cover data and the estimates of the local site characteristics. The evaluation of the model in Chapter 4 indicates that the wind resource assessment is very sensitive to the values of the surface roughness parameters. For instance, a site located near some buildings entail that the local parameters will be subject to uncertainties due to the changes in the building height, density as well as the roughness elements that cannot be easily captured by simple site categorisation.

Small-scale perturbations to the mean wind flow due to the local obstructions, and the effects of local orography on a smaller scale than the resolution of the reference site may present additional errors. Another source of uncertainty worthy of mention is the surface parameter on a regional scale, such as the regional displacement height. This data is usually assumed to be the highest of the displacement heights from the land cover data in the region, an assumption that could result in overestimates of the wind resource, particularly with regions characterised by heterogeneous land cover. Interestingly, a number of these draw backs can be improved upon if the methodology is applied in a site-specific context, where detailed site information is taken into consideration. However, this will mean that some of the advantages of the approach is lost. An interesting topic worthy of further research is to explore the impact of detailed local site information on the applicability of the methodology. Although, this was considered in the build environment by Millward-Hopkins (2013) using detailed building information in an urban area.

Furthermore, the analysis in Chapter 4 revealed that the uncertainties arising from the estimation of the Weibull parameters is an additional possible source of a small error. However, this could be improved upon by using wind atlas data that includes high resolution estimates of these parameters.

### **8.3.2 MCP approaches**

A major limitation of the MCP methods implemented in Chapter 5 is the use of a single reference data and site. Uncertainties from data-driven MCP approach tends to be more of the sources of data than the MCP method. Thus, a topic worthy of further research is to explore the degree of uncertainty using multiple non similar reference data. This has never done before presumably, due to the lack of interest into the research of small-scale wind resource assessment. The majority of researchers in the wind energy industry have focused on large-scale wind assessment.

Also, it will be informative to investigate the impact of different terrain types on the performance of the short-term onsite data on the MCP approaches. Using multiple reference sites at different terrain can be used to check for consistency of the methodology.

A further limitation of the MCP approaches in the current work is the use of hourly averages of the wind speeds and directions. Wind speeds and directions vary strongly on shorter timescales and this could have a significant impact on the wind power production. Thus, it will be useful to investigate whether the MCP approaches implemented in the current study are better able to capture these variations. However, one major barrier to undertaking such investigations is the lack of reference/target site wind data with high temporary resolutions.

The current study was also limited to two linear MCP approaches utilising a single input of the reference site wind speeds. Hence, there is scope to assess and compare several different MCP approaches that have been proposed in the literature, such as the Gaussian process regression and Weibull parameter scaling, etc. using data from multiple reference sites. Such a study could be used to check for sensitivity and as a benchmark against which new MCP approaches could be developed.

### 8.3.3 Design for a self-starting vertical axis wind turbine

The design presented in Chapters 6 and 7 utilise a multiplatform design code which comprises a vortex panel model and a double multiple streamtube model. The results of these design tools were combined to make predictions of the wind turbine performance. Several simplifications were adopted for this to work (see Section 6.4.2).

A clear issue with such an approach is that the aerofoil design and analysis is limited to the prediction of the lift and drag coefficients at angles that lie before, or just after, stall. At higher angles of attack, these simplifications becomes increasingly invalid, and convergence cannot be obtained anymore. In addition, these models do not account for three-dimensional or unsteady effects. Therefore, there is scope for the use of advanced models, such as CFD for the computations of the blade performance for the complete angles of attack range as well as 3D effects. The combination of an unsteady Panel method code, coupled with an integral Boundary Layer Equation solver, could potentially be a viable solution for the aforementioned limitations, at least for moderate angles of attack on the performance regions. The use of CFD models will be considered in the future works.

A further limitation is the values of the critical amplification factor,  $N_{crit}$  which were estimated in order to make a distinction between the upwind and downwind half cycles. A wind tunnel experiment is therefore proposed to obtain more accurate and reliable data to validate the simulations. In addition, it would be useful to perform a field performance measurement of small-scale wind turbine utilising cambered sections with low minimum drag, high lift-drag ratio and high stall angles at low Reynolds numbers. Such a test will increase the understanding of small-scale wind turbines before they can be fully utilised and deployed in decentralised power generations.

## 8.4 Research impacts

The contribution of the work presented in this thesis can be used as a step towards developing a systematic low-cost methodology to wind resource assessment in the context of small-scale wind energy.

The boundary layer model presented in Chapter 4 offers a low cost methodology that can be used in assessing the wind resource potential at a wide range of sites against a defined viability criterion. The model output

revealed an improved wind resource performance compared to the widely used NOABL-MCS approach. Furthermore, the results revealed the likely uncertainties associated with the implementation of the methodology, which should be used as a guide to make investment decisions.

To reduce these uncertainties, the MCP approaches evaluated in Chapter 5 can be used. Results based on these approaches indicate lower uncertainties in the predicted wind resources. The analysis of the error metrics as a function of the training seasons can be used to assess the added value of onsite measurements as well as the most appropriate seasons in which to conduct measurement campaigns. This will enable small-scale wind energy developers and investors to identify the most suitable assessment technique to apply, subject to the availability of time and funds.

Overall, it is envisaged that the wind resource assessment methodologies developed in Chapters 4 and 5 could be combined to develop a rapid and systematic approach to small-scale wind resource assessment. As a minimum, a boundary layer methodology should be deployed to screen for viable sites against a defined viability criterion. This would give an indication of the resource potentials as well as the likely associated uncertainties, as described in Chapter 4. Based on this preliminary screening, and the scale of the investment, the most promising sites could be identified for further evaluation by conducting short-term onsite measurements and long-term correlation using the best performing MCP approach described in Chapter 5. This would guarantee a more reliable power projection. Following this procedure will reduce the likelihood of installing small-scale wind turbines in non-viable sites that do not spin and ultimately maximises the investment decisions by reducing the financial risk associated with wind resource assessments that are often time consuming and expensive.

In addition, the design of a small-scale vertical axis wind turbine based on the Darrieus principles demonstrate that self-starting can be achieved. This is an interesting finding because the inability of the conventional Darrieus turbine has limited its application, particularly in decentralised power applications. Thus, if a small-scale vertical wind turbine with self-starting capabilities can be manufactured at a relatively lower cost than the widely used horizontal axis

wind turbines, a resurgent of interest and confidence in this class of turbine could occur.

#### **8.4.1 The big picture**

Overall, despite the promising prospects of the UK small-scale wind resource, the future projections of generated energy from small-scale wind turbines indicate that only a small part of the total energy use will be required from low carbon sources. However, wind turbines have become a key player in the future of renewable energy, and hence, a strongly growing small-scale wind industry has the potential to reduce our energy and environmental problems and contribute to the awareness of new energy systems. Clearly, the growing concern around poorly designed and siting of wind turbines in non-viable sites as well as other environmental impacts are some of the reasons why people tend to reject wind energy. Thus, stakeholders and developers in the small-scale wind industry should ensure that the best available approaches are adopted in the assessment of potential sites in order to design and install turbines at appropriate sites and with a full understanding of the associated uncertainties inherent in such approaches as well as the limitations of the design codes.

## Bibliography

- Abbott, I and Doehoff, A.V. (1949) *Theory of wing sections*. New York: Dover Publications, Inc.
- Abbott, I.H., and Von Doenhoff, A.E. (1959) *Theory of Wing Sections: Including a Summary of Aerofoil Data*. New York: Dover Publications.
- Ackerman, T and Soder, L. (2000) Wind energy technology and current status, a review. *Renewable and Sustainable Energy Reviews* 4, 315-374.
- Ahmed, M.R and Sharma, K (2015) Wind energy resource assessment for the Fiji Islands: Kadavu Island and Suva Peninsula. *Renewable energy* 89:168-180.
- Ahmed, S, A.S. (2012) Electricity generation from the first wind farm situated at the Ras Ghareb, Egypt. *Renew Sustain Energy Rev* 16 (13): 1630–1635.
- Akpinar, E.K and Akpinar S. A. (2005) Statistical analysis of wind speed data used in installation of wind energy conversion systems. *Energy Conversion and Management* 46 (4) 515–532.
- Albers, A and Klug, H. (1999) High quality wind speed measurements for site assessment. *DEWI Magazine* 15:6–16.
- Allen, S.R., Hammond, G.P. and McManus, M.C. (2008) Energy analysis and environmental life cycle assessment of a micro-wind turbine. *Proceedings of the Institution of Mechanical Engineers Part A-Journal of Power and Energy*, 222(A7): 669-684.
- American Wind Energy Association (2009) “Small Wind Turbine: Global Market Study”, [online] available from [http://www.awea.org/learnabout/smallwind/upload/2009\\_AWEA\\_Small\\_Wind\\_Global\\_Market\\_Study.pdf](http://www.awea.org/learnabout/smallwind/upload/2009_AWEA_Small_Wind_Global_Market_Study.pdf) [12<sup>th</sup> June, 2013].
- Anderson M.A Review of MCP techniques (2004) [Online] available from: <http://www.res-group.com/media/234585/a%20review%20of%20mcp%20techniques.pdf>.

- Ayotte, K.W. and Hughes, D.E. (2004) Observations of boundary-layer wind-tunnel flow over isolated ridges of varying steepness and roughness *Boundary-Layer Meteorology*, 112:525–556.
- Angel Wind Energy Company. 2013 [Online]. Available from:
- Archer, C.L and Caldeira, K. (2009). Global Assessment of High Altitude Wind Power. *Energies* 2, 307-319; doi: 10.3390/en20200307.[http://www.awec2010.com/public/img/media/archer\\_caldeira.Pdf](http://www.awec2010.com/public/img/media/archer_caldeira.Pdf).
- Aris, C.A. (2013) Wind power reassessed: a review of the UK wind resource for electricity generation [Online] available from <<https://static1.squarespace.com/static/56eddde762cd9413e151ac92/t/56f71e527c65e4881ff6eac2/1459035746943/Assessment7.pdf>> [accessed 15/7/16].
- Aslam, B.M.M., Hayat, N., Farooq, A.U., Ali, Z., Jamil, R.S and Hussain, Z. (2012) Vertical Axis wind turbine- a review of various configurations and design techniques. *Renew & Sustainable Energy Rev.* 16: 1926-1939.
- Achberger, C., Ekstrom, M and Barring, L (2002) Estimation of local near-surface wind conditions - a comparison of WASP and regression based techniques. *Meteorological Applications*, 9(2): 211-221.
- AWS Scientific Inc. & National Renewable Energy Laboratory (U.S.) (1997) *Wind Resource Assessment Handbook - fundamentals for conducting a successful monitoring program.* <http://www.nrel.gov/wind/pdfs/22223.pdf> [accessed 15/7/16].
- Bahaj, A.S., Myers, L. and James, P.A.B. (2007) Urban energy generation: Influence of micro-wind turbine output on electricity consumption in buildings. *Energy and Buildings*, 39(2): 154-165.
- Baker, J. R., (1983) “Features to Aid or Enable Self-Starting of Fixed Pitch Low Solidity Vertical Axis Wind Turbines” *Journal of Wind Engineering and Industrial Aerodynamics* 15 (1–3), 369-380.
- Bardsley, W.E. and Manly, B.F.J. (1983) Regression-based estimation of long-term mean and variance of wind-speed at potential aerogenerator sites. *Journal of Climate and Applied Meteorology*, 22(2): 323-327.



- <program.com/Library/Reports%20on%20the%20natural%20wind/Small-scale Wind Energy - Technical Report.pdf> [accessed 15/7/16].
- . (1994) Best Practice Guidelines for Wind Energy Development. <<http://nature.berkeley.edu/biometlab/espm129/notes/>> [accessed 15/7/16].
- Baldocchi, D. (2012) Wind and Turbulence, Part 2, surface boundary layer theory and principles (lecture series). [University of California, Berkley. Unpublished work]. [Online] available from:
- Barros, V.R. and Estevan, E.A. (1983) On the evaluation of wind power from short wind records. *Journal of Climate and Applied Meteorology* 22(6): 1116- 1123.
- Bass, J. MCP: Pitfalls & common mistakes. In: AWEA wind resource & project assessment workshop, Minneapolis, MN, USA; 30 September–1 October 2009.
- Bass, J.H, Rebbeck, M., Landberg, L., Cabre, M., Hunter, A. (2000) An improved Measure Correlate Predict Algorithm for the prediction of the long term wind climate in regions of complex environment. Joule project report JOR3-CT98- 0295,EU.
- Bayly, D.A (1981) Kentfield JAC. A vertical axis cyclogiro type wind turbine with freely-hinged blades in Proc. of 16th Intersoc. Energy Conversion Eng. Atlanta, Georgia, Aug. 9-14.
- Beck, A (2004) “Turning to Stealth Technology” Power Engineering International.
- Belabes, B, Youcefi, A, Guerri, O, Djamai, A and Kaabeche, A (2015) Evaluation of wind energy potential and estimation of cost of using wind turbines for electricity generation in north Algeria. *Renewable and Sustainable Energy Reviews*. 51:1245–1255.
- Berg, D.E. (1990) Customised Aerofoils and Their Impact on VAWT Cost of Bergey Wind Power Company. 2013 [Online]. Available from: <http://www.bergey.com> [accessed 12.09.15].
- Bergey, M. (2002), AWEA Small Wind Turbine Committee, Road Map, a 20-year Industry Plan for Small Wind Technology, AWEA/Dept of Energy, USA.

- Best, M., Brown, A., Clark, P., Hollis, D. et al., (2008) Small-scale Wind Energy–Technical Report. Met Office. [Online] available from: <https://www.wind-power-program.com/Library/Reports%20on%20the%20natural%20wind/Small-scale%20Wind%20Energy%20-%20Technical%20Report.pdf> [accessed 12. 06. 2013].
- Betz, A. (1966) Introduction to the Theory of Flow Machines. (D. G. Randall, Trans.) Oxford: Pergamum Press.
- Bianchini, A., Balduzzi, F., Rainbird, J.M., Peiro, J. et al. (2016) An experimental and numerical assessment of aerofoils polars for use in Darrieus wind turbines-Part 1: flow curvature effects. *Journal of Engineering for Gas Turbines and Power* 16 (138), 032602-1.
- Bostan, I., Gheorghe, A., Dulgheru, V., Sobor, I., Bostan, V. and Sochirean, A. (2013) Resilient Energy Systems. Springer: London.
- Boyle, G. (2004) Renewable energy, power for a sustainable future, Oxford University Press, Oxford, England, p. 244.
- BP (2012) Statistical Review of World Energy [online] available from <http://www.bp.com/extendedsectiongenericarticle.do?categoryId=9041566&contentId=7075262> [accessed 20.01. 2013].
- Bradley, E.F. (1968) A micrometeorological study of velocity profiles and surface drag in the region modified by a change in surface roughness. *Quarterly Journal of the Royal Meteorological Society*, 1968. 94(401): 361-379.
- Bradshaw, P. (1975) Possible origin of Prandtl's mixing-length theory. *Nature*, 249: 135-136.
- Brochier, G., Frauni e, P., Begui er, C., and Paraschivoui, I. (1986) "Water Channel Experiments of Dynamic Stall on Darrieus Wind Turbine Blades" *Journal of Propulsion*, 2 (5), 445–449.
- Brower, M.C. (2012) Chapter 12. *Wind resource assessment*. Hoboken: John Wiley & Sons Inc.
- Brown, B. G., Katz, R. W., and Murphy, A. H. (1984) Time series models to simulate and forecast wind speed and wind power. *Journal of Climate and Applied Meteorology* 23(8):1184–1195.

- Burton, T., Jenkins, N., Sharpe, D and Bossanyi, E. (2011) *Wind Energy Handbook U.S* : Wiley and Sons.
- Bussel van, G.J.W and Mertens, S.W. (2005) *Small Wind Turbines for the Built Environment*. The Fourth European & African Conference on Wind Engineering Prague, 11-15<sup>th</sup> July 2005.
- BWEA (2009) *Small Wind Systems, UK market report* London, April 2009, pp. 1-20.  
Energy, Sandia National Laboratories, SAND90-1148C.  
[http://www.energy.ca.gov/windguidelines/documents/other\\_guidelines/BWEA-BPG.PDF](http://www.energy.ca.gov/windguidelines/documents/other_guidelines/BWEA-BPG.PDF).
- Carbon Trust (2008) *Small-scale wind energy-policy insights and practical guidance*.
- Carmoy, D. (1978) "The USA Faces the Energy Challenge" *Journal of Energy Policy* 6, 36-52.
- Carta, J.A., Ramirez, P. and Velazquez, S. (2009) A review of wind speed probability distributions used in wind energy analysis - Case studies in the Canary Islands. *Renewable & Sustainable Energy Reviews*, 13 (5): 933-955.
- Carta, J.A., Velázquez, S. and Cabrera, P. (2013) A review of measure-correlate-predict (MCP) methods used to estimate long-term wind characteristics at a target site. *Renewable and Sustainable Energy Reviews* 27:362-400.
- Carvalho, D., Rocha, A., Gómez-Gesteira, M., and Santos, C. S. (2014) WRF wind simulation and wind energy production estimates forced by different reanalyses: Comparison with observed data for Portugal. *Applied Energy*, 117(0):116–126.
- Celik, A.N., A. Makkawi, and T. Muneer (2010) Critical evaluation of wind speed frequency distribution functions. *Journal of Renewable and Sustainable Energy* 2 (1).
- Celik, A.N., Muneer, T. and P. Clarke (2007) An investigation into micro wind energy systems for their utilization in urban areas and their life cycle assessment. *Proceedings of the Institution of Mechanical Engineers Part A - Journal of Power and Energy*, 2007. 221(A8): 1107-1117.
- Centre for Ecology and Hydrology (2007) *Land Cover Map (25m raster, GB)*. [Online] Available from: <<http://www.ceh.ac.uk>. > [12.05. 2016].

- Chandel, C.C, Murthy, K.S.R, (2014) Ramasamy P. Wind resource assessment for decentralised power generation: Case study of a complex hilly terrain in western Himalayan region. *Subst. Energy Tech. and Assessments* 2014; 8:18–33.
- Chands, P.K. and Tokekar, S.V. (1998) Expert-based maintenance: a study of its effectiveness. *IEEE Trans Reliab*, 47, 95-97.
- Chang, T.P. (2011). Estimation of wind energy potential using different probability density functions. *Applied Energy* 88 (5): 1848-1856.
- Cheng, H. and Castro, I.P. (2002) Near wall flow over urban-like roughness. *Boundary-Layer Meteorology*, 104 (2): 229-259.
- Chougule, P. (2014) Overview and design of self-acting pitch control mechanism for vertical axis wind turbine using multibody simulation approach. *Journal of Physics conference series* 524. Doi: 10.1088/1742-6596/524/1/012055.
- Classens, M.C. (2006) The Design and Testing of Aerofoils for Application in Small Vertical Axis Wind Turbines, Master's Thesis, Delft University of Technology [online] Available from <[http://faculty.mu.edu.sa/public/uploads/13381829.239820061\\_17.pdf](http://faculty.mu.edu.sa/public/uploads/13381829.239820061_17.pdf) [[accessed 12. 05. 2015].
- Claussen, M. (1990) Area-Averaging of Surface Fluxes in a Neutrally Stratified, Horizontally Inhomogeneous Atmospheric Boundary Layer *Atmos. Environ.* 24A, 1349–1360.
- Clive, P. (2008) Non-linearity in MCP with Weibull distributed wind speeds. *Wind Engineering* 32(3):319-323.
- Commission on Environment and Development (1987) *Our Common Future*. Oxford: University Press.
- Consul, C. A., Willden, R. H. J., Ferrer, E., and Mcculloch, M. D. (2009) "Influence of Solidity on the Performance of a Cross-Flow Turbine" *Proceedings of the 8th European Wave and Tidal Energy Conference*. Uppsala, Sweden.
- Cook, N.J. (1997) "The Deaves and Harris ABL model applied to heterogeneous Terrain". *Journal of Wind Engineering and Industrial Aerodynamics* 66, 197–214.

- Crookes, R. (1985) Defence Research Centre, Salisbury, SA. Pers. comm.
- Dahl, K.S and Fuglsang, P. (1998). Design of the Wind Turbine Aerofoil Family RISO-A-XX, RISO National Laboratory, Roskilde, Denmark. December, 1998.  
[https://www.carbontrust.com/media/77248/ctc738\\_small-scale\\_wind\\_energy.pdf](https://www.carbontrust.com/media/77248/ctc738_small-scale_wind_energy.pdf).
- D'Ambrosio, M and Medaglia, M (2010) *Vertical Axis Wind turbines: History, Technology and Applications*. MSc thesis. [Online] available from <<http://hh.divaportal.org/smash/get/diva2:326493/FULLTEXT01>> [18<sup>th</sup> May, 2013].
- Dannemand, A. P. (1999) "Review of Historical and Modern Utilization of wind power" [online] available from <[www.risoe.dk/rispubl/VEA/dannemand.htm](http://www.risoe.dk/rispubl/VEA/dannemand.htm) > [[accessed 15. 03. 2015].
- Dahmouni, A.W, Salah, M.B., Askri, F., Kerkeni, C and Nasrallah, B (2011). Assessment of wind energy potential and optimal electricity generation in Borj-Cedria, Tunisia. *Renewable Sustainable Energy Rev* 15:815–20.
- Davenport, A.G. (1960) "Rationale for Determining Design Wind Velocities". *Journal of Structural Engineering, ASCE* 86, 39–68.
- Danao, L. A., Qin, N., and Howell, R. (2012) "A Numerical Study of Blade Thickness and Camber Effects on Vertical Axis Wind Turbines", *Proceedings of the Institution of Mechanical Engineers, Part A: Journal of Power and Energy*, pp. 15.
- Danao, L. A., and Howell, R. (2012) "Effects on the Performance of Vertical Axis Wind Turbines with Unsteady Wind Inflow: A Numerical Study," 50<sup>th</sup> AIAA Aerospace Sciences Meeting including the New Horizons Forum and Aerospace Exposition, Nashville, Tennessee.
- Danao, L.A.M (2012) *The Influence of Unsteady Wind on the Performance and Aerodynamics of Vertical Axis Wind Turbines*. PhD thesis, University of Sheffield.
- Darrieus, G.J.M. (1931) Turbine Having its rotating shaft transverse to the flow of the current. US Patent No. 1835081, 1931.
- Denson, W. (1998). The history of reliability prediction, failure causes for electronic systems, *IEEE Trans Reliab*, 47, 325.

- Department of Trade and Industry (2006) "The Energy Challenge: Energy Review Report 2006." Department of Trade and Industry, UK Government.
- Derrick, A. (1992) Development of the measure-correlate-predict strategy for site assessment. British Wind Energy Association Annual Conference, pp. 259-265.
- DECC (2012). Energy security strategy, URN 12D/349, Department of Energy and Climate Change.
- Dooling, R. "Avian Hearing and the Avoidance of Wind Turbines." NREL/SR-500-30844, National Renewable Energy Laboratory, Colorado, USA, June 2002.
- Drees, H.M. The cycloturbine and its potential for broad application. In: Proceedings of 2nd international symposium on wind energy systems, Amsterdam, October 3–6, 1978. 81–8.
- Drela, M. (1989) "XFOIL: An analysis and design system for low Reynolds number aerofoils". In Conference on Low Reynolds Number Aerofoil Aerodynamics, 1989.
- Drela, M and Giles, M. (1989) Viscous-inviscid analysis of transonic and low Reynolds number aerofoils, AIAA Journal Vol. 5, no 10.
- Drela, M. (1995) XFOIL 6.5 user guide Cambridge, MA: Massachusetts Institute of Technology.
- Department of the environment, UK Govt (2007) Planning and environmental policy group. [Online] available from <[http://www.planningni.gov.uk/index/policy/planning\\_statements\\_and\\_supplementary\\_planning\\_guidance/pps18-draft-renewable-energy.pdf](http://www.planningni.gov.uk/index/policy/planning_statements_and_supplementary_planning_guidance/pps18-draft-renewable-energy.pdf)>. [Accessed 15.7. 2016].
- Du, L., Berson, A., and Dominy, R. G. (2015) NACA0018 Behaviour at high angles of attack and at Reynolds numbers appropriate for small wind turbines, Proc. Inst. Mech. Eng., Part C, 229(11), 2007–2022. <<http://tools.energysavingtrust.org.uk/Publications2/Generating-energy/Field-trial-reports/Location-location-location-domestic-small-scale-wind-field-trial-report>>. [18.03. 2016].
- EC, Directive 2009/28/EC, OJ L 140/16, 5.6.2009, 2009.

- ECI Wind and Solar Company. 2013 [Online]. Available from: [http://www.eciwas.com/Products/Wind\\_Products/Proven/Proven\\_15kW\\_6kW\\_25kW.pdf](http://www.eciwas.com/Products/Wind_Products/Proven/Proven_15kW_6kW_25kW.pdf) [accessed 12.09.15].
- El-Ali, A., Moubayed, N. And Outbib, R. (2007) "A Comparison of Two MPPT Techniques for PV System" WSEAS Transaction on Environment and Development 12 (5), 770-779.
- Elliot, W.P. (1958) The growth of the atmospheric internal boundary layer. Transactions of the American Geophysical Union, 39: 1048-1054.
- Elsam Engineering A/S (2004) "Life Cycle Assessment of Offshore and Onshore Sited Wind Farms." Elsam Engineering A/S, October 2004.
- Emeis, S. (2013) Wind energy meteorology (1st ed.) New York: Springer.
- Encraft (2009). *Warwick Wind Trials Final Report*. [Online] available from: <http://www.warwickwindtrials.org.uk/resources/Warwick+Wind+Trials+FinalReport+.pdf> [accessed 11.11.15].
- Endurance Wind Power Company. 2013 [Online]. Available from:
- Energy Saving Trust (2009) Location, Location, Location. Domestic small-scale wind field trial report. [Online] available from:
- Energy Saving Trust, Location, Location, Location. Domestic small-scale wind field trial report, 2009.
- Environmental change Institute (2005) Wind Power and the UK Wind Resource [online] available from <http://www.eci.ox.ac.uk/publications/downloads/sinden05-dtiwindreport.pdf> [accessed 18.03.13].
- ESRU (2015) Wind Resource UK Content. [Online]. Available from: [http://www.esru.strath.ac.uk/EandE/Web\\_sites/03-04/wind/content/wind%20resource.html](http://www.esru.strath.ac.uk/EandE/Web_sites/03-04/wind/content/wind%20resource.html) [accessed 11.11.15].
- Euroserv'er (2015) Wind Energy Barometer [online] available from [http://www.energiesrenouvelables.org/observer/stat\\_baro/observ/barojde16\\_WindEnergy\\_EN.pdf](http://www.energiesrenouvelables.org/observer/stat_baro/observ/barojde16_WindEnergy_EN.pdf) [15. 03. 2013].
- European Commission (2013). SWIP H30 project period report. Blades aerodynamics technical report. Revision 01. [Online] available from <http://swipproject.eu/wp-content/uploads/swip-periodic-report-2.pdf> [18. 03. 2015].

- European Wind Energy Association (1999). Wind Force 10- A Blueprint to achieve 10% of the World's Electricity from wind power by 2020. Published by European Wind Energy Association, London, UK/Forum for Energy and Development, Copenhagen, Denmark and Greenpeace International.
- EWEA (2009) Wind energy – the facts (1st ed.) London: Earthscan.
- Ezio, S and Claudio, C. (1998) Exploitation of wind as an energy source to meet the world's electricity demand. *Wind Eng.*, Vol. 74-76, 375-87. <http://www.endurancewindpower.com> [accessed 12.09.15]. [accessed 12.02.16].  
<[http://www.gwec.net/wpcontent/uploads/2015/02/GWEC\\_GlobalWindStats2014\\_FINAL\\_10.2.2015.pdf](http://www.gwec.net/wpcontent/uploads/2015/02/GWEC_GlobalWindStats2014_FINAL_10.2.2015.pdf)> [19. 04. 2015].
- Fanucci, J. and Walters, R. (1976) "Innovative Wind Machines: The Theoretical Performance of a Vertical-Axis Wind Turbine" In Proceedings of the vertical-axis wind turbine technology workshop, L. Wetherholt, eds. Albuquerque, NM, USA, pp. 61-93.
- Fisher, B., Kukkonen, J., Piringer, M., Rotach, M.W., Scatzmann, M. (2005) Meteorology Applied to Urban Air Pollution: Concepts from Cost 715, European Geo Sciences Union, Atmospheric Chemistry and Physics Discussions [online] available from <[http://www.cgrer.uiowa.edu/people/carmichael/GURME/acpd-5-7903\\_p.pdf](http://www.cgrer.uiowa.edu/people/carmichael/GURME/acpd-5-7903_p.pdf)> [14<sup>th</sup> May, 2013].
- Fleming, P.D. and Probert, S.D. (1984) "The Evolution of Wind-Turbines: A Historical Review." *Journal of Applied Energy* 18,163-77.
- Forrest, S.S. and Eggleston, D. M. (1985) *Wind Turbine Engineering Design*. New York: Van Nostrand Reinhold.
- Frantsi, A., Kalli, H., Larjola, J and Montonen, J. (1984) "Direct Heat Production through the use of a Straight-Blade VAWTs" *presented at European Wind Energy Conference, Hamburg, 1984*.
- Garratt, J.R. (1990) The Internal Boundary-Layer - A Review. *Boundary-Layer Meteorology*, 50(1-4): 171-203.
- Garratt, J.R. (1990) The Internal Boundary-Layer - A Review. *Boundary-Layer Meteorology* 50 (1-4): 171-203.



- Gauld, R (2009) Orkney Renewable Energy Case Studies Original Bargar Hill Research Project [online] available from <<http://www.oref.co.uk/orkneys-energy/wind/>>. [15.03.13].
- Gerdes, G and Strack, M. (1999) Long-term correlation of wind measurement data. *DEWI Magazine* 15:18–24.
- Gibescu M, Ummels BC, Kling WL. Statistical wind speed interpolation for simulating aggregated wind energy production under system studies. 2006 [Online]. Available from: <http://ieeexplore.ieee.org/stamp/stamp.jsp?tp=&arnumber=4202376>
- Gipe, P. (1991) “Wind Energy Comes of Age in California and Denmark” *Journal of Energy Policy* 19,756-67
- Gipe, P. (1995) “Design as if People Matter: Aesthetic Guidelines for the Wind
- Gipe, P. (1995) *Wind Energy Comes of Age*. USA: Wiley.
- Gipe, P. (2004) *Wind power: renewable energy for home, farm, and business*. Chelsea Green Publishing, 2004.
- Glauert, H. (1963) in Durand, W.F. (Ed.) *Airplane Propellers, Aerodynamic Theory* Global Wind Energy Council (2015) *Global Wind Statistics 2014*. [Online] available from
- Gökçek, M, Erdem, H.H, Bayülken, A. (2007) A techno-economical evaluation for installation of suitable wind energy plants in Western Marmara Turkey. *Energy Explor. Exploit.* 25: 407–428.
- Goode, K. and Belcher, S.E. (1999) On the parameterisation of the effective roughness length for momentum transfer over heterogeneous terrain. *Boundary-Layer Meteorology*, 1999. 93(1): 133-154.
- Goselin, G.M. (2007) A review of wind energy technologies. *Renewable and Sustainable Energy reviews*, Vol. 11, pp.1118.
- Gourieres, D.L. (1982) *Wind Power Plants Theory and Design*. Headington Hill II: Pergamon Press Ltd.
- Green, S (2004) “Gotland: The HVDC Pioneer.” *Power Engineering International*. [Online] available from <http://www.powerengineeringint.com/articles/print/volume-12/issue-7/features/hvdc-systems-gotland-the-hvdc-pioneer.html> [accessed 17.11.2016].

- Grimmond, C.S.B. and T.R. Oke, (1999) Aerodynamic properties of urban areas derived from analysis of surface form. *Journal of Applied Meteorology* 38: 1262-1292.
- Grylls, W., Dale, B., and Sarre, P.E. A theoretical and experimental investigation into the variable pitch vertical axis wind turbine. In: *Proceedings of 2nd international symposium on wind energy systems*, Amsterdam, October 3–6, 1978. pp. E9-101–18.
- Gunturu, U.B and Sclosser, C.A (2012) Characterisation of wind power resources in the United States. *Atmos. Chem. Phys.* 12 (20):9687-702. Industry” In “American Wind Energy Association Conference,” Washington, DC, March 30.
- Hamann, R.J. and Toren van, M.J.L (2007) *Systems Engineering and Technical Management Techniques, Parts I-II, Lecture notes*, TUDelft.
- Hammarlund, K. and Martensson, A. (1999) “Planning for Acceptance - Windpower in a Social Landscape” In “European Wind Energy Conference,” Nice, France.
- Hansen, A., Butterfield, C and Cui, X. (1990) Yaw loads and motions of a horizontal axis wind turbine. *Journal of Solar Energy Engineering* 112 (4), 310–314. March 1-5.
- Hansen, M.O.L. (2008) *Aerodynamics of Wind Turbines (2nd Edition)*. London: Earthscan.
- Harrison, R., Hall, E. and Snel, H. (2000) *Large Wind Turbines-Design and Economics* England: John Wiley and Sons.
- Hameed, M.S and Afaq, S.K (2012) “Design and Analysis of a Straight Bladed Vertical Axis Wind Turbine using Analytical and Numerical Techniques”. *Journal of Ocean Engineering* 57 (2013), 248-225.
- Healy, J. V. (1978a) “The Influence of Blade Thickness on the Output of Vertical Axis Wind Turbines” *Journal of Wind Engineering* 2 (1), 1-9.
- Healy, J. V. (1978) “The Influence of Blade Camber on the Output of Vertical-Axis Wind Turbines”. *Journal of Wind Engineering*, 2(3), 146-155.
- Hau, E. (2006) *Wind Turbines, Fundamentals, Technologies, Application, Economics*, Verlag, Berlin: Springer.

- Heath, M.A., Walshe, J.D. and Watson, S.J. (2007) Estimating the potential yield of small building-mounted wind turbines. *Wind Energy* 10 (3): 271–287.
- Hilton, D. J. (1984) "A low cost Darrieus Wind Machine for farm use," presented at Agricultural Engineering, Bundaberg, 1984.
- Hill, N., Dominy, R., Ingram, G. and Dominy, J. (2009) Darrieus turbines: The physics of self-starting. *Proceedings of the Institution of Mechanical Engineers, Part A: Journal of Power and Energy* 223(1), 21–29.
- Hirsch, H and Mandal, A.C. (1987) "A Cascade theory for the Aerodynamic Performance of Darrieus Wind Turbine" *Journal of Wind Eng.* 11(3), 164-75.
- HM Government, *The Carbon Plan: Delivering our low carbon future*, 2011.
- Holme, O. (1977) "A Contribution to the Aerodynamic Theory of the Vertical-Axis Wind Turbine" In *Proceedings of the International Symposium on Wind Energy Systems*, H. S. Stephens, et al., eds. Cambridge, England, pp. 55-72.
- Howard, T. and Clark, P. (2007) Correction and downscaling of NWP wind speed forecasts. *Meteorological Applications*, 14 (2): 105-116.
- Hubbert, M.K. (1971). *The energy resources of the Earth*. *Scientific American*, 225, pp. 60-70.  
<[http://www.eia.gov/outlooks/ieo/pdf/0484\(2016\).pdf](http://www.eia.gov/outlooks/ieo/pdf/0484(2016).pdf)> [7.06. 2013].
- IEC (2006) International Standard 61400-2. Wind Turbines Part 2. Design Requirements for Small Wind Turbines.
- Iida, A; Mizuno, A. and Fukudome, K. (2004) Numerical Simulation of Aerodynamic Noise Radiated form Vertical Axis Wind Turbines. Kyoto, Japan, Proc. Of ICA 2004, the 18th International Congress on Acoustics, 2004.
- International Energy Agency (2003). *Energy Balances of Non-OECD Countries 2000-2001*, Paris: IEA and OECD.
- International Energy Agency (2016). *International Energy Outlook 2016 with Projections to 2040*. [Online]. Available from:
- International Renewable Energy Agency (IRENA). *Renewable Energy Technologies: Cost Analysis Series 1* (5):1–64. International Standard IEC 61400-1. Wind Turbine Design Requirements. 2008 [Online].

Available from: <http://homes.civil.aau.dk/rrp/BM/BM8/r.pdf> [accessed 12.09.15].

IPPC (2007) The Landmark 2007 IPCC Report on Climate Change [online] available from

<<http://www.wunderground.com/resources/climate/ipcc2007.asp?MR=1>> [7<sup>th</sup> June 2013].

Islam, M., David, S., Ting, K and Fartaj, A. (2008) “Aerodynamic Models for Darrieus-Type Straight Bladed Vertical Axis Wind Turbines” *Journal of Renewable and Sustainable Energy Reviews* 12 (4), 1087–1109.

<[http://www.energy.ca.gov/windguidelines/documents/other\\_guidelines/2006-05-12\\_BCKGRD\\_ENVIRMTL\\_ASSMNT.PDF](http://www.energy.ca.gov/windguidelines/documents/other_guidelines/2006-05-12_BCKGRD_ENVIRMTL_ASSMNT.PDF)> [accessed 15.7.16].

for Stand-Alone Applications” Ph.D. thesis, Griffith University, Gold Coast, Australia.

Jackson, P.S. and Hunt, J.C.R. (1975) Turbulent wind over a low hill

Jacobs, E. and Sherman, A. (1937) Aerofoil Characteristics As Affected by Variations of the Reynolds Number. Technical Report No. 586, NACA. [Online] available from

<[http://ntrs.nasa.gov/archive/nasa/casi.ntrs.nasa.gov/19930091662\\_1993091662.pdf](http://ntrs.nasa.gov/archive/nasa/casi.ntrs.nasa.gov/19930091662_1993091662.pdf)> [13<sup>th</sup> March 2013].

Jain, P. (2011) *Wind Energy Engineering*. McGrawHill: New York.

James, P.A.B.; Sissons, M.F; Bradford, J.; Myers, L.E; Bahaj, A.S; Anwar, A. and Green, S. (2010) Implications of the UK field trial of building mounted horizontal axis micro-wind turbines. *Energy Policy*, 2010. 38(10): 6130-6144.

Jamieson, P. (1998). Design challenges for growing sector. *Wind Directions*, April 1998, UK, pp. 16- 17.

Jha, A.R. (2010) *Wind Turbine Technology* UK: CRC Press.

Jimenez, A.C (2013) Wind resource assessment report: Mille Lacs India reservation, Minnesota. [Online] available from

<http://www.nrel.gov/docs/fy14osti/60429.pdf> [accessed 21.11.16].

Jimenez, B., Monnich, K., and Durante, F. (2012) Comparison between NCEP/NCAR and MERRA reanalysis data for long term correction in

- wind energy assessment. In Proceedings of the EWEA Annual Event 2012, Copenhagen, Denmark.
- Jung, S., Vanli, A. O., and Kwon, S.D. (2013) Wind energy potential assessment considering the uncertainties due to limited data. *Applied Energy*.
- Justus, C.G., Mani, K. and Mikhail, A.S. (1979) Inter annual and month-to-month variations of wind speed. *Journal of Applied Meteorology*, 1979. 18(7): 913-920.
- Justus, C.G., W.R. Hargraves, and A. Yalcin (1976) Nationwide assessment of potential output from wind-powered generators. *Journal of Applied Meteorology* 15 (7): 673-678.
- Kaimal, J.C and Finnigan, J.J (1994) *Atmospheric boundary layer flows*. New York, USA: Oxford University Press.
- Kentfield, J.A.C. (1978) A hybrid cyclogiro-Darrieus rotor wind turbines. Proc. of 1st Brazilian Energy Congress, Rio de Janeiro, Dec.; Vol.B: 448-463.
- Kingsley, A and Whittam, B (2005) *Wind Turbines and Birds. A Background Review for Environmental Assessment*
- Kirby, A (2004) "MoD 'Threatening UK Energy Plans'" BBC News Online, March 1 2004.
- Kirke, B. K., (1998) "Evaluation of Self-Starting Vertical Axis Wind Turbines"
- Klimas, P.C. (1984) Tailored Aerofoils for Vertical Axis Wind Turbines Sandia National Laboratories, SAND84-1062.
- Koksal and Hughes (2005) Vertical Axis Wind Turbine. Design Project MECH 4010. Department of Mechanical Engineering, Dalhousie University, December, 2005.
- Kooiman, S. J., and Tullis, S. W. (2010) "Response of a Vertical Axis Wind Turbine to Time Varying Wind Conditions Found within the Urban Environment" *Journal of Wind Engineering* 34(4), 389-401.
- Kristoffersen, J.R. (2005) "The horns Rev Wind Farm and the Operational Experience with the Wind Farm Main Controller" *Copenhagen Offshore Wind 2005*, 26-28 October 2005.
- Kubik, M.L., Brayshaw, P.J.C and Barlow, J.F. (2013) Exploring the role of reanalysis data in simulating regional wind generation variability over Northern Ireland. *Renewable Energy* 57:558-561.

- Q. J. R. Meteorology. Soc., 101: 929–955.
- Lambert, T and Ferguson, T. (2012) Windographer database interface specification. [Online] available from  
<<https://www.windographer.com/media/downloads/WindographerDatabaseInterfaceSpecification-Rev7.pdf>> [accessed 22.7.16].
- Landberg, L., Myllerup, L., Rathmann, O., Petersen, E.L., Jørgensen, B.H., Niels, B.J. et al. (2003) Wind resource estimation – an overview Wind Energy 6:261–271.
- Landscape Design Associates (2000) “Cumulative Effects of Wind Turbines: A Guide to Assessing the Cumulative Effects of Wind Energy Development.” ETSU 248 Bibliography W/14/00538/REP, UK Department of Trade and Industry.
- Langtree, W. (2010) Wind resource and site assessment W Tong (Ed.), Wind power generation and wind turbine design, MA: WIT Press, 49–87.
- Lantz, E., Wiser, R and Hand, M. (2012) IEA Wind Task 26: The Past and Future Cost of Wind Energy [online] available from  
<[https://www.ieawind.org/index\\_page\\_postings/WP2\\_task26.pdf](https://www.ieawind.org/index_page_postings/WP2_task26.pdf)> [13.09.2015].
- Lapin, E.E. (1975) *Theoretical Performance of Vertical Axis Wind Turbines*. ASME Paper, 75-WA/Ener-1, the winter annual meeting, Houston, TX, USA.
- Larsen, H. C., 1975, "Summary of a Vortex Theory for the Cyclogiro" Proceedings of the 2nd US National Conferences on Wind Engineering Research, Colorado State University, Colorado, USA.
- Lazauskas, L. (1992) Three pitch control systems for vertical axis wind turbines compared, Wind Engineering, 16 (5):269-283.
- Leishman J.G., Bhagwat M.J., and Bagai A. (2002) “Free-Vortex Filament Methods for the Analysis of Helicopter Rotor Wakes”, Journal of Aircraft, 39 (5), 759-775.
- Li, Q.S., Zhi, L., .H., Hu, F. (2009) “Field Monitoring of Boundary Layer Wind Characteristics in Urban Area” Journal of Wind and Structures 12, 553–574.
- Li,S. and Yan,L. (2010) Numerical Study on the Performance effect of solidity on Straight-Bladed Vertical Axis Wind turbine. Scientific Research.

- Liléo, S., Berge, E., Undheim, O., Klinkert, R and Rolv, E. et al. (2013) Long-term correction of wind measurements, state-of-the-art, guidelines and future work. Elforsk report 13:18.
- Love, M. (2003) Land Area and Storage Requirements for Wind and Solar Generation to Meet the US Hourly Electrical Demand. MSc Dissertation, University of Victoria, Victoria, Canada.
- Mabry, S. (2012) company profile, Mistaya Engineering. [Online] available from
- Mahri, Z.L. and Rouabah, M.S. (2008) "Calculation of Dynamic Stresses using Finite Element Method and Prediction of Fatigue Failure for Wind Turbine Rotor" WSEAS Transactions on Applied and Theoretical Mechanics 3 (1), 28-41.
- Makridakis, S., Wheelwright, S.C and Hyndman, R.J. (1998) Forecasting Methods and applications (3rd ed.), New York: Wiley.
- Martin-Martínez, S., et al., (2012) Wind Power Variability and Singular Events. Advances in Wind Power.
- Marten, D., Wendler, J., Pechlivanoglou, G., Nayeri, C.N., and Paschereit, C.O. (2013) QBLADE: An Open Source Tool for Design and Simulation of Horizontal and Vertical Axis Wind Turbines. International Journal of Emerging Technology and Advanced Engineering Volume 3, Special Issue 3: ICERTSD 2013, Feb 2013, 264-269.
- Mandal, A.C. (1986) Aerodynamics and Design Analysis of Vertical Axis Darrieus Wind Turbines. PhD dissertation, Vrije Universiteit, Brussels, Belgium.
- Mandal, A.C. and Hirsch, H. (1987) A Cascade "Theory for the Aerodynamic Performance of Darrieus Wind Turbines" *Journal of Wind Engineering* 11 (3), 164–175.
- McIntosh, S.C., Babinsky, H., Bertenyi, T. (2008) Unsteady power output of vertical axis wind turbines operating within a fluctuating free stream, 46<sup>th</sup> AIAA aerospace sciences meeting and exhibit, Reno Nevada.
- Mason, P.J. (1988) The formation of a really-averaged roughness lengths. Quarterly Journal of the Royal Meteorological Society, 114 (480): 399-420.

- Mason, P.J. and Sykes, R.I. (1979) Three-dimensional numerical integrations of the Navier–Stokes for flow over surface-mounted obstacles *J. Fluid Mech.*, 91:433–450.
- Manwell, J.F; McGowan, J.G and Rogers, A.L. (2009) *Wind Energy Explained Theory Design and Applications*. US: Willey Publishing.
- Mathew, S. (2006) *Wind Energy. Fundamental Resource Analysis and Economics*. Verlag Berlin Heidelberg: Springer.
- Mahrt, L. (1996) The Bulk Aerodynamic Formulation over Heterogeneous Surfaces, *Boundary-Layer Meteorology* 78, 87–119.
- Met Office (2008) A Report by the Met Office to accompany the Carbon Trust Report, Small-Scale Wind Energy – Policy Insights and Practical Guidance [online] available from <<http://www.carbontrust.com/media/85174/small-scale-wind-energy-technical-report.pdf>> [14. 05.14].
- Met Office (2012) Met Office Integrated Data Archive System (MIDAS) Land and Marine Surface Stations Data (1853 - current). NCAS British Atmospheric Data Centre.
- Mickael, E. (2007) 38 Meter Wind turbine blade Design [online] available from <[http://ns7.freeheberg.com/~mach085/38\\_meter\\_wind\\_turbine\\_blade\\_design.pdf](http://ns7.freeheberg.com/~mach085/38_meter_wind_turbine_blade_design.pdf)> [20<sup>th</sup> Feb. 2013].
- Mina, G and Clive, P. Assessing the influence of neighbouring wind farms on one another. In: Proceedings of the EWEA annual conference and exhibition, Bella Center, Copenhagen, Denmark; 16–19 April 2012.
- Millward-Hopkins, J.T., Tomlin, A.S., Ma, L., Ingham, D. and Pourkashanian, M. (2011) The predictability of above roof wind resource in the urban roughness sublayer. *Wind Energy*, 225-43.
- Millward-Hopkins, J.T. (2013) Predicting the wind resource available to roof-mounted wind turbines in urban areas. PhD thesis, Energy Research Institute, University of Leeds.
- Migliore, P.G. and Fritschen, J.R. (1982) Darrieus Wind Turbine Airfoil Configurations, A subcontract report, Solar Energy Research Institute, SERU/TR-11045-1.
- Mortimer, A. (1994) A new correlation/prediction method for potential wind farm sites. Proceedings of the BWEA.



- Muraca, R.J., Stephens, M.V., Dagenhart, J.R. (1975) *Theoretical Performance of Cross-Wind Axis turbines with Results for a Catenary Vertical Axis Configuration*. [Online] available from <<http://www.ntis.gov/search/product.aspx?ABBR=N7611032> [11. 02. 2014].
- Mcintosh, S. C., Babinsky, H., and Bertenyi, T. (2007) Optimizing the Energy Output of Vertical Axis Wind Turbines for Fluctuating Wind Conditions”, 45th AIAA Aerospace Sciences Meeting and Exhibit, Reno, Nevada.
- Mcintosh, S. C., Babinsky, H., and Bertenyi, T. (2008) “Unsteady Power Output of Vertical Axis Wind Turbines Operating within a Fluctuating Free-Stream”, 46th AIAA Aerospace Sciences Meeting and Exhibit, Reno, Nevada.  
<[http://www.windssystemsmag.com/media/pdfs/Articles/2012\\_August/0812\\_Profile.pdf](http://www.windssystemsmag.com/media/pdfs/Articles/2012_August/0812_Profile.pdf)> [accessed 22.7.16].
- Microgeneration Certification Scheme (2013) MIS 3003, Issue 3.2, 17/04/2013. [Online] Available from: <<http://www.microgenerationcertification.org/installers/installers/installer-standards>> [12. 05. 2016].
- Newman, B.G. (1983) “Actuator-Disc Theory for Vertical-Axis Wind Turbines” *Journal of Wind Energy Engineering and Industrial Aerodynamics* 15 (1983), 347-355.
- Nedaei, M. (2014) Wind resource assessment in Hormozgan province in Iran. *Int.J. of Subst. Energy* 3:651–692.  
<http://www.doc.govt.nz/Documents/science-and-Technical/sfc289entire.pdf> [accessed 20.06.16].
- Oke, T.R. (1987) *Boundary Layer Climates*. Methuen and Co.: New York.
- Oliver, A, Zarling, K (2010) The effect of seasonality on wind speed prediction bias in the plains. In: Proceedings of the AWEA 2010 windpower conference and exhibition, Dallas Texas, USA; May 23–25.
- Ostowari, C., and Naik, D. (1984) Post-stall Studies of Untwisted Varying Aspect Ratio Blades with an NACA 4415 Aerofoil Section - Part I, *Journal of Wind Engineering*, 8(3): 176–194.

- Paraschivoiu, I. (1981) Double-Multiple Streamtube Model for Darrieus Wind Turbines. Second DOE/NASA Wind turbines dynamics workshop, NASA CP-2186, Cleveland, OH, February, 1981. 19–25.
- Paraschivoiu, I. (2002) *Wind Turbine Design with Emphasis on Darrius Concept* Canada: Polytechnic International Press.
- Paraschivoiu, I; Delclaux, F; Fraunie, P; Beruier, C. (1983) “Aerodynamic analysis of the Darrieus Rotor including Secondary Effects” *Journal of Energy* 7(5), 416-21.
- Patel, B and Kevat, V. (2013) Performance prediction of straight bladed Darrieus wind turbine by single stream tube model. *International Journal of Advanced Engineering Tech.* 4 (2): 86-89.
- Perea, R. A., Amezcua, J and Probst, O (2011) Validation of three new measure-correlate-predict models for the long-term prospection of the wind resource. *Journal of Renewable and Sustainable Energy* 3 (2) DOI: 10.1063/1.3574447.
- Peterson, E.W. (1969) Modification of mean flow and turbulent energy by a change in surface roughness under conditions of neutral stability. *Quarterly Journal of the Royal Meteorological Society* 95 (405): 561-575.
- Powlesland, R.G.(2009) *Impacts of wind farms on birds: A review* Press, W.H., Teukolsky, S.A., Vetterling, W.T., Flannery, B.P. (1992) *Numerical recipes in Fortran 77* (2nd ed.), vol. 1 New York: Cambridge University Press.
- Putnam, P.C (1948) *Power from the wind* (1st eds.) New York: Van Nostrand Reinhold Company.  
<http://www.renewableuk.com/en/renewable-energy/wind-energy/uk-wind-energy-database/index.cfm> [02.03.16].
- Ragheb, M. (2016) Orography and wind turbine sitting available from <http://mragheb.com/NPRE%20475%20Wind%20Power%20Systems/Orography%20and%20Wind%20Turbine%20Siting.pdf> [11.05.16].
- Ragheb, M. and Ragheb, A.M. (2011) *Wind Turbines Theory - The Betz Equation and Optimal Rotor Tip Speed Ratio, Fundamental and Advanced Topics in Wind Power*, Dr. Rupp Carriveau (Ed.), ISBN: 978-953-307-508-2, InTech, available from:

<<http://www.intechopen.com/books/fundamental-and-advanced-topicsin-wind-power/wind-turbines-theory-the-betz-equation-and-optimal-rotor-tip-speed-ratio>> [20.051. 2013].

- Ramirez, P. and Carta, J.A. (2005) Influence of the data sampling interval in the estimation of the parameters of the Weibull wind speed probability density distribution: a case study. *Energy Conversion and Management Energy* 46 (15-16): 2419-2438.
- Ramkissoon, R and Manohar, K. (2013) Increasing the power output of the Darrieus Vertical Axis Wind Turbine, *British journal of Applied Science & Technology* 3 (1):77 90.
- Rao, K.S., Wyngaard, J.C. and Coté, O.R. (1974) The Structure of the Two-Dimensional Internal Boundary Layer over a Sudden Change of Surface Roughness. *Journal of the Atmospheric Sciences*, 31(3): 738-746.
- Raupach, M.R. (1994) Simplified expressions for vegetation roughness length and zero-plane displacement as functions of canopy height and area index. *Boundary-Layer Meteorology*, 71, (1-2): 211-216.
- Renewable UK (2010) Small Wind Systems Quarterly News Bulletin.
- Renewable UK (2013) Small and Medium Wind UK Market Report [online] available from <[file:///C:/Users/Charles/Downloads/final\\_ruk13-013\\_small\\_medium\\_wind\\_market\\_report.pdf](file:///C:/Users/Charles/Downloads/final_ruk13-013_small_medium_wind_market_report.pdf)> [29<sup>th</sup> Sept, 2015].
- Renewable UK. UK wind energy database. 2013 [Online]. Available from: REUK.co.uk. (2007) *Darrieus Wind Turbines*. [Online] available from: <<http://www.reuk.co.uk/Darrieus-Wind-Turbines.htm>> [13.03 2013].
- Rienecker, M.M, Suarez M.J, Gelato R, Todling R, Backmeister J, Liu E, et al. (2011) MERRA: NASA's modern-era retrospective analysis for research and applications. *Journal of Climate* 2011; 24 (14), 3624–3648.
- Righter, R.W. (1996) "Pioneering in Wind Energy: The California Experience" *Journal of Renewable Energy* 9,781-4.
- Ritter, M., Shen, Z., Cabrera, B.L., Odening, M and Deckert, L. (2014) Designing an index for assessing wind energy potential. SFB 649 discussion paper 2014-052. [Online] available from

<<http://sfb649.wiwi.hu-berlin.de/papers/pdf/SFB649DP2014-052.pdf>>  
[accessed 11.7.16].

Robert, G. (1982) Wind turbine generators. USA: MIT Press.

Rogers, A.L., Rogers, J.W. and Manwell, J.F. (2006) Uncertainties in results of measure-correlate-predict analyses. European Wind Energy Association annual conference, Athens.

Rogers, A.L., Rogers, J.W., Manwell, J.F. (2005) Comparison of the performance of four measure-correlate-predict algorithms, *Journal of Wind Engineering and Industrial Aerodynamics*, 93:243–264.

Rohatgi, J. and Nelson, V. (1994) Wind Characteristics: An Analysis for the Generation of Wind Power. *Alternative Energy Institute: Burgess Publishing*.

Rojas, R. (1996) Neural networks: a systematic introduction. Berlin: Springer.

Romo Perea, A., Amezcua, J. and Probst, O. (2011) Validation of three new measure-correlate-predict models for the long-term prospection of the wind resource. *Journal of Renewable and Sustainable Energy*, 3(2).

Rose, S and Apt, J. (2015) What can Reanalysis data tell us about wind power? *Renewable Energy* 83 (94): 963-969.

Rosser, M. (1997) 70% penetration of wind energy into a rural grid - 2.4 MW of wind capacity interconnected with a 14 MW diesel power station. In: *Proceedings Wind Energy Workshop 1997*, Asia Pacific Wind Energy Centre, and Centre for Electrical Power Engineering. Calyton, Australia: Monash University.

of National Development and Energy, Canberra, Aust. Report NERDDP/EG/81/25.

Samaraweera, Pathirathna K.A.B (2013) Development of Darrieus type vertical axis wind turbine for stand- alone applications, University of moratuwa, Srilanka.

Sandia Report (1982) *Proceedings of the Vertical Axis Wind Turbine Design Technology Seminar for Industry* eds. By Sidney F and Johnston, Jr. [Online] available from

<<http://energy.sandia.gov/wp/wp-content/gallery/uploads/Sand80-0984.pdf>> [20<sup>th</sup> Jan. 2013].

- Savonius, S.J. (1931) The S-Rotor and its applications. *Mech Eng.* 53 (5):333–8.
- Schmid, H. P. and Bunzli, B.: (1995) The Influence of Surface Texture on the Effective Roughness Length. *Quart. J. Roy. Meteorology. Soc* 121, 1–21.
- Schmid, H.P. and Oke, T.R. (1990) A model to estimate the source area contributing to turbulent exchange in the surface-layer over patchy terrain. *Quarterly Journal of the Royal Meteorological Society*, 116 (494) 965-988.
- Scruton, C. (1981) *An Introduction to Wind Effects on Structures*, England: Oxford University Press.
- Seguro, J.V. and Lambert, T.W. (2000) Modern estimation of the parameters of the Weibull wind speed distribution for wind energy analysis. *Journal of Wind Engineering and Industrial Aerodynamics*, 85(1): 75-84.
- Selig, M.S., Guglielmo, J.J; Broeren, A.P and Giguere. P (1995). Summary of Low- Speed Aerofoil Data. Virginia Beach, Virginia: Soar Tech Publications.
- Sharma, J.S., Kar, S.K and Kumar, A. (2012) Wind Energy Status in India. *A Short Review* 16: 157-1164.
- Sharpe, D. (1990) Wind turbine aerodynamics. In: Freris L, ed. *Wind Energy Conversion Systems*. New York: Prentice Hall, 54–117.
- Sharpe, D; Burton, T; Jenkins, N; Bossanyi, E. (2001) *Wind Energy Handbook*. West Sussex, UK: John Wiley and Sons, Ltd.
- Sheldahl, R. E., and Klimas, P. C. (1981) Aerodynamic characteristics of seven symmetrical aerofoil sections through 180-degree angle of attack for use in aerodynamic analysis of vertical axis wind turbines,” Sandia National Laboratories, Albuquerque, NM, Technical Report No. SAND80-2114.
- Sheldahl, R., Klimas, P., and Feltz, L. (1980) Aerodynamic Performance of a 5-meter-Diameter Darrieus Turbine with Extruded Aluminium NACA-0015 blades. Technical Report SAND80-0179, Sandia National Laboratories.

- Shephard, D.G. (1990) Historical Development of the Wind Mill NASA contractor Report 4337 DOE/NASA/5255-1 [online] available from <<http://wind.nrel.gov/public/library/shepherd.pdf>> [13. 03. 2013].
- Sheppard, C.J.R (2009) Analysis of the Measure-correlate-Predict Methods for wind resource assessment. Master's thesis, Humboldt State University, Areta, CA.
- Simiu, E., Scanlan, R.H. (1996) *Wind Effects on Structures—Fundamentals and Applications to Design*. John Wiley & Sons, Inc., pp.42–43.
- Sissons, M.F., et al. (2011) Pole-mounted horizontal axis micro-wind turbines: UK field trial findings and market size assessment. *Energy Policy* 39(6): 3822-3831.
- Skibin, D. (1984) On the evaluation of wind power from short wind records—comment. *Journal of Climate and Applied Meteorology* 23 (10):1477-1479.
- Smulders, P. T. and Folling, F. J. (1984) “Wind Energy and Cooling”, presented at European Wind Energy Conference, Hamburg.
- Sobol, I.M. (1967) On the distribution of points in a cube and the approximate evaluation of integrals. *U.S.S.R. Computational Mathematics and mathematical physics*, 7(4): 86-112.
- Solomon, S., Qin, D., Manning, M., Chen, Z., Marquis, M., Averyt, K.B., Tignor, M. and Miller, H.L. (editors). *Climate Change (2007) the Physical Science Basis. Contribution of Working Group I to the Fourth Assessment Report of the Intergovernmental Panel on Climate Change*. Cambridge University Press, Cambridge, United Kingdom and New York, NY, USA, 2007.
- South, P., Mitchell, R and Jacobs, E. (1983). *Strategies for the Evaluation of Advanced Wind Energy Concepts*. Solar Energy Research Institute, Golden, CO, USA, pp. 153.
- Spera, D. A. (2009) *Wind Turbine Technology: Fundamental Concepts in Wind Turbine Engineering*, Second Edition U.S: ASME Press.
- Spera, D.A (2008) Models of lift and drag coefficients of stalled and unstalled aerofoils in wind turbines and wind tunnels. NASA/CR-2008-215434.
- Stimmel, R. (2008) *AWEA Small Wind Turbine Global Market Study 2009*, Washington DC. [Online] available from

<[http://www.awea.org/learnabout/smallwind/upload/2009\\_AWEA\\_Smallwind\\_Global\\_Market\\_Study.pdf](http://www.awea.org/learnabout/smallwind/upload/2009_AWEA_Smallwind_Global_Market_Study.pdf)> [10. 03. 2013].

- Storer, R.G. (1981) End of Grant Report "Vertical Axis Wind Turbine." Dept
- Strickland, J.H. (1976) *A Performance Prediction Model for the Darrieus Turbine*. International Symposium on Wind Energy Systems, Cambridge, UK, September 7–9, C3-39–54.
- Stull, R.B. (1988) *An Introduction to Boundary Layer Meteorology*. Dordrecht, Boston: Kluwer Academic Publisher.
- Summers, D. M. and Tangler, J.L. (2000) Wind Tunnel Tests of Two aerofoils for Wind Turbines operating at High Reynolds Numbers, *ASME Wind Energy Symposium, Nevada* [online] available from <<http://www.nrel.gov/docs/fy00osti/27891.pdf>> [20. 01. 2013].
- Surugiu, L. and Paraschivoiu, I (1999) "Acceptability, Environmental and Social Aspects of Wind Energy" In "European Wind Energy Conference," Nice, France, March 1-5.
- results for aerofoil NACA0018," *Wind Eng.*, 32(6), 525–537.
- Taylor, M., Mackiewicz, P., Brower, M.C, Markus, M (2004) An analysis of wind resource uncertainty in energy production estimates. In: *Proceedings of the European wind energy conference & exhibition*, London, UK, 22–25 November.
- Taylor, P.A. and Lee, R.J. (1984) Simple guidelines for estimating wind speed variations due to small scale topographical features. *Climatological Bulletin*, 18 (2): 3-32.
- Technical University of Denmark. (2013) WAsP - the wind atlas, analysis and application program. [Online] <available from: <http://www.wasp.dk/>> [20.03.2016].
- Templin, R.J. (1974) *Aerodynamic Performance Theory for the NRC Vertical-Axis wind Turbines*. NRC Lab Report LTR-LA
- The British Wind Energy Association (2000) "End of an Era at Burgar Hill," BWEA 13 November 2000.
- Thøgersen, M., et al. (2007) Measure-correlate-predict methods: case studies and software implementation. European Wind Energy Association annual conference, Milan.

- Thomas, R.L and Robbins, W.H. (1980) "Large Wind-Turbine Projects in the United States Wind Energy Program" *Journal of Wind Eng. Ind. Aerodyn* 5,323-35.
- Tillman, J.P. (2011) Improvements to vertical axis wind turbine blades to aid in self-starting, School of Technology , Eastern Illinois University.
- Timmer, W. A. (2008) Two-dimensional low-Reynolds number wind tunnel
- Timmer, W. and van Rooij, R. (2001) The Performance of New Wind Turbine Blade Tip and Root aerofoils up to High Angles-of-attack, Delft University of Technology, In Proceedings of the 2001 European Wind Energy Conference, July 2001, Copenhagen. pp. 26.
- Tingting, G., Dianwen, W., Jihui, X., and Shaohua, L. (2009) "The Method of Large-Scale Wind Turbine Blades Design Based on MATLAB Programming", IEEE International Conference on Sustainable Power Generation Nanjing, China 6-7 April 2009.
- Tong, W. (2010) *Fundamental of wind energy. Wind Power Generation and Wind Turbine Design*. U.S: Wit Press.
- Tuller, S.E. and A.C. Brett (1984). The characteristics of wind velocity that favour the fitting of a Weibull distribution in wind-speed analysis. *Journal of Climate and Applied Meteorology* 23(1): 124-134.
- Tyndall Centre (2005) "Decarbonising the UK: Energy for Climate Conscious Future." Tyndall Centre for Climate Change Research, Norwich.  
<https://www.ons.gov.uk/census/2011census/2011censusdata>  
 [accessed 02.03.16].
- UCL (2013) UCL energy Institute [online] available from  
<http://www.bartlett.ucl.ac.uk/energy/research/themes/buildings>  
 [13.05.2013].
- UK Census Data. 2011 [Online]. Available from:
- van Hulle, F (2005) "Large Scale Integration of Wind Energy in the European Power Supply: Analysis, Issues and Recommendations". EWEA, Brussels.
- Vandenbereghe, D, Dick E. (1986) A theoretical and experimental investigation into the straight bladed wind turbine with second order harmonic pitch control. *Wind Engineering*, 10: 122-138.

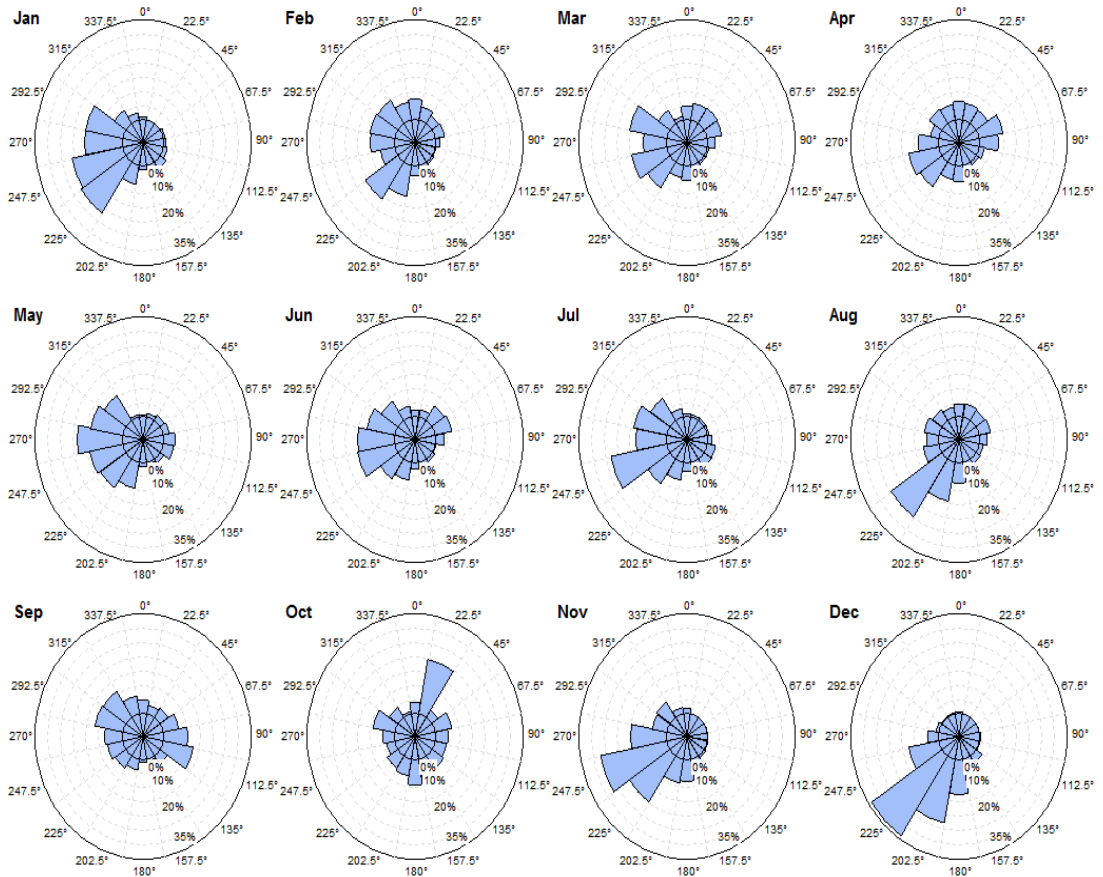


- Vestas (2011) Wind Energy Annual Report [Online] available from <[http://www.unglobalcompact.org/system/attachments/14224/original/12020\\_8CA\\_UK\\_08\\_AnnualReport2011.pdf?1330075458](http://www.unglobalcompact.org/system/attachments/14224/original/12020_8CA_UK_08_AnnualReport2011.pdf?1330075458)> [17.01.2013].
- Viterna, L.A and Corrigan. R. (1981) Fixed-pitch rotor performance of large HAWTs; DOE/NASA workshop on large HAWTs; Cleveland, Ohio, 28-30 July.
- Wakui, T., Tanzawa, Y., Hashizume, T. and Nagao, T. (2005) Hybrid configuration of Darrieus and Savonius rotors for standalone wind turbine-generator systems. *Electrical Engineering in Japan* 150 (4), 13–22.
- Walker, J.F and Nicholas, J. (1997) *Wind energy technology*. Chichester, UK: Wiley.
- Walker, S.L. (2011) Building mounted wind turbines and their suitability for the urban scale-a review of methods of estimating urban wind resource. *Energy and Buildings*, 43(8): 1852-1862.
- Walters D.K. and Cokljat, D (2008) A Three-Equation Eddy-Viscosity model for Reynolds Averaged Navier Stokes simulations of transitional flow. *Journal of Fluids Engineering*, 130, issue 11-12.
- Weekes, S.M. (2014) *Small-Scale Wind Energy: Methods for Wind Resource Assessment*. PhD thesis, PhD thesis, Energy Research Institute, University of Leeds.
- Weekes, S.M. and Tomlin, A.S. (2013) Evaluation of a semi-empirical model for predicting the wind energy resource relevant to small-scale wind turbines. *Renewable Energy* 50:280-288.
- Weibull, W. (1951) A Statistical Distribution Function of Wide Applicability. *Journal of Applied Mechanics-Transactions of the ASME*, 18(3): 293-297.
- White F.M. (2005) *Viscous Fluid Flow (3rd Edition)*. India: McGraw-Hill.
- Wieringa, J. (1976) An objective exposure correction method for average wind speeds measured at a sheltered location. *Quarterly Journal of the Royal Meteorological Society*, 102 (431): 241-253.

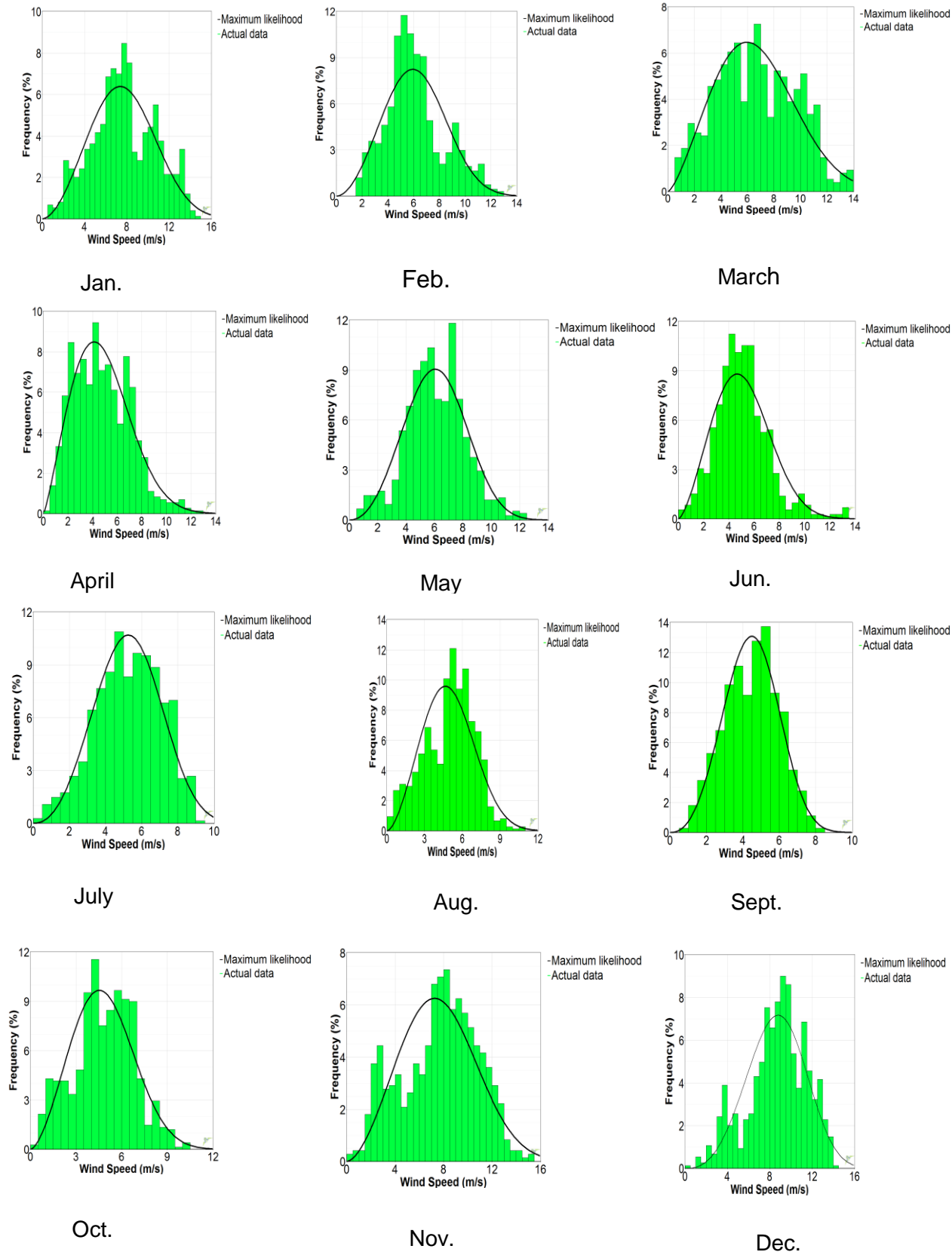
- William, P.K., Wilfried, B., (1986) "Wind Profile Constants in a Neutral Atmospheric Boundary Layer over Complex Terrain" *Boundary Layer Meteorology* 34, 35–54.
- Wilson, R. E (1980) "Wind-Turbine Aerodynamics," *Journal of Wind Engineering and Industrial Aerodynamics*, 5 (3–4), 357-372.
- Wilson, R.E and Lissaman, P.B.S. (1974) *Applied Aerodynamics of Wind Power Machines* US: Oregon State University Press.
- Windographer (2015) Mistaya Engineering Inc. 109 Arbour Ridge Heights NW, Calgary AB T3G 3Z1, Canada [accessed on 22. 03. 2013].
- Wood, D. (2011) *Small Wind Turbines: Analysis, Design and Applications* London: Springer.
- Worasinchai, S., Ingram, G. and Dominy, R. (2011). A low-Reynolds-number, high-angle-of-attack investigation of wind turbine aerofoils. *Proceedings of the Institution of Mechanical Engineers, Part A: Journal of Power and Energy* 225(6), 748–763.
- World Wind Energy Association (2014). Wind Resource Assessment Report. [Online] available from <<http://www.wwindea.org/wwea-publishes-world-wind-resource-assessment-report>> [14. 09. 2015].
- Wong, R., Webster, S. and Vosper, S (2012) High-resolution dynamical downscaling techniques for wind resource assessment. European Wind Energy Association annual conference, Copenhagen.
- Zervos, A. (2009) Wind Power as a main stream energy source. Proc. Of the 2009 European Wind Energy conference. Marseille, March 2009.
- Zhang, J., Draxl, C., Hopson, T., Monache, D.L., Vanvyve, E and Hodge, B. (2015) Comparison of numerical weather prediction based deterministic and probabilistic wind resource assessment methods. *Applied Energy* 156: 528-541.
- Zhang, M.H. (2015) Wind resource assessment and micro-siting. China: China machine press.
- Zheng H, Kusaik A. Prediction of wind farm power ramp rates: A data mining approach. *Journal of Solar and Energy Engineering* 2008; 131(3): doi:10.1115/1.3142727.

## Appendix I

(a) Wind roses for every month of the year 2015 at 10 m for Beighton site.



(b) Wind frequency for every month of the year 2015 at 10 m for Beighton site.

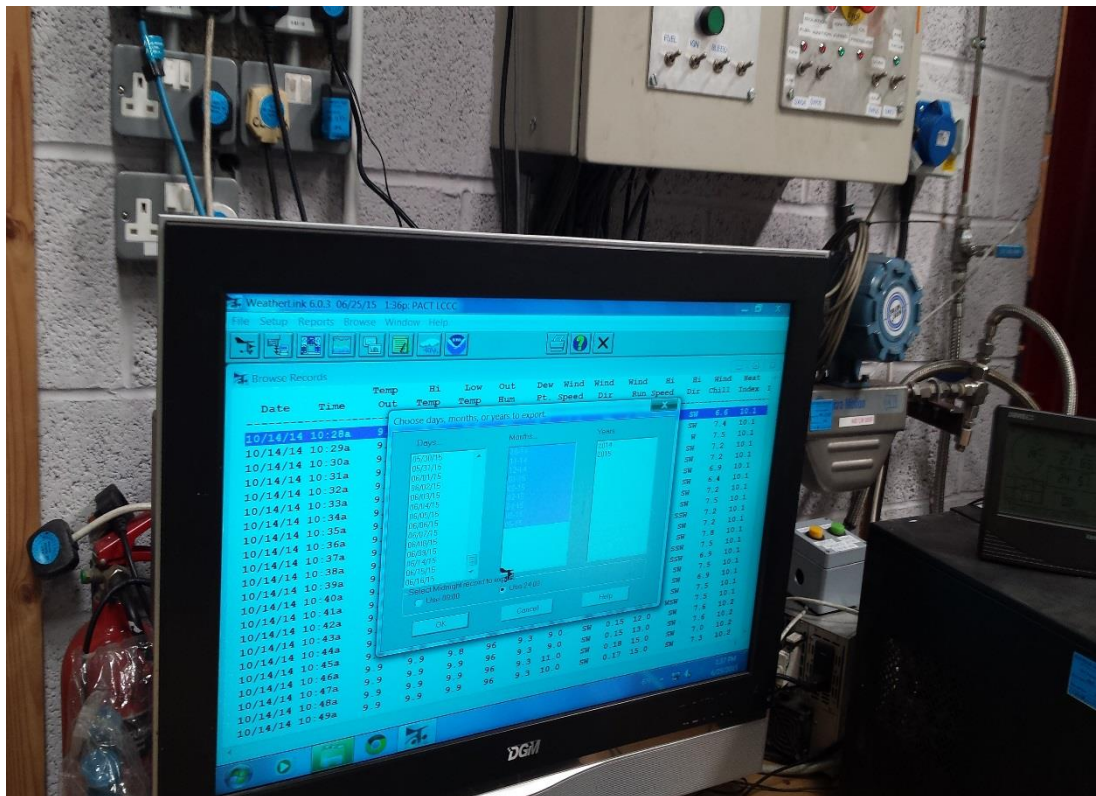


**Appendix II: Photographs of the experimental set up**

(a): The wind sensors clamped on a mast at the PACT site, Beighton.



(c): The Vantage PRO 2 data receiver and recorder



(d): LCD monitor where the data are captured